

Microfluidic Techniques

METHODS IN MOLECULAR BIOLOGY™

John M. Walker, SERIES EDITOR

- 335 Fluorescent Energy Transfer Nucleic Acid Probes: Designs and Protocols**, edited by Vladimir V. Didenko, 2006
- 334 PRINS and In Situ PCR Protocols: Second Edition**, edited by Franck Pellestor, 2006
- 333 Transplantation Immunology: Methods and Protocols**, edited by Philip Hornick and Marlene Rose, 2006
- 332 Transmembrane Signaling Protocols: Second Edition**, edited by Hydar ali and Haribabu Bodduluri, 2006
- 331 Human Embryonic Stem Cell Protocols**, edited by Kursad Turksen, 2006
- 330 Nonhuman Embryonic Stem Cell Protocols, Vol. II: Differentiation Models**, edited by Kursad Turksen, 2006
- 329 Nonhuman Embryonic Stem Cell Protocols, Vol. I: Isolation and Characterization**, edited by Kursad Turksen, 2006
- 328 New and Emerging Proteomic Techniques**, edited by Dobrin Nedelkov and Randall W. Nelson, 2006
- 327 Epidermal Growth Factor: Methods and Protocols**, edited by Tarun B. Patel and Paul J. Bertics, 2006
- 326 In Situ Hybridization Protocols, Third Edition**, edited by Ian A. Darby and Tim D. Hewitson, 2006
- 325 Nuclear Reprogramming: Methods and Protocols**, edited by Steve Pells, 2006
- 324 Hormone Assays in Biological Fluids**, edited by Michael J. Wheeler and J. S. Morley Hutchinson, 2006
- 323 Arabidopsis Protocols, Second Edition**, edited by Julio Salinas and Jose J. Sanchez-Serrano, 2006
- 322 Xenopus Protocols: Cell Biology and Signal Transduction**, edited by X. Johné Liu, 2006
- 321 Microfluidic Techniques: Reviews and Protocols**, edited by Shelley D. Minteer, 2006
- 320 Cytochrome P450 Protocols, Second Edition**, edited by Ian R. Phillips and Elizabeth A. Shephard, 2006
- 319 Cell Imaging Techniques, Methods and Protocols**, edited by Douglas J. Taatjes and Brooke T. Mossman, 2006
- 318 Plant Cell Culture Protocols, Second Edition**, edited by Victor M. Loyola-Vargas and Felipe Vázquez-Flota, 2005
- 317 Differential Display Methods and Protocols, Second Edition**, edited by Peng Liang, Jonathan D. Meade, and Arthur B. Pardee, 2005
- 316 Bioinformatics and Drug Discovery**, edited by Richard S. Larson, 2005
- 315 Mast Cells: Methods and Protocols**, edited by Guha Krishnaswamy and David S. Chi, 2005
- 314 DNA Repair Protocols: Mammalian Systems, Second Edition**, edited by Daryl S. Henderson, 2006
- 313 Yeast Protocols: Second Edition**, edited by Wei Xiao, 2005
- 312 Calcium Signaling Protocols: Second Edition**, edited by David G. Lambert, 2005
- 311 Pharmacogenomics: Methods and Protocols**, edited by Federico Innocenti, 2005
- 310 Chemical Genomics: Reviews and Protocols**, edited by Edward D. Zanders, 2005
- 309 RNA Silencing: Methods and Protocols**, edited by Gordon Carmichael, 2005
- 308 Therapeutic Proteins: Methods and Protocols**, edited by C. Mark Smales and David C. James, 2005
- 307 Phosphodiesterase Methods and Protocols**, edited by Claire Lugnier, 2005
- 306 Receptor Binding Techniques: Second Edition**, edited by Anthony P. Davenport, 2005
- 305 Protein–Ligand Interactions: Methods and Applications**, edited by G. Ulrich Nienhaus, 2005
- 304 Human Retrovirus Protocols: Virology and Molecular Biology**, edited by Tuofu Zhu, 2005
- 303 NanoBiotechnology Protocols**, edited by Sandra J. Rosenthal and David W. Wright, 2005
- 302 Handbook of ELISPOT: Methods and Protocols**, edited by Alexander E. Kalyuzhny, 2005
- 301 Ubiquitin–Proteasome Protocols**, edited by Cam Patterson and Douglas M. Cyr, 2005
- 300 Protein Nanotechnology: Protocols, Instrumentation, and Applications**, edited by Tuan Vo-Dinh, 2005
- 299 Amyloid Proteins: Methods and Protocols**, edited by Einar M. Sigurdsson, 2005
- 298 Peptide Synthesis and Application**, edited by John Howl, 2005
- 297 Forensic DNA Typing Protocols**, edited by Angel Carracedo, 2005
- 296 Cell Cycle Control: Mechanisms and Protocols**, edited by Tim Humphrey and Gavin Brooks, 2005
- 295 Immunochemical Protocols, Third Edition**, edited by Robert Burns, 2005
- 294 Cell Migration: Developmental Methods and Protocols**, edited by Jun-Lin Guan, 2005
- 293 Laser Capture Microdissection: Methods and Protocols**, edited by Graeme I. Murray and Stephanie Curran, 2005
- 292 DNA Viruses: Methods and Protocols**, edited by Paul M. Lieberman, 2005
- 291 Molecular Toxicology Protocols**, edited by Phouthone Keohavong and Stephen G. Grant, 2005
- 290 Basic Cell Culture Protocols, Third Edition**, edited by Cheryl D. Helgason and Cindy L. Miller, 2005

METHODS IN MOLECULAR BIOLOGY™

Microfluidic Techniques

Reviews and Protocols

Edited by

Shelley D. Minteer

*Department of Chemistry
Saint Louis University, St. Louis, MO*


HUMANA PRESS  TOTOWA, NEW JERSEY

© 2006 Humana Press Inc.
999 Riverview Drive, Suite 208
Totowa, New Jersey 07512

www.humanapress.com

All rights reserved. No part of this book may be reproduced, stored in a retrieval system, or transmitted in any form or by any means, electronic, mechanical, photocopying, microfilming, recording, or otherwise without written permission from the Publisher. Methods in Molecular Biology™ is a trademark of The Humana Press Inc.

All papers, comments, opinions, conclusions, or recommendations are those of the author(s), and do not necessarily reflect the views of the publisher.

This publication is printed on acid-free paper. 
ANSI Z39.48-1984 (American Standards Institute)

Permanence of Paper for Printed Library Materials.

Cover illustrations: Figure 3 from Chapter 15, "Microtextured Polydimethylsiloxane Substrates for Culturing Mesenchymal Stem Cell," by Erik T. K. Peterson and Ian Papautsky. Figure 1 from Chapter 14 "Microfluidic Chambers for Cell Migration and Neuroscience Research," by Anne M. Taylor, Seog Woo Rhee, and Noo Li Jeon.

Production Editor: Jennifer Hackworth

Cover design by Patricia F. Cleary

For additional copies, pricing for bulk purchases, and/or information about other Humana titles, contact Humana at the above address or at any of the following numbers: Tel.: 973-256-1699; Fax: 973-256-8341; E-mail: orders@humanapr.com; or visit our Website: www.humanapress.com

Photocopy Authorization Policy:

Authorization to photocopy items for internal or personal use, or the internal or personal use of specific clients, is granted by Humana Press Inc., provided that the base fee of US \$30.00 per copy is paid directly to the Copyright Clearance Center at 222 Rosewood Drive, Danvers, MA 01923. For those organizations that have been granted a photocopy license from the CCC, a separate system of payment has been arranged and is acceptable to Humana Press Inc. The fee code for users of the Transactional Reporting Service is: [1-58829-517-6/06 \$30.00].

eISBN: 1-59259-997-4
ISSN: 1064-3745

Library of Congress Cataloging-in-Publication Data

Microfluidic techniques : reviews and protocols / edited by Shelley D.Minteer.

p. ; cm. -- (Methods in molecular biology ; 321)

Includes bibliographical references and index. ISBN 1-58829-517-6 (alk. paper)

1. Biochips--Laboratory manuals.
 2. Microfluidics--Laboratory manuals.[DNLM: 1. Microfluidics--methods--Laboratory Manuals. 2. Microchip Analytical Procedures--methods--Laboratory Manuals. 3. Microfluidics--instrumentation--Laboratory Manuals. 4. Miniaturization--methods--Laboratory Manuals. QT 25 M626 2006]
- I. Minteer, Shelley D.
II. Series: Methods in molecular biology (Clifton, N.J.) ; v. 321.

R857.B5M54 2006
610'.28--dc22

2005010945

Preface

Microfluidic Techniques highlights recent advances in microfluidic techniques for biological applications. The first section of the book contains chapters that focus on the most popular techniques for fabrication of microchips (photolithography, laser ablation, and soft lithography), while the remaining chapters will focus on microfluidic techniques for bioanalytical assays and bioprocesses, such as DNA analysis, PCR, immunoassays, and cell reactors.

The chapters found here should provide molecular biologists and biochemists with the state-of-the-art technical information required to perform readily reproducible microscale bioassays and bioprocessing in the laboratory.

Shelley D. Minter

Contents

Preface	v
Contributors	ix

1 Overview of Advances in Microfluidics and Microfabrication <i>Shelley D. Minter and Christine M. Moore</i>	1
---	---

PART I MICROFABRICATION METHODS

2 Introduction to Microfabrication Techniques <i>Rabih Zaouk, Benjamin Y. Park, and Marc J. Madou</i>	5
3 Fabrication of Polydimethylsiloxane Microfluidics Using SU-8 Molds <i>Rabih Zaouk, Benjamin Y. Park, and Marc J. Madou</i>	17
4 Fabrication of Microelectrodes Using the Lift-Off Technique <i>Benjamin Y. Park, Rabih Zaouk, and Marc J. Madou</i>	23
5 Laser Ablation as a Fabrication Technique for Microfluidic Devices <i>Emanuel A. Waddell</i>	27
6 Reversible, Room Temperature Bonding of Glass Devices for Microfluidics <i>Loranelle L. Lockyear</i>	39

PART II BIOLOGICAL APPLICATIONS

7 Solid-Phase Extraction in Packed Beds on Glass Microdevices <i>Loranelle L. Lockyear</i>	47
8 Fabrication of Micromachined Magnetic Particle Separators for Bioseparation in Microfluidic Systems <i>Jin-Woo Choi</i>	65
9 Hydrogel-Immobilized Antibodies for Microfluidic Immunoassays: <i>Hydrogel Immunoassay</i> <i>Gloria Thomas, Emad M. El-Giar, Laurie E. Locascio, and Michael J. Tarlov</i>	83

10	Polymerase Chain Reaction in Miniaturized Systems: <i>Big Progress in Little Devices</i> Kalee D. Spitzack and Victor M. Ugaz	97
11	Polymerase Chain Reaction on Microchips Maria C. Carles and Nikolaus J. Sucher	131
12	A Sensitive Sandwich DNA Array Using Fluorescent Nanoparticle Probes Xiaojun Zhao, David T. Pierce, and Yanfu Huan	141
13	Microfluidic Ethanol Biobatteries on a Microchip Shelley D. Minteer and Christine M. Moore	157
14	Microfluidic Chambers for Cell Migration and Neuroscience Research Anne M. Taylor, Seog Woo Rhee, and Noo Li Jeon	167
15	Microtextured Polydimethylsiloxane Substrates for Culturing Mesenchymal Stem Cells Erik T. K. Peterson and Ian Papautsky	179
16	Contraction Study of a Single Cardiac Muscle Cell in a Microfluidic Chip Xiujun (James) Li and Paul C. H. Li	199
17	Microscale Integrated Sperm Sorter Yaokuang Chung, Xiaoyue Zhu, Wei Gu, Gary D. Smith, and Shuichi Takayama	227
	Index	245

Contributors

MARIA C. CARLES • *Department of Molecular and Experimental Medicine, The Scripps Research Institute, La Jolla, CA*

JIN-WOO CHOI • *Department of Electrical Engineering, Louisiana State University, Baton Rouge, LA*

YAOKUANG CHUNG • *Department of Biomedical Engineering, University of Michigan, Ann Arbor, MI*

EMAD M. EL-GIAR • *Department of Chemistry, Mississippi State University, MS State, MS*

WEI GU • *Department of Chemical Engineering, University of Michigan, Ann Arbor, MI*

YANFU HUAN • *Department of Chemistry, University of North Dakota, Grand Forks, ND*

NOO LI JEON • *Department of Biomedical Engineering, University of California–Irvine, Irvine, CA*

PAUL C. H. LI • *Department of Chemistry, Simon Fraser University, Burnaby, BC, Canada*

XIUJUN (JAMES) LI • *Department of Chemistry, Simon Fraser University, Burnaby, BC, Canada*

LAURIE E. LOCASCIO • *Chemical Science and Technology Laboratory, National Institute of Standards and Technology, Gaithersburg, MD*

LORANELLE L. LOCKYEAR • *Department of Chemistry, Bethany College, Lindsborg, KS*

MARC J. MADOU • *Department of Mechanical Engineering, University of California-Irvine, Irvine, CA*

SHELLEY D. MINTEER • *Department of Chemistry, St. Louis University, St. Louis, MO*

CHRISTINE M. MOORE • *Department of Chemistry, St. Louis University, St. Louis, MO*

IAN PAPAUTSKY • *Department of Electrical and Computer Engineering and Computer Science, University of Cincinnati, Cincinnati, OH*

BENJAMIN Y. PARK • *Department of Mechanical Engineering, University of California-Irvine, Irvine, CA*

ERIK T. K. PETERSON • *Department of Electrical and Computer Engineering and Computer Science, University of Cincinnati, Cincinnati, OH*

DAVID T. PIERCE • *Department of Chemistry, University of North Dakota, Grand Forks, ND*

- SEOG WOO RHEE • *Department of Biomedical Engineering, University of California–Irvine, Irvine, CA*
- GARY D. SMITH • *Departments of Obstetrics and Gynecology, Urology, and Molecular and Integrative Physiology, University of Michigan, Ann Arbor, MI*
- KALEE D. SPITZACK • *Department of Chemical Engineering, Texas A&M University, College Station, TX*
- NIKOLAUS J. SUCHER • *Department of Neurology/Neuroscience, Children's Hospital and Harvard Medical School, Boston, MA*
- SHUICHI TAKAYAMA • *Department of Biomedical Engineering and Macromolecular Science and Engineering Program, University of Michigan, Ann Arbor, MI*
- MICHAEL J. TARLOV • *Chemical Science and Technology Laboratory, National Institute of Standards and Technology, Gaithersburg, MD*
- ANNE M. TAYLOR • *Department of Biomedical Engineering, University of California–Irvine, Irvine, CA*
- GLORIA THOMAS • *Department of Chemistry, Mississippi State University, MS State, MS*
- VICTOR M. UGAZ • *Department of Chemical Engineering, Texas A&M University, College Station, TX*
- EMANUEL A. WADDELL • *Department of Chemistry, University of Alabama–Huntsville, Huntsville, AL*
- RABIH ZAOUK • *Department of Mechanical Engineering, University of California–Irvine, Irvine, CA*
- XIAOJUN ZHAO • *Department of Chemistry, University of North Dakota, Grand Forks, ND*
- XIAOYUE ZHU • *Department of Biomedical Engineering, University of Michigan, Ann Arbor, MI*

Overview of Advances in Microfluidics and Microfabrication

Shelley D. Minteer and Christine M. Moore

Miniaturized instrumentation and reactors have attracted great interest in the last decade. The first reported use of a microchip was in 1979, when a gas chromatograph air analyzer was fabricated on a silicon wafer (1). It was not until several years later, when flow injection analysis was performed on a chip, that microchips gained attention (2). Over the last decade, research in integrated microfluidic devices (which are typically referred to as lab-on-a-chip devices or micro total analysis systems [μ TAS]) has expanded to include sample preparation, fluid handling, microreactors, separation systems, cell handling, and cell culturing. The incorporation of these techniques has led to microfluidic devices that have been used to perform capillary electrophoresis-based separations, magnetic microparticle-based separations, immunoassays, DNA analysis, and clinical diagnostics, along with the design of highly efficient microreactors (3,4). They have been applied in medical analysis, environmental monitoring, biochemical analysis, and microchemistry (4).

Advantages of such systems include high performance, design flexibility, reagent economy, miniaturization, and automation (3). The use of small flow channels, typically between 1 and 100 μ M is important when considering the networks of microscopic channels in substrates in which analytes are transported, mixed, and separated (5). Miniaturization allows high-throughput screening, portability, and high-density arrays on a small scale. By decreasing the dimensions of devices, space, time, and the amount of analyte decrease (5). Smaller apparatuses are lower in cost, consume less energy and material, and are minimally invasive when referring to a biological application. The use of less material is protecting our limited resources and the disposability of the microdevices helps to avoid contamination. More sophisticated systems can be

built using small parts, and further development of science can occur because the macro laws do not always apply to microsystems (6).

Although this book focuses on biological applications of microchip technology, it is divided into two sections. The first section describes fabrication techniques. It contains detailed background and methods for photolithography, soft lithography, and laser ablation. The second section provides details of the different applications of microchip technology in molecular biology. Methods for DNA amplification through PCR-on-a-chip, DNA sequencing and separation, magnetic separations, immunoassays, cell culturing, and cell analysis are described.

References

1. Terry, S. C., Jerman, J. H., and Angell, J. B. (1979) A gas chromatograph air analyzer fabricated on a silicon wafer. *IEEE Trans. Electron Devices* **26**, 1880–1886.
2. Ruzicka, J. (1983) Flow injection analysis: from test tube to integrated microconduits. *Anal. Chem.* **55**, 1040–1053.
3. Zhan, W., Alvarez, J., and Crooks, R. M. (2003) A two-channel microfluidic sensor that uses anodic electrogenerated chemiluminescence as a photonic reporter of cathodic redox reactions. *Anal. Chem.* **75**, 313–318.
4. McDonald, J. C. and Whitesides, G. M. (2002) Poly(dimethylsiloxane) as a material for fabricating microfluidic devices. *Acc. Chem. Res.* **35**, 491.
5. Duffy, D. C., McDonald, J. C., Schueller, O. J. A., and Whitesides, G. M. (1998) Rapid prototyping of microfluidic systems in poly(dimethylsiloxane). *Anal. Chem.* **70**, 4974–4984.
6. Madou, M. J. (2002) *Fundamentals of Microfabrication: The Science of Miniaturization*, 2nd ed., CRC Press, Boca Raton, FL.

I _____

MICROFABRICATION METHODS

Introduction to Microfabrication Techniques

Rabih Zaouk, Benjamin Y. Park, and Marc J. Madou

Summary

The advent of photolithography literally brought about the integrated circuit (IC) revolution of the latter part of the twentieth century. Almost all electronic devices that we use today have one or more ICs inside. Improving lithography techniques led to smaller and smaller transistors, which translated into faster and more efficient computing machines. Photolithography also powered the advent of MicroElectroMechanical Systems (MEMS), which are now starting to become more and more diverse in commercial products from mechanical to biomedical devices, helping to change the way people perceive the applicability of IC technology. In this chapter, we examine basic photolithography techniques and their uses in soft lithography and MEMS.

Key Words: Photolithography; microlithography; lithography; soft lithography; microfabrication; MicroElectroMechanical Systems; BioMEMS, microfluidics.

1. Photolithography: An Overview

The word *lithography* (Greek for the words *stone* [*lithos*] and *to write* [*gráphein*]) refers to a process invented in 1796 by Aloys Senefelder. Senefelder found that stone (he used Bavarian limestone) when properly inked and treated with chemicals could transfer a carved image onto paper (*1*).

The most widely used form of lithography is photolithography. In this process, a pattern is transferred to a photosensitive polymer (a photoresist) by exposure to a light source through an optical mask. An optical mask usually consists of opaque patterns (usually chrome or iron oxide) on a transparent support (usually quartz) used to define features on a wafer. The pattern in the photoresist is then further transferred to the underlying substrate by subtractive (etching) or additive (deposition) techniques. The combination of accurate alignment of a successive set of photomasks and exposure of these successive

patterns leads to complex multilayered structures. Photolithography has matured rapidly by continuous improvements in the ability to resolve ever-smaller features. Research in high-aspect-ratio resist features, driven by the field of MicroElectroMechanical Systems (MEMS), is also being actively pursued, as opposed to the essentially two-dimensional processes used traditionally. This is especially important in the fabrication of microfluidic molds.

Photolithography and pattern transfer involve a set of process steps as summarized in **Fig. 1**. As an example, we use an oxidized silicon (Si) wafer and a negative photoresist to transfer a pattern from a mask to a layer of silicon dioxide. An oxidized wafer (**Fig. 1A**) is coated with a 1- μm -thick negative photoresist layer (**Fig. 1B**). After exposure (**Fig. 1C**), the wafer is rinsed in a developing solution or sprayed with a spray developer, which removes the unexposed areas of photoresist and leaves a pattern of bare and photoresist-coated oxide on the wafer surface (**Fig. 1D**). The resulting photoresist pattern is the negative image of the pattern on the photomask. In a typical next step after development, the wafer is placed in a solution of HF or a mixture of HF and NH_4F that attacks the oxide at a much faster rate than the photoresist or the underlying Si (**Fig. 1E**). The photoresist prevents the oxide underneath from being attacked. Once the exposed oxide has been etched away, the remaining photoresist can be stripped off with a solution that only attacks the photoresist, such as a strong acid (e.g., H_2SO_4) or an acid-oxidant combination (e.g., piranha, $\text{H}_2\text{SO}_4\text{:H}_2\text{O}_2$) (**Fig. 1F**). Other liquid strippers include organic solvent strippers and alkaline strippers (with or without oxidants). The oxidized Si wafer with etched windows in the oxide (**Fig. 1F**) now awaits further processing. Recently, photoresists are increasingly being used in applications in which the resist is a permanent part of the final device rather than just a sacrificial layer for patterning the substrate.

2. Basic Photolithography Techniques

Each implementation of the photolithographic process has its own specific requirements, but there is a basic common flow of process that are common to most procedures. In this section, we introduce the basic lithography steps of preparation of wafer, resist application, exposure, development, and pattern transfer.

2.1. Preparation of Wafer

2.1.1. Cleaning of Wafer

Physical contaminants such as dust particles can hinder the lithography process by preventing light from exposing the photoresist or by disturbing the surface uniformity of a coated photoresist. Chemical contaminants may also react with various materials used in the lithography process, creating unwanted effects.

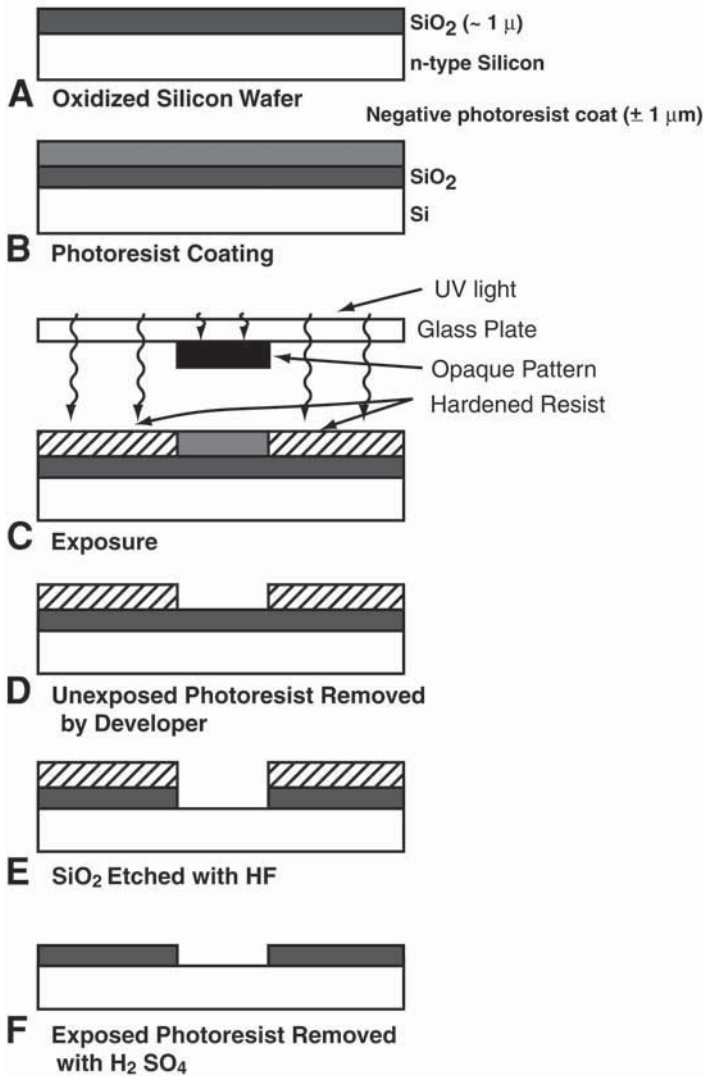


Fig.1. Process flow of basic photolithography followed by pattern transfer. The example uses (A) an oxidized Si wafer and a negative photoresist system. The process steps are (B) photoresist coating, (C) exposure, (D) development, (E) oxide etching, and (F) resist stripping and oxide etching. These steps are explained in detail in the text.

A silicon wafer is the most commonly used platform for microfabrication, but there is a trend toward different substrate materials, especially in the field of BioMEMS (see **Subheading 4.**). A variety of cleaning methods can be used to prepare a wafer for the lithography process. Usually, new wafers do not need further cleaning, because they are cleaned before shipping and are kept in a contamination-free container. If cleaning of the wafer is necessary, a variety of methods (HF dip, RCA1, RCA2, use of piranha, and so on) can be used to remove different types of contaminants. The presence of water or water vapor compromises the adhesion between the photoresist and the wafer. Before the photoresist is applied, a dehydration bake is performed to remove water from the surface of the wafer. Adhesion can be further promoted by applying an adhesion promoter (hexamethyldisilazane) or by roughening the surface of the wafer by plasma etching. This is referred to as wafer priming.

2.1.2. Oxide Growth

In many cases, an oxide layer is desired as a mask for subsequent processes (e.g., an etch or an implant process) or as an insulating layer. This is usually achieved by heating a silicon wafer to between 900 and 1150°C in a dry or humidified oxygen stream in a tube furnace.

2.2. Resist Spinning and Soft Bake

As the first step in the lithography process itself, a thin layer of an organic polymer, a photoresist sensitive to ultraviolet (UV) radiation, is deposited on the oxide surface (see **Fig. 1B**). The liquid photoresist is dispensed onto a wafer that is held by a vacuum chuck in a resist spinner. The wafer is then spun in one or more steps at precisely controlled speeds. The spin speed (between 1500 and 8000 rpm) allows the formation of a uniform film. At these speeds, the centrifugal force causes the liquid to flow to the edges, where it builds up until expelled when the surface tension is exceeded. The resulting polymer thickness, T , is a function of spin speed, solution concentration, and molecular weight (measured by intrinsic viscosity). The spin curves for various photoresists can be obtained from the manufacturer. The spinning process is of primary importance to the effectiveness of pattern transfer. The quality of the resist coating determines the density of defects transferred to the device under construction.

After spin coating, the resist still contains up to 15% solvent and may contain built-in stresses. The wafers are therefore soft baked (prebaked) at 75–100°C to remove solvents and stress, and to promote adhesion of the resist layer to the wafer.

Negative and Positive Tone

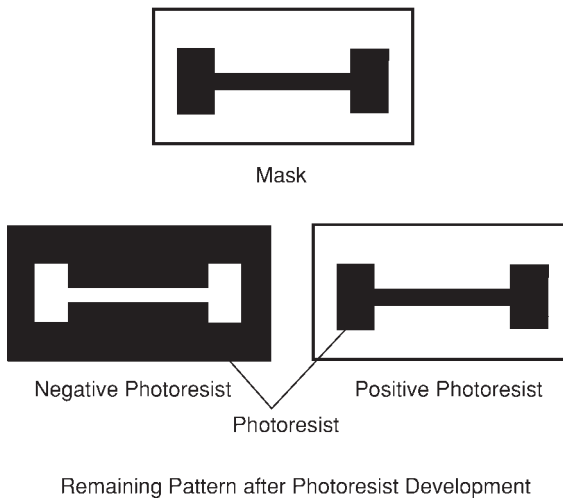


Fig. 2. Resulting patterns after exposure and development of a positive- and negative-tone photoresist. The opaque image on the mask is transferred as is onto the positive photoresist. The image is reversed in the case of a negative photoresist.

2.3. Exposure and Postexposure Treatment

Pattern transfer onto a photoresist is done by shining light through the mask (see Fig. 1C). One typically uses the g-line (435 nm) or i-line (365 nm) of a mercury lamp. In general, the smallest feature that can be printed using projection lithography is roughly equal to the wavelength of the exposure source.

The action of light on a photoresist either increases or decreases the resist solubility depending on whether it is a positive or negative photoresist, respectively. Thus, for a positive-tone photoresist, the opaque pattern on the mask will determine the features remaining in the resist layer after development (see Fig. 2). Conversely, after development of a negative photoresist, the clear pattern of the mask determines the remaining photoresist features (Fig. 2). The profile of the photoresist side walls (see Fig. 3) is critical to many applications such as patterning of hard-to-etch metals (lift-off) and mold fabrication. Figure 4 illustrates the use of a lift-off profile in the lift-off process. The resist wall profile can be controlled by adjusting resist tone, exposure dose, developer strength, and development time, as well as by other means.

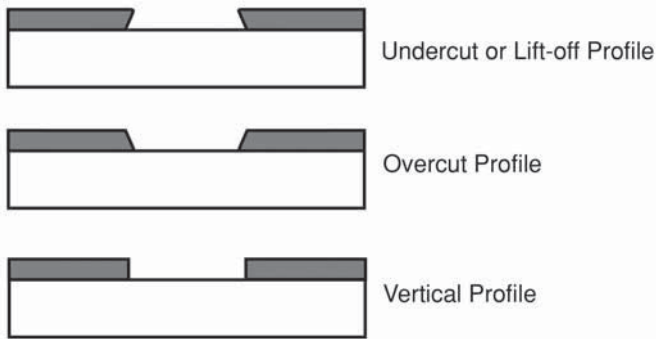


Fig. 3. The three different photoresist profiles. The undercut (lift-off) profile is used mostly in the patterning of metals in a process called “lift-off” (see Fig. 4). The overcut profile is the profile that is normally obtained from a positive-tone photoresist. The vertical profile achieves the best pattern fidelity, but is relatively difficult to obtain.

Post-exposure treatment is often desired because the reactions initiated during exposure might not have run to completion. To halt the reactions or to induce new ones, several post-exposure treatments can be used: postexposure baking, flood exposure with other types of radiation, treatment with reactive gas, and vacuum treatment.

2.4. Development, Descumming, and Postbaking

During the development process, selective dissolving of resist takes place (see Fig. 1D). Development can be done using a liquid (wet development), a gas, or plasma (dry development). Positive resists are typically developed in aqueous alkaline solutions (e.g., tetramethyl ammonium hydroxide), and negative resists in organic solvents.

Unwanted residual photoresist sometimes remains after development. Descumming is a procedure for removing this unwanted photoresist with a mild plasma treatment. In this process, highly energetic oxygen ions react and essentially burn away the unwanted photoresist.

Postbaking or hard baking removes residual solvents and anneals the film to promote interfacial adhesion of the resist that has been weakened either by developer penetration along the resist/substrate interface or by swelling of the resist (mainly for negative resists). Hard baking also improves the hardness of the film. Improved hardness increases the resistance of the resist to subsequent etching and deposition steps. Postbaking is usually done at higher temperatures (120°C) and for longer times (e.g., 20 min) than soft baking or prebaking.

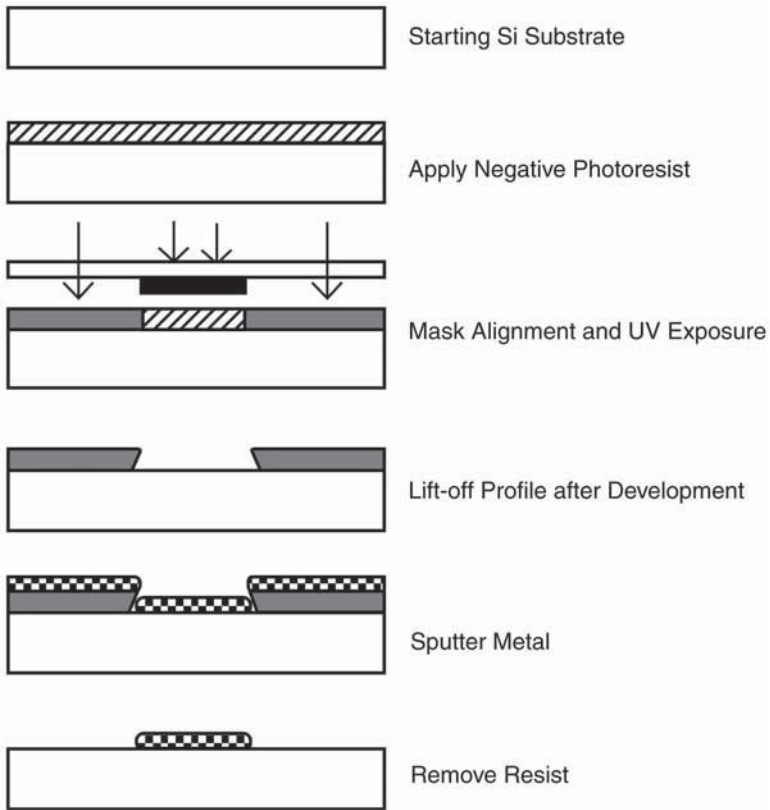


Fig. 4. Example of lift-off sequence using negative resist as sacrificial layer. This method is used in cases in which the metal is difficult to etch (e.g., gold or platinum).

2.5. Pattern Transfer

In cases in which the photoresist is a permanent part of the final device (e.g., microfluidics, carbon MEMS [C-MEMS]), further processing may not be necessary. In most other cases, the sacrificial photoresist pattern is used as a mask for etching (subtractive) or deposition (additive) on the underlying substrate (a subtractive process; *see Fig. 1E*). In a subtractive process, the resist acts as a protective barrier to the etching agent, which can be a liquid solution, a gas, or plasma. After pattern transfer, the resist can be removed for further process steps. Similarly, pattern transfer can involve a deposition technique: chemical vapor deposition or e-beam evaporation.

3. Soft Lithography

Soft lithography (2–4) techniques incorporate an imprint step, in which the topography of a template defines patterns created on a substrate. In soft lithography, a patterned elastomer is used as a stamp, mold, or mask to generate micropatterns and microstructures instead of using a rigid photomask. These methods include replica molding, micro-contact printing, micromolding in capillaries, and micro-transfer molding (5). The major advantage of soft lithography is its short turnaround time; it is possible to go from design to production of replicated structures in <24 h. The method is low in cost and, unlike photolithography, soft lithography is applicable to almost all polymers and, thus, many materials that can be prepared from polymeric precursors. Because soft materials are used, deformation of the stamp or mold, low reproducibility (owing to distortion), and defects (yield) are problems that prevent this technology from being a viable manufacturing technique, but it is widely used in research settings (2).

An example of soft lithography frequently used in creating microfluidics is polydimethylsiloxane (PDMS) molding. In this method, high-aspect-ratio microfluidics can be fabricated using SU-8 negative photoresist (MicroChem, Newton, MA) molds. SU-8 is a chemically amplified negative photoresist with high transparency. The high transparency allows light to penetrate through thick layers of photoresist, thus creating near vertical sidewall profiles. As a form of soft lithography, SU-8 structures have been used as molds for microfluidic applications. In these applications, PDMS is first poured onto the patterned SU-8 mold. The PDMS is cured, removed, and then pressed or bonded onto a flat substrate to create microchannels. **Figure 5** shows a scanning electron microscopy (SEM) micrograph of a PDMS microchannel for a microfluidic system.

4. MicroElectroMechanical Systems (MEMS)

MEMS, or the science of miniaturization, refers to a class of devices that have at least one of their dimensions in the micrometer range. Whereas IC devices involve only electrical components (transistors, diodes, capacitors, and so on), MEMS devices take advantage of a wide range of other phenomena from mechanical to biological (BioMEMS). The materials and fabrication methods used in MEMS are much more varied than those used for IC fabrication (in which one deals principally with Si, oxides, and metals patterned using photolithography). In contrast to the IC industry, in which the devices are carefully packaged and protected from the environment, MEMS devices, such as pressure or glucose sensors, often must have surfaces that are directly exposed to the environment in which they are sensing. Examples of successfully com-

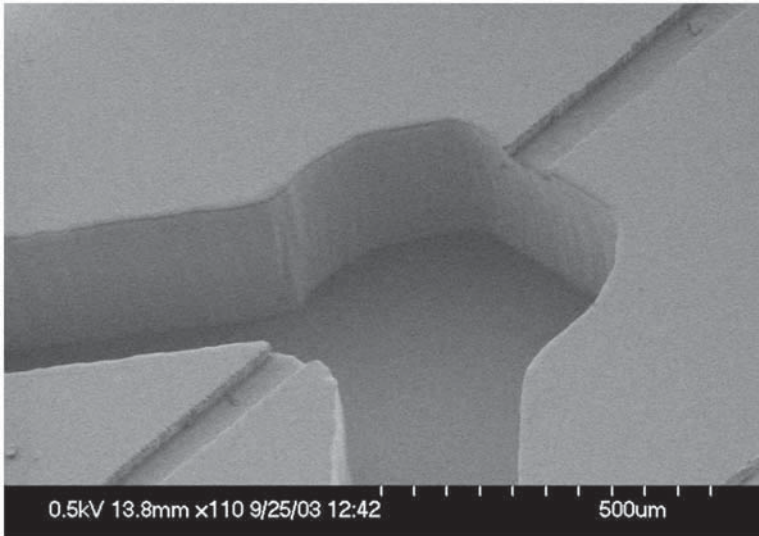


Fig. 5. SEM micrograph showing a PDMS microchannel used for hybridization of DNA on a microfluidic platform. (Courtesy of Guangyao Jia, Madou Research Group, UCI.)

mercialized mechanical devices are accelerometers, gyroscopes, tilt meters, membrane pressure sensors, micromirrors, optical MEMS switches, and inkjet printheads. Commercial BioMEMS devices include glucose sensors, lab-on-chip systems, and DNA arrays. Because of the irreversible chemical reactions involved and contamination considerations, BioMEMS devices tend to be disposable.

5. Nontraditional Materials

Different materials that are being used or investigated for use in MEMS processes include polymers, ceramics, nitinol (shape memory alloys), biomaterials, and carbon. The Madou research group at UCI (see <http://mmadou.eng.uci.edu>) has been actively pursuing research in C-MEMS derived from pyrolyzed photoresist. Patterned SU-8 photoresist is converted into carbon electrodes by subjecting the photoresist to high temperatures in an inert environment in a process called pyrolysis. C-MEMS electrodes can be easily patterned into complex three-dimensional geometries that were previously difficult or expensive to fabricate using conventional carbon electrode fabrication methods. In addition, the electrochemical properties of carbon make it an excellent electrode material (6). High-aspect-ratio carbon structures (see Fig. 6) can be obtained from SU-8 photoresist structures (see Fig. 7). These high-aspect-

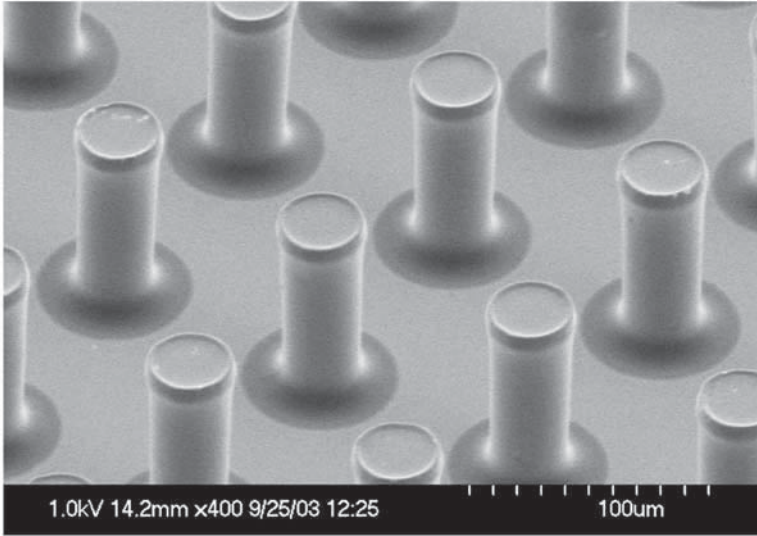


Fig. 6. SEM micrograph of carbon (C-MEMS) posts obtained by pyrolyzing SU-8 negative photoresist. (Courtesy of Chunlei Wang, Madou Research Group, UCI.)

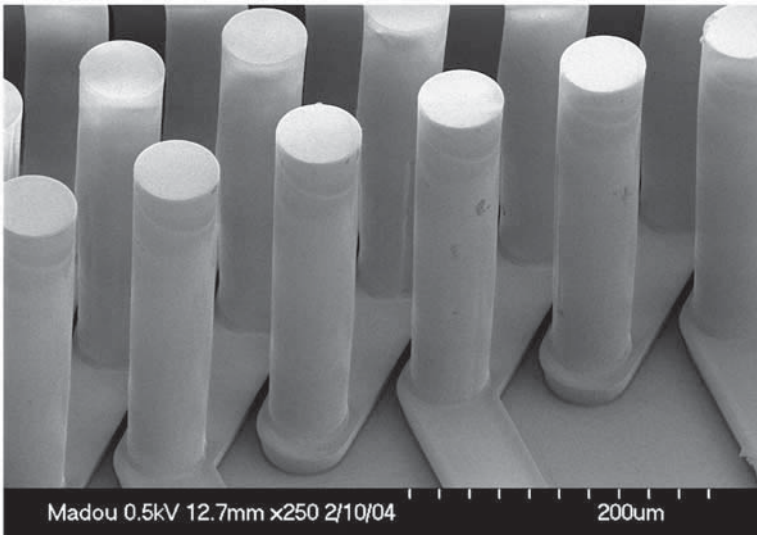


Fig. 7. SEM micrograph of a high-aspect-ratio SU-8 negative photoresist structure taken before structure was pyrolyzed into carbon. The resulting electrodes and interconnects were used for battery research. (Courtesy of Chunlei Wang, Madou Research Group, UCI.)

ratio carbon structures are being investigated for their potential use in batteries, and chemical and biosensing applications.

6. Conclusion

In this chapter, we introduced lithography as an important tool for microfabrication. The application domain of lithography has greatly expanded beyond the IC world to encompass fabrication of mechanical and biological devices. The fact that some DNA arrays are nowadays made through lithography illustrates this point. With the advent of MEMS, different materials and high-aspect-ratio fabrication techniques have also been introduced. The field of microfabrication is so vast that it would be impossible to give a comprehensive review in the context of one short chapter. The reader is therefore referred to textbooks (7,8) and recent reviews for a more thorough investigation.

References

1. Compton. (1994) *Compton's Interactive Encyclopedia (Interactive Multimedia)*, Compton's New Media, Carlsbad, CA.
2. Xia, Y. and Whitesides, G. M. (1998) Soft lithography. *Annu. Rev. Mater. Sci.* 28, 153–184.
3. Kumar, A. and Whitesides, G. M. (1993) Features of gold having micrometer to centimeter dimensions can be formed through a combination of stamping with an elastomeric stamp and an alkanethiol 'ink' followed by chemical etching. *Appl. Phys. Lett.* 63, 2002–2004.
4. Kumar, A., Abbot, N. L., Kim, E., Biebuyck, H., and Whitesides, G. M. (1995) Patterned self-assembled monolayers and meso-scale phenomena. *Acc. Chem. Res.* 28, 219–226.
5. Xia, Y., Rogers, J. A., Paul, K. E., and Whitesides, G. A. (1999) Unconventional methods for fabricating and patterning nanostructures. *Chem. Rev.* 99, 1823–1848.
6. Kinoshita, K. (1988) *Carbon, Electrochemical and Physicochemical Properties*, John Wiley and Sons, New York.
7. Madou, M. J. (2002) *Fundamentals of Microfabrication: The Science of Miniaturization*, 2nd ed., CRC Press, Boca Raton, FL.
8. Gad-el-Hak, M. (2002) *The MEMS Handbook*, CRC Press, Boca Raton, FL.

Fabrication of Polydimethylsiloxane Microfluidics Using SU-8 Molds

Rabih Zaouk, Benjamin Y. Park, and Marc J. Madou

Summary

We detail the widely prevalent technique of polydimethylsiloxane (PDMS) molding using SU-8 for creating microfluidic chambers and channels. Although other techniques such as injection molding are more apt for mass manufacturing and cost-effective, PDMS molding is used almost exclusively for rapid prototyping in corporate and research environments because of its simplicity and fast turnaround time.

Key Words: Polydimethylsiloxane; SU-8; soft lithography; microfluidics; molding.

1. Introduction

This chapter details the process of creating microfluidic channels in polydimethylsiloxane (PDMS) using SU-8 as a mold. This relatively easy process is widely used in the research environment for prototyping of microfluidic devices. **Figure 1** represents the process flow for the creation of PDMS microfluidics.

2. Materials

2.1. Equipment

1. Ultraviolet (UV) flood exposure machine (*see Note 1*).
2. Photoresist spinner.
3. Oven or hot plate (*see Note 2*).

2.2. Supplies (*see Note 3*)

1. Silicon (Si) wafer (*see Note 4*).
2. SU-8 photoresist (MicroChem, Newton, MA) (*see Note 5*).
3. SU-8 photoresist developer (MicroChem).

From: *Methods in Molecular Biology*, vol. 321: *Microfluidic Techniques: Reviews and Protocols*
Edited by: S. D. Minteer © Humana Press Inc., Totowa, NJ

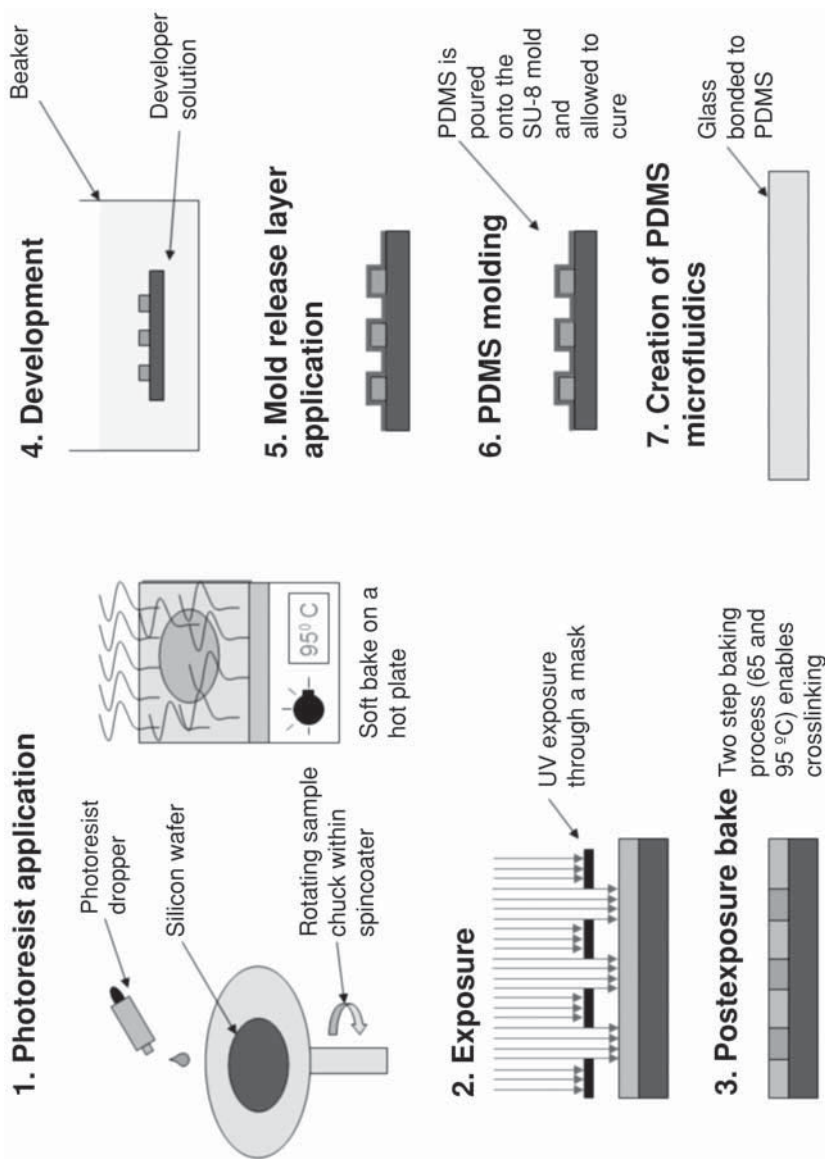


Fig. 1. Process flow for creating PDMS microfluidics using SU-8 molds.

4. Acetone.
5. Isopropyl alcohol.
6. Sylgard 184 Silicone Kit (Dow Corning, Midland, MI).
7. Mold release (*see Note 6*): trimethylchlorosilane (Sigma-Aldrich, St. Louis, MO) or tridecafluoro-1,1,2,2-tetrahydrooctyl-1-trichlorosilane (United Chemical Technology, Bristol, PA).

3. Methods

3.1. Mask Fabrication

Drawing and computer-aided design (CAD) programs such as Macromedia Freehand® and Autodesk AutoCAD® can be used to design masks for the fluidic device. Although glass or quartz masks are used for fabrication of devices with small features, a transparency (much cheaper) can be used as a mask for devices with relatively large feature sizes ($>50\ \mu\text{m}$). The mask design can be simply printed with a high-resolution printer on a regular transparency.

3.2. Application of SU-8 Photoresist

The SU-8 photoresist is spun onto a Si wafer using the photoresist spinner at a speed that achieves the required thickness. For example, to get a $100\text{-}\mu\text{m}$ -thick layer of SU-8 using SU-8 100, the wafer should be spun at 500 rpm for 5 s, to spread out the photoresist, then at 3000 rpm for 30 s, to achieve the final thickness (*see Note 7*). The wafer should then be soft baked for the required time at the required temperature (*see Note 8*). For our example of a $100\text{-}\mu\text{m}$ -thick-layer of SU-8, the soft bake time is 10 min at 65°C , and 30 min at 95°C . The two-step bake is done to reduce internal stresses owing to thermal effects.

3.3. Exposure

The transparency photomask is clamped between the Si wafer coated with SU-8 photoresist and a blank glass plate. The photoresist is exposed in a UV exposure machine at the required dose ($400\ \text{mJ}/\text{cm}^2$ in our example).

3.4. PostExposure Bake

After exposure, a postexposure bake (*see Note 8*) is performed to crosslink selectively the exposed portions of the photoresist (1 min at 65°C and 10 min at 95°C for our example).

3.5. Development

SU-8 developer is poured in a beaker, and a spray bottle with new SU-8 developer is made ready. The sample is developed in the SU-8 developer until all unexposed SU-8 is removed. To determine whether all the unexposed SU-8

is removed, the sample is removed from the beaker, rinsed with new developer, rinsed with isopropyl alcohol, and then blown dry gently with nitrogen air.

3.6. Application of Mold Release Layer

A mold release layer is created by exposing it to a vapor of tridecafluoro-1,1,2,2-tetrahydrooctyl-1-trichlorosilane in a desiccator for 2 h. Two or three drops from a dropper should suffice.

3.7. PDMS Molding

The PDMS oligomer and crosslinking prepolymer of PDMS agent from a Sylgard 184 kit is mixed in a ratio of 10:1. A convenient way of mixing these agents is to place both in a disposable plastic bag, heat seal, and mix manually. The two liquids can also be mixed using a disposable fork. The mixture can then be placed under vacuum for degassing. The PDMS mixture is poured onto an Si/Su-8 mold and cured for 1 h at 65°C (*see Note 9*). Unused material can be stored in a refrigerator or freezer for later use. After cooling, the PDMS can be carefully peeled off the mold (*see Note 10*). This process yields a transparent polymer sheet that contains channels and chambers that correspond to the positive relief of the photoresist.

3.8. Creation of PDMS Microfluidics

In a final step, the PDMS film is sealed to a flat surface to complete the microfluidics. The PDMS can be sealed with manual pressure to create fluidic devices that do not need to withstand high pressures. Otherwise, oxygen plasma can be used to treat both a glass substrate and the PDMS film. If these are immediately pressed together, a tight bond will be created.

4. Notes

1. An alignment machine is needed for multilayer molds. The aligner has the ability to align masks to the existing patterns for multiple exposure steps.
2. All bake times are given with respect to baking on a hot plate. An oven can be used for all the bakes, but the bake times may differ.
3. Protective equipment including chemical gloves and safety goggles should be worn at all times. Refer to the Material Safety Data Sheet of all chemicals for toxicity, flammability, and handling information before starting any process.
4. Too thin of a Si wafer can cause the mold to break easily. Standard Si wafers are 500 μm thick.
5. Store in a tightly closed container in a cool environment away from sunlight. Handle only under yellow light.
6. Handle and store under nitrogen. This material has an extremely low flash point (-18°C).

7. Bubbles will often be present after spinning of the photoresist. These bubbles can be promptly removed by puncturing the bubbles carefully with a sharp object.
8. After all baking steps, the sample must be allowed to cool slowly (at least 15 min) to room temperature before any further processing is done, to reduce internal stresses. This thermal relaxation time is crucial for survival of the mold.
9. The curing process for the PDMS can be done at room temperature for an extended time (24 h or more) to facilitate removal of the PDMS from the mold. A well-polished Si wafer (without an oxide layer) seems to work best as the substrate to promote detachment of the PDMS from the mold.
10. Removal can be facilitated by using a knife to cut the PDMS around the edges of the wafer.

Fabrication of Microelectrodes Using the Lift-Off Technique

Benjamin Y. Park, Rabih Zaouk, and Marc J. Madou

Summary

The lift-off technique is one of the most prevalent methods for fabricating microelectrodes on a flat surface (e.g., a silicon [Si] wafer). It represents an alternative for metal-etching techniques that often utilize hazardous chemicals in order to define a pattern. This chapter presents an example of patterning gold electrodes on an Si wafer.

Key Words: Photoresist; gold; lift-off technique; chlorobenzene; Si wafer.

1. Introduction

In many cases, a pattern of metallic electrodes and interconnects is desired. Some metals such as platinum and gold are not easily etched away and, therefore, standard chemical patterning methods cannot easily be used. In this chapter, we detail a procedure for obtaining gold electrodes or interconnects (*see Fig. 1*). These electrodes can be used for electrokinetic manipulation, local application of voltage or current, DNA immobilization, and so on.

2. Materials

2.1. Equipment

1. Ultraviolet (UV) flood exposure machine.
2. Sputtering machine (or an evaporation machine).
3. Photoresist spinner.
4. Oven or hot plate.

2.2. Supplies (see *Note 1*)

1. Oxidized silicon (Si) wafer (or any flat nonconductive substrate).
2. Crucible for an E-beam evaporator.
3. Gold (evaporation material).

From: *Methods in Molecular Biology*, vol. 321: *Microfluidic Techniques: Reviews and Protocols*
Edited by: S. D. Minton © Humana Press Inc., Totowa, NJ

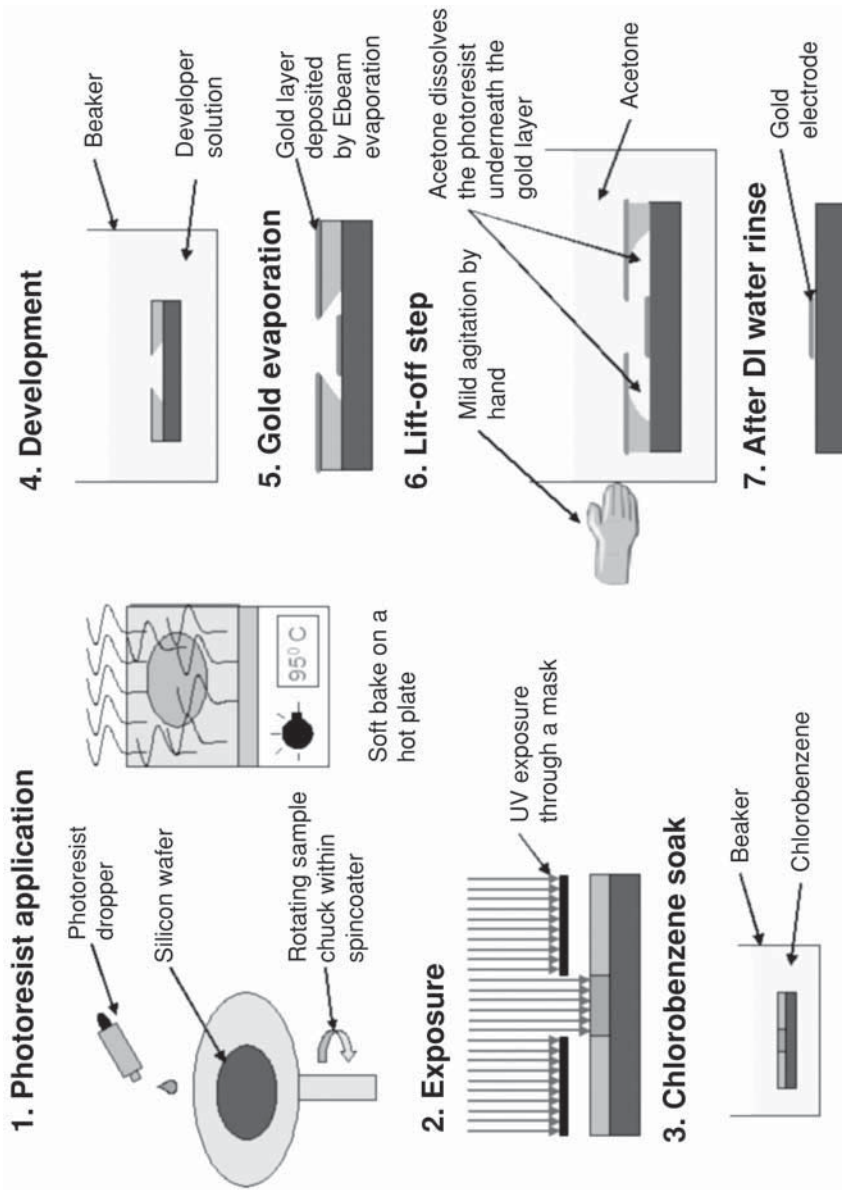


Fig. 1. Process flow for fabrication of gold microelectrodes using lift-off technique.

4. Chrome or titanium (evaporation material) (*see Note 2*).
5. Shipley Microposit® SC 1827 positive photoresist (MicroChem, Newton, MA) (*see Note 3*).
6. Photoresist developer: Microposit MF 319 or Microposit MF 351 (MicroChem).
7. Acetone.

3. Methods

3.1. Mask Fabrication

Drawing and computer-aided design (CAD) programs such as Macromedia Freehand® and Autodesk AutoCAD® can be used to design masks for the fluidic device. Although glass or quartz masks are used for fabrication of devices with small features, a transparency (much cheaper) can be used as a mask for devices with relatively large feature sizes ($>50\ \mu\text{m}$). The mask design can be simply printed with a high-resolution printer on a regular transparency.

3.2. Application of Shipley 1827 Photoresist

Shipley 1827 photoresist is spun onto an Si wafer using a photoresist spinner at 3000 rpm for 30 s to achieve a 2.7- μm -thick layer of photoresist. The photoresist thickness must be much greater than the final metal layer because a positive photoresist is used as a sacrificial layer. There must be a discontinuity in the metal layer to allow the acetone to dissolve the photoresist underneath the gold layer during the lift-off step. The wafer should then be soft baked on a hot plate for 2 min.

3.3. Exposure

A transparency photomask is clamped between the Si wafer coated with the photoresist and a blank glass plate. The photoresist is exposed in a UV exposure machine for the amount of time required to achieve a dose of 100 mJ/cm². The sample can be dipped in chlorobenzene solution for 5 min before development to help the lift-off process (*see Note 4*).

3.4. Development

Although different concentrations of the developer solution can be used to develop the photoresist, it is prudent to use a dilute solution for slower and more controlled development. The sample should be developed in the developer solution until all unexposed photoresist is removed. Periodic checking, visually or under a microscope, will ensure that the photoresist is completely developed. The wafer surface that is not covered with photoresist has to be completely void of photoresist residue for better metal adhesion.

3.5. Metal Deposition

A 500- to 5000-Å layer of gold is deposited in a sputtering or evaporation machine onto the sample. An adhesion layer is usually deposited before the gold (*see Note 2*). For better adhesion, an oxygen plasma step can be used before metal deposition (*see Note 5*).

3.6. Lift-Off

The sample, covered in gold, is placed into a bath of acetone. The photoresist underneath the gold will be attacked by the acetone, and slight agitation should selectively remove the gold leaving the gold electrode patterns. Physical abrasion using a lintfree wipe can help remove strongly adhered gold fragments. The final sample should be cleaned in deionized water.

4. Notes

1. Protective equipment including chemical gloves and safety goggles should be worn at all times. Refer to the Material Safety Data Sheet for toxicity, flammability, and handling information before starting any process.
2. A 15- to 100-Å layer of chrome or titanium is usually deposited onto the sample before gold deposition in order to promote adhesion.
3. Store in a tightly closed container in a cool environment away from sunlight. Handle only under yellow light.
4. A 5-min chlorobenzene soak can be done after exposure and before development to create a lift-off profile for easier lift-off. The chlorobenzene causes the top surface of the photoresist to swell and become more resistant to the developer. As a substitute to the chlorobenzene soak and to ensure discontinuities in the deposited gold layer, relatively thick photoresist layers (>2 μm) can be used.
5. A descumming step using oxygen plasma can be done prior to metal deposition. This ensures that the wafer surface is free of resist residue for better adhesion of the metal.

Laser Ablation as a Fabrication Technique for Microfluidic Devices

Emanuel A. Waddell

Summary

The use of microfluidic devices is making rapid inroads in the modern laboratory. Traditionally, devices have been manufactured in silica owing to its well-understood surface chemistry and micromachining techniques that are ubiquitous in the microelectronics industry. Recently researchers have begun to utilize devices fabricated from polymer substrates as an alternative to glass. Reasons include total cost and the ability to tailor physical and chemical properties. However, traditional microfabrication techniques of molds that are used to fabricate polymer devices by imprinting or injection molding are subject to similar limitations as those associated with silica. In a research and development environment, it is important that researchers have access to fabrication techniques that are rapid and easily implemented with a variety of polymer substrates. Laser ablation has been proven to be such a technique, and this chapter describes the fabrication of a simple injection tee utilizing this technique. This chapter also examines the practical details involved in laser ablation from the perspective of a scientist who desires to utilize a turn-key system.

Key Words: Microfluidic devices; laser ablation; laser fluence; polymer substrates; microfabrication.

1. Introduction

Traditionally, microfluidic devices have been fabricated in silica or glass owing to their well-understood physical and chemical properties. These substrates have the following advantages:

1. They have well-established surface chemistries.
2. They allow easy transfer of existing technologies (such as capillary electrophoresis and DNA hybridization protocols) to miniaturized systems.
3. They allow easy fabrication using techniques developed for silicon.
4. They have general chemical inertness.
5. They have very low electrical conductivity (*I*).

From: *Methods in Molecular Biology*, vol. 321: *Microfluidic Techniques: Reviews and Protocols*
Edited by: S. D. Minter © Humana Press Inc., Totowa, NJ

However, using silica or glass as a substrate material has some disadvantages, such as low limiting aspect ratios obtained through chemical etching, a time-consuming fabrication process, and fragility resulting from their inherent brittleness. Polymers provide an alternative to the aforementioned substrates, and there are many methods for fabricating microfluidic devices from polymer substrates. Some of the more popular methods include LIGA (German for Lithographic Galvanoformung Abformung-lithography, electroplating, and molding) (2–4), imprinting (5–9), and laser ablation (10–12). LIGA-based methods require a lithographic step in which a pattern is formed that is transferred to a metal template utilizing photoresist. The metal template is then used to fabricate micron-size channels in a plastic substrate by either an imprinting method or a plastic reformulation method. In the imprinting method, the metal template is pressed against the plastic substrate at high pressure and usually at a temperature approaching the glass transition temperature, which is the temperature at which a plastic transitions from a solid state to a liquid (glassy) state. In some instances, the imprinting step may be accomplished at room temperature. In the plastic reformulation method, the plastic is heated past its glass transition temperature and poured into a mold, where it is allowed to cool to room temperature. After cooling, it is then released from the mold. In soft lithography, the unpolymerized plastic is poured into a manufactured mold. The polymerization step takes place in the mold and the final product is released from the mold following polymerization. The primary drawback of this method is the time and cost involved in manufacturing a mold. In addition, a mold may be utilized only a finite number of times (tens to hundreds) before it must be discarded.

Martynova et al. (9) first reported wire imprinting in the literature in 1996. In this method, high-gage wire (small diameter) is laid in the desired format on the polymer substrate. The wire serves as a template and is pressed against the substrate in the previously described manner. This method is fairly easy to implement and is low cost, but it is limited in the design complexity of fluidic circuits. In addition, the template must be redesigned after the manufacture of a single circuit. This limits reproducibility and becomes tedious when fabricating more than several circuits. Finally, it is difficult to attain high aspect ratios with this method.

Briefly, laser ablation is the phenomenon of laser light interacting with material such that chemical bonds are broken and the associated rapid increase in temperature and pressure ejects the resultant chemical product. This phenomenon was first reported in 1973 when the damage of laser optics by intense 10.3- μm radiation was observed (13). Srinivasan (14) first reported the laser ablation of polymers, when he described the laser ablation of polyethylene terephthalate (PET) in 1982. Although laser ablation of ceramics, glass, and met-

Table 1
Common Wavelengths of Pulsed Lasers

Laser	Wavelength (nm)
Excimer	
F ₂	157
ArF	193
KrF	248
XeCl	308
N ₂	337
Nd:YLF	1054
Ti:sapphire	700–1080
Nd:YAG	1064, 532
	355, 266
CO ₂	10,600

als has been reported, typically, when laser ablation is utilized as a tool for fabricating microfluidic devices, polymer substrates are utilized. With laser ablation micromachining, polymeric devices are fabricated by focusing the output of a laser onto the surface of a polymer. Either moving the surface relative to a fixed laser beam with a two-dimensional (2D) stage or moving the focused beam relative to a fixed substrate creates the fluidic circuit.

This chapter examines the practical details involved in laser ablation, from the perspective of a scientist who desires to utilize a turnkey system. Turnkey systems are available from several manufacturers, including, but are not limited to, New Wave Research (Fremont, CA), Resonetics (Nashua, NH), Potomac Photonics (Lanham, MD), and J.P. Sercel Associates (Hollis, NH). The major components of a laser ablation system are (1) a laser light source, (2) steering and imaging optics and beam delivery, and (3) a movable stage.

2. Materials

The light source in a laser ablation system usually consists of a high-intensity pulsed laser source (**Table 1**). The wavelength of the emitted radiation may range from the deep ultraviolet (UV) to the infrared (IR) region of the spectrum. The wavelength of the emitted radiation has a direct impact on the materials one is able to ablate. As a general rule, the deep UV (<480 nm) is utilized to ablate transparent, nondoped polymers, with more effective ablation occurring at shorter wavelengths. Such wavelengths are typically accessible by excimer lasers, which have pulse durations in the nanosecond range and peak intensities of 3–400 mW. It is important to note that as the wavelength of the ablation laser decreases in the UV, the energy necessary to ablate a poly-

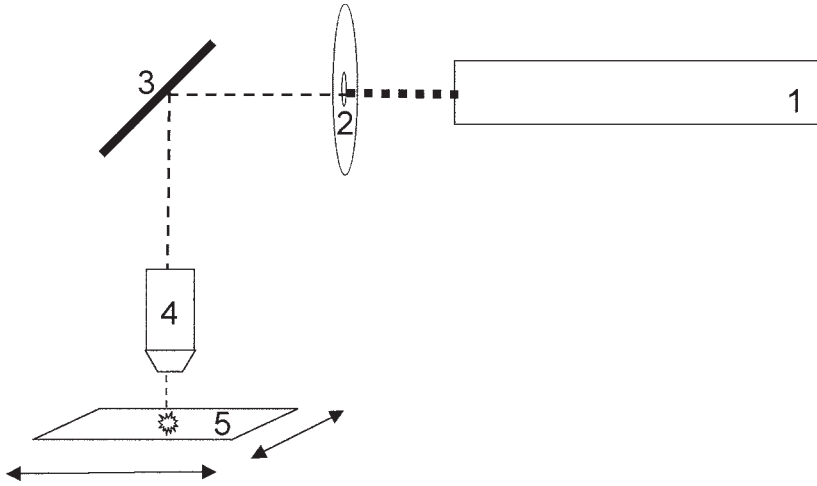


Fig. 1. Simplified schematic of a laser ablation micromachining system. The dashed line denotes the path of laser emission. Radiation is emitted by the laser (1), the beam passes through an aperture (2) and is steered by a turning mirror (3) through the focusing objective (4). The substrate (5) is mounted on a computer-controlled *x-y* stage.

mer also decreases. This is a direct result of the increased electronic absorption cross-section of polymers at shorter wavelengths that improves the efficiency of light absorption. In many instances, doped polymers, which are doped with dyes that absorb at particular wavelengths, are used. In these instances, visible wavelengths emitted from pulsed Nd:YAG lasers may be used. If the dye absorbs in the IR region of the spectrum, near-IR and IR light sources such as the Ti:Sapphire laser or CO₂ laser may be used.

The steering and imaging optics are the set of lenses, mirrors, and apertures that are used to “steer” the laser beam from its origination point to the sample stage. The optics must be able to withstand the high amounts of energy at the wavelengths being propagated by the laser. In this instance, in which the excimer laser is used, the optics are manufactured from quartz or sapphire. The aperture is usually a spherical or rectangular opening that ranges from 10 μm to several millimeters and is used to define spatially the laser beam. The discussion here follows the simplified schematic in **Fig. 1**, which is based on a typical laser micromachining system. After the light is emitted from the laser (1), it passes through an aperture (2) and is steered by a mirror (3) through the focusing objective (4). Ablation occurs at the polymer surface (5), which is placed on a 2D stage.

The programmable stage (Aerotech, Pittsburgh, PA) is typically 2D and in the ideal setting is integrated with the laser utilized for laser ablation. The motion of the stage is controlled via user input or preprogrammed commands. In both instances, the speed of the stage may be varied. A manually controlled stage offers the advantage of the ability to ablate simple microfluidic devices without having to program the stage. This is helpful for rapid design and testing of simple devices in which one is interested in “proof of concept,” material compatibility with the lasing wavelength, or a “free-hand” modification of an existing device. Manual control of a motorized stage is typically accomplished via the use of a joystick, which is intuitive and replicates direction and speed as directed by the user. In most instances, the joystick will have a “fire” button that turns the laser on and off.

However, for day-to-day reproducibility and for the production of tens to hundreds of devices, the ability to program a stage is indispensable. Commonly referred to as the “direct write” method, because the laser directly “writes” the pattern into the desired substrate, the programming of the stage may be accomplished by the use of computer numerical control (CNC) commands. The CNC commands are simplistic statements that may be programmed in a style similar to the Beginner’s All-Purpose Symbolic Instruction Code. CNC commands instruct the movement of the stage (coordinates and velocity) and the firing of the laser (on–off control and repetition rate) as well as the control of any associated accessories such as vacuum stages and process gases. Because of the complexity of some fluidic circuits, this programming method may be time-consuming and tedious, but comprehension of the technique is essential for troubleshooting and modification of existing programs.

The graphic method of programming is predicated on the translation of computer-aided design (CAD) drawings into the Data eXchange File (DXF) format. The DXF format may then be translated to CNC commands with the use of a conversion utility such as Gcode2000 (Andrew Clayton, Salisbury, NC). The advantage of this process is that the microfluidic circuit may be designed in a graphical interface such as CorelDraw or AutoCAD that assists in visualization, digital archiving amenable to modification, and speed and ease of design. The CAD method does not require detailed programming by the user, which eliminates extensive training. The amount of modification required after translation is dependent on the CAD and translation programs utilized.

The physical morphology of the microfluidic channels is determined by a number of parameters including the laser fluence, the spot size of the focused laser output, the translation speed of the x - y stage, the repetition rate of the laser firing, the nature of the substrate being ablated, and the local chemical environment under which ablation occurs. The laser fluence is typically expressed

as the energy per unit area (mJ/cm^2). At low fluence, the laser has no visible effect on the polymer substrate; however, as the fluence is increased, there is a point at which there is sufficient power density to break chemical bonds and remove material from the substrate. This is known as the ablation threshold (15). Using a laser fluence that is too low results in a lack of any observable ablation, laser-induced periodic structures, and/or alterations in surface charge without a physical loss of material (16,17). The geometric spot size of the focused laser beam is defined by the demagnification of the focusing objective and the size and shape of the mask utilized. The aperture is typically a circle or a square that has dimensions ranging from tens of micrometers to a few millimeters. After passing through the aperture, the light is focused through a lens onto the substrate surface. The energy received per unit time determines the depth of ablation and is defined by the rate of the x - y stage movement, the repetition rate of the laser firing, and the laser fluence. A slow rate of x - y stage movement and a high laser-firing repetition rate translate to a higher number of pulses and an increased depth for a defined area. However, the depth of focus of the laser spot limits the depth of a channel (or feature), because as the laser spot moves out of focus, the fluence decreases. This problem may be circumvented when etching deeper structures, if the focus is readjusted for subsequent passes.

The laser-firing repetition rate and the velocity of the x - y stage also determine the gross roughness of the microfluidic channel. The physical morphology of the channels is also a function of the local atmosphere under which ablation occurs (18). For example, ablation under water results in wedge-shaped channel profiles and is thought to be the result of self-focusing or re-focusing of the laser beam as it passes through water. In addition to the self-focusing effect, the water assists in the removal of debris that is usually left behind in the laser ablation process. It has been determined that the physical morphology of the ablated region is dependent on the temporal profile, the spatial profile, and the wavelength of the laser pulse. The longer the laser pulse length, the greater the fluence required to ablate the substrate, because the ablation of the surface of the polymer is a function of the energy deposited per unit time (15). Ablation pulse lengths may range from hundreds of femtoseconds to tens of nanoseconds and are dependent on the physical characteristics of the laser used. For a corresponding fluence of $30 \text{ mJ}/\text{cm}^2$, the power density may range from 1.5 mW for a pulse length of 20 ns to a power density of 1.5 petawatts for a pulse length of 20 fs . Similarly, for a given substrate material, different ablation wavelengths afford different limiting aspect ratios; that is, the shorter the wavelength, the greater the aspect ratio. A poor spatial profile of the laser beam results in poor feature quality and reproducibility because it dictates the geometric shape of the ablated area.

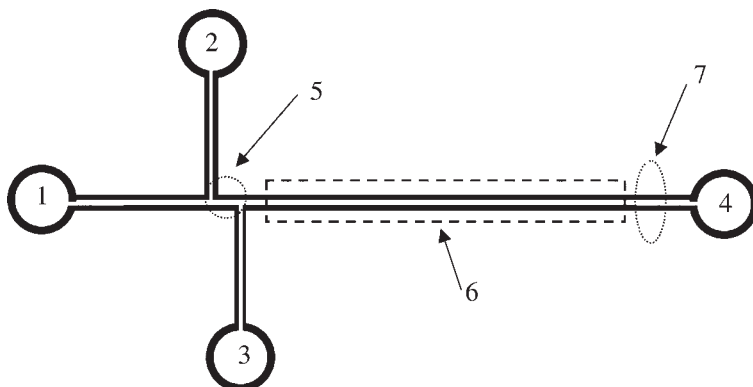


Fig. 2. Schematic of double-tee injection system: (1) Mobile phase (buffer) well; (2) sample well; (3) waste well no. 1; (4) waste well no. 2; (5) injection plug; (6) separation channel; (7) detection zone.

In general, the laser ablation of polymer substrates to fabricate microfluidic devices is a rapid process. Once initial testing of the laser ablation system is successfully accomplished, simple devices may be fabricated in a matter of hours with modifications being easily made.

3. Methods

In this experiment, a basic cross-tee injection design as depicted in [Fig. 2](#) is fabricated in a 1 × 3 in. section of polymethylmethacrylate (Goodfellow, Devon, PA). Because the actual separation is not included in the scope of this work, injection and separation voltages are not discussed. However, it is possible to ensure channel connectivity by monitoring the current as a function of voltage in the device. The steps for fabricating a device in polymer substrate are as follows:

1. Cut the polymer by either scoring the plastic and breaking, cutting with shears, or using a band saw or rotary tool. The sample should be cut into a 1 × 3 in. piece. Typically, the thickness of the polymer ranges from 500 μm to 2 mm.
2. Remove any protective coating from the plastic and sonicate in a 50:50 mixture of water and ethanol for 5 min. Sonication assists in removing any debris and adhesive residue. After sonication, blow-dry the sample using a nitrogen stream.
3. Place the plastic on the stage and engage the stage vacuum. The vacuum ensures that the plastic is held flat during the ablation process. This is critical in order to maintain focus during the machining process.
4. Focus the imaging objective such that the top face of the plastic is in focus. This is accomplished by focusing on the edge of the plastic (*see Notes 1–3*).

5. Fire several shots of the laser in order to ensure that ablation occurs at the pre-defined power levels and focus. If this does not occur either refocus the imaging objective or increase the laser fluence. Increasing the intensity of the laser or decreasing the attenuation may result in increased laser fluence (*see* **Notes 1–3**).
6. Utilizing the joystick, move the piece such that the start point for machining is under the microscope objective.
7. Initiate the ablation process. Make note of the local atmosphere; that is, is the ablation occurring under an inert gas such as nitrogen, in a vacuum, or under a solvent such as methanol or water (*see* **Notes 4–6**).
8. After micromachining of the piece has been completed, ensure that the laser has stopped firing before attempting to remove the plastic. After removing the plastic from the stage, sonicate in a solution of 50:50 ethanol:water in order to remove any particulates that may remain on the surface.
9. Seal the device. This may be accomplished by one of two methods. The first method involves placing a cured sample of polydimethylsiloxane (PDMS) on top of the ablated sample. A cork borer is utilized to cut circles in the PDMS to form wells. The wells are cut before placing of the PDMS on the ablated sample. This method allows one to form a reversible seal of PDMS and polymethyl methacrylate. The second method involves placing an identical section of 1 × 3 in. of polymer on top of the ablated substrate and placing the pair under pressure and low heat approaching the glass transition temperature. The combination of heat and pressure permanently seals the device.

4. Notes

1. Laser light may permanently damage vision. Ensure that all personnel have been properly trained in laser use and that all safety protocols are followed. *Always* wear goggles approved for the wavelength of laser emission.
2. Ensure that the fluence of the laser remains constant. Some lasers may require a warm-up period during which shots are continually fired until the fluence remains constant.
3. An absorption spectrum of the polymer sample proves to be helpful when determining the appropriate wavelength for ablation. Ablation occurs in regions of strong absorption.
4. A slow stage movement and a high laser repetition rate result in smoother channels.
5. Reproducible results are readily obtained when the system is placed in a vibration-free environment. This may be accomplished by placing the system on a damped optical table or a marble slab.
6. A sample program for micromachining a double-tee injection system was written for a laser micromachining system (LMT-4000 Laser Micromachining System) purchased from Potomac Photonics equipped with a KrF pulsed (7 ns) excimer (248 nm) laser and an Aerotech Unidex 500 PC-based motion controller.


```

rot x,y,0
;rotates the stage coordinates to the home position
pr in un me un/se
;prompts the stage to move in metric units per second
ou 1,1; vacuum chuck
;turns on the vacuum chuck
ou 0,1; process gas
;turns on process gas to blow across stage
ou 2,1; process vacuum
;turns on vacuum to remove large debris from surface being machined
;*****LIST OF VARIABLES*****
;V1 is rep rate of laser for channel ablation
;V4 is dummy counter
;V7 is feed rate for making channels
;V33 is dummy variable for vertical channel
;V36 is total length of channel
;V5 is dummy counter
;V17 is the number of loops for ablating channel in CHANNEL
;V7 is feed rate for CHANNEL
;V53 is dummy counter
;V72 is distance of double tee from waste reservoir
;V82 is length of injection plug
;***PROGRAM DESCRIPTION AND INPUT QUESTIONS***
me di "This program ablates a channel and double Tee."
;me di commands prints phrases in quotations to computer monitor
me di "The user is prompted for the length of the channel, the feed rate,"
me di "and the laser repetition rate, as well as the length of the injection"
me di "plug"
me di ""
me di ""
me di+V1 "What repetition rate should the laser be run for ablation?"
;for the Potomac System the laser may be run at 1 Hz, 10 Hz, 100 Hz, or 200
;Hz
me di+V17 "How many loops do you want to make to ablate column?"
me di "(even number)"
me di+V7 "What is the feed rate for making channels?"
;feed rate is the velocity at which the stage moves
me di+V36 "Please enter total length of channel in mm."
me di+V82 "What is length of injection plug? (microns)"

```

```

;injection plug length is the distance between the “arms” of the double tee
me di+V72 “What is distance of double tee from waste reservoir? (mm)”
me di+V76 “What is length of sample injection channel? (mm)”
me di+V78 “What is length of sample injection waste channel? (mm)”
;*****CALCULATIONS*****
V82=V82/1000; convert microns to mm
;*****PROGRAM*****
me di “Position joystick for 0,0. Channel ablates to left.”
SU :JOYSTICK
;SU denotes a subroutine
V53=1
SU :CHANNELLEFT
g1 xV72 y0
g1 x0 yV76
V33=V76
SU :VERTICALCHANNEL
g1 x0 y-V76
g1 x-V82 y0
V33=V78
SU :VERTICALCHANNEL
ou 2,0
ou 0,0
EXIT; end program
;***SUBROUTINE CHANNELLEFT***
:CHANNELLEFT
  V5=1
  psop,1,0,1,V1
  ;psop command defines the pulse train of the laser, V1 defines repetition
  psof,1
  ;psof command turns laser on (1) and off (2)
  LOOP V17
  g1 xV36 y0 fV7
  ;g1 is a positioning command with x and y denoting coordinates
  ;f is a velocity command
  g1 x-V36 y0 fV7
  wa on
  ;wa on is a pause until all previous commands are completed
  me di “PASS %V5 of %V17”
  V5=V5+1
  NEXT

```

```

    psof,0
RETURN
;*****END CHANNELLEFT*****
;*****SUBROUTINE VERTICALCHANNEL*****
:VERTICALCHANNEL
    V5=1
    psop,1,0,1,V1
    psof,1
    LOOP V17
    g1 x0 y-V33 fV7
    g1 x0 yV33 fV7
    wa on
    me di "PASS %V5 of %V17"
    V5=V5+1
    NEXT
    psof,0
RETURN
;*****END VERTICALCHANNEL*****
;*****SUBROUTINE JOYSTICK*****
:JOYSTICK
    sl x y; allows use of joystick
    wa on; wait on completion of command
    SU :SETASHOMEPOSITION
RETURN
;*****END JOYSTICK*****
;*****SUBROUTINE SETASHOMEPOSITION*****
:SETASHOMEPOSITION
    ;g1 x1 y3
    so po x y; set current x y position as software position
    so ho x y; set current x y position as software home
RETURN
;*****END SETASHOMEPOSITION*****

```

References

1. Soper, S. A., Ford, S. M., Qi, S., McCarley, R. L., Kelly, K., and Murphy, M. C. (2000) Polymeric microelectromechanical systems. *Anal. Chem.* **72**, 642A–651A.
2. Ford, S. M., Kar, B., Mcwhorter, S., et al. (1998) Microcapillary electrophoresis devices fabricated using polymeric substrates and X-ray lithography. *J. Microcolumn Sep.* **10**, 413–422.
3. Lowe, H. and Ehrfeld, W. (1999) State-of-the-art in microreaction technology: concepts, manufacturing and applications. *Electrochim. Acta* **44**, 3679–3689.

4. Lehr, H. and Ehrfeld, W. (1994) Advanced microstructure products by synchrotron-radiation lithography. *J. Phys. IV* **4**, 229–236.
5. Xu, J. D., Locascio, L. E., Gaitan, M., and Lee, C. S. (2000) Room-temperature imprinting method for plastic microchannel fabrication. *Anal. Chem.* **72**, 1930–1933.
6. Duffy, D. C., McDonald, J. C., Schueller, O. J. A., and Whitesides, G. M. (1998) Rapid prototyping of microfluidic systems in poly(dimethylsiloxane). *Anal. Chem.* **70**, 4974–4984.
7. Xia, Y. N. and Whitesides, G. M. (1998) Soft lithography. *Annu. Rev. Mater. Sci.* **28**, 153–184.
8. Zhao, X. M., Xia, Y. N., and Whitesides, G. M. (1997) Soft lithographic methods for nano-fabrication. *J. Mater. Chem.* **7**, 1069–1074.
9. Martynova, L., Locascio, L. E., Gaitan, M., Kramer, G. W., Christensen, R. G., and Maccrehan, W. A. (1997) Fabrication of plastic microfluid channels by imprinting methods. *Anal. Chem.* **69**, 4783–4789.
10. Roberts, M. A., Rossier, J. S., Bercier, P., and Girault, H. H. (1997) UV laser machined polymer substrates for the development of microdiagnostic systems. *Anal. Chem.* **69**, 2035–2042.
11. Lee, H. J., Fermin, D. J., Corn, R. M., and Girault, H. H. (1999) Marangoni flow in micro-channels. *Electrochem. Commun.* **1**, 190–193.
12. Rossier, J. S., Schwarz, A., Reymond, F., Ferrigno, R., Bianchi, F., and Girault, H. H. (1999) Microchannel networks for electrophoretic separations. *Electrophoresis* **20**, 727–731.
13. Emmony, D.C., Howson, R.P., and Willis, L. J. (1973) Laser mirror damage in germanium at 10.6 micrometers. *Appl. Phys. Lett.* **23**, 598–600.
14. Srinivasan, R. (1982) Action of far ultraviolet-radiation (185-nm) on poly(ethylene-terephthalate) films—a method for controlled dry-etching, *Polymer* **23**, 1863–1864.
15. Srinivasan, R. and Braren, B. (1989) Ultraviolet-laser ablation of organic polymers. *Chem. Rev.* **89**, 1303–1316.
16. Lippert, T., Nakamura, T., Niino, H., and Yabe, A. (1997) Laser induced chemical and physical modifications of polymer films: dependence on the irradiation wavelength. *Appl. Surf. Sci.* **110**, 227–231.
17. Lazare, S. and Drillhole, D. (1997) Submicrometre ablation on polymer surfaces. *J. Photochem. Photobiol. A* **106**, 15–20.
18. Waddell, E. A., Locascio, L. E., and Kramer, G. W. (2002) UV laser micromachining of polymers for microfluidic applications. *J. Assoc. Lab. Automat.* **7**, 78–82.

Reversible, Room Temperature Bonding of Glass Devices for Microfluidics

Loranelle L. Lockyear

Summary

This chapter describes a procedure for bonding glass microdevice substrates to their top plates by contact alone. This method results in devices that are robustly bonded but that can be separated, cleaned, and reused. For glass chips that have been used for applications involving the transport of hard particles, cells, or other biological material, reversible bonding provides a way of increasing the chip's lifetime and utility. Glass microdevices that are cleaned following this procedure can be successfully used many times for electrophoresis or pressure-driven applications.

Key Words: Room temperature bonding; reversible glass bonding; glass microdevices.

1. Introduction

Glass microchips are often designed so that there are many individual devices on a single piece of glass, the substrate. A second piece of glass, the top plate, is required to close the channels and to provide access holes. Usually, these two pieces of glass are cleaned, aligned with each other, bonded by contact, and then thermally bonded at high temperature. This chapter gives detailed instructions for reversibly bonding microfluidic chips made of thin glass. The substrate and top plate are contact bonded, but not thermally bonded.

Obviously, an etching or micromachining process is very cost-effective if several devices can be incorporated on a single substrate. If the devices are designed to trap or transport beads (1,2), cells (3,4), or other materials that can leave debris in the channel, a device can be easily plugged with the debris. If, after all the devices on a given chip have been used, the chip can be cleaned and reused, then the cost-effectiveness of the chip is increased. This is convenient when the debris blocks the channels after only a few uses, or when cross-contamination of biological samples precludes multiple uses of the same

device. For example, a glass chip containing 16 separate devices was used to study the electrokinetic movement of cells and beads in channels of various dimensions and with assorted barriers in the channels. After a single use, a given device was plugged and/or contaminated with cell debris or beads that had become trapped in the channels. If the chip had been thermally bonded, a maximum of 16 experiments could have been performed with a given chip before the chip would have needed to be discarded. The reversible bonding procedure enabled the repeated use of the chip (all 16 devices) over hundreds of experiments.

Because this bonding is reversible, there is no need to match the types of glass used, but the directions presented in this chapter were perfected for use with Corning 0211 glass (600 μm thick, and 3 or 4 in. on a side), available from Paragon Optical. Devices bonded by this procedure can be used for electrophoresis or pressure-driven flow without leaking (5).

2. Materials

2.1. Solutions and Reagents

1. Acid piranha solution: prepare by carefully adding 3 parts concentrated sulfuric acid to 1 part 30% hydrogen peroxide, by volume. Use caution and mix slowly. Warm the solution on a hot plate to reuse.
2. Isopropanol or acetone.
3. Detergent solution: dissolve one teaspoon of Sparkleen 1 powder (Fisher) in 1 L of water.

2.2. Equipment

1. *Optional*: Spin-Rinse Dryer (Semitool single stack or equivalent).
2. High-pressure washer (MicroAutomation 2066 or equivalent).
3. Wafer frame tape applicator and mounting station (ADT model 961 or equivalent).
4. At least one substrate and one top plate with access holes (*see Note 1*), although the method described herein is usually done in batches to save time.

3. Methods

All work with chip substrates before they are bonded to top plates should be done in a Class 100 clean facility (Class 10 preferred).

3.1. Procedure for New Chips

1. Place the substrate and top plate into a warm, but not boiling, acid piranha bath for at least 10 min (*see Note 2*).
2. Using plastic forceps, remove the substrate and top plate from the acid piranha and place in a Spin-Rinse Dryer holder (*see Note 3*).

3. Place the holder in the Spin-Rinse Dryer, run at default settings, and then remove the holder from Spin-Rinse Dryer.
4. Mount the substrate and top plate on separate wafer frames using ultraviolet (UV) tape. Before use, be sure that the wafer frames are clean. (Remove old pieces of tape, and use isopropanol or acetone on a Kimwipe to remove adhesive residue and particles from the wafer frames.) The substrate and top plate should be mounted on their wafer frames with the surfaces to be bonded facing out.
5. Using detergent solution and a soft sponge, wash the surface of the substrate for 2 min. Place in a high-pressure (HP) washer for three wash cycles, zero dry cycles.
6. Remove the wafer frame from the HP washer; wash the surface with a sponge again for 2 min. Place the wafer frame in the HP washer for five wash cycles, three dry cycles (turn on the drying lamp during the drying time).
7. Remove the wafer frame (with substrate) from the HP washer and place carefully in a holding rack for later use. Place the frame in a rack with the glass surface facing down, to prevent any particles from depositing before bonding. If any particles or water droplets should remain on the glass, the surface may be blown clean with a jet of nitrogen at high pressure.
8. Repeat **steps 6 and 7** for the top plate. Remove the wafer frame (with the top plate) from the HP washer and place on a clean work surface (glass surface facing up).
9. Place an additional wafer frame on top, to use as a spacer. (Again, be sure to clean the wafer frame with isopropanol or acetone first, to remove particles.) Remove the substrate on the wafer frame from the holding rack and position it on top of the stack with the exposed glass surface facing down (*see Fig. 1*).
10. Carefully pick up the stack and hold it up to the light, so that the channels can be seen. Once the channel ends are lined up with the access holes in the top plate, carefully put the stack back down on the work surface. Starting at one corner of the glass, press the two pieces together across the diagonal to contact bond them.
11. If one has been very diligent in cleaning the glass, there should be no, or very few, Newton rings (rainbow-colored rings around dust particles or rough glass areas). Newton rings on channels will cause liquid to leak in between the glass plates in these room temperature–bonded chips. If there are several Newton rings, and they cross channels, remove the glass pieces from the UV tape (*see Note 4*) and start over at **step 4**. If the Newton rings are centered around the access holes on the top plate, the holes are poorly drilled and a different top plate should be used, if possible.

3.2. Procedure for Previously Used Chips

1. Remove all reservoirs from the top surface of the top plate. If the reservoirs were attached with epoxy, scrape off as much of the epoxy as possible. Clean the top plate with methanol on a Kimwipe to remove any residue.
2. Take the lid from a plastic Petri dish and fill it about halfway with water. Place the chip in the water-filled dish. Using a spatula or knife blade at the corner of the chip, carefully pry the two glass pieces apart. Water will quickly get between the

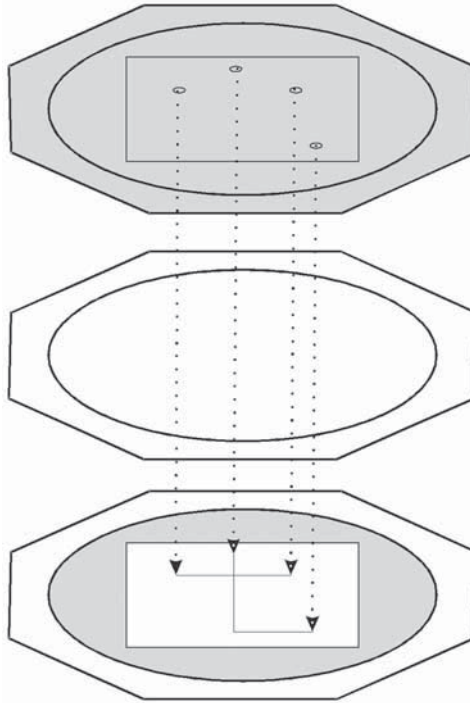


Fig. 1. Illustration of glass plates mounted on wafer frames. An additional, clean wafer frame is used as a spacer to keep the glass plates apart until they are pressed together at the corner. The gray shading represents the mounting tape used to secure the glass to the wafer frame.

plates, and the two pieces will come apart very easily. If the top plate is good (i.e., no rough holes, cracks, and so on), it can be used again (*see Note 5*).

3. Place the substrate on a wafer frame using UV tape, then into the HP washer for five wash cycles, zero dry cycles.
4. Remove the wafer frame from the HP washer; use detergent solution and a soft sponge to wash the surface of the substrate for 2 min. Place in the HP washer for five wash cycles, zero dry cycles. The purpose of these steps is to try to remove as many particles as possible from the surface of the substrate.
5. Remove the substrate from the wafer frame.
6. Perform all steps in **Subheading 3.1**.

4. Notes

1. Here, the substrate is the piece of glass with channels etched in it; the substrate may also have drilled access holes. The top plate is used to close the channels and

- may or may not have drilled access holes, depending on whether the substrate itself is drilled.
2. Prepare the acid piranha solution in a beaker whose diameter is slightly larger than the width of the glass plates. Plates can be kept from sticking together by placing glass Pasteur pipets or stirring rods between the plates.
 3. Use of the Spin-Rinse Dryer is not required. If a Spin-Rinse Dryer is not available, replace **steps 2 and 3 in Subheading 3.1.** with the following: use plastic forceps to remove the substrate and top plate from the acid piranha solution and place them in a clean beaker of ultrapure water, again separating the plates with glass Pasteur pipets or stirring rods. When ready to proceed with **step 4 in Subheading 3.1.** blow each plate dry with nitrogen at high pressure before attempting to place on the wafer frame.
 4. The glass pieces can be separated in one of two ways: carefully pull up on the corners of the wafer frames one at a time until the pieces of UV tape pop apart. Note that this is an easy way to break one or both pieces of glass. Alternatively, cut the UV tape away from the wafer frames and remove the glass sandwich from the tape. Then, follow **step 2 in Subheading 3.2.**, and start over at **step 4 in Subheading 3.1.**
 5. **Steps 3–5 in Subheading 3.2.** may be omitted if the chip has never contained beads or other hard particles.

Acknowledgment

Special thanks go to D. Jed Harrison, in whose laboratories these procedures were performed and perfected.

References

1. Verpoorte, E. (2003) Beads and chips: new recipes for analysis. *Lab Chip* **3**, 60N–68N.
2. Jemere, A. B., Oleschuk, R. D., Ouchen, F., Fajuyigbe, F., and Harrison, D. J. (2002) An integrated solid-phase extraction system for sub-picomolar detection. *Electrophoresis* **23**, 3537–3544.
3. Li, P. C. H., de Camprieu, L., Cai, J., and Sangar, M. (2004) Transport, retention, and fluorescent measurement of single biological cells studied in microfluidic chips. *Lab Chip* **4**, 174–180.
4. Li, P. C. H. and Harrison, D.J. (1997) Transport, manipulation, and reaction of biological cells on-chip using electrokinetic effects. *Anal. Chem.* **69**, 1564–1568.
5. Chiem, N., Lockyear-Shultz, L., Andersson, P., Skinner, C., and Harrison, D. J. (2000) Room temperature bonding of micromachined glass devices for capillary electrophoresis. *Sens. Actuators B* **63**, 147–152.

II

BIOLOGICAL APPLICATIONS

Solid-Phase Extraction in Packed Beds on Glass Microdevices

Loranelle L. Lockyear

Summary

This chapter provides a detailed description of a network of channels that includes a chamber for trapping beads in a microfluidic device. Instructions are included for the packing and use of the bead bed for solid-phase extraction (SPE). The SPE procedure may be used, e.g., as a filter to clean up a dirty sample prior to analysis, or as a means of pre-concentration for a dilute sample. Once the bead bed is in place, it may be used multiple times without sample breakthrough.

Key Words: Solid-phase extraction; preconcentration, packed column; glass microdevices; beads; microfluidics.

1. Introduction

Microfluidic methods of analysis have gained popularity partly because they require small sample and reagent volumes, and because they can provide data in a very short analysis time. The “lab-on-a-chip” concept has, at its core, the idea of incorporating multiple sample-handling steps on a single microfluidic device. Since the inception of the lab-on-a-chip concept, many researchers have perfected various parts of the micro-total analysis system (μ -TAS). These individual pieces of the μ -TAS have included, e.g., injectors, separation channels, pre- and postcolumn reactors, and detectors, most of which are integrated within the channel design on the chip. Recently, small beads (micrometer scale) have been employed on microchips to enhance further the capability of the μ -TAS (*1*).

Beads (or microspheres) can be employed for many purposes on a microchip. In the context of biological applications, beads have been used on-chip for protein digestion (*2,3*), determination of enzyme substrates (*2,4*), immunoassay (*5–7*), and many other examples (*1*), including highly sensitive analyte

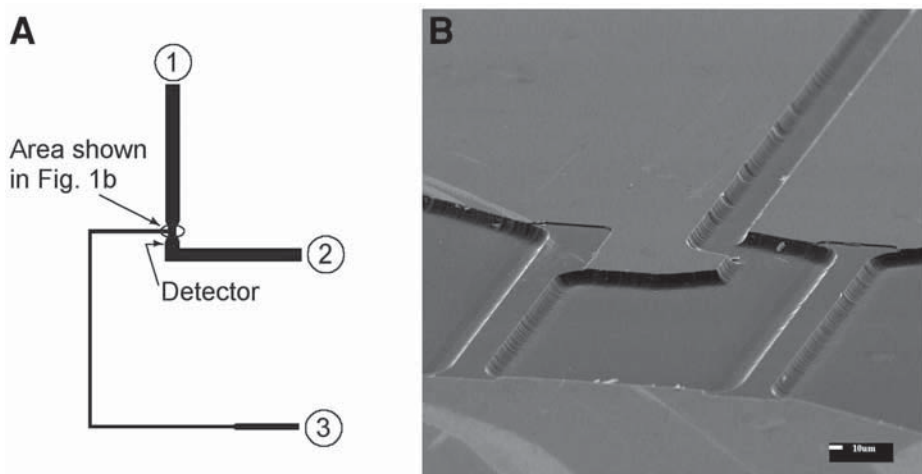


Fig 1. (A) Microfluidic device used for solid phase extraction, and (B) scanning electron microscope image showing detail of chamber in which beads are trapped. The channel reservoirs are numbered to match the description in the text. Reservoir 3 is the bead inlet channel and is used only to prepare the packed bed. (Reprinted with permission from **ref. 8**. Copyright 2000 American Chemical Society.)

preconcentration by immunoaffinity chromatography and solid-phase extraction (SPE) (8–11).

This chapter is intended to provide an introduction to the use of beads retained in a chamber on-chip, by describing how to quickly obtain easily observable SPE data. SPE is commonly used to remove contaminants and/or to concentrate compounds of interest prior to analysis. In the case described here, reverse-phase packing material, normally used for packing liquid chromatography columns, comprises the beads used for this integrated SPE chamber. **Figure 1** shows the device and an image of the chamber used to trap the SPE beads. The weirs are etched to be only $1\ \mu\text{m}$ from the cover plate, whereas the other channels are etched to a depth of $10\ \mu\text{m}$. This configuration provides the cavity that contains the beads. **Figure 2** is a drawing of the cross-section of the bead chamber. The beads are electrokinetically loaded via a side channel and locked in place by changing solution conditions. The sample solution is electrokinetically driven through the bead bed for a given period of time, during which the analyte is preferentially bound to the beads. After a wash step to remove any remaining sample from the incoming channel, the solvent conditions are changed to allow the beads to release the bound analyte from the bed. The analyte is then detected as a narrow, concentrated band as it exits the bead chamber.

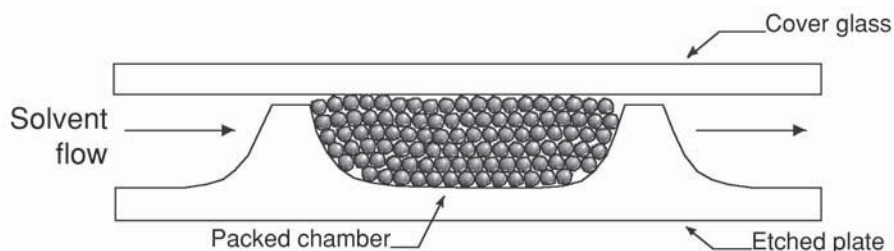


Fig 2. Cross-sectional view of packed bead chamber, perpendicular to main channel used for introducing sample during preconcentration. Weir height allows solvent to flow through the bed, but the beads cannot escape the chamber via the main channel. (Reprinted with permission from ref. 8. Copyright 2000 American Chemical Society.)

Once comfortable with the SPE technique, the user can experiment with other analytes that can be preconcentrated with reverse-phase beads, such as amino acids labeled with fluorescent tags (10). Alternatively, the user can make use of different types of beads, including those functionalized with enzymes (4), protein A (11), or antibodies (6,7), to perform similar work on systems of greater interest and usefulness in biological applications.

2. Materials

2.1. Solutions and Reagents

1. Detergent solution: dissolve one teaspoon of Sparkleen 1 powder (Fisher) in 1 L of water.
2. Methanol, reagent grade.
3. Acetone, semiconductor grade.
4. Access to nitrogen at high pressure.
5. Acid piranha solution: prepare by carefully adding three parts concentrated sulfuric acid to one part 30% hydrogen peroxide, by volume. Use caution and mix slowly.
6. Positive photoresist: Waycoat HPR 504 (Olin Hunt Specialty Products).
7. Photoresist developer: Microposit 354 (Shipley).
8. Aqua regia: prepare by carefully adding one part concentrated HNO_3 to three parts concentrated HCl , by volume. Use caution and mix slowly.
9. Chromium etch solution (Cyantek Cr-7S or equivalent).
10. Concentrated $\text{HF}/\text{HNO}_3/\text{H}_2\text{O}$ (20:14:66 by volume).
11. Dexter Epoxi Patch (EPK-1C) epoxy kit.
12. Acetonitrile, high-performance liquid chromatography (HPLC) grade, filtered through a 0.45- μm Nylon-6,6 filter.
13. 50 mM Ammonium acetate buffer (pH 8.5), prepared by combining 4.03 g of ammonium acetate and 3.38 mL of ammonium hydroxide in 1.0 L of ultrapure water.

14. Mixed acetonitrile/buffer solution, prepared by combining equal volumes of filtered acetonitrile and 50 mM ammonium acetate buffer.
15. BODIPY 493/503 (product no. D-3922; Molecular Probes, Eugene, OR). Store the solid reagent in a -20°C freezer and protect from light. Prepare a stock solution (approx 0.38 mM) by dissolving 10 mg of BODIPY in 100 mL of HPLC-grade methanol. (This solution will be saturated; that is, the BODIPY will probably not completely dissolve.) Dilute this stock solution as follows: 26.3 μL of stock in 10.0 mL of ammonium acetate buffer, then 10.0 μL of this solution diluted in 10.0 mL of ammonium acetate buffer to give the desired approx 1.0 nM solution. Refrigerate and protect all BODIPY solutions from light. (It is sufficient to cover the flask or vial with aluminum foil.) If the BODIPY solutions are refrigerated, they will remain stable for several weeks. Allow solutions to come to room temperature before use.
16. Reverse-phase chromatographic beads: Spherisorb ODS1 (3- μm particle diameter, product no. PSS820034; Waters), prepared as a 2-mg/mL slurry in filtered HPLC-grade acetonitrile. The slurry itself is not to be filtered.

2.2. Instrumentation

2.2.1. Chip Design and Fabrication

Figure 3 shows the device used for SPE on-chip; it has been enlarged to show detail but is not drawn to scale. Several such devices may be fabricated on a 3×3 in. (or 4×4 in.) plate of glass. Directions for fabricating the device are given in **Subheading 3.1**.

1. Computer with installed computer-aided design (CAD) program, such as AutoCAD (Autodesk) or L-Edit (Tanner Research).
2. Corning 0211 glass plates (3×3 in. or 4×4 in.), 600 μm thick (Paragon Optical).
3. Ultrasonic cleaning bath.
4. Physical vapor deposition system (Lesker CMS-18 or equivalent).
5. Photoresist coater-developer (Solitec Model 4110 or equivalent).
6. Photoresist convection oven(s) (Fisher cat. no. 13-247-725 or equivalent).
7. Contact mask aligner (Quintel Q-6000 Ultraline or equivalent).
8. Clean-room microscope (Leitz Ergolux or equivalent).
9. Profilometer (Tencor Alpha-Step 500 or equivalent).
10. Programmable electric muffle furnace (Ney model 6-525 or equivalent).
11. Aluminum oxide (Al_2O_3) ceramic plate(s), such as Coors Superstrate (*see Note 1*).

2.2.2. Chip Operation

1. Optical table (Newport or equivalent) connected to earth ground.
2. Uniphase Model 2011 (or equivalent) argon ion laser (488 nm) operated at 4.0 mW.
3. Focusing lens(es), as required to focus the laser spot on the channel (Melles Griot or equivalent). In this work, rather large channels are used, and the laser is easily focused within their confines.

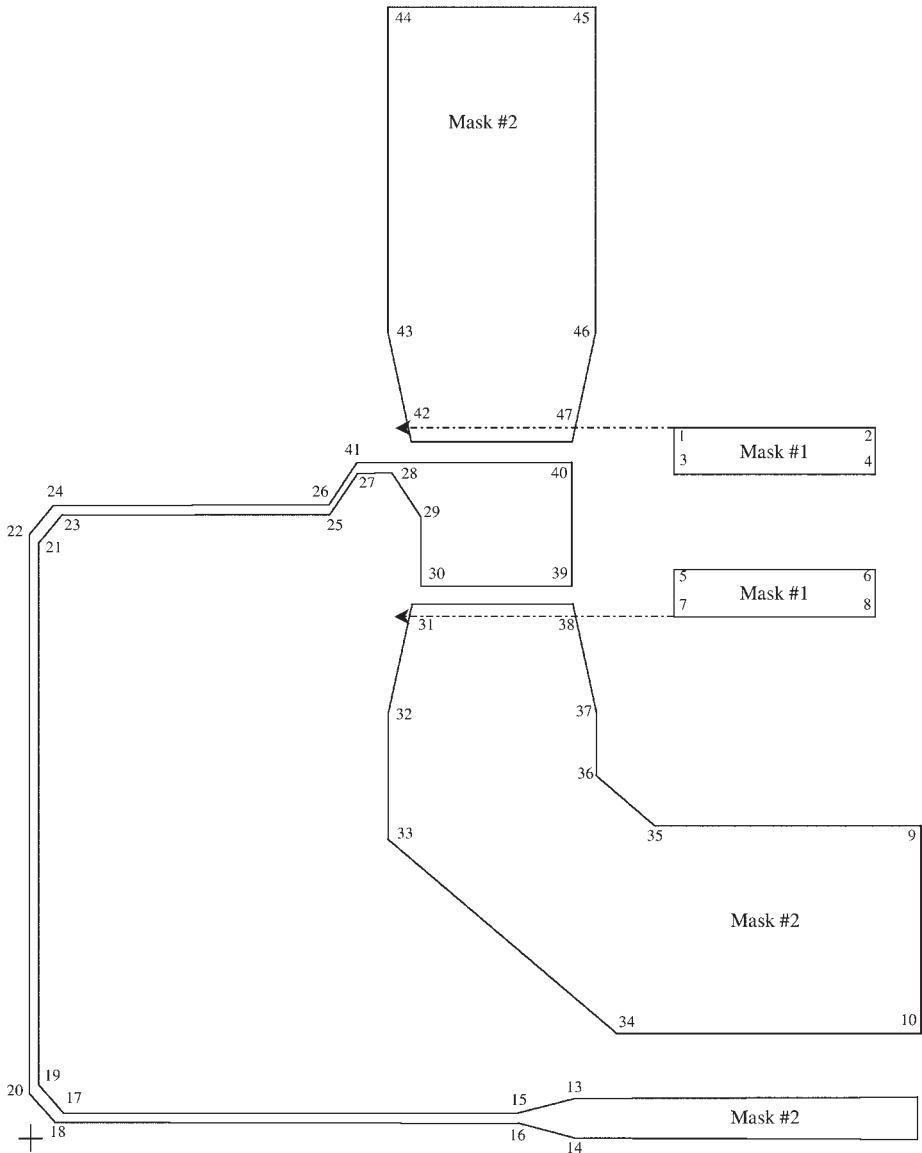


Fig. 3. Drawing of device (not to scale) showing design of mask features for the two masks required. The cross at the bottom left is the origin, and each corner is given a number that corresponds to the coordinates listed in [Table 1](#) relative to the origin. The dotted lines show where the mask no. 1 features will appear overlaid on the mask no. 2 features.

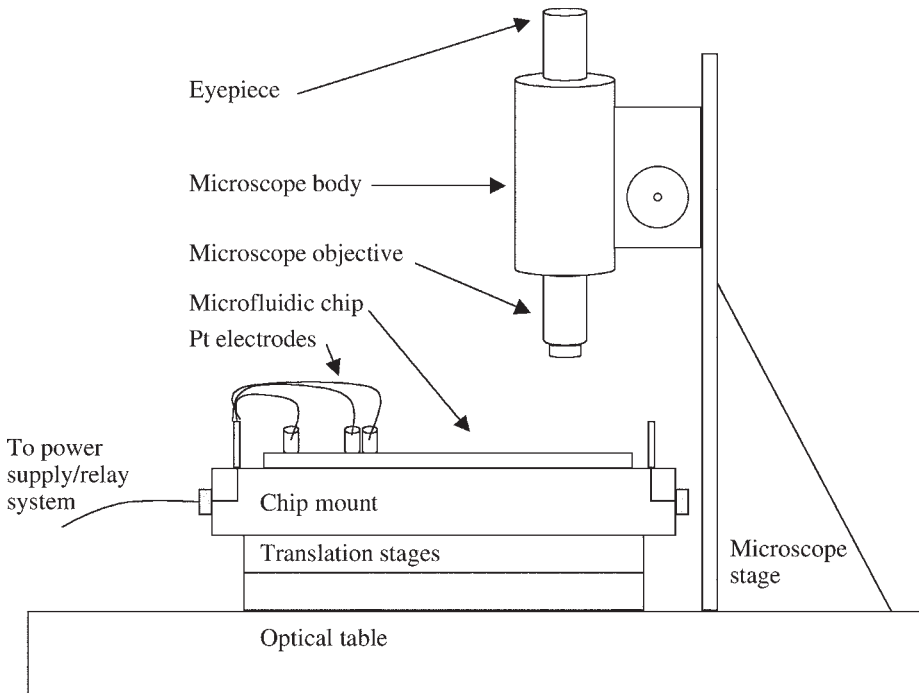


Fig. 4. Possible design for assembly of parts 4–7 in **Subheading 2.2.2**. (not drawn to scale).

4. Translation stages (nominally two stages) with manual actuators for x - and y -positioning of the chip (Newport 433 or equivalent).
5. Chip mount to be attached to top translation stage (see Fig. 4 for arrangement of parts 4–7). The chip mount design should keep the top surface of the chip free for the incoming laser beam and the detection path and provide a way to deliver voltage to the reservoirs (see Note 2).
6. Leitz Wetzlar 25 \times , 0.35-NA microscope objective on a Melles Griot microscope body. The microscope body is attached to a stage that is screwed to the optical table for stability.
7. Microscope eyepiece (Melles Griot or equivalent).
8. 530-nm Emission filter (Melles Griot or equivalent).
9. Photomultiplier tube (PMT) housing equipped with a Hamamatsu R1477 PMT, socket, and power supply.
10. Electronic filter for PMT signal: Krohn-Hite Model 3342 six-pole 25-Hz Butterworth filter.
11. High-voltage power supplies and relay system, as shown in Fig. 5.

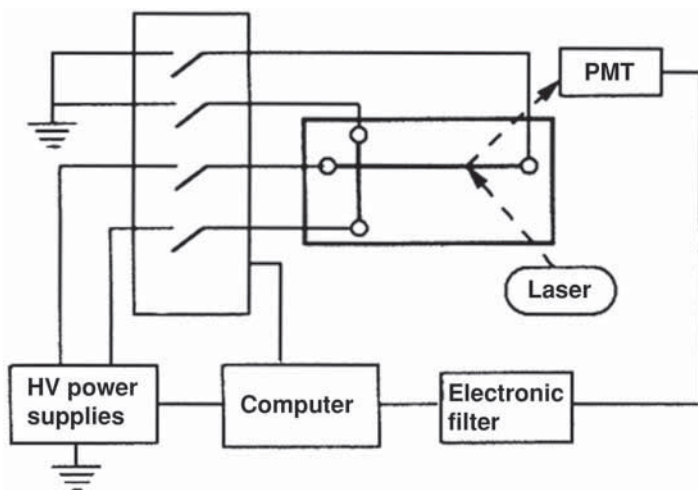


Fig. 5. Power supply and relay system used for computer control of electroosmotic flow within microfluidic device and for data acquisition of laser-induced fluorescence signal. HV, high-voltage. (Adapted and reprinted with permission from **ref. 12**. Copyright 1994 American Chemical Society.)

12. PC with LabVIEW (or equivalent) program for running a high-voltage power supply/relay system and collecting PMT signal. PMT signal should be sampled at a frequency of 50 Hz.

3. Methods

3.1. Device Fabrication

All chips are fabricated in Corning 0211 glass using conventional wet chemical etching as described in this section. To prepare the device, two photomasks are required: one to etch the tops of the weirs to a depth of 1 μm , and the other to etch the channels to a depth of 10 μm (*see Note 3*).

1. Using a CAD program, e.g., AutoCAD or L-Edit, lay out the design of the chip. The device layout is shown in **Fig. 3**, and dimensions for a single device are given in **Table 1** (*see Note 4*). Each device is rather small, so several such devices can and should be produced on each 3 \times 3-in (or 4 \times 4 in.) piece of glass (*see Note 5*).
2. Once the mask is designed, send the file to a mask manufacturer to have a master produced (*see Note 6*).
3. Place Corning 0211 glass plates in a large beaker, wafer holder, or other suitable container, and separate the plates with glass or plastic spacers. Fill the container with Sparkleen detergent solution (enough to cover the glass plates completely),

Table 1
Coordinates to Be Used for Drawing Masks of Device Shown in Fig. 3
Relative to Origin in Bottom Left Corner of Fig. 3

No.	x-Coordinate (μm)	y-Coordinate (μm)
1	4120	10,275
2	4400	10,275
3	4120	10,215
4	4400	10,215
5	4120	10,045
6	4400	10,045
7	4120	9985
8	4400	9985
9	10,720	8655
10	10,720	8095
11	10,715	200
12	10,715	0
13	7710	200
14	7710	0
15	7510	105
16	7510	95
17	20	105
18	10	95
19	10	115
20	0	105
21	10	10,115
22	0	10,125
23	20	10,125
24	10	10,135
25	4120	10,125
26	4120	10,135
27	4140	10,165
28	4190	10,165
29	4210	10,115
30	4210	10,045
31	4140	9985
32	3980	9585
33	3980	8655
34	4540	8095
35	5100	8655
36	4540	9215
37	4540	9585

(continued)

Table 1 (Continued)

No.	x-Coordinate (μm)	y-Coordinate (μm)
38	4380	9985
39	4380	10,045
40	4380	10,216
41	4140	10,216
42	4140	10,275
43	3980	10,675
44	3980	17,545
45	4540	17,545
46	4540	10,675
47	4380	10,275

and place in an ultrasonic cleaning bath for 3–5 min.

4. Replace the detergent solution with reagent-grade methanol, and clean in the ultrasonic bath again for 3–5 min.
5. Repeat **step 4** using semiconductor-grade acetone and then deionized water.
6. Dry the plates with nitrogen at high pressure.
7. Vapor deposit a metal layer under vacuum (below 10^{-6} torr) on the surface of the glass. The metal layer must nominally be comprised of 200 Å of chromium and 1000 Å of gold.
8. Submerge the glass plates in warm, but not boiling, acid piranha solution to remove trace organics, and rinse with deionized water.
9. Spin coat a 1.4- μm -thick layer of positive photoresist (Waycoat HPR 504) on the metal surface using a photoresist coater-developer at 3500 rpm.
10. Bake at 110°C for 5 min. This will provide the surface shown in the cross-section in **Fig. 6A**.
11. Using a contact mask aligner, position master mask no. 1 (*see Note 7*) on the surface of the photoresist, and expose the photoresist using ultraviolet light (*see Fig. 6B*).
12. Apply Microposit 354 to develop the photoresist. This will provide the definition of the mask features, as shown in **Fig. 6C**.
13. Bake at 120°C for 5 min to harden the remaining photoresist.
14. Etch the metal layer with aqua regia and Cr etch to achieve the metal etch (*see Fig. 6D*). This will leave exposed glass in the desired pattern.
15. Etch the glass in a slowly stirred mixture of concentrated HF/HNO₃/H₂O (20:14:66) for the amount of time needed to achieve the desired channel depth, as in **Fig. 6E**. Corning 0211 etches at a rate of approx 1 μm in 10 s. The etch rate can be confirmed through the use of a profilometer after fixed etch times (*see Note 8*). After the etch time, immediately immerse the substrate in, or rinse the surface with, clean deionized water.

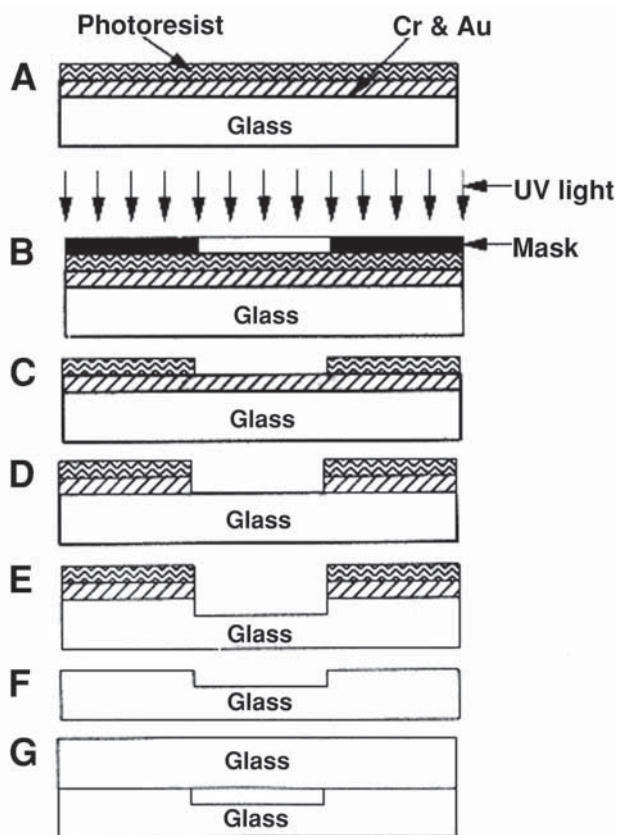


Fig. 6. Stepwise illustration of wet chemical etch process. (A) Glass substrate with a chrome-gold layer and photoresist coating is shown. (B) Exposure of the photoresist through the mask master is shown. (C) After the photoresist has been developed, mask features are defined on the chrome-gold layer. (D) The metal layer has been etched in the desired pattern, leaving glass exposed in this pattern. (E) The glass has been etched to the proper depth. (F) The photoresist and metal layers have been removed. (G) A cover plate has been bonded to the etched plate to yield a network of closed channels. (Reprinted with permission from **ref. 12**. Copyright 1994 American Chemical Society.)

16. Remove the remaining photoresist with Microposit 354. Also remove the remaining metal from the surface using the aqua regia and Cr etch from **step 14**. Rinse well with deionized water, and blow the surface dry with nitrogen at high pressure. This will result in an etched glass substrate, such as that shown in **Fig. 6F**.
17. Inspect the etched features under a microscope to ensure that they are smooth. Also use a profilometer to confirm that the features are the proper dimensions.

Table 2
Heating Program for Bonding Corning 0211 Glass Chips

Stage	Rate (°C/min)	Temp (°C)	Time (h)
1	10	440	0.5
2	2	473	0.5
3	2	592	6.0
4	4	473	0.5

18. Repeat **steps 7–17** this time using master mask no. 2, to etch the channels.
19. Clean and bond the substrate to a drilled cover plate to achieve the closed chip, as in **Fig. 6G**. Cleaning and contact bonding may be achieved as described in Chapter 6. If a permanently bonded chip is *not* desired, skip to **step 22** in this section.
20. If a permanent bond (between substrate and cover plate) is desired, place inside the programmable muffle furnace the contact-bonded chip on a flat Al₂O₃ ceramic plate with the white side facing up. Be sure that the furnace door is closed.
21. Enter the heating program as follows:
 - a. Press the Temp/Cycle Time button.
 - b. Press the Stage button. Enter 1.
 - c. After Rate, enter 10 (°C/min).
 - d. After Temp, enter 440 (°C).
 - e. After Time, enter 0.5 (h).
 - f. Repeat **steps b–e** for Stages 2–4 entering the parameters from **Table 2**.
 - g. Check the program by pressing the Temp/Cycle Time button again, followed by the Stage button. Press 1 for the first stage of the program, and simply press Enter if the rate, temperature, and time are correct for that stage. (If not, just enter the correct number.) Repeat this for all stages of the program.
 - h. After the program has been checked for accuracy, press the Start button.
 - i. Allow the furnace to cool to nearly room temperature before opening the door. When the furnace temperature has reached between 80 and 100°C, the furnace door can be opened slightly to speed cooling to room temperature.
 - j. Inspect the cooled chip carefully for areas that did not bond properly. If any nonbonded areas cross a channel, the thermal bonding will have to be repeated, with small metal weights placed over the channel where the bonding was ineffective.
22. Cut plastic pipet tips, plastic tubing, or glass tubing to the desired size for reservoirs, and attach them with Epoxi Patch to the cover plate, centered over the access holes. Allow the epoxy to cure at room temperature for 24 h before use (see **Note 9**).

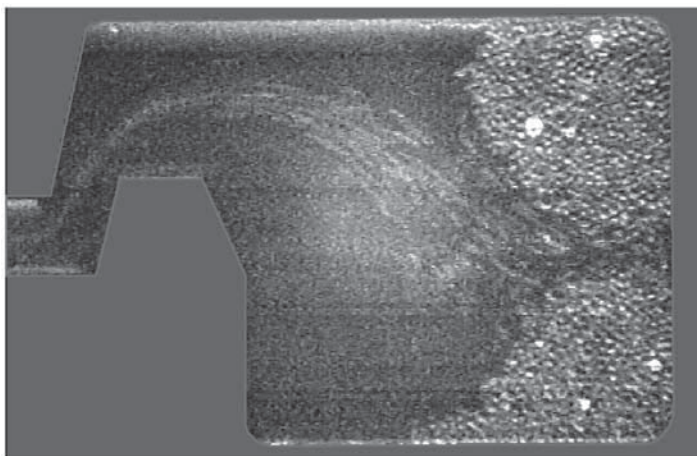


Fig. 7. Photograph of beads entering chamber via electroosmotic flow. The background surrounding the chamber has been colored to provide contrast. (Reprinted with permission from ref. 8. Copyright 2000 American Chemical Society.)

3.2. Preparation of Extraction Bed

All solutions to be used on-chip other than the bead slurry are delivered by sterile syringes and needles, and are filtered through a 0.2- μm -pore-size cellulose acetate syringe filter.

1. Install the eyepiece in the microscope body above the chip mount. Align the chip under the microscope objective so that the bead chamber is visible (*see Note 10*).
2. Fill all reservoirs with acetonitrile (*see Note 11*), and check to be sure that no air is trapped in any channels (*see Note 12*).
3. Replace acetonitrile in reservoir 3 with bead slurry; *see Fig.1* for reservoir numbers.
4. Insert electrodes in the reservoirs.
5. Apply positive high voltage at reservoir 3 starting with 200 V with reservoirs 1 and 2 grounded.
6. Slowly ramp up the voltage at reservoir 3 from 200 to 800 V by increasing by 100 V every 30–60 s. Beads should begin entering the chamber at voltages ranging between 600 and 800 V (*see Note 13*), as shown in **Fig. 7**.
7. After the bed is completely packed, ramp the voltage down to 100–200 V for the last 30 s. Now a sizeable portion of the bead introduction channel should also be filled with beads. Cease application of voltage, and ensure that the bed is intact.
8. Carefully remove the slurry from reservoir 3, and replace it with acetonitrile (*see Note 14*). Remove the acetonitrile from reservoirs 1 and 2, and replace it with the mixed acetonitrile/buffer solution.

9. Apply positive high voltage at reservoir 1, starting at 200 V, with reservoir 2 grounded, and reservoir 3 biased at +400 V.
10. Ramp up the voltage at reservoir 1 from 200 to 800 V by increasing by 100 V every 30 s.
11. After 2–5 min at 800 V, ramp down the voltage as in **step 7**.
12. Replace the mixed acetonitrile/buffer solution in reservoirs 1 and 2 with the pH 8.5 ammonium acetate buffer, and repeat **steps 9–11** (see **Note 15**).

3.3. Solid-Phase Extraction On-Chip

1. To visualize the steps involved with preconcentration, simply observe the bead bed through the eyepiece (see **Note 10**). To record the fluorescence of the BODIPY before and after concentration, leave the eyepiece in place. Watching through the eyepiece, move the chip toward reservoir 2 so that the bead bed is just out of sight. Carefully remove the eyepiece, and replace it with the emission filter and PMT assembly (see **Subheading 2.2.2.**, **items 8–10**).
2. To conduct a blank run, place ammonium acetate buffer in reservoirs 1 and 2. Leave acetonitrile in reservoir 3 throughout the experiment, replenishing as needed.
3. If recording with PMT, start data collection, and immediately apply +200 V to reservoir 2 with reservoir 1 grounded for 60 s. Reservoir 3 should be floating (not grounded, and no voltage applied). This step simply provides a background, which may be subtracted from subsequent run data to yield a smoother baseline.
4. To load the sample, place 1 nM BODIPY solution in reservoir 2 with buffer in reservoir 1 and acetonitrile in reservoir 3.
5. If recording with a PMT, start data collection, and immediately apply +200 V for 90 s to reservoir 2 with reservoir 1 grounded and reservoir 3 floating. This step will result in the concentration of BODIPY on the first few layers of beads, as shown in **Fig. 8**. The fluorescence intensity recorded here will correspond to the fluorescence of the 1 nM BODIPY solution. Although it will have the appearance of a baseline signal, its intensity should increase slightly when the BODIPY enters the vicinity of the bead bed, as shown in the “sample load” signal in **Fig. 9**.
6. To flush the sample channel, replace the 1 nM BODIPY solution in reservoir 2 with ammonium acetate sample channel. (Reservoir 2 should still contain buffer, and reservoir 3 acetonitrile.)
7. Apply +200 V to reservoir 2 with reservoir 1 grounded and reservoir 3 floating for 60 s. The purpose of this step is to wash any remaining BODIPY from the channel onto the bead bed. If recording, one should be able to see a small reduction in the fluorescence intensity when the BODIPY in the channel has been replaced with buffer, as in the “buffer flush” signal in **Fig. 9**.
8. To perform elution, place acetonitrile in all reservoirs. If recording with a PMT, start data collection, and immediately apply +500 V to reservoir 1 with reservoir 2 grounded and reservoir 3 floating. This step will cause the band of BODIPY to be released from the beads; the band should be moving back toward reservoir 2

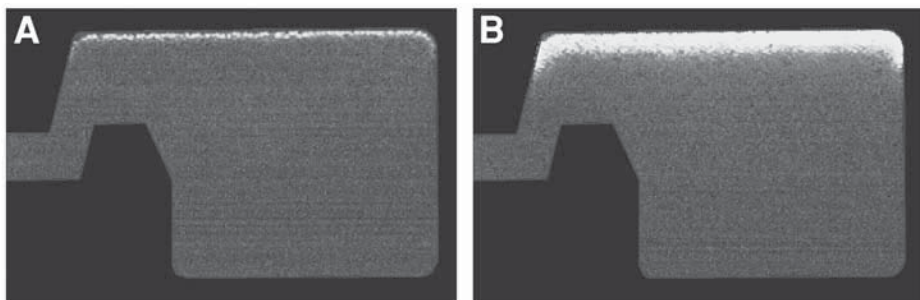


Fig. 8. Photographs of fluorescence of BODIPY on first few layers of beads deposited after (A) 1 min and (B) 2 min of pre-concentration. The background surrounding the chamber has been colored to provide contrast. (Reprinted with permission from *ref. 8*. Copyright 2000 American Chemical Society.)

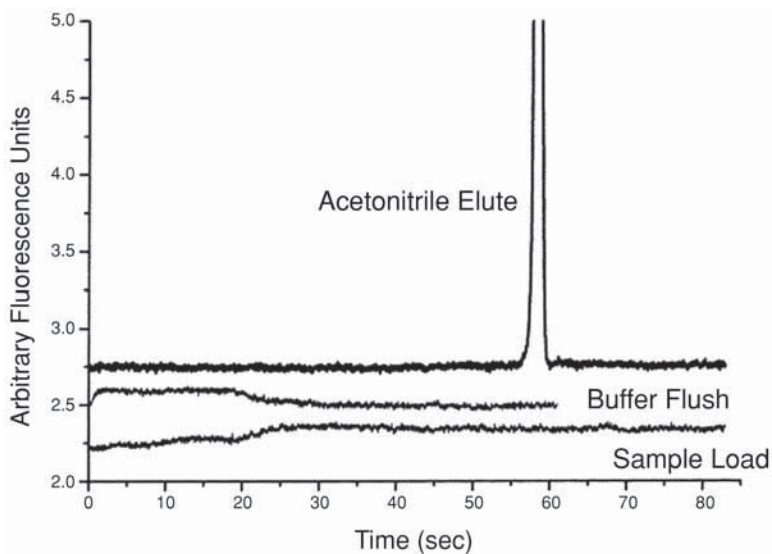


Fig. 9. Three traces of fluorescence signal: one as BODIPY approaches bead channel (sample load), one during channel-washing step (buffer flush), and one as concentrated BODIPY is removed from the SPE bed (acetonitrile elute). Traces have been offset vertically to distinguish each trace from the others. (Reprinted with permission from *ref. 8*. Copyright 2000 American Chemical Society.)

now. The PMT signal should show the BODIPY band as a narrow peak, as in the “acetonitrile elute” signal in **Fig. 9**.

9. To perform reequilibration, place ammonium acetate buffer in reservoirs 1 and 2 with acetonitrile remaining in reservoir 3.
10. Apply +500 V to reservoir 2 with reservoir 1 grounded and reservoir 3 floating. Ramp the voltage down from +500 to +200 V over the course of 2 to 3 min. This will reequilibrate the bead bed with buffer, in preparation for another preconcentration experiment.
11. To repeat this experiment, start over at **step 3**.

4. Notes

1. These plates must be extremely flat to prevent deformation of glass during bonding.
2. A Plexiglas chip mount can be homemade with banana plugs on each end, for supplying high voltage. The banana plugs should be soldered to smaller plugs at the top of the chip mount. These smaller plugs are used to attach light-gage Pt wires (all but the ends covered with insulating plastic tubing) to the power supplies. These Pt wires are used as the electrodes in the chip reservoirs.
3. All fabrication steps that involve manipulation, cleaning, and etching of the glass plates should be performed in a class 100 clean-room environment.
4. All voltages and times given in later sections assume the use of the exact channel dimensions given here.
5. Be sure to include marks in the masks that will assist with mask alignment. Because two masks are involved in this process, it is imperative that they both be properly aligned.
6. Determine whether the mask fabrication facility uses a positive or negative photoresist. If negative, the drawn features in the design file will correspond to the channels desired. If positive, the drawn features in the design file will correspond to everything except the channels desired (the channels would come out instead as raised features in the final product). The mask manufacturer can reverse the image, but it will cost more, take longer, and may result in errors in mask fabrication. It is advisable to reverse the image oneself, before sending it off for mask fabrication.
7. **Steps 7–17** will be followed twice: first with mask no. 1, which defines only the weirs, and then with mask no. 2, which defines the channels.
8. Because glass is etched isotropically, it will etch in the x and y (horizontal) directions at the same rate that it etches in the z (vertical) direction. The channel width will be equal to $(2 \times \text{etch depth}) + \text{mask width}$. If a channel is $10 \mu\text{m}$ wide in the original mask and is etched $10 \mu\text{m}$ deep, it will be $30 \mu\text{m}$ across ($2 \times 10\text{-}\mu\text{m}$ etch depth + $10\text{-}\mu\text{m}$ mask width). Similarly, a $30\text{-}\mu\text{m}$ -wide mask feature etched $10 \mu\text{m}$ deep will result in a $50\text{-}\mu\text{m}$ -wide channel. The metal layer is also undercut by the etching of the glass (i.e., the glass is etched out from under the metal layer). Thus, channels etched in glass have curved sides and a flat bottom, as shown in **Fig. 10**.

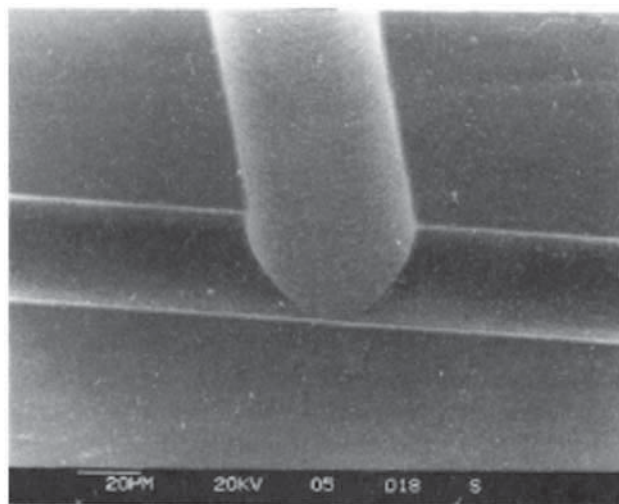


Fig. 10. Electron micrograph of a channel intersection showing the geometry of an etched glass channel. (Reprinted with permission from **ref. 12**. Copyright 1994 American Chemical Society.)

9. After reservoirs are attached, place the chip in a plastic Petri dish (with a lid) for storage, to keep particles from entering the channels when not in use.
10. The eyepiece should be employed to monitor visually the bead chamber as it is packed and locked in place, or during preconcentration experiments. Alternatively, the eyepiece may be replaced with a small charge-coupled device video camera connected to a video screen and recorder.
11. Do not treat channels with aqueous reagents prior to use. Only fill with acetonitrile (or whatever organic packing solvent is used) to avoid entrapped air.
12. If air is trapped in a channel, use a vacuum to pull solution through one reservoir. Once all the trapped air has been removed, refill the reservoirs with solutions to keep air from reentering the channels.
13. Devices can be packed by applying a vacuum to reservoirs 1 or 2 (or both), but the packing is not as complete or as uniform as when voltage is used for packing. If the application of voltage results in incomplete packing, it may be followed up with a vacuum applied at reservoirs 1 or 2 (or both). The combination of voltage and vacuum used for packing the chamber will depend on individual device characteristics. The user should be prepared to employ either or both to achieve a completely packed bed.
14. Empty and refill each reservoir in turn starting with reservoir 3. Take care not to remove so much solution from the reservoir that the bead bed is disturbed or that air enters any channel. If the bed is damaged, repeat **steps 2–7** in **Subheading 3.2**.

15. As the acetonitrile is driven out of the bed by the aqueous buffer solution, the refractive index should visibly change. The beads will noticeably agglomerate and appear “locked” in place. At this stage, the extraction bed is ready for use.

Acknowledgments

Special thanks go to D. Jed Harrison, in whose laboratories these experiments were done. I also thank Paul Li for designing the devices used in this work, and Rick Oleschuk for collaborating on this research and for working with other Harrison group members to continue it.

References

1. Verpoorte, E. (2003) Beads and chips: new recipes for analysis. *Lab Chip* **3**, 60N–68N.
2. Wang, C., Oleschuk, R., Ouchen, F., Li, J., Thibault, P., and Harrison, D. J. (2000) Integration of immobilized trypsin bead beds for protein digestion within a microfluidic chip incorporating capillary electrophoresis separations and an electrospray mass spectrometry interface. *Rapid Commun. Mass Spectrom.* **14**, 1377–1383.
3. Lin, L. J., Ferrance, J., Sanders, J. C., and Landers, J. P. (2003) A microchip-based proteolytic digestion system driven by electroosmotic pumping. *Lab Chip* **3**, 11–18.
4. Richter, T., Shultz-Lockyear, L. L., Oleschuk, R. D., Bilitewski, U., and Harrison, D. J. (2002) Bi-enzymatic and capillary electrophoretic analysis of non-fluorescent compounds in microfluidic devices: determination of xanthine. *Sens. Actuators B* **81**, 369–376.
5. Sato, K., Yamanaka, M., Takahashi, H., Tokeshi, M., Kimura, H., and Kitamori, T. (2002) Microchip-based immunoassay system with branching multichannels for simultaneous determination of interferon- γ . *Electrophoresis* **23**, 734–739.
6. Sato, K., Tokeshi, M., Odake, T., et al. (2000) Integration of an immunosorbent assay system: Analysis of secretory human immunoglobulin A on polystyrene beads in a microchip. *Anal. Chem.* **72**, 1144–1147.
7. Sato, K., Tokeshi, M., Kimura, H., and Kitamori, T. (2001) Determination of carcinoembryonic antigen in human sera by integrated bead-bed immunoassay in a microchip for cancer diagnosis. *Anal. Chem.* **73**, 1213–1218.
8. Oleschuk, R. D., Shultz-Lockyear, L. L., Ning, Y., and Harrison, D. J. (2000) Trapping of bead-based reagents within microfluidic systems: on-chip solid-phase extraction and electrochromatography. *Anal. Chem.* **72**, 585–590.
9. Oleschuk, R. D., Jemere, A. B., Shultz-Lockyear, L. L., Fajuyigbe, F., and Harrison, D. J. (2000) Utilization of bead based reagents in microfluidic systems, in *Micro-Total Analysis Systems 2000*, Proceedings Volume (Van den Berg, A., Olthuis, W., and Bergveld, P., eds.), Kluwer Academic, Dordrecht, The Netherlands, pp. 11–14.

10. Jemere, A. B., Oleschuk, R. D., Ouchen, F., Fajuyigbe, F., and Harrison, D. J. (2002) An integrated solid-phase extraction system for sub-picomolar detection. *Electrophoresis* **23**, 3537–3544.
11. Jemere, A. B., Oleschuk, R. D., Taylor, J., and Harrison, D. J. (2001) Microchip-based selective preconcentration using protein A immunoaffinity chromatography, in *Micro-Total Analysis Systems 2001*, Proceedings Volume (Ramsey, J. M. and van den Berg, A., eds.), Kluwer Academic, Dordrecht, The Netherlands, pp. 501–502.
12. Fan, Z. H. and Harrison, D. J. (1994) Micromachining of capillary electrophoresis injectors and separators on glass chips and evaluation of flow at capillary intersections. *Anal. Chem.* **66**, 177–184.

Fabrication of Micromachined Magnetic Particle Separators for Bioseparation in Microfluidic Systems

Jin-Woo Choi

Summary

Fabrication of micromachined magnetic particle separators is introduced with an emphasis on magnetic particle-based bioseparation in microfluidic systems. The most attractive aspect of the magnetic separation technique in biochemistry and biotechnology is ease of manipulation of biomolecules, which are immobilized on magnetic particles. Embedded electromagnets in the microfluidic channel are described for on-chip magnetic particle separation for lab-on-a-chip applications. An example of microfluidic systems with a magnetic particle separator and integrated microfluidic components is also presented for rapid magnetic particle-based bioseparation and immunoassay.

Key Words: Bioseparation; magnetic particle; microfluidic system; microfabrication; superparamagnetic particle.

1. Introduction

1.1. Background

In recent molecular biology and biotechnology, cell or biomolecule separation is considered to be one of the most complex and difficult tasks. New separation technologies capable of treating dilute solutions in both small- and large-scale processes even in the presence of particulate matter are necessary for the future development of biochemistry and biotechnology at all levels. Among several available bioseparation techniques, magnetic separation technique using magnetic particles has been considered to be one of the most promising and can be used in a wide range of applications if it is appropriately developed.

Conventional magnetic separation methods have been used for a long time as standard techniques in a variety of laboratory and industrial applications,

which include the enrichment of low-grade iron ore, removal of weakly magnetic colored impurities from kaolin clay, removal of magnetic pollutants from stack gases from several industrial processes, desulfurization of coal, and removal of ferromagnetic impurities from large volumes of boiler water in both conventional and nuclear power plants. Their applications to biochemistry and biotechnology, however, were restricted and of limited use until the 1970s. Since then, magnetic separation, labeling, and targeting techniques have found many useful and interesting applications in various areas such as molecular biology, cell biology, and microbiology. Further, intensive research is being performed in other areas employing the unique properties of magnetic particles.

The idea of using magnetic separation techniques in cell separation is not new, but it has enjoyed a resurgence of interest over the last decade (1–5). This has primarily been caused by the development of new magnetic particles with improved properties for various cell separation procedures such as cancer cell separation. Many researchers have also reported the feasibility of using magnetic beads for immunomagnetic cell separation (6–9), immunoassay, and drug delivery applications (10–13). The most attractive aspect of the magnetic separation technique in biochemistry and biotechnology is the ease of manipulation of biomolecules, which are immobilized on magnetic particles. Once target biological cells or molecules are immobilized on magnetic particles, the target biomolecules can be separated from a sample solution, manipulated in various reagents, and easily transported to a desired location by controlling magnetic fields produced from a permanent magnet or an electromagnet. Another advantage is the large surface area of the immobilization substrate owing to a large number of binding sites, resulting in a high population of target biomolecules and, hence, a high detection signal.

In this chapter, magnetic separation in biomedical applications is briefly introduced and the fabrication of micromachined magnetic particle separators is presented.

1.2. Magnetic Particles for Bioseparation

Magnetic separations in biology and biotechnology have diversified in recent years. Applications in the nucleic acid realm include products for mRNA isolation from cells or previously purified total RNA preparations, solid-phase cDNA library construction, double-stranded DNA (dsDNA) and single-stranded DNA (ssDNA) purification, solid-phase DNA sequencing, and a variety of hybridization-based methodologies. Magnetic beads are also finding uses in protein purification; immunology; and the isolation of a wide range of specific mammalian cells, bacteria, viruses, subcellular organelles, and individual proteins. There are also products that employ magnetic particles for more con-

ventional isolation and purification methods, such as affinity/ion exchange and charcoal trapping of small analytes.

A common use of superparamagnetic particles is for immunospecific cell separations (14–17). Specific antibody and magnetic particles are mixed together first to immobilize the antibody onto the surface of magnetic particles. The antibody-tagged magnetic particles are then incubated with a solution containing the cells, proteins, and/or antigens of interest. The magnetic particles bind to the surfaces of the desired cells and/or proteins, and these biomolecules can then be collected in a magnetic field by collecting the magnetic particles. Methods of this type have been used to isolate or remove numerous cell types, including lymphocytes (cells that control immune response), tumor cells, or specific antigens. In addition to loading superparamagnetic particles with biomolecules, other examples of tagging the desired biomaterial with individual particles have been reported. Other application areas are mRNA isolation from cells or previously purified total RNA preparations, solid-phase cDNA library construction, dsDNA and ssDNA purification, and a variety of hybridization-based methodologies (18). An example of magnetic particle-based bioseparation is illustrated in Fig. 1.

1.3. Magnetic Particles and Magnetic Separation

The basic concept of magnetic separations in biotechnologies including lab-on-a-chip systems is to bind the biomaterial of interest selectively, such as a specific cell, protein, or DNA fragment, to a magnetic particle and then separate it from its surrounding matrix using a magnetic field for manipulation or purification of biological cells/molecules. Magnetic beads of iron oxide (Fe_2O_3 or Fe_3O_4) with diameters ranging from a few nanometers to a few micrometers are typically used for such separations. These magnetic particles are called superparamagnetic particles, meaning that they are attracted to a magnetic field but retain no residual magnetism after the field is removed. The material, which is halfway between ferromagnetic and paramagnetic property, has superparamagnetism. As the size of magnetic elements scales below a range of a few tens of nanometers, a superparamagnetic phase emerges in which the room temperature thermal energy overcomes the magnetostatic energy well of the element, resulting in zero hysteresis. In other words, although the element itself is a single-domain ferromagnet, the ability of an individual magnetic domain to store magnetization orientation information is lost when its physical dimensions are below a threshold. Therefore, suspended superparamagnetic particles tagged to the biomaterial of interest can be removed from a matrix using a magnetic field, but they do not agglomerate or stay suspended in the solution after removal of the magnetic field. If the magnetic components (generally iron oxide) are small enough, they will respond to a magnetic field but

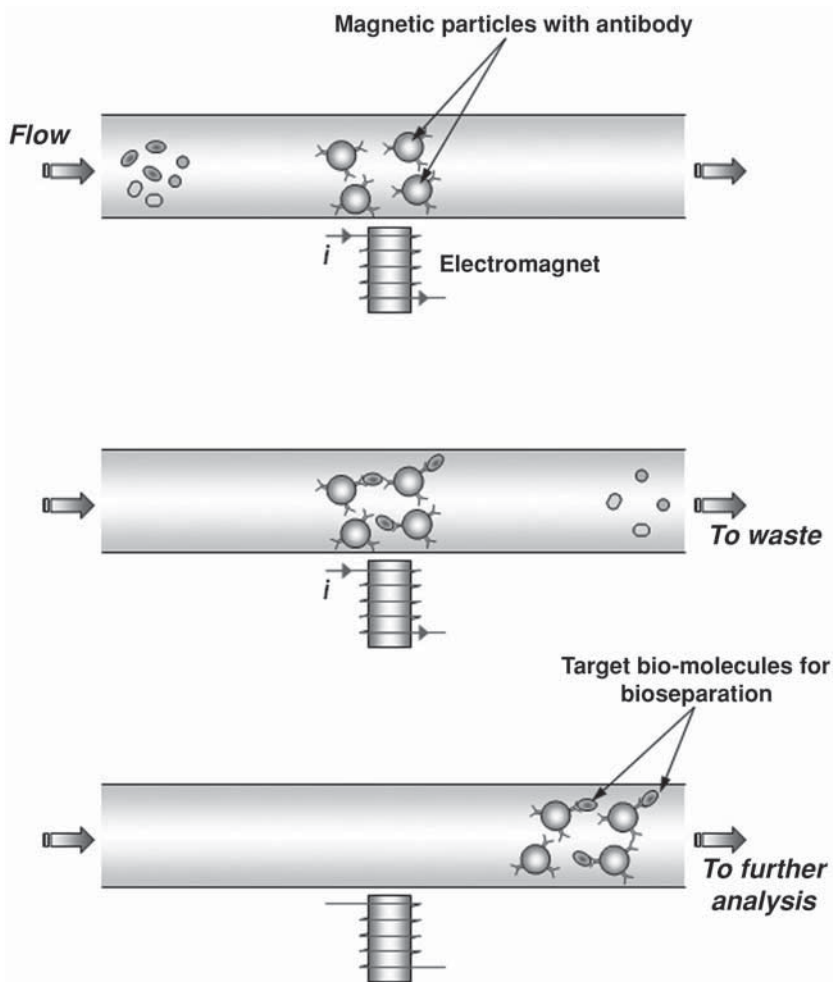


Fig. 1. Example of magnetic particle-based bioseparation in microfluidic channel. i , electric current.

will be incapable of becoming independently magnetic. This is important, because it results in particles that are attracted by a magnetic force owing to a magnetic field (*see Note 1*) and yet lose all attraction for each other in the absence of a magnetic field, thereby allowing efficient separation and complete resuspension. **Figure 2** illustrates a general structure of magnetic beads that contain superparamagnetic nanoparticles in a polymeric shell.

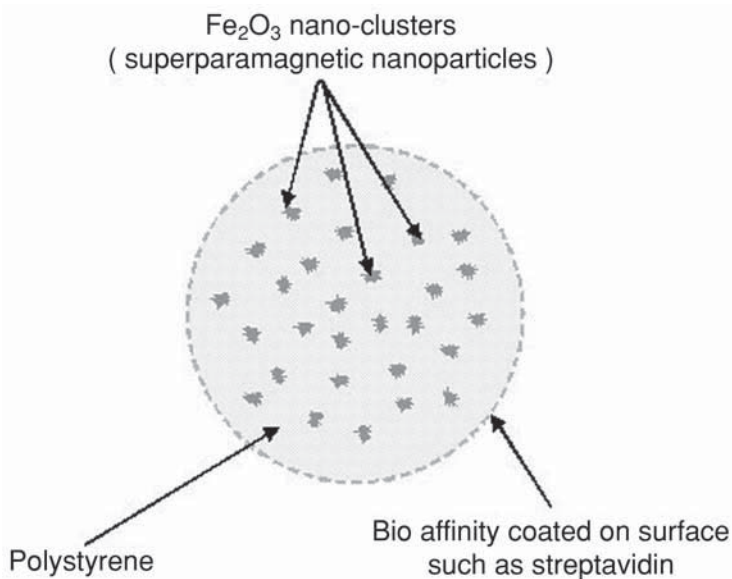


Fig. 2. General structure of superparamagnetic particles.

2. Materials

1. Pyrex glass wafer (2-in.) (Pyrex 7740; Corning).
2. n-Type silicon (Si) wafer 2-in. (100) with thermally grown silicon dioxide (*see Note 2*).
3. Photoresist (Shipley 1818, AZ4620, AZ4400) and developer (Microposit 351, AZ400K).
4. Polyimide (PI2611; DuPont).
5. Copper (Cu) electroplating solution: 120 g/L of copper sulfate ($\text{CuSO}_4 \cdot 5\text{H}_2\text{O}$), and 100 g/L of sulfuric acid (H_2SO_4).
6. Permalloy ($\text{Ni}_{81}\text{Fe}_{19}$) electroplating solution: 200 g/L of nickel sulfate ($\text{NiSO}_4 \cdot 6\text{H}_2\text{O}$), 5 g/L of nickel chloride ($\text{NiCl}_2 \cdot 6\text{H}_2\text{O}$), 8 g/L of ferrous sulfate ($\text{FeSO}_4 \cdot 7\text{H}_2\text{O}$), 25 g/L of boric acid (H_3BO_3), 3 g/L of sodium saccharin ($\text{C}_7\text{H}_4\text{NNaO}_3\text{S} \cdot 2\text{H}_2\text{O}$), and H_2SO_4 for pH control (to 2.5).
7. Copper etchant (*see Note 3*):
 - a. CuSO_4 (4 g) + NH_4OH (100 mL) + H_2O (150 mL).
 - b. H_2SO_4 (100 mL) + H_2O_2 (100 mL) + H_2O (1000 mL).
8. Titanium (Ti) etchant: 0.2% hydrofluoric acid.
9. Silicon (Si) wet etchant potassium hydroxide (KOH), 40% by weight, (*see Note 3*).
10. Si dioxide etchant (Buffered Oxide Etch; Fisher).
11. Magnetic beads: estapor carboxylate-modified superparamagnetic beads from Bangs Laboratories, Inc. (*see Note 4*).

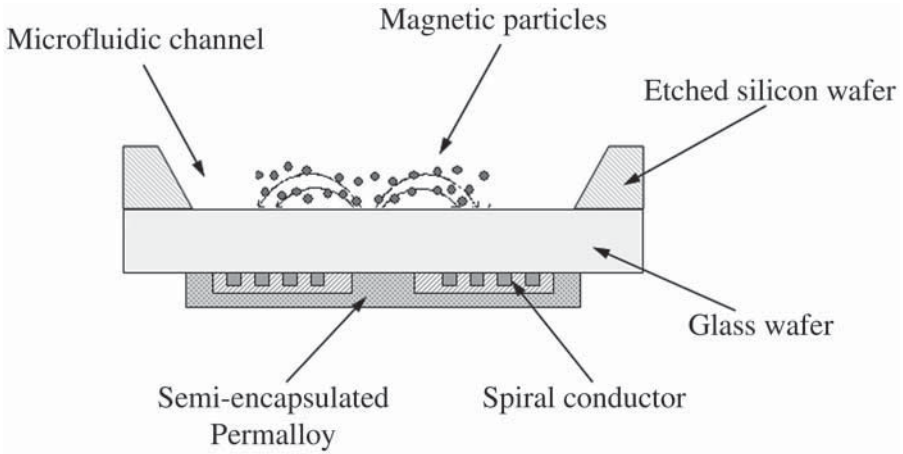


Fig. 3. Cross-sectional view of magnetic particle separator with semi-encapsulated spiral electromagnet.

3. Methods

3.1. Magnetic Particle Separator With Semi-Encapsulated Spiral Electromagnet

Considering the design parameters to maximize the magnetic force on a magnetic particle (*see Note 1*), a magnetic particle separator with semiencapsulated spiral electromagnets can be designed and fabricated for microfluidic magnetic particle separation as shown in **Fig. 3**. The magnetic flux path from the bottom of the channel creates the magnetic field and its gradient for the separation. A planar spiral-type electromagnet is placed on the bottom of the flow channel that consists of Pyrex glass and an etched Si wafer bonded to each other. For a specific design reported by Choi et al. (**19**), the width of the conductive coil of the electromagnets is 50 μm and the thickness is 25 μm . The spiral coils have 12 turns with 30- μm spacing between each conductive line. Anisotropic etching of an Si wafer, which is bonded to a glass wafer, forms the wall of the channel. The magnetic flux path in the bottom of the channel creates a magnetic field gradient necessary for the separation. From the back side of the glass wafer (the other side of the channel), the flux is confined by a semiencapsulated Permalloy ($\text{Ni}_{81}\text{Fe}_{19}$) core, which has a high permeability. This semiencapsulated Permalloy structure reduces the field losses on the back side and serves as a structural support for the inductor/insulator layer. Detailed fabrication steps are summarized next:

1. Deposit Titanium (Ti) (300 \AA) and copper (Cu) (3000 \AA) layers on a glass wafer using electron beam evaporation. The layers act as a seed layer.

2. Using standard AZ 4620 photolithography, form a 25- μm -thick photoresist electroplating mold.
3. Electroplate a Cu spiral inductive component up to 20 μm with a current density of 10 mA/cm².
4. Remove the photoresist mold in acetone. In addition, etch away the 3000- \AA -thick Cu layer and 300- \AA -thick Ti seed layer in Cu etchant (*see Note 5*) and Ti etchant, respectively (*see Note 6*). After each wet process, rinse the wafer in deionized water.
5. After hard baking (*see Note 7*) of the wafer, using standard AZ 4620 photolithography, form a mold for Permalloy electroplating.
6. Cure the Permalloy electroplating mold at 200°C for 1 h on a hot plate under a fume hood (*see Note 8*).
7. Deposit a seed layer of Ti/Cu for Permalloy electroplating using electron-beam evaporation. The thickness of the seed layer is 300 \AA for Ti and 3000 \AA for Cu. Conduct Permalloy electroplating with a current density of 5 mA/cm².
8. Remove the Ti/Cu seed layer in Cu and Ti etchant (*see Note 9*).
9. To fabricate the channel, perform KOH anisotropic etching on a double-sided, polished 2-in. Si (100) wafer with a silicon dioxide layer on both sides. Define the channel pattern using standard Shipley 1818 photolithography and silicon dioxide etching in buffered oxide etch. The back side of the wafer has to be protected during this step. After removing the photoresist in acetone, anisotropically etch the Si wafer completely through in KOH (40% by weight) solution at 80°C.
10. Remove the remaining silicon dioxide in buffered oxide etch, and bond the unprocessed side of the glass wafer to the Si wafer using a low-temperature (250°C) electrostatic bonding technique. If a complete microchannel is necessary, another glass wafer with drilled inlet/outlet holes can be bonded to the other side of the Si wafer using the same electrostatic bonding technique. Schematic fabrication steps are illustrated in **Fig. 4**.

3.2. Magnetic Particle Separator With Planar Electromagnet

A magnetic particle separator with a semiencapsulated spiral electromagnet has a relatively simple structure. One downside is the long distance from micromachined electromagnets to the microfluidic channel, which means that the source of magnetic fields is far away (at least the thickness of the glass wafer [250 μm]) from the magnetic particles to be separated. As a result, if higher flow velocity is required in microfluidic applications, higher electric current to separate magnetic particles in the microfluidic channel is often necessary. A shorter distance between the source of magnetic fields and the microfluidic channel where the magnetic particles of interest will flow is advantageous. Therefore, a magnetic particle separator with a planar electromagnet that is fabricated using planar serpentine conductors and semi-encapsulated in Ni/Fe Permalloy has been introduced. To improve the capability of

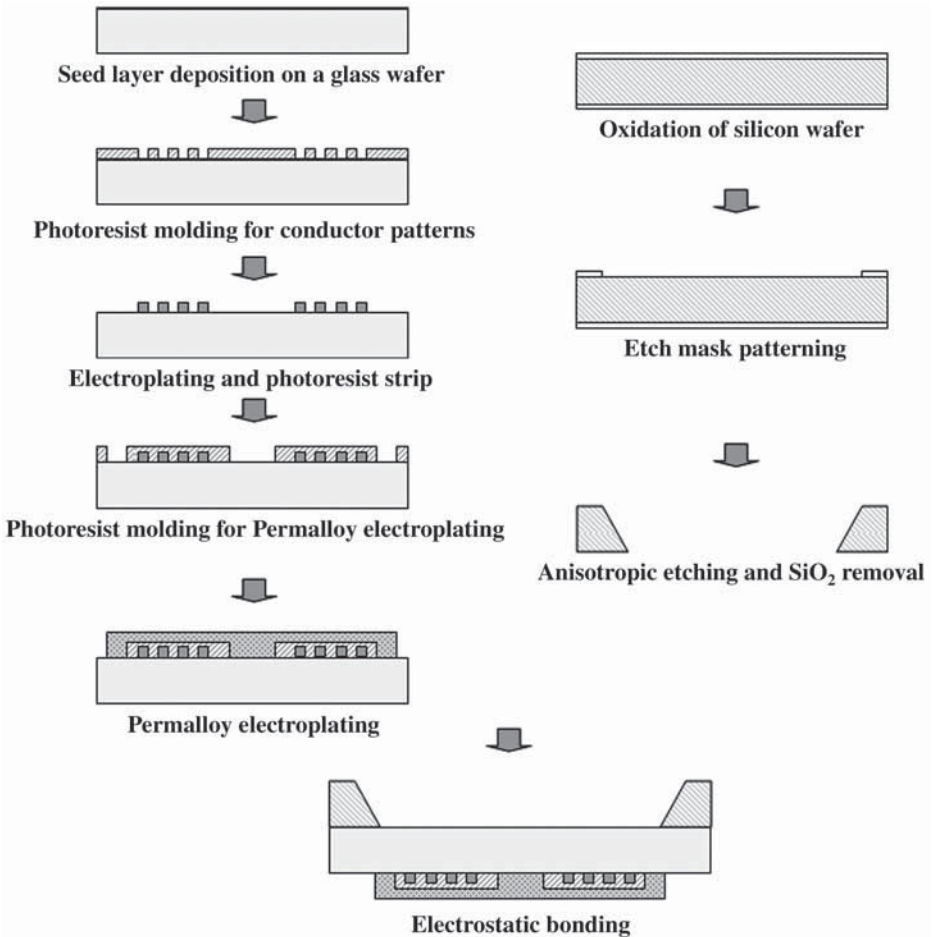


Fig. 4. Fabrication steps of magnetic particle separator with semi-encapsulated spiral electromagnet.

magnetic particle separation, the inside walls of the microchannel consist of the embedded planar electromagnets, which will attract or release the magnetic beads that immobilize the target biomolecules. Considering the size of the bead of interest and the difficulties in fabrication, the width of the serpentine conductor was chosen as $10\ \mu\text{m}$. The current applied to the serpentine conductor ($10\ \mu\text{m}$ width and spacing) produces magnetic fields through the microfluidic channel and forces magnetic beads to move onto the embedded planar electromagnet. The separated magnetic particles are captured and held in the continuous fluid flow if the magnetic force on a magnetic particle is larger than the

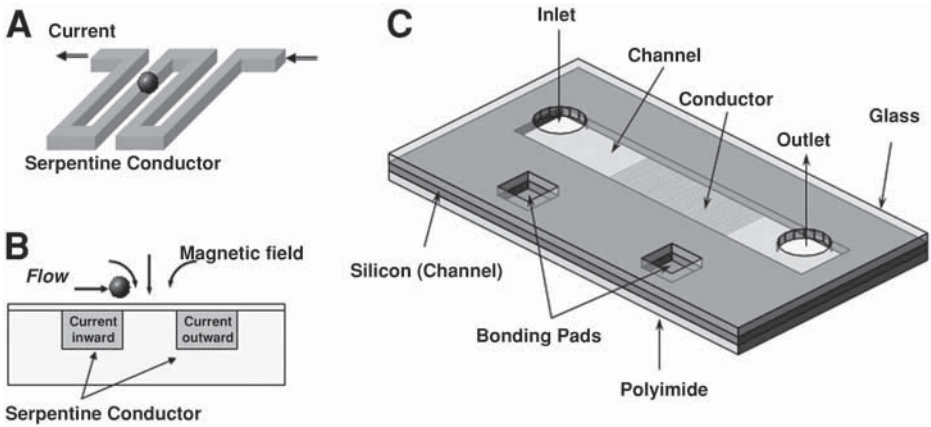


Fig. 5. Inductive component for magnetic separation: (A) serpentine conductor structure; (B) embedded serpentine conductor as an electromagnet; and (C) schematic illustration of microfluidic magnetic particle separator.

fluidic force on the magnetic particle. A serpentine conductor and an electromagnet are fabricated using an electroplating technique based on the thick photoresist lithography process. Electroplated high-permeability Permalloy ($\text{Ni}_{81}\text{Fe}_{19}$) is used as the magnetic material. The inductive component for magnetic separation is the embedded serpentine electromagnets, as illustrated in **Fig. 5**. Applied electric current generates nonuniform magnetic fields to separate and hold magnetic particles in a microfluidic channel (20). **Figure 6** briefly illustrates the fabrication process.

1. The process starts with a 2-in. oxidized n-type Si (100) wafer that forms the substrate for fabricating both the conductor and the microfluidic channel. Deposit Ti (300 Å)/Cu (3000 Å) layers using electron-beam evaporation to seed electroplating onto a double-sided polished n-type Si (100) wafer with 1- μm -thick silicon dioxide.
2. Using standard AZ 4400 photolithography, form a 7- to 8- μm -thick photoresist electroplating mold.
3. Fill the mold with 5- μm -thick electroplated copper. Set the current density to 10 mA/cm² during electroplating.
4. On completion of the electroplating, remove the photoresist mold in acetone followed by Cu and Ti seed layer etching (*see Note 5*).
5. To insulate the serpentine conductor coil from the Permalloy structure, spin-coat polyimide (PI-2611) and fully cure at 350°C in a convection oven for 1 h.
6. To fabricate the Permalloy structure, deposit a seed layer and form a thick photoresist mold up to 25 μm for electroplating using standard AZ 4620 photolithography.

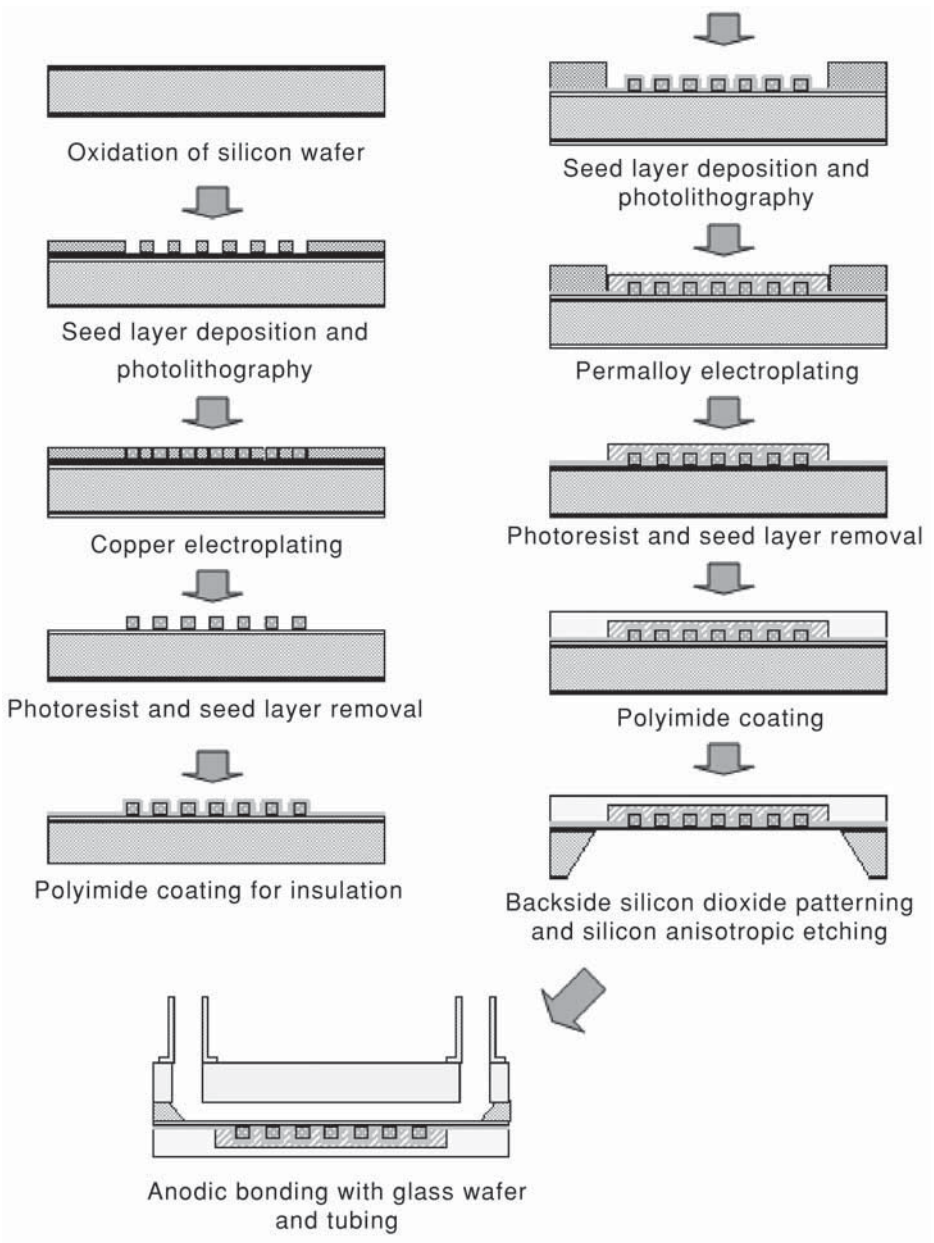


Fig. 6. Fabrication process of magnetic particle separator with planar serpentine electromagnet.

7. Electroplate the Permalloy and then perform mold removal and seed layer etching from the wafer (*see Note 9*). Spin polyimide on the wafer in multiple coats to protect the inductive components and fully cure.
8. Fabricate an 800- μm -wide and 250- μm -deep channel on the back side of the Si wafer by anisotropic etching in KOH (40% by weight) solution at 80°C. During etching in KOH, the polyimide-covered side of the wafer must be protected from the solution. Then remove the silicon dioxide layer used as an etching mask in buffered oxide etch.
9. Place a glass (Pyrex) wafer with mechanically drilled inlet and outlet holes on the etched side of the Si wafer and anodically bond at 250°C.
10. Glue tubings on both the inlet and outlet. Connect the inlet tubing to fluidic control equipment (e.g., syringe pump).
11. The magnetic beads used in this experiment are commercially available superparamagnetic particles (Bangs) supplied as an aqueous dispersion with 60% solid content of magnetite (*see Note 4*). First, inject the magnetic beads into the microchannel. Then, turn the direct current (DC). This initiates the separation of beads. During separation, the unseparated beads are washed away with the fluid flow. After completely washing out the unseparated beads, release the separated beads by turning off the applied DC. Key separation steps are shown in **Fig. 7** (*see Note 10*).

4. Notes

1. According to electromagnetic field theory, the magnetization density \mathbf{M} is introduced to account for the effects of magnetizable materials. The most common constitutive law for \mathbf{M} takes the form

$$\mathbf{M} = \chi_m \mathbf{H} \quad (1)$$

in which χ_m is the magnetic susceptibility and \mathbf{H} is the magnetic field intensity. **Equation 1** is based on the assumption that the material is both isotropic and linear, in other words, that \mathbf{M} is proportional to \mathbf{H} and in the same direction, which is reasonably true in superparamagnetic materials. Assuming N as the number of atoms in unit volume and \mathbf{m} as the magnetic moment, \mathbf{H} can also be expressed as

$$\mathbf{M} = N\mathbf{m} \quad (2)$$

The magnetic beads are assumed to be spherical and have a low density in the suspension. Therefore, interactions between the particles are not considered. For this case, the magnetic force \mathbf{F} has the form

$$\mathbf{F} = \nabla U = \nabla (\mathbf{m} \cdot \mathbf{B}) \quad (3)$$

in which U is the magnetic energy. Applying basic vector calculation, **Eq. 3** can be rewritten as

$$\mathbf{F} = \mathbf{B} \times (\nabla \times \mathbf{m}) + \mathbf{m} \times (\nabla \times \mathbf{B}) + (\mathbf{B} \cdot \nabla) \mathbf{m} + (\mathbf{m} \cdot \nabla) \mathbf{B} \quad (4)$$

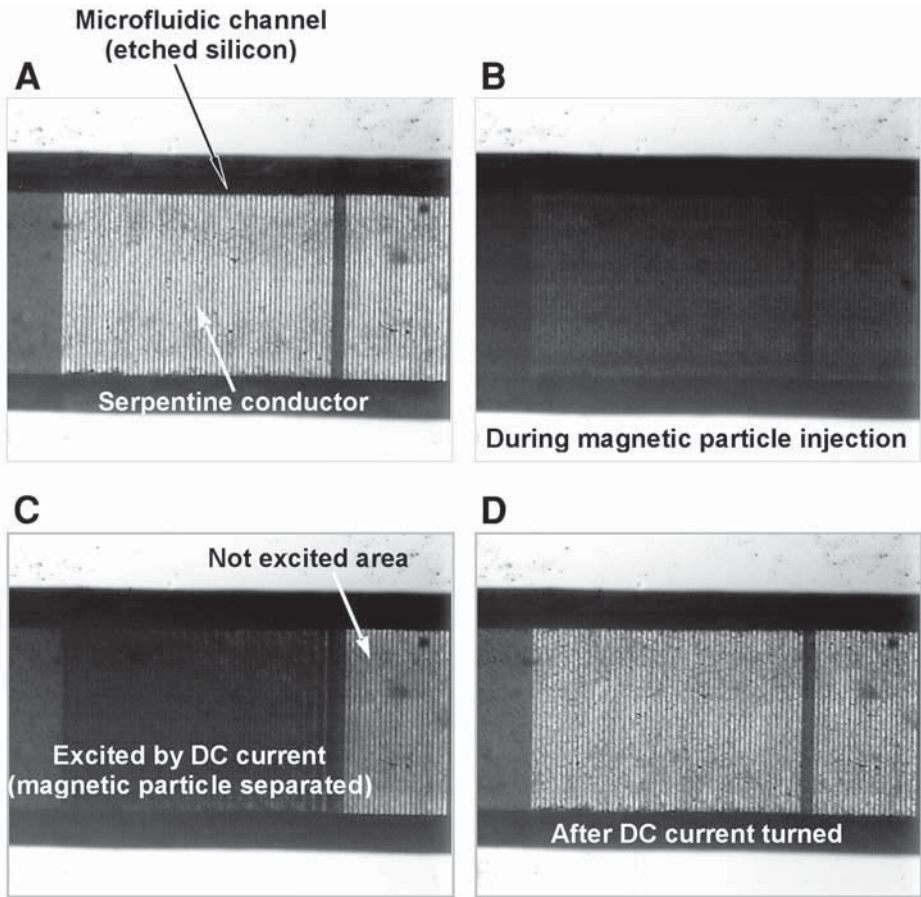


Fig. 7. Key microphotographs of magnetic particle separation test results: (A) before injection of magnetic particles; (B) after injection of the magnetic particles; (C) separation and holding magnetic particles; (D) after complete release.

Based on the assumption that there is no interaction between the particles, the first and the third terms are zero. In addition, the absence of source current at the location of \mathbf{m} makes the second term zero. By combining Eqs. 1 and 2 into 4, the magnetic force of attraction from the field on the particle is

$$\mathbf{F} = (\mathbf{m} \cdot \nabla) \mathbf{B} = V \chi_m (\mathbf{H} \cdot \nabla) \mathbf{B} \quad (5)$$

in which V is the volume of the particle.

By choosing the x direction along the channel, the x -directional force is

$$F_x = V \chi_m \left(H_x \frac{\partial}{\partial x} + H_y \frac{\partial}{\partial y} \right) B_x = V \chi_m \left(H_x \frac{\partial B_x}{\partial x} + H_y \frac{\partial B_x}{\partial y} \right) \quad (6)$$

From **Eq. 6**, since V and χ_m depend on the selected magnetic beads, the controllable parameters of the separation device are the strength (H_x and H_y) and the gradient ($\partial B_x/\partial x$ and $\partial B_y/\partial y$) of the magnetic field. In microfluidic systems, the field depends on the performance of the inductive component, which is limited by the allowable size and microfabrication process. The field strength is, however, usually limited in a microstructure because it is not easy to apply a large current owing to its small size, although the field gradient is easier to maximize by choosing an appropriate structure or geometry.

2. Silicon nitride (Si_3N_4) on both sides of an Si wafer is also acceptable. In such cases, a reactive ion etching technique has to be employed to etch Si_3N_4 film.
3. Etchant (a) is general Cu etchant in microfabrication but it also etches Permalloy. Etchant (b) gives a good selectivity over Permalloy and it does not etch Permalloy.
4. The magnetic beads used in this experiment are commercially available superparamagnetic particles (Bangs Laboratories, Inc.) supplied as an aqueous dispersion with 60% solid content of magnetite. This magnetic bead consists of a ferrite core (magnetite) with median diameters of 0.8–1.3 μm . The magnetic bead density is 2.2 g/mL. The beads are coated with the usual polystyrene and carboxylic acid–modified shell to isolate iron from the surface, so that they can be used for adsorption as well as covalent attachment.
5. Although any etchant (*see Note 3*) can be used, the first etchant (mixture of CuSO_4 , NH_4OH , and H_2O) is recommended. The etch rate is approx 1000 $\text{\AA}/\text{min}$ at room temperature.
6. The etch rate is approx 100 $\text{\AA}/\text{min}$ at room temperature.
7. Hard baking requires more than 20 min in a 120°C convection oven to dehydrate the sample fully.
8. This layer of photoresist works as both electroplating mold and insulation layer between the Permalloy encapsulation structure and the Cu conductor, as shown in **Fig. 3**.
9. Etchant that does not etch Permalloy (mixture of H_2SO_4 , H_2O_2 , and H_2O) should be used to protect the electroplated Permalloy structure.
10. After completely washing out the unseparated beads, biosamples can be injected for actual bioseparation. A simple concept of magnetic bead–based bioseparation with a microfabricated electromagnet for the application of on-chip immunoassay is shown in **Fig. 8**. The analytical concept is based on sandwich immunoassay and electrochemical detection (**21**). Antibody-coated magnetic particles are introduced to the electromagnet and separated by applying the magnetic fields. While one holds the antibody-coated magnetic beads, antigens are injected into the channel. Only target antigens are immobilized and, thus, separated onto the magnetic bead surface owing to antibody-antigen reaction. Other antigens get washed out with the flow. Because the only target antigens are collected by magnetic beads, target antigens are also “filtered.” Next, enzyme-labeled secondary antibodies are introduced and incubated with the immobilized antigens. The chamber is then rinsed to remove all unbound secondary antibodies. Substrate solution, which will react with enzyme, is injected into the channel and the elec-

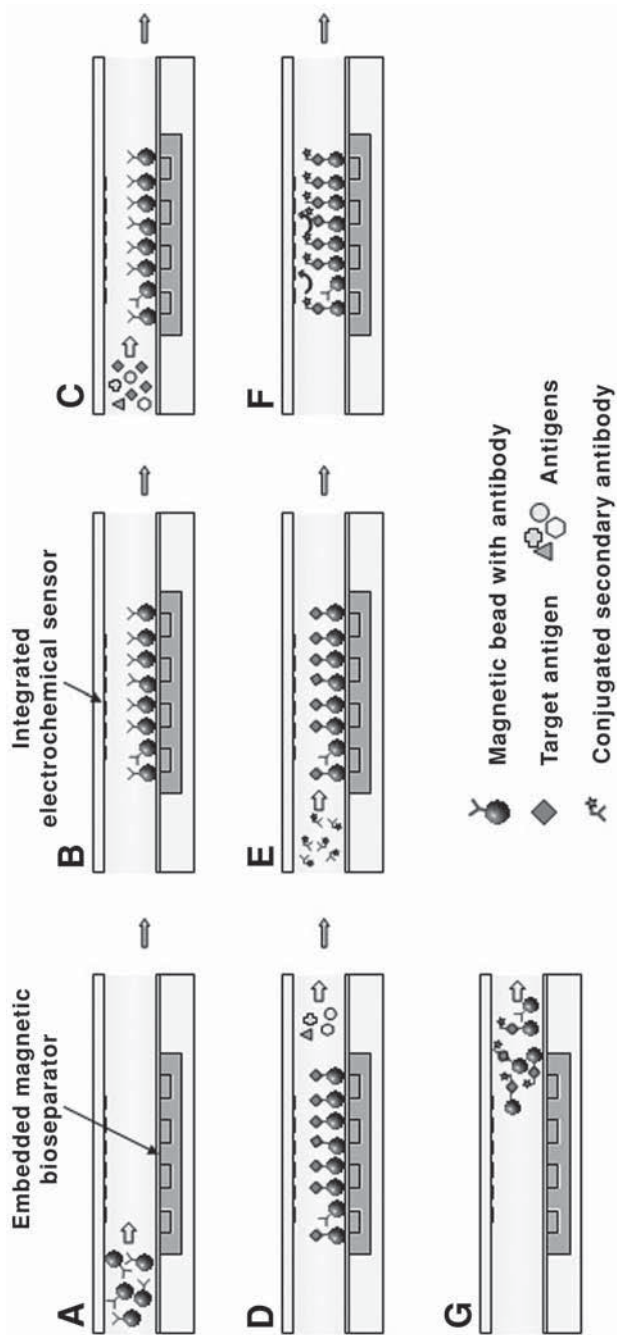


Fig. 8. Conceptual illustration of biosampling and immunoassay procedure using magnetic bead approach: (A) injection of magnetic beads; (B) separation and holding of beads; (C) flowing samples; (D) immobilization of target antigen; (E) flowing labeled antibody; (F) electrochemical detection; (G) washing out of magnetic beads, making bioseparator ready for another immunoassay.

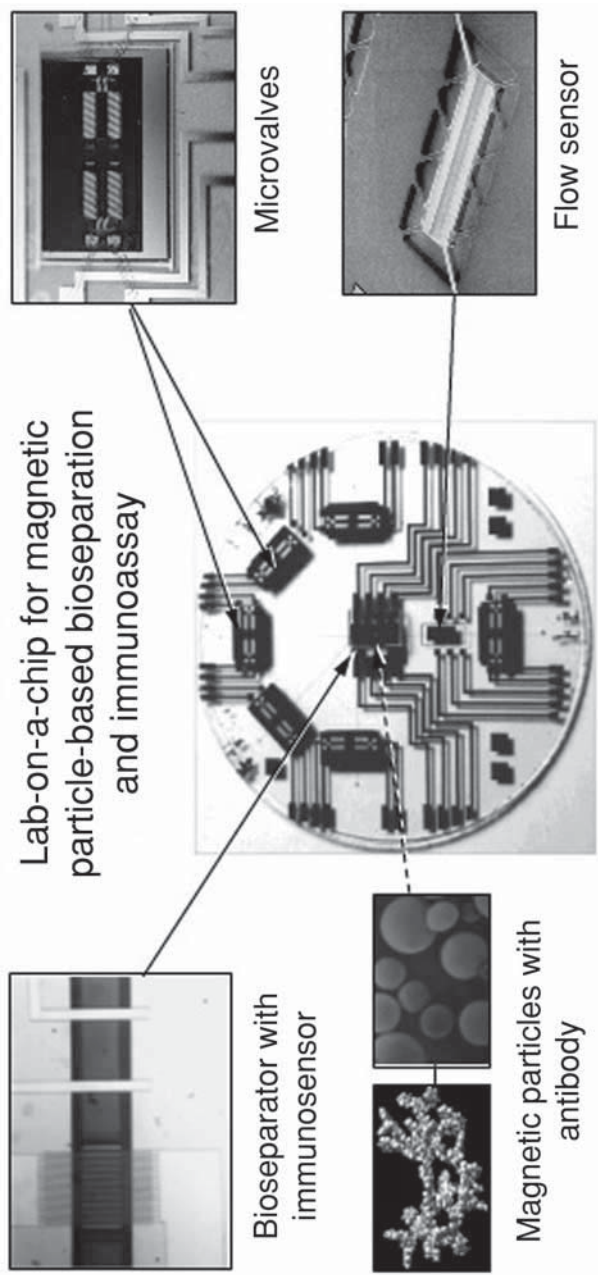


Fig. 9. Generic microfluidic system for biochemical detection using magnetic particle-based bioseparation.

trochemical detection is performed. Finally, the magnetic beads are released to the waste chamber and the bioseparator is ready for another immunoassay. One of the sample microfluidic systems is shown in [Fig. 9](#).

References

1. Melville, D., Paul, F., and Roath, S. (1975) High gradient magnetic separation of red cells from whole blood. *IEEE Trans. Magn.* **Mag-11**, 1701.
2. Whitesides, G. M., Kazlauskas, R. J., and Josephson, L. (1983) Magnetic Separations in Biotechnology. *Trends Biotechnol.* **1**, 144–148.
3. Roath, S., Smith, A., and Watson, J. H. P. (1990) High gradient magnetic separation in blood and bone marrow processing. *J. Magnetism. Magn. Mater.* **85**, 285–289.
4. Chikov, V., Kuznetsov, A., Shapiro, A., Winoto-Morbach, S., and Mueller-Ruchholtz, W. (1993) Single cell magnetophoresis and its diagnostic value. *J. Magnetism. Magn. Mater.* **122**, 367–370.
5. Miltenyi, S., Muller, W., Weichel, W., and Radbruch, A. (1990) High-gradient magnetic cell-separation with MACS. *Cytometry* **11**, 231–238.
6. Partington, K. M., Jenkinson, E. J., and Anderson, G. A. (1999) Novel method of cell separation based on dual parameter immunomagnetic cell selection. *J. Immunol. Methods* **223**, 195–205.
7. Hartig, R., Hausmann, M., and Cremer, C. (1995) Continuous focusing of biological particles by continuous immunomagnetic sorter: technique and applications. *Electrophoresis* **16**, 789–792.
8. Yu, H. (1998) Use of an immunomagnetic separation–fluorescent immunoassay (IMS–FIA) for rapid and high throughput analysis of environmental water samples. *Anal. Chim. Acta* **376**, 77–81.
9. Panphilov, A. S. and Bekish, O.-J. L. (1997) Updating of magnetosensitive microspheres from styrene technology for immunomagnetic cell separation. *Immunol. Lett.* **56**, 462.
10. Ghassabian, S., Ehtezazi, T., Forutan, S. M., and Mortazavi, S. A. (1996) Dexamethasone-loaded magnetic albumin microspheres: preparation and in vitro release. *Intl. J. Pharmaceutics* **130**, 49–55.
11. Goodwin, S., Peterson, C., Hoh, C., and Bittner, C. (1999) Targeting and retention of magnetic targeted carriers (MTCs) enhancing intra-arterial chemotherapy. *J. Magnetism Magn. Mater.* **194**, 132–139.
12. Pulfer, S. K., Ciccotto, S. L., and Gallo, J. M. (1999) Distribution of small magnetic particles in brain tumor-bearing rats. *J. Neuro-Oncol.* **41**, 99–105.
13. Lubbe, A. S., Bergemann, C., Brock, J., and McClure, D. G. (1999) Physiological aspects in magnetic drug-targeting. *J. Magnetism Magn. Mater.* **194**, 149–155.
14. Deng, M. Q., Lam, K. M., and Cliver, D. O. (2000) Immunomagnetic separation of cryptosporidium parvum oocysts using MACS microbeads and high gradient separation columns. *J. Microbiol. Methods* **40**, 11–17.
15. Makarovskiy, A. N., Ackerley, W., Wojcik, L., et al. (1997) Application of immunomagnetic beads in combination with RT-PCR for the detection of circulating prostate cancer cells. *J. Clin. Lab. Anal.* **11**, 346–350.

16. Cudjoe, K. C., Hagtvedt, T., and Dainty, R. (1995) Immunomagnetic separation of salmonella from foods and their detection using immunomagnetic particle (IMP)-ELISA. *Intl. J. Food Microbiol.* **27**, 11–25.
17. Wright, A. P., Fitzgerald, J. J., and Colello, R. J. (1997) Rapid purification of glial cells using immunomagnetic separation. *J. Neurosci. Methods* **74**, 37–44.
18. Bosnes, M., Dggerdal, A., Rian, A., Korsnes, L., and Larsen, F. (1997) Magnetic separation in molecular biology, in *Scientific and Clinical Applications of Magnetic Carriers* (Hafeli, E. A., et al., eds.), Plenum, New York, pp. 311–322.
19. Choi, J.-W., Liakopoulos, T. M., and Ahn, C. H. (2001) An on-chip magnetic bead separator using spiral electromagnets with semi-encapsulated permalloy. *Biosens. Bioelectron.* **16**, 409–416.
20. Choi, J.-W., Ahn, C. H., Bhansali, S., and Henderson, H. T. (2000) A new magnetic bead-based, filterless bio-separator with planar electromagnet surfaces for integrated bio-detection systems. *Sens. Actuators B* **68**, 34–39.
21. Choi, J.-W., Oh, K. W., Thomas, J. H., et al. (2002) An integrated microfluidic biochemical detection system for protein analysis with magnetic bead-based sampling capabilities. *Lab Chip* **2**, 27–30.

Hydrogel-Immobilized Antibodies for Microfluidic Immunoassays

Hydrogel Immunoassay

**Gloria Thomas, Emad M. El-Giar, Laurie E. Locascio,
and Michael J. Tarlov**

Summary

The integration of immunoassays in microfluidic devices is a rapidly developing research area combining the power of immunoassays with the inherent benefits of microfluidics. Here, a general overview of microfluidic-based immunoassays is presented along with a method for immobilizing antibodies in polyacrylamide gel plugs set in microfluidic channels. These antigen-specific hydrogels can be rapidly formed by photopolymerizing monomer solutions mixed with antibodies or other large proteins. The resulting antigen-specific hydrogels contain pore sizes appropriate for physical entrapment of large antibodies while remaining permeable to smaller proteins. The open structure of these hydrogels enables the capture and concentration of target antigens present at low concentrations. Such physical entrapment provides a conceptually simple method of immobilization compared with immobilization of proteins on surfaces and offers advantages such as resistance to chemical and thermal denaturation.

Key Words: Microfluidic immunoassays; antibody immobilization; microdevice; hydrogel; polyacrylamide gel plug.

1. Introduction

Since their introduction to the scientific community in 1959 (*1*), immunoassays have become popular and powerful analytical methods for quantitative determination of analytes in a wide range of applications including clinical diagnostics (*2–5*), biochemical studies (*6–8*), pharmaceutical analyses (*9–12*), and environmental monitoring (*13–20*). Annual sales for immunoassay reagents and supplies are \$2 billion in the United States and \$7 billion worldwide. These powerful methods have several important characteristics, including specific-

ity, selectivity, simple procedures and instrumentation, and universal application (21–25). The high specificity is based on the antibody/antigen recognition. High sensitivity arises from the use of low background detection methods such as radioactive, fluorescent, or chemiluminescent labeling.

Conventional microplate-based immunoassays are generally carried out in either homogeneous or heterogeneous formats (26). Homogeneous immunoassays have the advantages of being rapid, easy to perform, and readily amenable to automation (27–29); however, they are also less sensitive and prone to interferences. Although heterogeneous immunoassays overcome these limitations and can also be used for both low and high molecular weight analytes (30–34), these assays are limited by diffusion and, thus, tend to be slow and labor-intensive (owing to multiple wash steps) and require relatively long assay times. In addition, automation can be rather costly.

The integration of immunoassays in microfluidic devices is a rapidly developing research area that has the potential to overcome many of the challenges in immunoassays (35). Advantages include reduced assay time; negligible sample, solvent, and reagent consumption; high performance and high throughput; and enhanced sensitivity (35–47). Most of the immunoassays published to date use electroosmotic pumping to drive fluid flow and to separate electrophoretically bound and nonbound fractions.

Many microfluidic methods, like their 96-well-plate predecessors, rely on covalent tethering of biomolecules to microchannel walls. Another recent approach is to use sol-gel technologies for immobilization. For example, the integration of polyethylene glycol plugs (48) or micropatches (49) into the channels of microfluidic systems for DNA and glucose sensing, respectively, has been demonstrated.

This chapter describes a method for immobilizing antibodies within microfluidic polyacrylamide gel plugs (hydrogels) for immunoassays. These antigen-specific hydrogels can be rapidly created by photopolymerizing monomer solutions mixed with antibodies or other large proteins. The resulting hydrogels physically entrap the large antibodies, while remaining permeable to target antigens that can be captured and concentrated in the antibody-containing hydrogels. This technology has been previously demonstrated for covalent immobilization of DNAs for specific hybridization of target sequences (50,51).

2. Materials

Certain commercial equipment, instruments, or materials are identified in this chapter to specify the experimental procedure adequately. Such identification does not imply recommendation or endorsement by the National Institute of Standards and Technology, nor does it imply that the materials or equipment identified are necessarily the best available for the purpose indicated.

2.1. Microdevice Fabrication

1. Polycarbonate (PC) sheets (McMaster-Carr, Atlanta, GA).
2. Ultraviolet (UV) transparent poly(methyl methacrylate) (PMMA) sheets (Acrylite OP-4; Cryo, Mt. Arlington, NJ).
3. Excimer laser ablation system (LMT-4000; Potomac Photonics, Lanham, MD).

2.2. Surface Treatment

1. 3-Methacryloxypropyltrimethoxysilane (BindSilane; Pharmacia Biotech, Piscataway, NJ).
2. UV/O₃ cleaner (UVOCS, Montgomeryville, PA).

2.3. Hydrogel Photopolymerization

1. Monomer: acrylamide/bis-acrylamide (19:1) monomer solution (nominally 40 g/L).
2. Catalyst: tetraethyl-methylenediamine (TEMED) (Aldrich, Milwaukee, WI).
3. Photoinitiator: riboflavin (light sensitive).
4. 1X Phosphate buffer (pH 7.20).
5. Fluoresbrite Polychromatic Red 1.0- μ m beads, 2.67% solids (Polysciences, Warrington, PA).
6. Antibody: anti-bovine albumin immunoglobulin G (IgG) (Sigma-Aldrich, St. Louis, MO).
7. Fluorescein isothiocyanate (FITC) (for hydrogel characterization).
8. Human IgG clone (FITC conjugate) (for hydrogel characterization).
9. Research-grade fluorescence microscope (Leica DM LB).

2.4. Antigen Capture and Analysis

1. Complement antigen: bovine serum albumin (BSA), FITC conjugate.
2. Noncomplement antigen: human prostatic acid phosphatase (PAP)-purified protein.
3. Platinum electrodes and power supply (Sorensen).

3. Methods

The following methods entail fabrication of the hybrid PC/PMMA microdevice, surface treatment of the microchannels, photopolymerization of the hydrogels, and antigen capture and analysis. Details are provided here for the hydrogel immobilization of antibodies for implementation in immunoassays, with less emphasis on laser ablation of microchannels. Laser ablation as a fabrication technique is described elsewhere (52,53) and also in Chapter 5.

3.1. Microdevice Fabrication

Hybrid PC/PMMA microdevices are used in this work. The PC and PMMA sheets are cut into 1 \times 3 in. sections by first scoring the sheets on a cutting board (*see Note 1*). PC is used as the microchannel substrate owing to its compatibility with the wavelength of the ablation system and the favorable smooth-

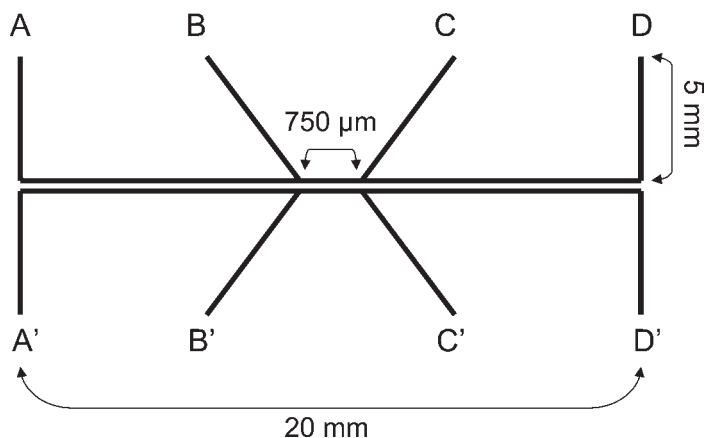


Fig. 1. Microchannel pattern.

ness and shape of the resulting channels. The PMMA lid is chosen owing to its optical transparency in both the wavelength region used for photopolymerization of the hydrogels and the wavelength region of fluorescence detection. The protective polymer film is removed from the PC base before laser ablation of microchannels. In the PMMA lid, well reservoirs are mechanically drilled before removing the protective film using a benchtop drill press (*see Note 2*).

3.1.1. Laser Ablation of Microchannels

Microchannels are ablated in PC bases (*see Note 3*). (*See Fig. 1* for a schematic of the configuration of the microchannels.) Briefly, the 248-nm excimer laser system used (LMT-4000; Potomac Photonics) contains a laser light source, a circular aperture (1.5-mm diameter) for shaping and reducing the size of the beam, a focusing lens (10 \times compound), a visible light source, a charge-coupled device (CCD) camera to image the ablation process, and a computer-controlled x - y stage equipped with a vacuum to hold the substrate in place. Nitrogen is swept over the ablation surface using a gas nozzle and a vacuum nozzle located opposite is used to remove debris. The frequency of pulses is set to 200 Hz, with a constant pulse of 7 ns. To form the channels, a motion program is written using simple movement commands to move the sample stage with respect to the laser beam linearly at a rate of 0.5 mm/s on the x - y stage (*see Note 4*). Each microchannel is thus written eight times to form channels that are approx 50 μ m wide and 95 μ m deep with slightly rounded bottoms.

3.1.2. Microdevice Assembly

After ablation, any remaining ablated material is removed by gently wiping with an EtOH damp tissue and rinsing. The PC base is then sonicated in a 1:1 solution of EtOH:H₂O for 30 min. The two components (PC base and PMMA lid) are clamped together between glass plates and thermally bonded at 103°C for 30 min in a circulating air oven (*see Note 5*). Devices can be reused (*see Note 6*).

3.2. Surface Treatment

The laser-ablated microchannels are treated for better adhesion of the hydrogel within the microfluidic channel by placing the assembled device in a UV/O₃ cleaner for 20 min (*54*). Immediately afterward, the channels are filled with a solution of 3-methacryloxypropyltrimethoxysilane and allowed to stand for approx 2 h at room temperature (*see Note 7*). The microchannels are then copiously rinsed with 18 M Ω -cm of water to remove unreacted silane and stored dry until use.

3.3. Hydrogel Photopolymerization

In general, hydrogels are formed by photopolymerization of a solution of acrylamide/bisacrylamide monomer (10 g/L of monomer, 2.5 g/L of crosslinker—equivalent to a “10T2.5C” polyacrylamide gel), riboflavin (15 μ mol/L), and TEMED (10 mmol/L). For antibody entrapment, the desired antibody is added to the monomer solution before introduction to the microfluidic channels. For characterization of either blank or antibody hydrogels, FITC or FITC-labeled antibody, respectively, is instead included in the monomer solution.

For *in situ* photopolymerization, monomer solution is added first to one well reservoir and then to fill all the microchannels using manual pressure. Before exposure to UV light and photoinitiation, fluid flow is minimized in all channels by balancing the volume in the well reservoirs using Fluoresbrite beads (0.00007%), which are added to the monomer solution for visualization (*see Note 8*). To effect photopolymerization, a square-shaped aperture is used to optically define an area for illumination at 340–380 nm by a mercury arc lamp (*see Fig. 2*). After polymerization, fluidic channels are rinsed and filled with buffer (*see Fig. 3* and *Note 9*). Devices are sealed with Parafilm and refrigerated until use.

3.4. Antigen Capture and Analysis

To test for antigen capture, hydrogels are electrokinetically filled with the antigen sample (0.26 g/L of BSA in phosphate buffer), allowed to incubate, then subjected to electrophoresis with fresh buffer (*see Figs. 1* and *4* and *Note*

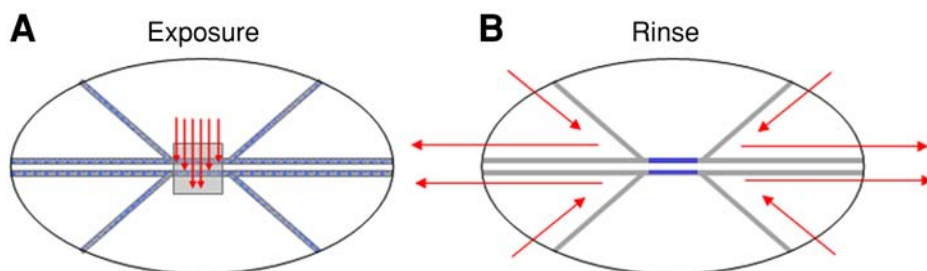


Fig. 2. Photopolymerization of hydrogels: (A) exposure; (B) rinse.

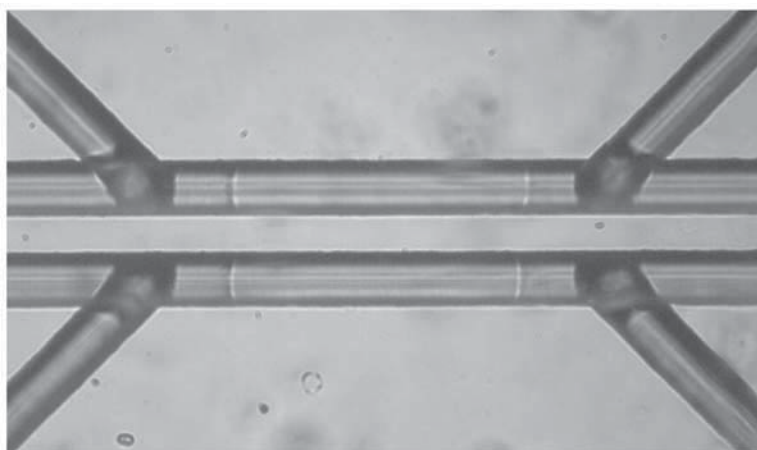


Fig. 3. Bright-field image of blank hydrogels.

10). First, antigen samples are placed in well A and all the other wells contain neat phosphate buffer. To electrokinetically load the hydrogel with sample, platinum electrodes are placed in wells A and D and connected to a 40-V power supply (Sorensen). Wells B and C are left “floating.” In this manner, the hydrogel is electrokinetically filled with the sample solution at 40 V for 5 min at room temperature, then allowed to stand at room temperature in the dark for 30 min. After incubation, microchannels AB and CD are rinsed well with buffer using pressure-driven flow. The hydrogels are then subjected to a 40-V electrokinetic rinse with buffer solution.

The capture of fluorescently labeled antigens in the hydrogel plugs is detected by fluorescence imaging of hydrogel plugs using a Leica DM LB fluorescence microscope equipped with a 10× objective, mercury arc lamp, appropriate filters, and a gray-scale CCD camera. Fluorescence images are captured during

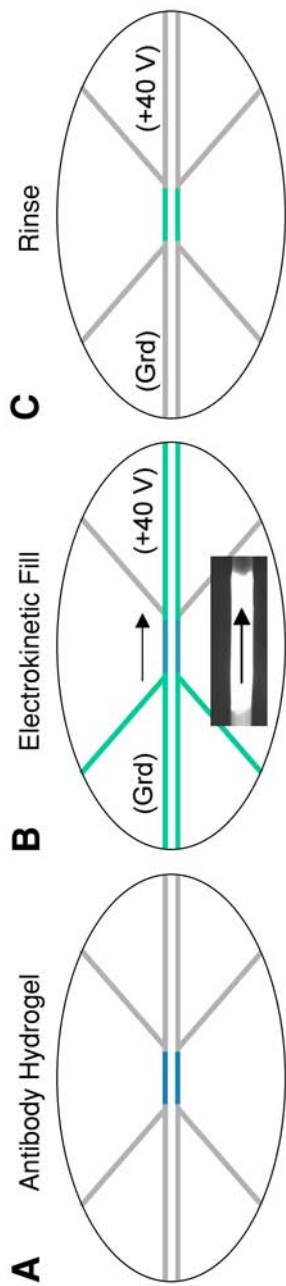


Fig. 4. Antigen capture: (A) antibody hydrogels; (B) electrokinetic filling of hydrogels with Fluorescein isothiocyanate (FITC) labeled sample (inset shows electrokinetic filling of anti-bovine serum albumin [BSA] hydrogel with FITC-BSA); (C) manual rinse of microchannels and electrokinetic rinse of hydrogels with phosphate buffer. Grd, ground.

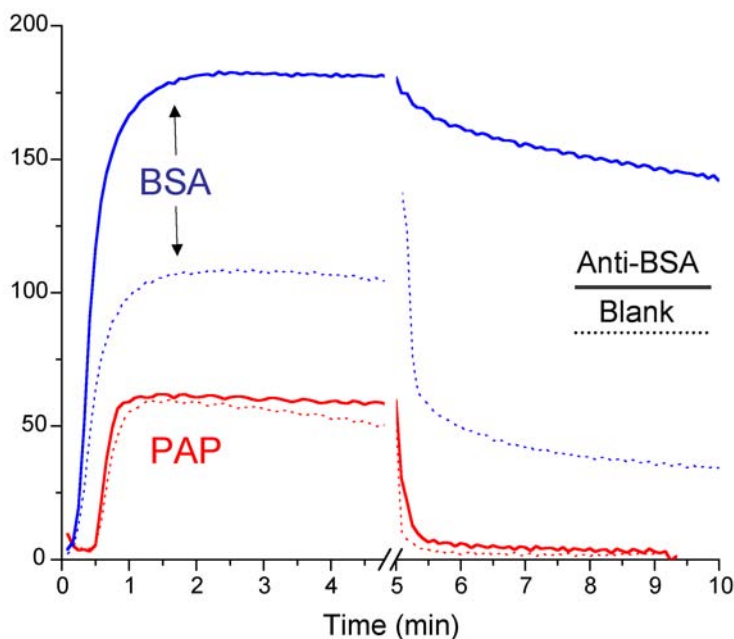


Fig. 5. Analysis of bovine serum albumin (BSA) and prostatic acid phosphatase (PAP) samples on anti-BSA and blank hydrogels.

electrokinetic filling and rinsing of the hydrogels using digital “frame-grabber” software (Scion Image, Frederick, MD) (*see Note 11*). For analysis, the fluorescence intensity of the hydrogels is digitally analyzed, frame by frame, to monitor capture of antigen.

Using this method, selective and quantitative capture of BSA (over human PAP, a noncomplementary protein of similar size) is possible using anti-BSA hydrogels (55) (*see Fig. 5*). The hydrogels are also able to concentrate trace levels of analyte for enhanced detection relative to solution-phase measurements. Although some nonspecific binding of BSA to blank hydrogels is observed, signal-to-background levels are significant. It is expected that this method can be adapted to other models by optimizing the hydrogel composition (total acrylamide, total crosslinking agent, polymerization time, buffer, and temperature).

4. Notes

1. The rough edges of devices cut from scored sheets or saws can be smoothed to a clear, transparent edge by lightly sanding first with rough-grit sandpaper, followed by sanding using a finer grit. Proper safety procedures should be exercised in operating cutting boards and power tools.

2. Mechanical drilling with the protective film intact results in less breakthrough in the underside of the device and cleaner edges in the well reservoir.
3. Laser light may permanently damage vision. Ensure that all personnel have undergone training in laser safety and that all safety protocols are followed. *Always* wear goggles approved for the wavelength of laser emission.
4. Decreases in laser power over the ablation process can result in channels of varying depth. The program can be devised to write the microchannels in an appropriate order and manner in order to normalize power fluctuations throughout the device.
5. Thermal annealing of the lid can be accomplished under light pressure in a hydraulic press with heated plates, or by clamping the device components between microscope slides using metal office binder clips in an oven.
6. Devices can be reused by physically delaminating the base and lid and dissolving the hydrogel using a 1.0 M NaOH solution for 30 min to 1 h. It is recommended that new PMMA lids be used for each device.
7. A disposable plastic syringe fitted with a short bit of rubber tubing works well for moving fluids through microchannels. The fluid is first placed in the well reservoir using a micropipettor. The syringe is applied to the top of the device such that the tubing forms an airtight seal around the well. The plunger is depressed to apply manual pressure. Conversely, vacuum can be applied to one well to draw fluid through microchannels from another well.
8. Flow can be minimized in the microfluidic channels by adding/removing solution from wells using a micropipettor while observing the Fluoresbrite beads using the microscope, or by filling the device and allowing it to stand until the wells are level and siphoning ceases.
9. A higher degree of polymerization and/or crosslinking at the horizontal ends of the gel plugs is often noticeable. This may be attributed to diffusion of monomer and crosslinking agent into the optically defined polymerization zone during polymerization.
10. Care should be taken to avoid bubbles, which can be observed or indicated by fluctuations in current. Often bubbles can become trapped at the edge of the hydrogel but are easily dislodged by thorough pressure-driven flow using buffer. In this work, the current in the microchannels was monitored by using a voltmeter to measure the voltage drop across a 100-k Ω resistor connected to the power supply in series with the microchannel.
11. To minimize photobleaching of the fluorophore during image acquisition, the shutter to the light source should be left closed and opened for image acquisition at established intervals.

Acknowledgments

We thank Drs. Kim Olsen and Rebecca Zangmeister for valuable conversations and technical contributions to this work. We also thank the National Research Council and the National Institute of Standards and Technology for a postdoctoral fellowship that supported this work.

References

1. Yalow, R. S. and Berson, S. A. (1959) Assay of plasma insulin in human subjects by immunological methods. *Nature* **184**, 1648–1649.
2. Clarke, W. (2004) Immunoassays for therapeutic drug monitoring and clinical toxicology, in *Handbook of Analytical Separations* (Hempel, G., ed.), Elsevier Science, Amsterdam, the Netherlands, pp. 95–112.
3. Peruski, A. H. and Peruski, L. F. Jr. (2003) Immunological methods for detection and identification of infectious disease and biological warfare agents. *Clin. Diagn. Lab. Immunol.* **10**, 506–513.
4. Oliva, A. G., Cruz, H. J., and Rosa, C. C. (2001) Immunosensors for diagnostics. *Sens. Update* **9**, 283–312.
5. Gosling, J. P. and Basso, L. V., eds. (1994) *Immunoassay: Laboratory Analysis and Clinical Applications*, Butterworth-Heinemann, Boston, MA.
6. Clausen, C. A. and Green, F. III. (1997) Antibody-mediated immunochemistry and immunoassay in plant-related diseases, in *Methods in Plant Biochemistry and Molecular Biology*, CRC Press, Boca Raton, FL, pp. 73–88.
7. Work, T. S. and Work, E., eds. (1982) *Laboratory Techniques in Biochemistry and Molecular Biology: An Introduction to Radioimmunoassay and Related Techniques*. Vol. 6, Pt. 2, 2nd ed., Elsevier, Amsterdam, the Netherlands.
8. Woodhead, J. S. and Thompson, R.J. (1981) Immunological techniques in biochemical investigation. *Methods Neurobiol.* **1**, 425–454.
9. Lee, J. W. and Colburn, W. A. (2002) Immunoassay techniques. *Drugs Pharm. Sci.* **117**, 225–312.
10. Widdop, B. (2001) Drugs of abuse, in *Immunoassay Handbook*, 2nd ed. (Wild, D., ed.), Nature Publishing Group, London, UK, pp. 781–816.
11. Findlay, J. W. A., Smith, W. C., Lee, J. W., et al. (2000) Validation of immunoassays for bioanalysis: a pharmaceutical industry perspective. *J. Pharm. Biomed. Anal.* **21**, 1249–1273.
12. Cook, C. E. (1992) New approaches in immunoassay techniques. *Top. Pharm. Sci. 1991, Proc. Int. Congr. Pharm. Sci. International Pharmaceutical Federation (F.I.P.)*, 51st pp. 295–305.
13. Knopp, D. and Niessner, R. (2004) Biomonitors based on immunological principles, in *Solid Wastes: Assessment, Monitoring and Remediation* (Twardowska, T., Allen, H., Kettrup, A., and Lacy, W., eds.), Elsevier Science, Amsterdam, the Netherlands, pp. 505–537.
14. Schneider, R. J. (2003) Environmental immunoassays. *Anal. Bioanal. Chem.* **375**, 44–46.
15. Mallat, E., Barcelo, D., Barzen, C., Gauglitz, G., and Abuknesha, R. (2001) Immunosensors for pesticide determination in natural waters. *Trends Analyt. Chem.* **20**, 124–132.
16. Van Emon, J. M. (2001) Immunochemical applications in environmental science. *J. AOAC Int.* **84**, 125–133.
17. Lee, N. A. and Kennedy, I. R. (2001) Environmental monitoring of pesticides by immunoanalytical techniques: validation, current status, and future perspectives. *J. AOAC Int.* **84**, 1393–1406.

18. Kaufman, B. M. (1996) Applications of immunoassay to pesticide analysis, in *Progress in Food Contaminant Analysis* (Gilbert, J., ed.), Blackie Academic and Professional, London, UK, pp.187–218.
19. Aga, D. S. and Thurman, E. M. (1997) Environmental immunoassays: alternative techniques for soil and water analysis. *ACS Symp. Ser.* **657**, 1–20.
20. Stanker, L. H., Watkins, B. E., and Vanderlaan, M. (1991) *Environmental monitoring by immunoassay*. Pesticide Chemistry: Advances in international research, development, and legislation: proceedings of the Seventh International Congress of Pesticide Chemistry (IUPAC), Hamburg, 1990.
21. Ekins, R. (1993) Principles of immunoassays: principles of non-competitive methods. *Methods Immunol. Anal.* **1**, 227–257.
22. Wengatz, I., Harris, A. S., Gilman, S. D., et al. (1996) Recent developments in immunoassays and related methods for the detection of xenobiotics. *ACS Symp. Ser.* **646**, 110–126.
23. Fukal, L. and Kas, J. (1989) The advantages of immunoassay in food analysis. *Trends Anal. Chem.* **8**, 112–116.
24. Wild, D., ed. (2001) *The Immunoassay Handbook, 2nd ed.*, Nature Publishing Group, London, UK.
25. Deshpande, S. S., ed. (1996) *Enzyme Immunoassays: From Concept to Product Development*, Chapman and Hall, New York, NY.
26. Ngo, T. T. (1985) Enzyme mediated immunoassay: an overview, in *Enzyme-Mediated Immunoassay* (Ngo, T. T. and Lenhoff, H. M., ed.), Plenum Publishing, New York, NY, pp. 3–32.
27. Ullman, E. F. (2001) Homogeneous immunoassays, in *Immunoassay Handbook, 2nd ed.* (Wild, D., ed.), Nature Publishing Group, London, UK, pp. 177–197.
28. Ullman, E. F. (1999) Homogeneous immunoassays: historical perspective and future promise. *J. Chem. Educ.* **76**, 781–788.
29. Maiolini, R. (1987) Homogeneous phase immunoassays. *Technique Biologie* **13**, 108–117.
30. Wild, D. (2001) Separation systems, in *Immunoassay Handbook, 2nd ed.* (Wild, D., ed.), Nature Publishing Group, London, UK, pp. 149–158.
31. Singh, A. K., Kilpatrick, P. K., and Carbonell, R. G. (1996) Application of antibody and fluorophore-derivatized liposomes to heterogeneous immunoassays for d-dimer. *Biotechnol. Prog.* **12**, 272–280.
32. Guebitz, G. and Shellum, C. (1993) Flow-injection immunoassays. *Anal. Chim. Acta* **283**, 421–428.
33. Truchaud, A., Barclay, J., Yvert, J. P., and Capolaghi, B. (1991) Automated separation for heterogeneous immunoassays. *J. Auto. Methods Manage. Chem.* **13**, 49–51.
34. Edwards, J. C. and Moon, C. R. (1990) Enhanced detection systems for enzyme-linked heterogeneous immunoassays: luminescence. *Immunol. Ser.* **53**, 95–106.
35. Erickson, D. and Li, D. (2004) Integrated microfluidic devices. *Anal. Chim. Acta* **507**, 11–26.
36. Sia, S. K. and Whitesides, G. M. (2003) Microfluidic devices fabricated in poly(dimethylsiloxane) for biological studies. *Electrophoresis* **24**, 3563–3576.

37. Hatch, A., Weigl, B. H., Zebert, D., and Yager, P. (1999) Microfluidic approaches to immunoassays. *Proceedings of SPIE-The International Society for Optical Engineering* **3877**, 169–172.
38. Sato, K., Tokeshi, M., Odake, T., et al. (2000) Integration of an immunosorbent assay system: analysis of secretory human immunoglobulin A on polystyrene beads in a microchip. *Anal. Chem.* **72**, 1144–1147.
39. Wang, J., Ibanez, A., and Chatrathi, M. P. (2002) Microchip-based amperometric immunoassays using redox tracers. *Electrophoresis* **23**, 3744–3749.
40. Wang, J., Ibanez, A., Chatrathi, M. P., and Escarpa, A. (2001) Electrochemical enzyme immunoassays on microchip platforms. *Anal. Chem.* **73**, 5323–5327.
41. Wang, J., Ibanez, A., and Prakash Chatrathi, M. (2003) On-chip integration of enzyme and immunoassays: simultaneous measurements of insulin and glucose. *J. Am. Chem. Soc.* **125**, 8444–8445.
42. Sato, K., Tokeshi, M., Kimura, H., and Kitamori, T. (2001) Determination of carcinoembryonic antigen in human sera by integrated bead-bed immunoassay in a microchip for cancer diagnosis. *Anal. Chem.* **73**, 1213–1218.
43. Chiem, N. H. and Harrison, D. J. (1998) Microchip systems for immunoassay: an integrated immunoreactor with electrophoretic separation for serum theophylline determination. *Clin. Chem.* **44**, 591–598.
44. Chiem, N. and Harrison, D. J. (1997) Microchip-based capillary electrophoresis for immunoassays: analysis of monoclonal antibodies and theophylline. *Anal. Chem.* **69**, 373–378.
45. Bernard, A., Michel, B., and Delamarche, E. (2001) Micromosaic immunoassays. *Anal. Chem.* **73**, 8–12.
46. Cheng, S. B., Skinner, C. D., Taylor, J., et al. (2001) Development of a multichannel microfluidic analysis system employing affinity capillary electrophoresis for immunoassay. *Anal. Chem.* **73**, 1472–1479.
47. Buechler, K. F., Mcpherson, P., Anderberg, J., Nakamura, K., Lesefko, S., and Noar, B. (2001) Microarray immunoassays in the microfluidic Triage protein chip. *Micro Total Analysis Systems 2001, Proceedings μ TAS 2001 Symposium*, 5th, Monterey, CA, Oct. 21–25, 2001, pp. 42–44.
48. Seong, G. H., Zhan, W., and Crooks, R. M. (2002) Fabrication of microchambers defined by photopolymerized hydrogels and weirs within microfluidic systems: application to DNA hybridization. *Anal. Chem.* **74**, 3372–3377.
49. Zhan, W., Seong, G. H., and Crooks, R. M. (2002) Hydrogel-based microreactors as a functional component of microfluidic systems. *Anal. Chem.* **74**, 4647–4652.
50. Zangmeister, R. A. and Tarlov, M. J. (2004) DNA displacement assay integrated into microfluidic channels. *Anal. Chem.* **76**, 3655–3659.
51. Olsen, K. G., Ross, D. J., and Tarlov, M. J. (2002) Immobilization of DNA hydrogel plugs in microfluidic channels. *Anal. Chem.* **74**, 1436–1441.
52. Johnson, T. J., Ross, D., Gaitan, M., and Locascio, L. E. (2001) Laser modification of preformed polymer microchannels: Application to reduce band broadening around turns subject to electrokinetic flow. *Anal. Chem.* **73**, 3656–3661.

53. Waddell, E. A., Barker, S. L. R., Rose, D. J., Locascio, L. E., and Kramer, G. W. (2000) Laser ablation of polymer substrates for the fabrication of microfluidic devices. *Abstr. Pap. Am. Chem. Soc.* **220**, U91–U92.
54. Zangmeister, R. A. and Tarlov, M. J. (2003) UV graft polymerization of polyacrylamide hydrogel plugs in microfluidic channels. *Langmuir* **19**, 6901–6904.
55. Thomas, G., Locascio, L., and Tarlov, M. Hydrogel-bound antibodies for microfluidic analysis of proteins, submitted.

Polymerase Chain Reaction in Miniaturized Systems:

Big Progress in Little Devices

Kalee D. Spitzack and Victor M. Ugaz

Summary

A critical need exists for advanced technologies that enable genomic-based DNA analysis to be performed with significantly higher throughput and at a significantly lower cost than is attainable with current hardware. Miniaturized polymerase chain reaction systems offer an attractive platform to address these needs, combining the ability to perform rapid thermocycling with a portable device format that can be inexpensively mass produced. We review recent efforts aimed at developing these next-generation systems and discuss some of the practical considerations involved in adapting this technology for routine laboratory use.

Key Words: Polymerase chain reaction; DNA amplification; miniaturized systems; passivation; microfluidics; hybridization; convective-flow systems; continuous-flow systems; microfabrication.

1. Introduction

The ability to selectively amplify specific regions of interest within a larger DNA template to extremely high concentration levels is a key enabling technology in modern genomic analysis. For example, the success of the Human Genome Project has raised awareness of the value of genetic information and its potential to revolutionize the diagnosis and treatment of disease. However, a new generation of inexpensive and portable DNA analysis devices must be developed before the use of genomic data can truly become an integral part of standard medical diagnostic protocols (*1*). In addition, there is an increasing need for new and more powerful sensor technology to detect infectious disease agents and provide early warning capabilities for emerging biowarfare/bioterror threats. In each of these examples, the current inability to perform polymerase chain reaction (PCR) amplification of DNA in a rapid and inex-

From: *Methods in Molecular Biology*, vol. 321: *Microfluidic Techniques: Reviews and Protocols*
Edited by: S. D. Minton © Humana Press Inc., Totowa, NJ

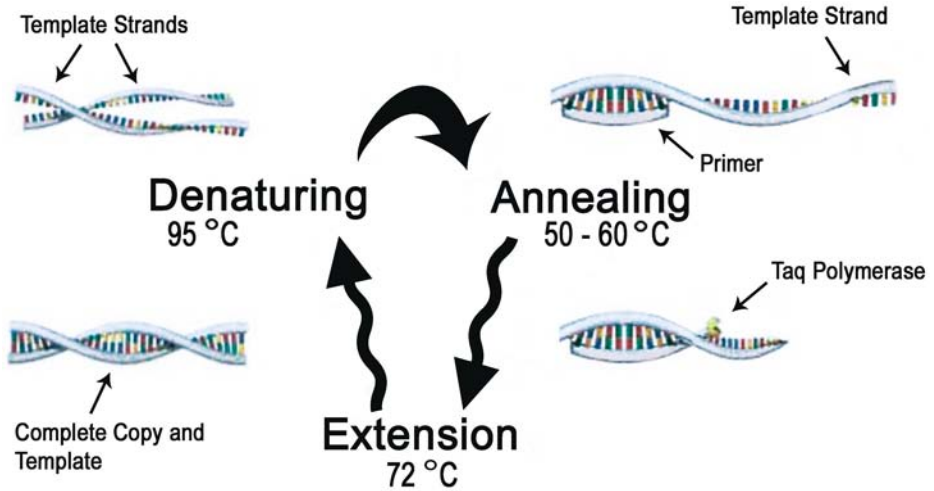


Fig. 1. Illustration of polymerase chain reaction (PCR) process. Exponential amplification of DNA is achieved by repetitively cycling the reagent mixture temperature among conditions associated with denaturing, annealing, and extension. (Adapted from ref. 48).

pensive format continues to pose significant challenges to efforts aimed at moving genomic analysis technology out of the laboratory and directly into settings where the information is most needed.

1.1. Principles of PCR Amplification

The underlying mechanics associated with PCR are fundamentally simple. A typical protocol involves first pipetting a PCR reagent cocktail (template DNA, primers, dNTPs, thermostable *Taq* polymerase enzyme, and so on) into plastic reaction tubes or multiwell plates. These tubes or plates are then inserted into a programmable thermocycling machine that repeatedly heats and cools the static reaction volume to temperatures corresponding to *denaturation* of the double-stranded target DNA (95°C), *annealing* of primers to complementary locations on the denatured single-stranded fragments (50–60°C), and enzyme-catalyzed *extension* to synthesize the complementary strands (72°C) (Fig. 1). Under ideal conditions, this scheme yields a doubling of dsDNA (double-stranded DNA) copies of the target region on completion of each cycle: $Y = (1 + x)^n$, in which Y is the copy yield, n is the number of cycles, and x is the mean efficiency per cycle. The total time required to complete one cycle of amplification includes the time over which the temperature of the reaction mixture is held constant at each temperature step (hold time), as well as the time required to heat and cool the reaction mixture between succes-

Table 1
Typical PCR Thermocycling Protocol Timescales

Step	Temperature (°C)	Hold time (s)	Reaction time
Denaturation	90–96	30–60	~Instantaneous
Annealing	55–60	30	~Instantaneous
Extension	72	60	~70 bases/s

From **ref. 2**.

sive steps (ramping time). Consequently, it is not uncommon for a 30- to 40-cycle amplification reaction to require 2 to 3 h of total time in order to reach completion, thereby imposing severe limitations on achievable throughput. Typical cycling protocols proceed according to the general steps outlined in **Table 1 (2)**, although many variations are possible to accommodate the needs of specific reaction systems.

1.2. Conventional Thermocycler Technology

The predominant thermocycler design employed in most laboratories consists of a metal heating block machined to maintain close physical contact with the reaction tubes or plates, and whose temperature is regulated by means of computer-controlled thermoelectric heaters. These systems remain popular owing to their relative simplicity; however, their attainable heating and cooling rates are restricted by the inherently high heat capacity of the thermal block itself. Moreover, because the reaction tubes or plates are constructed using plastic materials possessing relatively low thermal conductivities (e.g., polypropylene), the temperature must be held constant for a significant period of time at each step in order to allow the entire reagent volume to uniformly attain the desired temperature. These hold times are typically much longer than the timescales associated with the individual reaction processes at each step (**Table 1**).

More recent developments reflect ongoing efforts to better accommodate high-throughput operation by increasing heating and cooling rates and reducing hold times at each step in order to achieve faster cycling. One widely used scheme to accomplish this goal involves the use of thin glass microcapillaries instead of plastic reaction tubes. The principle advantage of this configuration is that it allows the reaction mixture to be distributed over a larger surface area in order to achieve more efficient heat transfer. Uniform heating and cooling can be achieved through the use of circulating airstreams (**3–7**), by encasing the capillary in silicon-resistive heaters (**8**), by fabricating heaters directly on the capillary walls (**9**), or by using non-contact-focused infrared (IR) techniques (**10**). The capillary format is also well suited for integration with downstream capillary electrophoresis (CE)-based analysis or real-time optical detection

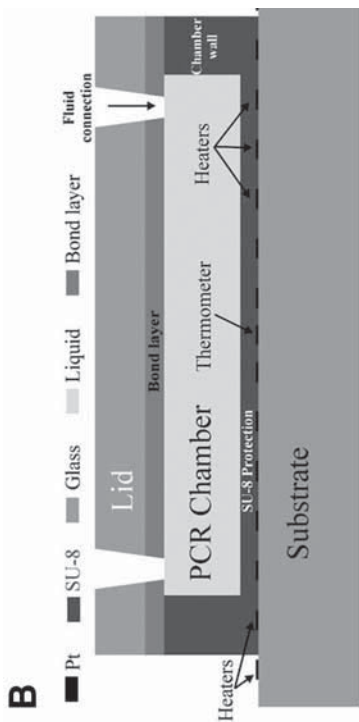
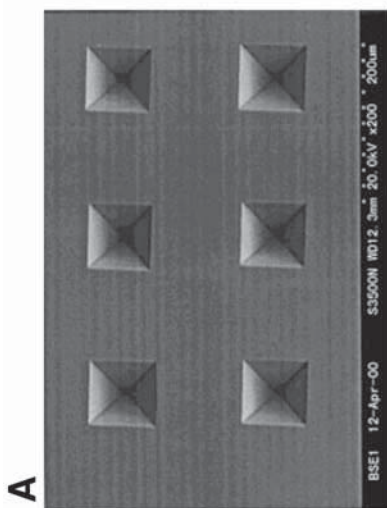
techniques. Although rapid cycle times have been demonstrated in these systems, the overall level of throughput can still be limited by issues associated with loading, sealing, and unloading the capillaries.

In this chapter, we review recent efforts aimed at developing advanced miniaturized thermocycling hardware capable of achieving even faster reaction speeds. Our goal is not only to convey the flavor of some of the exciting accomplishments that have been made to date (*11–19*), but also to highlight some of the practical considerations necessary to adapt this technology for performing routine PCR in the laboratory. To narrow the scope of the discussion, our review is limited to developments reported in refereed literature and conference proceedings, although evidence of additional progress can be found in patents and other unpublished sources.

2. PCR in Miniaturized Systems

The primary obstacle to achieving rapid PCR amplification with conventional benchtop thermocyclers is not the kinetics of the reaction itself but the substantial amount of thermal energy wasted by the need to repeatedly heat and cool hardware elements that do not actively participate in the reaction (e.g., metal thermal blocks). These difficulties have motivated recent efforts to explore the feasibility of performing PCR in miniaturized systems capable of delivering faster cycling times as a consequence of their higher surface-to-volume ratios, which provide improved heat transfer and temperature uniformity by placing more of the reaction volume in contact with the reactor walls. By virtue of their small size (typical reaction volumes range from microliters to nanoliters), miniaturized systems also offer the capability to dramatically reduce reagent consumption, thereby lowering the costs associated with performing PCR. The economic benefits of miniaturization extend even further to the hardware itself because photolithographic microfabrication techniques can be used to produce hundreds or thousands of devices at once (**Fig. 2A**), yield-

Fig. 2. (*opposite page*) Examples of microchip-based polymerase chain reaction (PCR) thermocyclers. (**A**) Scanning electron microscope image of an array of $80 \times 80 \mu\text{m}$ silicon PCR microreaction chambers. (Reproduced with permission from **ref. 44**, copyright 2001 American Chemical Society.) (**B**) Schematic cross-sectional slice of hybrid SU-8/glass PCR microchip incorporating integrated heating and temperature control circuitry. (Reproduced with permission from **ref. 50**, copyright 2004 Elsevier B.V.) (**C, D**) Portable rapid analysis thermocyclers: (**C**) Miniature Analytical Thermal Cycling Instrument (MATCI) (reproduced with permission from **ref. 64**, copyright 1998 American Chemical Society), and (**D**) Advanced Nucleic Acid Analyzer (ANAA) (reproduced with permission from **ref. 66**, copyright 1998 American Association for Clinical Chemistry).



ing per-device costs of \$1 or less. This highly desirable combination of characteristics has stimulated considerable interest in the area of microfabricated thermocycling systems. Most of these devices can be broadly categorized as either static PCR microchips (either employing an external heating source or incorporating on-chip temperature control) or dynamic continuous-flow PCR devices.

2.1. PCR Microchips

2.1.1. Design and Fabrication

Microfluidic chips capable of performing PCR are typically constructed from either glass or silicon substrates, or some combination of both. Although silicon and glass generally compare similarly in terms of price, silicon's higher thermal conductivity allows superior heating and cooling rates to be achieved, shortening the overall reaction time. Methods for depositing a variety of conductive and insulating thin films in order to construct integrated heaters and temperature sensors are also highly developed in silicon using processes adapted from the microelectronics industry, although similar methods can be applied to glass substrates as well. Silicon substrates also offer the possibility of embedding electronic circuitry to allow reaction, detection, and analysis functions to be performed within a single microchip platform (20). In terms of surface properties, both bare silicon and untreated glass surfaces typically yield poor PCR performance under high surface-to-volume conditions. Consequently, surface treatment techniques have been developed to remedy these problems in both substrates. Glass is an attractive material owing to its optical transparency, which allows visual inspection of the reaction chamber for abnormalities such as bubbling or evaporation, real-time monitoring of fluorescent probes to track reaction progress, and the use of other fluorescence-based detection schemes (e.g., CE, hybridization). In addition to devices constructed entirely from glass (21–29) or quartz (30), hybrid silicon/glass designs have been used to construct microchips with (31–38) (Fig. 2B) and without (39–45) integrated heating capabilities. The use of glass structures is not essential, however, because devices have also been constructed solely from silicon (46–48) and ceramics (49).

PCR microchips have also been constructed using plastic substrate materials such as SU-8 (a photopolymerized epoxy resin) (50), polyimide (51), or polydimethylsiloxane (PDMS) (52–55). More conventional plastics including polycarbonate (PC) (56,57) and cyclic olefins (58) have also been used and can be easily and inexpensively mass-produced using standard injection molding processes. Plastics are attractive because they offer a less expensive and easy-to-fabricate alternative, often with improved surface properties that reduce nonspe-

cific binding interactions; however, they may exhibit autofluorescence, which could interfere with the emission spectra of fluorescent probes used for optical detection. Finally, Strizhkov et al. (59) strayed from the conventional setup by conducting their PCR experiments on an array of polyacrylamide-based gel pads containing immobilized primers that enabled various targets to be amplified simultaneously.

PCR microchips can broadly be grouped into two subcategories: those requiring external temperature control (Table 2) and those incorporating integrated heating capability (Table 3). Devices without integrated heating can be thermocycled in a number of ways, including placing the microchip inside a conventional thermocycler (44,55), using custom heating and cooling fixtures (39–41,57,59–61), and even physically transporting the chip between individual heating blocks held at different temperatures (45). Fans are occasionally used to boost cooling rates in these systems (57). Rapid microchip thermocycling has also been demonstrated using focused infrared radiation as a heat source (51). Chips with integrated temperature control require additional fabrication steps for deposition of metals or other associated components onto the chip surface (Fig. 2B). These devices generally incorporate integrated feedback control systems that allow on-chip temperatures to be continuously and accurately monitored.

Aside from developments in the area of PCR microchips, advancements have been made in the design of portable stand-alone thermocycling instruments. Belgrader and colleagues and Bennett and colleagues have conducted a number of experiments using three rapid analysis thermocyclers: the Miniature Analytical Thermal Cycling Instrument (MATCI) (62–65), the Advanced Nucleic Acid Analyzer (ANAA) (66–68) (Fig. 2C), and the battery-powered Notebook Thermal Cycler (69,70). Each design features built-in silicon-based reaction chambers with integrated heating and fluorescence detection systems.

2.1.2. Surface Interactions

Reactor geometry is an important consideration in microchip-based PCR devices. While the inherently high surface-to-volume characteristic of miniaturized systems is beneficial from the standpoint of providing enhanced thermal conductivity and reduced reaction time, it can also magnify the effects of nonspecific surface interactions that act to degrade amplification efficiency. The use of ultrasmall reaction volumes also poses challenges associated with sample loading and unloading, in some cases requiring the use of specialized equipment to meter and dispense reagents accurately. Typical reaction volumes employed in PCR microdevices range between 5 and 30 μL , although experiments using smaller volumes (26,27,29,37,47,58,60,71), even down to picoliter levels (44,45) (Fig. 2A), have been reported.

Table 2
Summary of Experiments Performed Using PCR Microchips With Off-Chip Heating

Reference	Device materials	Reactor volume	Reagents	Template	Target size	Temperature (°C) ^a	Hold times ^a	Cycles/ reaction time	Analysis
39	Microfabricated chip (Si/glass)	15 μ L	AmpliTaq (0.1 U/ μ L)	Lambda DNA	500 bp	95 95, 55, 72 72	50 min 15 s, 15 s, 60 s 5 min	Not specified (3 min/cycle)	Agarose gel
40	Microfabricated chip (Si/glass)	Not specified	AmpliTaq (0.025 U/ μ L)	Lambda DNA	500 bp	94 94, —, 55 72	60 s 15 s, —, 15 s 5 min	30 cycles 58.5 min ^c	Agarose gel
41	Microfabricated chip (Si/glass) Silicon oxide layer Microfabricated chip (Si/glass) Silicon oxide layer	12 μ L	AmpliTaq (0.05 U/ μ L) AmpliTaq (0.03 U/ μ L)	Bacterial genomic Human genomic	1400 bp 100 bp	94 94, 55, 72 72 94 94, 53, 65 65	60 s 15 s, 60 s, 60 s 10 min 6 min 30 s, 30 s, 120 s 5 min	28 cycles 1 h 14 min ^d 35 cycles 1 h 54 min ^d	Agarose gel Agarose gel
42	Microfabricated chip (Si/glass)	12 μ L	Triton X-100 Taqstart antibody AmpliTaq (0.1 U/ μ L)	Human genomic Multiplex: Human genomic amplicons	1–2 kb 500– 1300 bp	94 94, 30/59, 72 94 94, 63, 65 65	8 min 60 s, 60 s, 180 s 5 min 10 s, 60 s, 60 s 10 min	8/28 cycles 3 h 8 min ^d 30 cycles 1 h 18 min ^d	CE (on-chip) CE (on-chip)
60	Microfabricated chip (Si/acrylic-based tape) Silicon oxide layer	0.5, 1, 2, 5.9 μ L	BSA AmpliTaq Gold (0.025–0.25 U/ μ L)	Human genomic	297 bp	50, 95 95, —, 60 72	2 min, 10 min 15 s, —, 60 s indefinitely	40 cycles 1 h 2 min ^d	Fluorescent probe
59	MAGIchip with polyacrylamide-based gel pads Quartz glass cover	30 μ L	BSA Stoffel Fragment (0.17 U/ μ L)	Bacterial genomic fragment	Not specified	95 95, 51–71, 72	120 s 30 s, 60 s, 40 s	25–35 cycles 56–78 min ^d	Agarose gel

44	Microfabricated chip (Si/glass) Silicon oxide layer	1.3 pL to 32 μ L	BSA AmpliTaq Gold (0.025 U/ μ L)	Plasmid DNA fragment	Not specified	95, 55, 72	60 s 60 s, 60 s, 60 s	40 cycles 2 h ^d	Fluorescent probe
45	Microfabricated chip (Si/glass) Silicon oxide layer	85 pL	BSA AmpliTaq Gold (0.025 U/ μ L)	Plasmid DNA fragment	100 bp	95, 55, 72	5 s, 5 s, 10 s	40 cycles 18 min	Agarose gel
51	Microfabricated chip (polyimide) IR heating	1.7 μ L	PEG AmpliTaq (0.2 U/ μ L)	Lambda DNA	500 bp	94, 68, 72, 72	10 s 2 s, 2 s, 2 s 10 s	15 cycles 200 s	CE
57	Microfabricated chip (PC plastic)	40 μ L	PEG BSA AmpliTaq (0.125 U/ μ L)	Bacterial genomic fragment	221 bp	94, 55, 72, 72	4 min 30 s, 30 s, 30 s 3 min	30 cycles 61 min ^c	Fluorescent probe
55	Microfabricated chip (PDMS)	Not specified	Dynazyme II (0.1 U/rxn ^b)	1.8 kb fragment	294 bp	50, 96, 96, —, 60	2 min, 1 min 20 s, —, 40 s	30 cycles ~1 h	Agarose gel

^aReaction temperatures are listed in the following format: denaturing, annealing, and extension. Omission of an annealing temperature indicates that a two-temperature cycling protocol was used. Preheating and final-extension temperatures are listed above and below the reaction temperatures, respectively. Reaction hold times are listed in the same order.

^bNeither a reactor volume nor a master mixture volume was given to determine the concentration in units per microliter.

^cTotal reaction time was calculated based on reported data for the total number of cycles, hold times, and ramp rates.

^dTotal reaction time was calculated based on reported data for the total number of cycles and hold times.

Table 3
Summary of Experiments Performed Using PCR Microchips Incorporating On-Chip Heating and Temperature Control

Reference	Device materials	Reactor volume	Reagents	Template	Target size	Temperature (°C) ^a	Hold times ^a	Cycles/ reaction time	Analysis
31	Microfabricated chip (Si/glass) Silicon rubber as chamber sealant	50 µL	AmpliTaq (0.025 U/µL)	M13 clone	142 bp	Not specified	Not specified	20 cycles 20 min	Agarose gel
46	Microfabricated chip (Si)	Not specified	AmpliTaq (0.025 U/µL)	M13 clone	268 bp	95, 65, 72	Not specified	23–31 cycles	Agarose gel
33	Microfabricated chip (Si/glass) Silicon oxide layer	5–10 µL	AmpliTaq (0.133 U/µL)	500 bp fragment	Not specified	93, 50, 70	Not specified	30 cycles 25 min	Agarose gel
64	MATCI	50 µL	AmpliTaq (0.1 U/µL) AmpliTaq (0.05 U/µL)	Human genomic 403 bp fragment	294 bp 369 bp, 321 bp	96 96, 55, 72 97, 42/48, 72	180 s 15 s, 15 s, 60 s 5 s, 10 s, 10 s	40 cycles 1 h 19 min 8, 29 cycles 25 min	Fluorescent probe Fluorescent probe
47	Microfabricated chip (Si) Silicon oxide layer BSA surface treatment	1.5 µL	AmpliTaq (0.01 U/µL)	Plasmid DNA	260 bp	94 94, 55, 72 72	60 s 5 s, 7 s, 5 s 60 s	30 cycles 10.5 min ^c	Agarose gel
62	MATCI Polypropylene insert	25 µL	BSA Taq Gold (0.16 U/µL)	Not specified	Not specified	94 94, 60, 72 72	30 s 30 s, 30 s, 30 s 10 min	30 cycles 1 h 15 min	Fluorescent probe
63	MATCI	25 µL	AmpliTaq (0.1 U/µL)	Not specified	266–281 bp 73 bp	94 94, 50, 72	30 s 2 s, 10 s, 10 s	40 cycles 20–30 min	Fluorescent probe
65	MATCI Polypropylene insert	18 µL	Pfu (0.02 U/µL)	Not specified	69 bp	94, 64, 72	4 s, 15 s, 15 s	Not specified ~35 min	Mass spectrometry
66	ANAA Polypropylene insert	25 µL	AmpliTaq (0.05 U/µL)	Not specified	Not specified	95 94, —, 60	30 s 4 s,—, 19/30 s	50 cycles 19.6– 28.8 min ^c	Fluorescent probe

67	ANAA	25 μ L	AmpliTaq (0.05 U/ μ L)	Bacterial spores	Not specified	95 95, —, 60	15 s 4 s, —, 10 s	50 cycles 12 min ^c	Fluorescent probe
68	ANAA	25 μ L	AmpliTaq (0.01 U/ μ L)	Not specified	Not specified	96 96, —, 56	15 s 1–4 s, —, 1–19 s	40 cycles 11.3– 25.3 min	Fluorescent probe
69	Battery-powered Notebook Thermal Cycler	100 μ L	Platinum Taq (0.05 U/ μ L)	Multiplex: bacterial spores	Not specified	95 95, —, 60	30 s 1 s, —, 6 s	45 cycles 19 min ^d	Fluorescent probe
34	Polypropylene walls	25 μ L	Platinum Taq (0.05 U/ μ L)	Human genomic	Not specified	95 95, —, 60	30 s 3 s, —, 20 s	45 cycles 17.8 min ^c	Fluorescent probe
	Microfabricated chip (Si/glass)	8 μ L	BSA AmpliTaq (0.25 U/ μ L)	3.9 kb fragment	300, 340, 500, 600 bp	95 95, 55, 72 72	4 min 30 s, 30 s, 60 s 5 min	35 cycles 1 h 27 min ^d	Agarose gel
	Silicon oxide or polymer coating								
37	Microfabricated chip (Si/glass)	3.6 μ L	Triton X-100 AmpliTaq (1.25 U/ μ L)	Plasmid DNA	323 bp	95 95, 55, 72 72	2 min 30 s, 30 s, 60 s 7 min	30 cycles 1 h 11 min ^d	Agarose gel
	Silicon oxide layer								
50	Microfabricated chip (SU-8/glass)	20 μ L	Hot start (conc. not given) ^b AmpliTaq (0.05 U/ μ L)	Yeast genomic	199 bp fragment	94 94, 59, 72 72	10 min 30 s, 30 s, 60 s 10 min	35 cycles 1 h 31 min ^d	CE (off-chip)
	Microfabricated chip (SU-8/glass)	20 μ L	AmpliTaq (0.05 U/ μ L)	Bacterial genomic fragment	Not specified	94 94, 45, 72 72	5 min 60 s, 60 s, 180 s 10 min	40 cycles 3 h 36 min ^d	CE (off-chip)
	Pretreatment with dichloromethylsilane								

^aReaction temperatures are listed in the following format: denaturing, annealing, and extension. Omission of an annealing temperature indicates that a two-temperature cycling protocol was used. Preheating and final-extension temperatures are listed above and below the reaction temperatures, respectively. Reaction hold times are listed in the same order.

^bNeither a reactor volume nor a master mixture volume was given to determine the concentration in units per microliter.

^cTotal reaction time was calculated based on reported data for the total number of cycles, hold times, and ramp rates.

^dTotal reaction time was calculated based on reported data for the total number of cycles and hold times.

Reagent additives are sometimes also used in microscale PCR in order to reduce unfavorable surface interactions at the reactor walls and provide improved performance. These additives are intended to preferentially complex with or neutralize nonspecific surface binding sites, leaving the PCR reagents unaffected and available to participate in the amplification process. The most commonly used “blocking” additives include bovine serum albumin (BSA) (10,22–29,34,35,44,45,53,57–62,72,73), polyethylene glycol (PEG) (51,57), and polyvinyl pyrrolidone (PVP) (21,28). The inner surfaces of the reaction chamber can also be prerinsed with these substances prior to the reaction as an alternative means of reducing undesirable surface effects (25,38,47,52,58). Other common reagent additives include surfactants such as Tween-20 (21,28,30,35) and Triton X-100 (28,37,38,42,61,72). These “enhancers” have been found to improve reaction performance in both microdevices and conventional benchtop-scale thermocyclers by creating a more favorable chemical environment for the PCR process. Finally, surface effects can also be dealt with by increasing the amount of enzyme added to the reaction mixture in order to compensate for the loss in amplification efficiency owing to the nonspecific binding interactions. Although this technique is effective, the relatively high cost of *Taq* polymerase makes it a less favorable passivation approach.

The importance of surface chemistry in microscale PCR and the passivation techniques used to minimize the adverse effects of nonspecific interactions at the reactor walls cannot be overstated (48,74–79). One way to combat these unfavorable interactions involves chemically altering the surfaces in contact with the PCR reagents using oxide or silane treatments. Deposition of a silicon oxide (SiO_2) layer is the most effective passivation technique for silicon surfaces (34,37,43,47), and silane layers (dichloromethylsilane, chlorotrimethylsilane, hexamethyldisilazane) are often employed for passivation of glass surfaces (21,28,30,35,50,80). Quite often, blocking agents are still added to the reaction mixture even after chemical passivation of the reactor surfaces has been performed in order to further ensure that unfavorable surface interactions are minimized (21,28,34,35,37,44,45,60). In some instruments, chemically inert inserts such as polypropylene liners are placed inside silicon reaction chambers in order to provide surface passivation (32,62,65,66,69).

2.1.3. Reagents

Successful PCR results have been reported using a wide range of template and target amplicon sizes. Generally, shorter DNA strands can be expected to allow the most rapid amplification owing to favorable kinetics associated with the denaturation and extension phases of the process. Although they are useful for device characterization studies, experiments focused solely on amplification of short fragments can yield data that may potentially lead to incorrect presumptions about reaction speed. Fortunately, most experiments have been

conducted using biologically relevant templates including plasmid DNA, genomic DNA, and lambda phage DNA, with target sizes ranging from 100 to 2000 bp. The number of template copies initially present also influences the efficiency and kinetics of PCR. For example, aliquots of amplified target DNA may be added to the reaction cocktail in order to improve the final product yield (81).

The choice of enzyme also plays a crucial role in miniaturized PCR systems, and researchers have experimented with different varieties and concentrations in order to optimize reaction performance. Conventional *Taq* polymerase (e.g., AmpliTaq) is the most common enzyme; however, *Pfu* (65), *Tth* (56,72), and Stoffel fragment (59) varieties have also been used successfully. Generally speaking, these enzymes provide similar results, although factors such as enhanced temperature stability (e.g., AmpliTaq Stoffel fragment) can be advantageous in allowing more latitude with device temperature control. Experiments have also been run using “hot-start” enzymes (e.g., AmpliTaq Gold, Platinum Taq), whose activity is triggered after an initial high-temperature activation period lasting between 30 s and 10 min (29,44,45,50,54,58,60,62,69). These enzymes offer the benefit of a reduced likelihood of nonspecific product formation prior to beginning the reaction. Similar results can be obtained by including TaqStart antibody in the reaction mixture (42,43). Because enzymes are relatively expensive and represent one of the primary costs associated with performing PCR, it is desirable to maintain standard concentration levels in the reaction mixture (approx 0.025–0.05 U/ μ L, although successful runs have been reported with enzyme concentrations as low as 0.01 U/ μ L [47]). Increasing the amount of enzyme to improve performance or compensate for unfavorable surface interactions (concentrations as high as 1.25 U/ μ L have been used [37]) tends to counteract some of the benefits of miniaturization (e.g., reduced reagent consumption) and is, therefore, usually an unattractive option.

2.1.4. Operational Parameters

In terms of device operation, the main parameters available to control the reaction are the temperature settings, hold times at each temperature, and total number of cycles. Temperature settings are typically varied within a limited range around a denaturing temperature of 95°C, an annealing temperature of 60°C, and an extension temperature of 72°C. The choice of annealing temperature offers the most flexibility depending on the choice of primers used in the reaction. A common variation employed in a number of systems is a two-temperature protocol, in which the annealing and extension steps are combined at a single temperature (8,30,38,54,55,60,66–69). An initial preheating step may be included in order to ensure complete template denaturation and/or activate hot-start enzymes (22–24,27,29,34,36–44,47,50,51,55,57–60,62–64,66–69,73). Similarly, an additional extension period of several minutes is sometimes added to allow final replication of incomplete copies (22–24,34,37–44,

47,50,51,57–60,62,73). “Touchdown” protocols in which the annealing temperature is gradually reduced during the course of the reaction to improve specificity have also been employed (24,27,29).

The choice of hold time depends on several parameters including heating/cooling rates and thermal conductivity of the reaction chamber (82–85). The highly efficient heat transfer characteristics associated with miniaturized systems normally allow hold times to be substantially reduced compared with conventional benchtop thermocyclers, resulting in much shorter total reaction times. Whereas conventional thermocyclers can take up to 2–3 h to complete a reaction, similar results can be achieved in 10–30 min using PCR microdevices (29,31–33,38,45,47,63,64,66,67,69). These times can be reduced even further when it is not necessary for the reaction to run to completion (25,26,51,68). Often, the reaction times reported for microchip devices do not include the time required for product analysis. For groups that employed real-time detection with fluorescent probes (8,44,54,60,71) or groups that used the rapid analysis thermocyclers (62–64,66–69), no additional time was necessary for analysis. However, for those that utilized an agarose gel (21,28,30,31,33–35,37,39,41,45–47,49,52,55,72,80), CE (22–27,29,32,38,42,43,50,53,58), or microarray hybridization (36,56,61,73), extra time was required. Also note that in the case of fluorescent probe detection, the use of carefully designed probes specific to the amplified target (e.g., TaqMan) is highly preferred over the use of nonspecific probes (e.g., SYBR green), because the small reaction volumes often make it difficult or impossible to perform parallel gel electrophoresis analysis to verify amplification of the correct product.

2.2. Integrated Microfabricated Systems

Integrated microfluidic devices designed to perform sequential sample extraction/purification, PCR amplification, and product analysis operations show great promise as self-contained lab-on-a-chip systems suitable for use in environments where portable low-power operation is a primary consideration (Table 4). One of the most compelling examples illustrating the power of miniaturized genomic analysis systems is the hybrid glass-silicon design developed by Burns et al. (20), capable of performing a series of liquid metering, thermal reaction, and analysis operations. This pioneering device was used to amplify a 106 bp DNA target via an isothermal strand displacement amplification process followed by gel electrophoresis with integrated photodetection of the fluorescently labeled reaction product, all within a single self-contained microchip. In terms of integrated PCR systems, early work focused on the design of systems coupling PCR with on-chip CE. Woolley et al. (32) were the first to demonstrate this concept using a hybrid system consisting of a 20- μ L microfabricated silicon PCR reactor bonded to the top of a glass CE microchip.

Unfavorable surface interactions at the reactor walls were avoided through the use of disposable polypropylene liners, and targets from both plasmid and bacterial genomic DNA templates were successfully amplified with cycling times as fast as 30 s/cycle. Products were detected using an external laser excited confocal fluorescence system with fluorescent dye added to the gel matrix. Subsequent refinements by the Mathies group to this basic design (26,27) integrated both the PCR reactor and CE unit into a single glass microchannel network (Fig. 3A). Reagents were loaded and sealed inside the 280-nL reactor using a valve manifold mounted on top of the chip, and temperature control was provided by thin-film heater and thermocouple elements affixed to the back side of the chip. Most recently, Lagally et al. (29) demonstrated multiplex PCR directly from whole bacterial cells using a microfabricated glass chip with integrated heating. Product was detected using fluorescently labeled primers.

The Ramsey group (22–25) has developed a family of glass microchips for performing integrated PCR and CE. The basic design consists of a 10- to 20- μ L reaction reservoir fabricated by drilling a hole in one of the glass substrates. After loading, the PCR reagents are covered with mineral oil or wax to prevent evaporation, and thermocycling is performed by placing the chip inside either a conventional thermocycler or specially designed thermoelectric fixture. After the reaction reaches completion, an intercalating dye is added to the reservoir and CE-based product analysis is performed using laser-induced fluorescence. This device has been used to perform successful PCR amplification of templates ranging from lambda DNA to bacterial and mouse genomic DNA.

Other approaches to integrating PCR and CE operations include the use of hybrid PDMS/glass microchips (52,53) and designs coupling a silicon PCR microchip with integrated heating to a glass CE chip (38). Finally, a group from ACLARA BioSciences has demonstrated an impressive plastic microfluidic chip with integrated temperature control incorporating novel on-chip photopolymerized gel valves that not only seal reagents inside the 29- to 84-nL PCR reactor but also allow the amplified products to be electrokinetically extracted through the valve material and directed into a CE channel for detection using laser-induced fluorescence (58). Device operation was demonstrated by amplifying targets from bacterial genomic DNA templates.

In addition to CE, devices designed to integrate other upstream and downstream sample processes have been reported. For example, Wilding et al. (43) used a hybrid glass/silicon device incorporating an etched filtration structure to isolate white blood cells from whole blood samples prior to performing PCR. Several groups have also explored integration of microchip PCR with microarray hybridization (36,61). A team from Affymetrix demonstrated this concept using a device incorporating a PC fluidic cartridge and GeneChip array

Table 4
Summary of Experiments Performed Using Integrated Microdevices Combining PCR With On-Chip Sample Preparation and/or Product Analysis

Reference	Device materials	Reactor volume	Reagents	Template	Target size	Temperature (°C) ^a	Hold times ^c	Cycles/ reaction time	Analysis
32	Microfabricated Si reactor bonded to glass CE chip Integrated heaters Polypropylene liner in reaction chamber	20 µL	<i>Taq</i> (0.05 U/µL)	Plasmid DNA	268 bp	96, 55, 72	2 s, 5 s, 2 s	30 cycles 15 min	CE (on-chip)
26	Microfabricated chip (glass/glass) External heating	280 nL	BSA <i>Taq</i> (0.05 U/µL)	Bacterial genomic 136 bp fragment	159 bp 136 bp	95, 56, 72 95, 53, 72	10 s, 15 s, 20 s 5 s, 15 s, 10 s	35 cycles 39 min 20 cycles 10 min	CE (on-chip) CE (on-chip)
27	Microfabricated chip (glass/glass) External heating	280 nL	BSA <i>Taq</i> (0.05 U/µL)	136, 231 bp fragments	136, 231 bp	95 94, 64–50, 72	1 min 5 s, 15 s, 10 s	30 cycles 15 min	CE (on-chip)
29	Microfabricated chip (glass/glass) Integrated heaters	200 nL	BSA Platinum <i>Taq</i> (1.5 U ^b)	2686 bp cloning vector Bacterial genomic	136 bp 348, 625 bp	95 94, 64–50, 72 95 94, 64–60, 72	1 min 5 s, 15 s, 10 s 1 min 10 s, 15 s, 15 s	30 cycles 15 min 35 cycles 23 min	CE (on-chip) CE (on-chip) CE (on-chip)
22	Microfabricated chip (glass/glass) External heating	10–25 µL	BSA Ampli Taq (0.025 U/µL)	Bacterial genomic Lambda DNA	219, 310 bp 500 bp	95 94, 55, 72 94, 37, 72 72	1 min 10 s, 15 s, 15 s 2 min, 3 min, 4 min 7 min	30 cycles 20 min 25 cycles 3 h 52 min ^e	CE (on-chip) CE (on-chip)
				Bacterial genomic	154, 264, 346 bp	94 94, 50, 72 72	2 min 2 min, 3 min, 4 min 7 min	25 cycles 3 h 54 min ^e	
				Plasmid DNA	410 bp	94 94, 50, 72 72	2 min 2 min, 3 min, 4 min 7 min	25 cycles 3 h 54 min ^e	

23	Microfabricated chip (glass/glass) External heating	12 μ L	BSA AmpliTaq (0.025 U/ μ L)	Lambda DNA	199, 500 bp	94, 50, 72 72	2 min, 3 min, 4 min 7 min	25 cycles 3 h 52 min ^c	CE (on-chip)
				Bacterial genomic	346 bp	94	4 min	25 cycles	
				Plasmid DNA	410, 550 bp	94, 50, 72 72	2 min, 3 min, 4 min 7 min	3 h 56 min ^c	
						94	4 min	25 cycles	
						94, 50, 72 72	2 min, 3 min, 4 min 7 min	3 h 56 min ^c	
24	Microfabricated chip (glass/glass) External heating	12 μ L	BSA AmpliTaq (0.04 U/ μ L)	Mouse genomic	107, 114, 121, 149 bp	95	4 min	21 cycles	CE (on-chip), agarose gel
						94, 60–50, 72 72	90 s, 90 s, 90 s 7 min	3 h	
25	Microfabricated chip (glass/glass) External heating Prerinsed with BSA	6 μ L	BSA AmpliTaq (0.025 U/ μ L)	Lambda DNA	199 bp	94, 50, 72	30 s, 20 s, 25 s	10–25 cycles 12.5– 31.25 min ^c	CE (on-chip)
43	Microfabricated chip (Si/glass) External heating SiO ₂ passivation	3.5 μ L	TaqStart antibody <i>Taq</i> (0.2 U/ μ L)	Human genomic	202 bp	94	5 min	30 cycles	CE (off-chip)
						94, 63, 65 65	10 s, 1 min, 1 min 10 min	1 h 20 min ^c	
56	PC cartridge Parylene-C passivation	~38 μ L	<i>rTth</i> polymerase or Taq Gold (1.5X normal conc) ^b	Serum samples	1.6 kb	93.5, 63, 72	20 s, 40 s, 90 s	45 cycles 1 h 53 min ^c	Hybridization
52	Microfabricated chip (PDMS/glass) External heating Prerinsed with BSA	30–50 μ L	BSA <i>Taq</i> (0.025 U/ μ L)	Lambda DNA	500 bp	94, 54, 72	30 s, 30 s, 30 s	25 cycles 52 min	Agarose gel
53	Microfabricated chip (PDMS/glass) External heating	30–50 μ L	BSA <i>Taq</i> (0.025 U/ μ L)	Lambda DNA	500 bp	94, 54, 72	30 s, 30 s, 30 s	25 cycles 52 min	CE (on-chip)

(continued)

Table 4 (Continued)

Reference	Device materials	Reactor volume	Reagents	Template	Target size	Temperature (°C) ^a	Hold times ^a	Cycles/reaction time	Analysis
61	MAGchip with polyacrylamide-based gel pads Quartz glass cover	30 µL	(NH ₄) ₂ SO ₄ Triton X-100 BSA AmpliTaq (0.08 U/µL)	Bacterial genomic fragment	Not specified	95, 66, 72	40 s, 45 s, 30 s	35–40 cycles 67–76 min ^c	Hybridization
58	Poly(cyclic olefin) chip Integrated heating Prerinse with BSA	29–84 nL	BSA AmpliTaq Gold (0.5 U/µL)	Bacterial genomic	232, 429, 559 bp	95 94, 56, 72 72	5 min 45 s, 30 s, 45 s 5 min	35 cycles 95–110 min ^c	CE (on-chip)
38	Microfabricated chip (Si/glass) Integrated heating Prerinse with BSA	3–10 µL	Triton X-100 Taq (0.025 U/µL)	Plasmid DNA Bird genomic	350 bp 350, 368 bp	96 96, 55 72 94 94, 48, 72 72	22 s 8 s, 8 s 4.5 min 2 min 35 s, 50 s, 50 s 8 min	30 cycles 8 min 36 cycles 1 h 31 min ^c	CE (on-chip)
73	Plastic chip Integrated heating	1 mL (total)	BSA AmpliTaq (0.05 U/µL)	Rabbit genomic Human genomic	221 bp Not specified	94 94, 55, 72 72 94 94, 55, 72 72	4 min 45 s, 45 s, 45 s 3 min 4 min 45 s, 45 s, 45 s 3 min	35 cycles 1 h 30 min 35 cycles 1 h 30 min	Hybridization Hybridization

^aReaction temperatures are listed in the following format: denaturing, annealing, and extension. Omission of an annealing temperature indicates that a two-temperature cycling protocol was used. Preheating and final-extension temperatures are listed above and below the reaction temperatures, respectively. Reaction hold times are listed in the same order.

^bNeither a reactor volume nor a master mixture volume was given to determine the concentration in units per microliter.

^cTotal reaction time was calculated based on reported data for the total number of cycles and hold times.

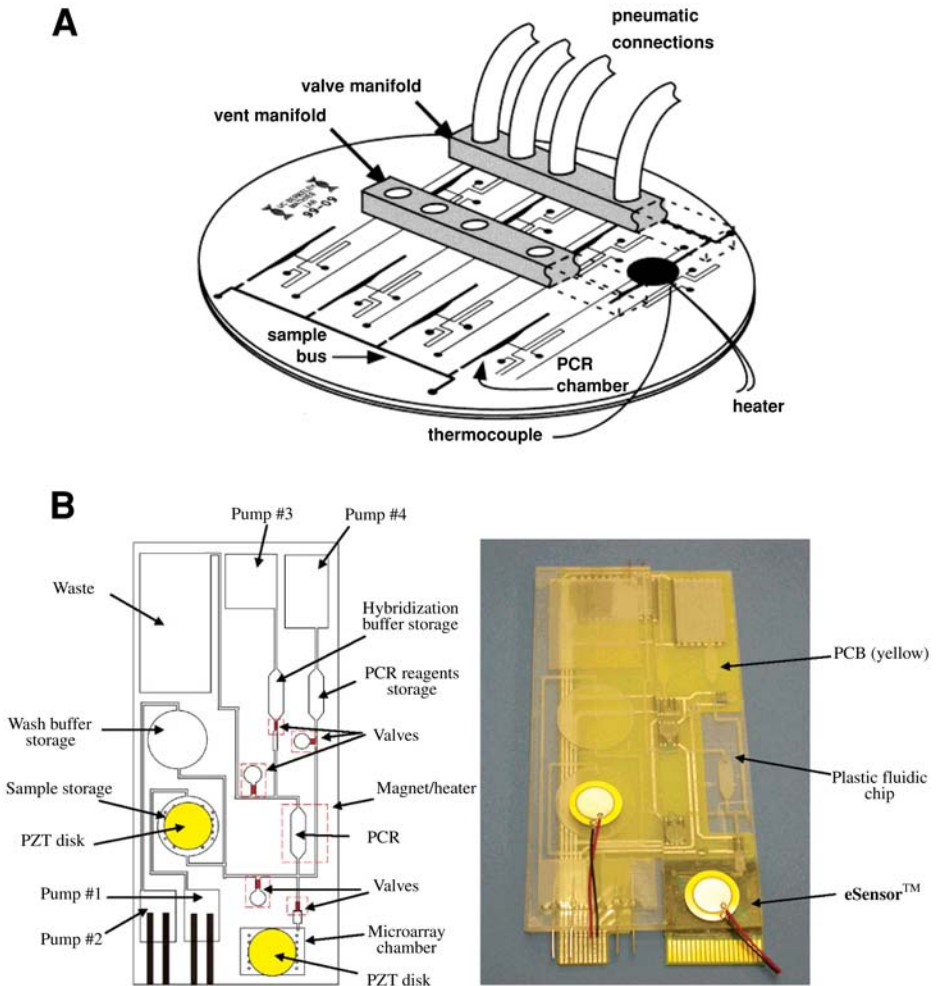


Fig. 3. Examples of integrated DNA analysis microdevices. (A) System combining polymerase chain reaction (PCR) with on-chip CE. (Reproduced with permission from ref. 27, copyright 2001 American Chemical Society.) (B) Self-contained biochip device incorporating ability to perform sample preparation, PCR, and microarray hybridization. (Reproduced with permission from ref. 73, copyright 2004 American Chemical Society.)

capable of performing sequential reverse transcription, PCR, enzymatic reactions, and hybridization (56). More recently, a team from Motorola has demonstrated a self-contained biochip device incorporating the ability to perform sample preparation (cell capture, concentration, purification, and lysis), PCR,

and hybridization using an integrated eSensor DNA microarray (**Fig. 3B**) (**73**). The device was used to detect pathogenic bacteria from whole rabbit blood and to perform single-nucleotide polymorphism analysis from diluted human blood samples.

2.3. Continuous-Flow PCR

The ability to perform rapid thermocycling depends, to a large extent, on the degree to which the associated high rates of heating and cooling can be precisely controlled in order to minimize temperature over- and undershoots that could adversely affect the reaction. One approach to addressing these complexities involves the use of so-called *continuous-flow* systems, in which PCR reagents are pumped through a channel network that passes through spatially distinct temperature zones corresponding to the denaturing, annealing, and extension steps of PCR (**Table 5**). This configuration is potentially advantageous because the need for dynamic temperature control is eliminated, while cycling times are determined by the flow rate used to pump reagents through the channel. Nakano et al. (**72**) were the first to successfully demonstrate this concept using an arrangement consisting of a 5 m length of Teflon capillary tubing (500 μm i.d.) whose flow path repeatedly passed through three constant-temperature oil baths. Subsequent advancements to this basic concept included the incorporation of on-line fluorescence detection (**71**) and the use of solid heating-block elements (**80**). In addition, these systems achieved reduction in reaction volumes to the microliter-to-nanoliter range by alternately coinjecting the PCR reagents and an inactive carrier liquid that confined the reagents inside discrete fluid plugs.

This concept was first adapted to a microchip format by Kopp et al. (**21**), who performed 20 cycles of continuous-flow PCR in a glass microfluidic chip mounted on independently heated copper blocks (**Fig. 4**). Later variations included integration of temperature control within the microchip (**30,35,83**) and the ability to extract products at selected locations along the flow path in order to vary the number of cycles (**28**). In all cases, external syringe pumps were used to transport reagents through the microchannel network. Device designs incorporating a closed-loop flow path have also been explored in order to provide the capability of adjusting the number of cycles performed. Chou et al. (**49**) employed laminated channels in a ceramic substrate combined with an external peristaltic pump, and Liu et al. (**54**) demonstrated a PDMS/glass microchip incorporating a 300 nL reactor with on-chip pumping capability. Finally, Chiou et al. (**81,86**) demonstrated PCR in a device incorporating an external bidirectional pumping system designed to shuttle a 1 μL reagent plug back and forth through a polytetrafluoroethylene (PTFE) capillary passing through three constant-temperature aluminum blocks. Generally speaking,

Table 5
Summary of Experiments Performed Using Continuous-Flow PCR Thermocyclers

Reference	Device materials	Reactor volume	Reagents	Template	Target size	Temperature (°C) ^a	Cycles/ reaction time	Analysis
72	Teflon capillary tube passing through 3 constant temperature oil baths Prerinse with Tris-HCl, MgCl ₂ , KCl	50 μ L (total)	BSA Triton X-100 Sodium cholate <i>Tth</i> polymerase (no amount given)	Plasmid DNA	230 bp, 1 kb	94, 55, 72	30 cycles 12–44 min	Agarose gel
21	Microfabricated chip (glass/glass) mounted on heated copper blocks Pretreatment with dichlorodimethylsilane	10 μ L (total)	Tricene Tween-20 PVP <i>Taq</i> (0.25 U/ μ L)	1 kb fragment	176 bp	95, 60, 77	20 cycles 1.5–18.7 min	Agarose gel
81	PTFE capillary External heating	1 μ L	Triton X-100 (extracted from <i>Taq</i>) <i>Taq</i> (0.18 U/ μ L)	Lambda DNA	524 bp	Variable (3-temperature protocol)	30 cycles 23 min	Agarose gel
35	Microfabricated chip (glass/Si) Integrated heaters Pretreatment with hexamethyldisilazane	10 μ L (total)	BSA Tween-20 PVP <i>Taq</i> (0.1 U/ μ L)	106 bp fragment Genomic Knockout vector	106 bp 379 bp 700 bp	94, 40, 72 94, 59, 72 94, 52, 72	25 cycles 35 min	Agarose gel
49	Laminated channels in ceramic substrate Integrated heaters	19 μ L (total)	<i>Taq</i> (more than normal)	209 bp fragment	209 bp	95, 52, 72	20 cycles 27 min	Agarose gel

Table 5 (Continued)
Summary of Experiments Performed Using Continuous-Flow PCR Thermocyclers

Reference	Device materials	Reactor volume	Reagents	Template	Target size	Temperature (°C) ^a	Cycles/reaction time	Analysis
54	Microfabricated chip (PDMS/glass) Integrated heaters	12 nL	AmpliTaq Gold (0.025 U/μL)	Human genomic Lambda DNA	294 bp 199 bp	95, —, 60 94, 55, 72	30–35 cycles 10–40 min	Fluorescent probe
30	Microfabricated chip (quartz/quartz) Integrated heaters Pretreatment with dichlorodimethylsilane	19 μL (total)	Tween-20 <i>Taq</i> (0.025 U/μL)	450 bp fragment	450 bp	94, —, 67	30 cycles 22.5–45 min	Agarose gel
71	Teflon capillary tube passing through 3 constant temperature water baths	300 nL	AmpliTaq (0.067 U/μL)	Human genomic	79, 148 bp	94, 54, 72	30 cycles 45 min	Fluorescent probe
28	Microfabricated chip (glass/glass) Mounted on heated copper blocks Pretreatment with dichlorodimethylsilane	2 μL	BSA Triton X-100 Tween-20 PVP <i>Taq</i> (0.5 U/μL)	230-bp fragment Human genomic	230 bp	95, 58, 72	30 cycles 6 min (variable)	Agarose gel
80	Fused silica capillary wrapped around 3 heating blocks Pretreatment with chlorotrimethylsilane	2 μL	<i>Taq</i> (0.025 U/μL)	Plasmid DNA Lambda DNA	323, 497 bp 500 bp	95, 60, 72	33 cycles 5.5–92 min	Agarose gel

^aReaction temperatures are listed in the following format: denaturing, annealing, and extension. Omission of an annealing temperature indicates that a two-temperature cycling protocol was used.

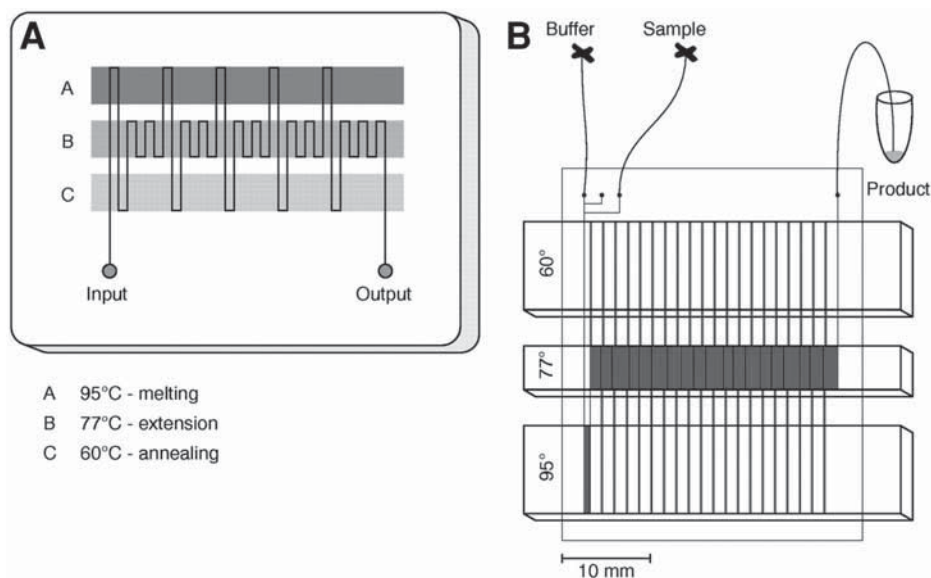


Fig. 4. (A) Schematic of microfabricated continuous-flow polymerase chain reaction (PCR) device. (B) Device layout. (Reproduced with permission from **ref. 21**, copyright 1998, the American Association for the Advancement of Science.)

surface passivation issues are of greater importance in continuous-flow systems because the PCR reagents experience a greater probability of interacting with the reactor walls as they flow through the extended channel network. Pre-treatment of the channel surfaces with various silanes and/or the use of additives in the reaction mixture is often employed to address this issue. Compatibility between the PCR mixture and carrier fluid, if used, is also an important consideration.

3. Convective-Flow PCR

Buoyancy-driven convective flows offer a novel and greatly simplified mechanism for performing thermally activated biochemical reactions such as PCR (**Table 6**). Convective flows occur throughout nature and are as well known in the field of physics as PCR is in the field of molecular biology. Under appropriate conditions, subjecting a confined fluid to a temperature gradient can generate a gravity-driven circulatory flow field capable of continually shuttling fluid elements through the temperature zones associated with denaturation, annealing, and extension processes (**Fig. 5A**). Because convective flow systems merely require two opposing surfaces of a PCR reactor to be maintained at constant temperatures associated with denaturing and annealing (the

Table 6
Summary of Experiments Performed Using Convective-Flow PCR Thermocyclers

Reference	Device materials	Reactor volume	Reagents	Template	Target size	Temperatures (°C) ^a	Cycles/ reaction time	Analysis
87	Cylindrical PC chambers	35 µL	AmpliTaq (0.1, 0.15 U/µL)	Human genomic	297 bp	97, —, 61	Not specified 1 h 30 min	Agarose gel
90	Cylindrical chamber between glass cover slips Heating with IR laser	20 µL	PureTaq beads (0.1 U/µL)	Lambda DNA	96 bp	95, —, 52	Not specified 25 min	Agarose gel
92	Teflon tubing Three heating blocks	119 µL	BSA <i>Taq</i> (0.05, 0.1 U/µL)	Bacterial genomic	305, 700 bp	95 (6 min) 94, 55, 72 72 (7 min)	35 cycles 1 h 13 min	Agarose gel
93	Polypropylene bag	75 µL	Platinum <i>Taq</i> (5 U/reaction) ^b	90 bp fragment	90 bp	94, —, 55	75 cycles 30 min	Agarose gel
89	Multiwell cylindrical PC chambers	30 µL	AmpliTaq (0.025 U/µL)	Bacterial genomic 191 bp, 3.9 kb fragments	58, 160 bp 191 bp	96, 61	Not specified 15–40 min	Agarose gel
	Fluoropolymer tubing Two thermoelectric heaters	15 µL	AmpliTaq (0.025 U/µL)	3.9 kb fragment	191 bp	95, 55, 72	40 cycles 1 h 30 min	
	PC loop channel	15 µL	AmpliTaq (0.1 U/µL)	Human genomic	297 bp	96, —, 58	Not specified 30 min	

^aReaction temperatures are listed in the following format: denaturing, annealing, and extension. Omission of an annealing temperature indicates that a two-temperature cycling protocol was used. Preheating and final-extension temperatures are listed above and below the reaction temperatures, respectively.

^bNeither a reactor volume nor a master mixture volume was given to determine the concentration in units per microliter.

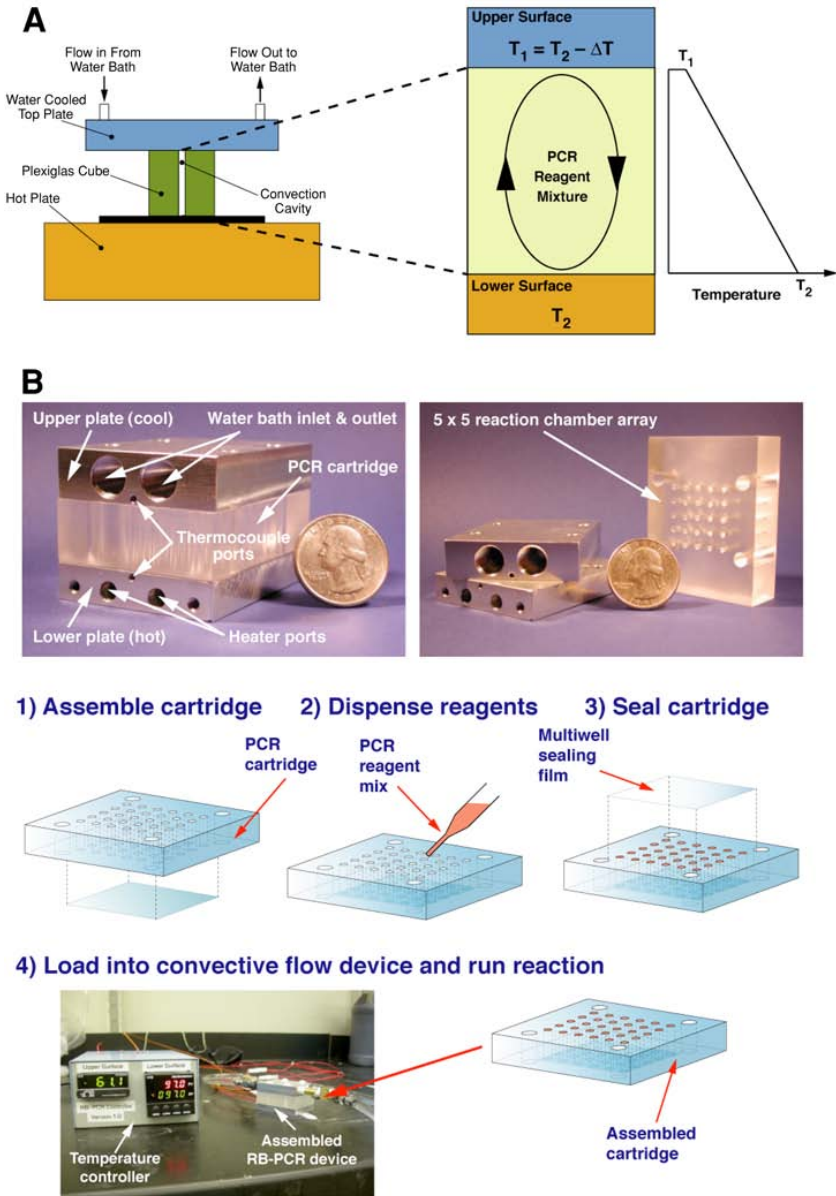


Fig. 5. (A) Schematic illustration of a convective-flow polymerase chain reaction (PCR) reactor and corresponding temperature distribution between upper and lower surfaces of cavity. (B) Prototype multiwell convective-flow PCR device consisting of a Plexiglas “PCR cartridge” incorporating a 5 × 5 array of reaction chambers, and illustration of assembly, loading, and operation processes. (Reproduced with permission from ref. 88, copyright 2004 Elsevier B.V.)

two reaction temperature extremes), the need for dynamic external temperature control is completely eliminated. Instead, amplification proceeds as the convected fluid packets circulate through the temperature field established within the reactor. Consequently, convective-flow systems allow a precise level of flow control to be exerted using purely passive techniques, eliminating the need for moving parts and complex actuation schemes. Because the convected reagents maintain a continual state of thermal equilibrium with their surroundings, rapid cycling times (approaching those attainable in microfluidic systems) can be achieved while still preserving a format that integrates readily with existing laboratory protocols.

Krishnan et al. (87) demonstrated the use of a convective-flow thermocycler incorporating a 35 μL cylindrical reactor to amplify successfully a 295 bp segment of the β -actin gene from a human genomic DNA template. Further studies have demonstrated the ability of convective-flow PCR systems to operate in a high-throughput format using multiwell devices consisting of interchangeable plastic reaction chamber “cartridges” incorporating arrays of cylindrical reactors sandwiched between two independently controlled constant-temperature aluminum plates (Fig. 5B) (88). The use of interchangeable PCR cartridges offers the flexibility to produce a wide range of layouts (e.g., conventional 96- or 384-well microplate formats) at minimal cost. This multiwell device was used to conduct a series of amplifications of a 191-base region associated with membrane channel proteins M1 and M2 of the influenza A virus, with amplification times ranging from 15 to 40 min, depending on template size (89).

Subsequent work has demonstrated convectively driven PCR in low-aspect-ratio cylindrical cavities using focused IR heating at the center of the cavity to drive the flow (90,91). Successful amplification has also been demonstrated in closed-loop convective-flow systems (89,92,93). These systems are attractive because of their ability to generate unidirectional flows along a closed path allowing residence times within desired temperature zones to be precisely controlled. The use of convective flows in miniaturized chemical and biochemical analysis systems is an emerging area of research, and more developments are likely owing to their desirable combination of reaction performance and operational simplicity. Convective-flow systems are also well suited for high-throughput operation because the reactors can be arrayed to preserve the same layouts found in traditional multiwell plate formats, enabling them to be filled and emptied using existing liquid-handling hardware.

4. General Method for Performing Microchip PCR

Widely standardized protocols have yet to emerge because miniaturized PCR and genomic analysis systems are still in a relatively early stage of development. The variety of current device designs makes it difficult to specify a

single generic process encompassing all possible steps. Here, we briefly list a basic process sequence with the primary aim of conveying a flavor for the modifications that would be necessary to existing protocols in order to adapt this technology for routine laboratory use.

4.1. Device Fabrication and Assembly

This step involves fabrication of device components (microchannels, temperature control circuitry, and so on), usually via photolithography or molding processes. These components are then assembled and interfaced with external electronic and mechanical hardware to perform such functions as reagent loading, automated thermal control, and product detection and analysis.

4.2. Cleaning and Surface Passivation

At a minimum, channels are thoroughly flushed with deionized water to remove any residue left over from the fabrication and assembly process. Additional surface passivation pretreatments may also be applied, either through chemical processes (e.g., silanization) or through the use of blocking agents (e.g., BSA).

4.3. Preparation of Sample

Owing to the small volumes employed, samples are typically prepared in a larger-volume master mix. Aliquots of the master mix can also be used for parallel control reactions run in a conventional thermocycler. If fluorescent probe detection is used, careful probe design is essential because the reaction volume may not be sufficient to verify amplification of the correct products via standard agarose gel analysis.

4.4. Loading of Sample and Reagents

Aliquots of PCR reagents and template DNA are loaded into the microreactor (either manually or using automated liquid-handling systems) and the device is sealed (either externally or using integrated on-chip valves). Proper sealing is a critical step in miniaturized systems owing to the extremely small volumes employed. Even a small amount of evaporation during thermocycling can result in loss of the entire sample or, at best, a drastic change in the relative concentrations of PCR reagents. Generally, care must also be taken to ensure that the samples are free of air pockets, which can lead to excess pressure buildup and/or nonuniform temperature distributions within the reactor.

4.5. Thermocycling

This part of the process is generally rapid and highly automated. Some systems may allow real-time monitoring of reaction progress.

4.6. Product Analysis

Some systems provide integrated product analysis using fluorescent probes, electrophoresis, or microarray hybridization techniques. Alternatively, products can be aspirated from the device for off-chip analysis. On-chip analysis is generally preferable because the extraction process can be difficult when ultrasmall reaction volumes are employed.

5. Conclusion

In this review, we have summarized some of the impressive progress that has been made in the development of miniaturized hardware systems for rapid PCR thermocycling. The benefits of miniaturization are extremely compelling, ranging from economic advantages associated with batch fabrication processes and reduced reagent consumption to the ability to construct portable devices for use outside conventional laboratory settings. Continued improvements, particularly regarding integrating sequential reaction, fluidic, and analysis steps *at the microscale* are still needed in order to construct truly self-contained lab-on-a-chip systems. These developments are likely to set the stage for a vast array of next-generation genomic analysis instrumentation incorporating enhanced capabilities to rapidly perform complex assays in a portable and inexpensive format.

References

1. Collins, F. S., Green, E. D., Guttmacher, A. E., and Guyer, M. S. (2003) A vision for the future of genomics research. *Nature* **422**, 835–847.
2. Cantor, C. R. and Smith, C. L. (1999) *Genomics: The Science and Technology Behind the Human Genome Project*, Wiley Interscience, New York.
3. Wittwer, C. T., Fillmore, G. C., and Hillyard, D. R. (1989) Automated polymerase chain-reaction in capillary tubes with hot air. *Nucleic Acids Res.* **17**, 4353–4357.
4. Wittwer, C. T., Fillmore, G. C., and Garling, D. J. (1990) Minimizing the time required for DNA amplification by efficient heat transfer to small samples. *Anal. Biochem.* **186**, 328–331.
5. Swerdlow, H., Jones, B. J., and Wittwer, C. T. (1997) Fully automated DNA reaction and analysis in a fluidic capillary instrument. *Anal. Chem.* **69**, 848–855.
6. Soper, S. A., Ford, S. M., Xu, Y. C., et al. (1999) Nanoliter-scale sample preparation methods directly coupled to polymethylmethacrylate-based microchips and gel-filled capillaries for the analysis of oligonucleotides. *J. Chromatogr. A* **853**, 107–120.
7. Zhang, N. Y., Tan, H. D., and Yeung, E. S. (1999) Automated and integrated system for high-throughput DNA genotyping directly from blood. *Anal. Chem.* **71**, 1138–1145.
8. Belgrader, P., Elkin, C. J., Brown, S. B., et al. (2003) A reusable flow-through polymerase chain reaction instrument for the continuous monitoring of infectious biological agents. *Anal. Chem.* **75**, 3446–3450.
9. Friedman, N. A. and Meldrum, D. R. (1998) Capillary tube resistive thermocycling. *Anal. Chem.* **70**, 2997–3002.

10. Huhmer, A. F. R. and Landers, J. P. (2000) Noncontact infrared-mediated thermocycling for effective polymerase chain reaction amplification of DNA in nanoliter volumes. *Anal. Chem.* **72**, 5507–5512.
11. Burke, D. T., Burns, M. A., and Mastrangelo, C. (1997) Microfabrication technologies for integrated nucleic acid analysis. *Genome Res.* **7**, 189–197.
12. Wilding, P. and Kricka, L. J. (1999) Micro-microchips: just how small can we go? *Trends Biotechnol.* **17**, 465–468.
13. deMello, A. J. (2001) DNA amplification: does ‘small’ really mean ‘efficient’? *Lab Chip* **1**, 24N–29N.
14. Schneegass, I. and Kohler, J. M. (2001) Flow-through polymerase chain reactions in chip thermocyclers. *Rev. Mol. Biotechnol.* **82**, 101–121.
15. Verpoorte, E. (2002) Microfluidic chips for clinical and forensic analysis. *Electrophoresis* **23**, 677–712.
16. deMello, A. J. (2003) Microfluidics—DNA amplification moves on. *Nature* **422**, 28–29.
17. Kricka, L. J. and Wilding, P. (2003) Microchip PCR. *Anal. Bioanal. Chem.* **377**, 820–825.
18. Wilding, P. (2003) Nucleic acid amplification in microchips, in *Biochip Technology* (Cheng, J. and Kricka, L. J., eds.), Taylor and Francis, New York, pp. 173–184.
19. Vilkner, T., Janasek, D., and Manz, A. (2004) Micro total analysis systems. Recent developments. *Anal. Chem.* **76**, 3373–3386.
20. Burns, M. A., Johnson, B. N., Brahmasandra, S. N., et al. (1998) An integrated nanoliter DNA analysis device. *Science* **282**, 484–487.
21. Kopp, M. U., deMello, A. J., and Manz, A. (1998) Chemical amplification: continuous-flow PCR on a chip. *Science* **280**, 1046–1048.
22. Waters, L. C., Jacobson, S. C., Kroutchinina, N., Khandurina, J., Foote, R. S., and Ramsey, J. M. (1998) Microchip device for cell lysis, multiplex PCR amplification, and electrophoretic sizing. *Anal. Chem.* **70**, 158–162.
23. Waters, L. C., Jacobson, S. C., Kroutchinina, N., Khandurina, J., Foote, R. S., and Ramsey, J. M. (1998) Multiple sample PCR amplification and electrophoretic analysis on a microchip. *Anal. Chem.* **70**, 5172–5176.
24. Dunn, W. C., Jacobson, S. C., Waters, L. C., et al. (2000) PCR amplification and analysis of simple sequence length polymorphisms in mouse DNA using a single microchip device. *Anal. Biochem.* **277**, 157–160.
25. Khandurina, J., McKnight, T. E., Jacobson, S. C., Waters, L. C., Foote, R. S., and Ramsey, J. M. (2000) Integrated system for rapid PCR-based DNA analysis in microfluidic devices. *Anal. Chem.* **72**, 2995–3000.
26. Lagally, E. T., Simpson, P. C., and Mathies, R. A. (2000) Monolithic integrated microfluidic DNA amplification and capillary electrophoresis analysis system. *Sens. Actuators B. Chem.* **63**, 138–146.
27. Lagally, E. T., Medintz, I., and Mathies, R. A. (2001) Single-molecule DNA amplification and analysis in an integrated microfluidic device. *Anal. Chem.* **73**, 565–570.
28. Obeid, P. J., Christopoulos, T. K., Crabtree, H. J., and Backhouse, C. J. (2003) Microfabricated device for DNA and RNA amplification by continuous-flow polymerase chain reaction and reverse transcription-polymerase chain reaction with cycle number selection. *Anal. Chem.* **75**, 288–295.

29. Lagally, E. T., Scherer, J. R., Blazej, R. G., et al. (2004) Integrated portable genetic analysis microsystem for pathogen/infectious disease detection. *Anal. Chem.* **76**, 3162–3170.
30. Sun, K., Yamaguchi, A., Ishida, Y., Matsuo, S., and Misawa, H. (2002) A heater-integrated transparent microchannel chip for continuous-flow PCR. *Sens. Actuators B Chem.* **84**, 283–289.
31. Northrup, M. A., Ching, M. T., White, R. M., and Watson, R. (1993) DNA amplification with a microfabricated reaction chamber, in *Transducers'93—the 7th International Conference on Solid-State Sensors and Actuators*, Hiroyuki, Fujita, Japan, pp. 924–926.
32. Woolley, A. T., Hadley, D., Landre, P., deMello, A. J., Mathies, R. A., and Northrup, M. A. (1996) Functional integration of PCR amplification and capillary electrophoresis in a microfabricated DNA analysis device. *Anal. Chem.* **68**, 4081–4086.
33. Poser, S., Schulz, T., Dillner, U., et al. (1997) Chip elements for fast thermocycling. *Sens. Actuators A Phys.* **62**, 672–675.
34. Lee, T. M. H., Hsing, I. M., Lao, A. I. K., and Carles, M. C. (2000) A miniaturized DNA amplifier: Its application in traditional Chinese medicine. *Anal. Chem.* **72**, 4242–4247.
35. Schneegass, I., Brautigam, R., and Kohler, J. M. (2001) Miniaturized flow-through PCR with different template types in a silicon chip thermocycler. *Lab Chip* **1**, 42–49.
36. Trau, D., Lee, T. M. H., Lao, A. I. K., et al. (2002) Genotyping on a complementary metal oxide semiconductor silicon polymerase chain reaction chip with integrated DNA microarray. *Anal. Chem.* **74**, 3168–3173.
37. Yoon, D. S., Lee, Y. S., Lee, Y., et al. (2002) Precise temperature control and rapid thermal cycling in a micromachined DNA polymerase chain reaction chip. *J. Micromechanics Microeng.* **12**, 813–823.
38. Rodriguez, I., Lesaicherre, M., Tie, Y., et al. (2003) Practical integration of polymerase chain reaction amplification and electrophoretic analysis in microfluidic devices for genetic analysis. *Electrophoresis* **24**, 172–178.
39. Wilding, P., Shoffner, M. A., and Kricka, L. J. (1994) PCR in a silicon microstructure. *Clin. Chem.* **40**, 1815–1818.
40. Wilding, P., Shoffner, M. A., Cheng, J., Hvichia, G., and Kricka, L. J. (1995) Thermal cycling and surface passivation of micromachined devices for PCR. *Clin. Chem.* **41**, 1367–1368.
41. Cheng, J., Shoffner, M. A., Hvichia, G. E., Kricka, L. J., and Wilding, P. (1996) Chip PCR. 2. Investigation of different PCR amplification systems in microfabricated silicon-glass chips. *Nucleic Acids Res.* **24**, 380–385.
42. Cheng, J., Waters, L. C., Fortina, P., et al. (1998) Degenerate oligonucleotide primed polymerase chain reaction and capillary electrophoretic analysis of human DNA on microchip-based devices. *Anal. Biochem.* **257**, 101–106.
43. Wilding, P., Kricka, L. J., Cheng, J., Hvichia, G., Shoffner, M. A., and Fortina, P. (1998) Integrated cell isolation and polymerase chain reaction analysis using silicon microfilter chambers. *Anal. Biochem.* **257**, 95–100.

44. Nagai, H., Murakami, Y., Morita, Y., Yokoyama, K., and Tamiya, E. (2001) Development of a microchamber array for picoliter PCR. *Anal. Chem.* **73**, 1043–1047.
45. Nagai, H., Murakami, Y., Yokoyama, K., and Tamiya, E. (2001) High-throughput PCR in silicon based microchamber array. *Biosens. Bioelectron.* **16**, 1015–1019.
46. Northrup, M. A., Gonzalez, C., Hadley, D., et al. (1995) A MEMS-based miniature DNA analysis system. *Transducers 95—the 8th International Conference on Solid-State Sensors and Actuators, and Eurosensors IX*. Stockholm, Sweden, pp. 764–767.
47. Daniel, J. H., Iqbal, S., Millington, R. B., et al. (1998) Silicon microchambers for DNA amplification. *Sens. Actuators A Phys.* **71**, 81–88.
48. Taylor, T. B., Harvey, S. E., Lebak, L., et al. (1998) Process control for optimal PCR performance in glass microstructures. *Biomed. Microdev.* **1**, 65–70.
49. Chou, C. F., Changrani, R., Roberts, P., et al. (2002) A miniaturized cyclic PCR device - modeling and experiments. *Microelectron. Eng.* **61**, 921–925.
50. El-Ali, J., Perch-Nielsen, I. R., Poulsen, C. R., Bang, D. D., Telleman, P., and Wolff, A. (2004) Simulation and experimental validation of a SU-8 based PCR thermocycler chip with integrated heaters and temperature sensor. *Sens. Actuators A Phys.* **110**, 3–10.
51. Giordano, B. C., Ferrance, J., Swedberg, S., Huhmer, A. F. R., and Landers, J. P. (2001) Polymerase chain reaction in polymeric microchips: DNA amplification in less than 240 seconds. *Anal. Biochem.* **291**, 124–132.
52. Hong, J. W., Fujii, T., Seki, M., Yamamoto, T., and Endo, I. (2000) PDMS (polydimethylsiloxane)-glass hybrid microchip for gene amplification, in *1st Annual International IEEE-EMBS Special Topic Conference on Microtechnologies in Medicine & Biology*. Lyon, France, pp. 407–410.
53. Hong, J. W., Fujii, T., Seki, M., Yamamoto, T., and Endo, I. (2001) Integration of gene amplification and capillary gel electrophoresis on a polydimethylsiloxane-glass hybrid microchip. *Electrophoresis* **22**, 328–333.
54. Liu, J., Enzelberger, M., and Quake, S. (2002) A nanoliter rotary device for polymerase chain reaction. *Electrophoresis* **23**, 1531–1536.
55. Liu, J., Hansen, C., and Quake, S. R. (2003) Solving the “world-to-chip” interface problem with a microfluidic matrix. *Anal. Chem.* **75**, 4718–4723.
56. Anderson, R. C., Su, X., Bogdan, G. J., and Fenton, J. (2000) A miniature integrated device for automated multistep genetic analysis. *Nucleic Acids Res.* **28**, E60.
57. Yang, J., Liu, Y., Rauch, C. B., et al. (2002) High sensitivity PCR in plastic micro reactors. *Lab Chip* **2**, 179–187.
58. Koh, C. G., Tan, W., Zhao, M., Ricco, A. J., and Fan, Z. H. (2003) Integrating polymerase chain reaction, valving, and electrophoresis in a plastic device for bacterial detection. *Anal. Chem.* **75**, 4591–4598.
59. Strizhkov, B. N., Drobyshv, A. L., Mikhailovich, V. M., and Mirzabekov, A. D. (2000) PCR amplification on a microarray of gel-immobilized oligonucleotides:

- Detection of bacterial toxin- and drug-resistant genes and their mutations. *Biotechniques* **29**, 844–857.
60. Taylor, T. B., WinnDeen, E. S., Picozza, E., Woudenberg, T. M., and Albin, M. (1997) Optimization of the performance of the polymerase chain reaction in silicon-based microstructures. *Nucleic Acids Res.* **25**, 3164–3168.
61. Tillib, S. V., Strizhkov, B. N., and Mirzabekov, A. D. (2001) Integration of multiple PCR amplifications and DNA mutation analyses by using oligonucleotide microchip. *Anal. Biochem.* **292**, 155–160.
62. Belgrader, P., Smith, J. K., Weedn, V. W., and Northrup, M. A. (1998) Rapid PCR for identity testing using a battery-powered miniature thermal cycler. *J. Forensic Sci.* **43**, 315–319.
63. Ibrahim, M. S., Lofts, R. S., Jahrling, P. B., et al. (1998) Real-time microchip PCR for detecting single-base differences in viral and human DNA. *Anal. Chem.* **70**, 2013–2017.
64. Northrup, M. A., Benett, B., Hadley, D., et al. (1998) A miniature analytical instrument for nucleic acids based on micromachined silicon reaction chambers. *Anal. Chem.* **70**, 918–922.
65. Ross, P. L., Davis, P. A., and Belgrader, P. (1998) Analysis of DNA fragments from conventional and microfabricated PCR devices using delayed extraction MALDI-TOF mass spectrometry. *Anal. Chem.* **70**, 2067–2073.
66. Belgrader, P., Benett, W., Hadley, D., et al. (1998) Rapid pathogen detection using a microchip PCR array instrument. *Clin. Chem.* **44**, 2191–2194.
67. Belgrader, P., Hansford, D., Kovacs, G. T. A., et al. (1999) A minisonicator to rapidly disrupt bacterial spores for DNA analysis. *Anal. Chem.* **71**, 4232–4236.
68. Belgrader, P., Benett, W., Hadley, D., et al. (1999) Infectious disease—PCR detection of bacteria in seven minutes. *Science* **284**, 449–450.
69. Belgrader, P., Young, S., Yuan, B., et al. (2001) A battery-powered notebook thermal cycler for rapid multiplex real time PCR analysis. *Anal. Chem.* **73**, 286–289.
70. Belgrader, P., Northrup, M. A., Benett, B., et al. (2002) Development of battery-powered portable instrumentation for rapid PCR analysis, in *Integrated Microfabricated Biodevices* (Heller, M. J. and Guttman, A., eds.), Marcel Dekker, New York, pp. 183–206.
71. Curcio, M. and Roeraade, J. (2003) Continuous segmented-flow polymerase chain reaction for high-throughput miniaturized DNA amplification. *Anal. Chem.* **75**, 1–7.
72. Nakano, H., Matsuda, K., Yohda, M., Nagamune, T., Endo, I., and Yamane, T. (1994) High-speed polymerase chain-reaction in constant flow. *Biosci. Biotechnol. Biochem.* **58**, 349–352.
73. Liu, R. H., Yang, J., Lenigk, R., Bonanno, J., and Grodzinski, P. (2004) Self-contained, fully integrated biochip for sample preparation, polymerase chain reaction amplification, and DNA microarray detection. *Anal. Chem.* **76**, 1824–1831.
74. Shoffner, M. A., Cheng, J., Hvichia, G. E., Kricka, L. J., and Wilding, P. (1996) Chip PCR. 1. Surface passivation of microfabricated silicon-glass chips for PCR. *Nucleic Acids Res.* **24**, 375–379.

75. Giordano, B. C., Copeland, E. R., and Landers, J. P. (2001) Towards dynamic coating of glass microchip chambers for amplifying DNA via the polymerase chain reaction. *Electrophoresis* **22**, 334–340.
76. Munro, N. J., Huhmer, A. F. R., and Landers, J. P. (2001) Robust polymeric microchannel coatings for microchip-based analysis of neat PCR products. *Anal. Chem.* **73**, 1784–1794.
77. Erill, I., Campoy, S., Erill, N., Barbe, J., and Aguilo, J. (2003) Biochemical analysis and optimization of inhibition and adsorption phenomena in glass-silicon PCR-chips. *Sens. Actuators B Chem.* **96**, 685–692.
78. Krishnan, M., Burke, D. T., and Burns, M. A. (2004) Polymerase chain reaction in high surface-to-volume ratio SiO₂ microstructures. *Anal. Chem.* **76**, 6588–6593.
79. Panaro, N. J., Lou, X. J., Fortina, P., Kricka, L. J., and Wilding, P. (2004) Surface effects on PCR reactions in multichip microfluidic platforms. *Biomed. Microdev.* **6**, 75–80.
80. Park, N., Kim, S., and Hahn, J. H. (2003) Cylindrical compact thermal-cycling device for continuous-flow polymerase chain reaction. *Anal. Chem.* **75**, 6029–6033.
81. Chiou, J., Matsudaira, P., Sonin, A., and Ehrlich, D. (2001) A closed cycle capillary polymerase chain reaction machine. *Anal. Chem.* **73**, 2018–2021.
82. Chaudhari, A. M., Woudenberg, T. M., Albin, M., and Goodson, K. E. (1998) Transient liquid crystal thermometry of microfabricated PCR vessel arrays. *J. Microelectromechanical Syst.* **7**, 345–355.
83. Lao, A. I. K., Lee, T. M. H., Hsing, I. M., and Ip, N. Y. (2000) Precise temperature control of microfluidic chamber for gas and liquid phase reactions. *Sens. Actuators A Phys.* **84**, 11–17.
84. Lin, Y. C., Yang, C. C., and Huang, M. Y. (2000) Simulation and experimental validation of micro polymerase chain reaction chips. *Sens. Actuators B Chem.* **71**, 127–133.
85. Erickson, D. and Li, D. (2002) Numerical simulations of a low power microchannel thermal cycling reactor. *Intl. J. Heat Mass Transfer* **45**, 3759–3770.
86. Chiou, J., Matsudaira, P., and Ehrlich, D. (2002) Thirty-cycle temperature optimization of a closed-cycle capillary PCR machine. *Biotechniques* **33**, 557–564.
87. Krishnan, M., Ugaz, V. M., and Burns, M. A. (2002) PCR in a Rayleigh-Bénard convection cell. *Science* **298**, 793.
88. Ugaz, V. M. and Krishnan, M. (2004) Novel convective flow based approaches for high-throughput PCR thermocycling. *J. Assoc. Lab. Automation* **9**, 318–323.
89. Krishnan, M., Agrawal, N., Burns, M. A., and Ugaz, V. M. (2004) Reactions and fluidics in miniaturized natural convection systems. *Anal. Chem.* **76**, 6254–6265.
90. Braun, D., Goddard, N. L., and Libchaber, A. (2003) Exponential DNA replication by laminar convection. *Phys. Rev. Lett.* **91**, 158,103.
91. Braun, D. (2004) PCR by thermal convection. *Modern Phys. Lett. B* **18**, 775–784.
92. Chen, Z., Qian, S., Abrams, W. R., Malamud, D., and Bau, H. (2004) Thermosiphon-based PCR reactor: experiment and modeling. *Anal. Chem.* **76**, 3707–3715.
93. Wheeler, E. K., Bennett, W., Stratton, P., et al. (2004) Convectively driven polymerase chain reaction thermal cycler. *Anal. Chem.* **76**, 4011–4016.

Polymerase Chain Reaction on Microchips

Maria C. Carles and Nikolaus J. Sucher

Summary

The polymerase chain reaction (PCR) provides an *in vitro* method for rapid enzymatic amplification of fragments of DNA. Microchip-based PCR devices (with reaction volumes from picoliters to microliters) have been realized using various combinations of silicon, glass, and/or plastic materials. Passivation of exposed surfaces in the microreactor is critical for successful PCR. Silicon and plastic surfaces can be passivated by silanization. With surface passivation, PCR can be performed efficiently and economically in chip-based microreactors. The reduced thermal mass of microchips allows for extremely fast temperature ramping. PCR protocols established for benchtop reactors may need to be adjusted accordingly when transferred to microchips. Here, we provide detailed protocols for microchip PCR including procedures for surface passivation and bonding of glass to silicon with ultraviolet curable glue, because both procedures have a major influence on the success or failure of the PCR.

Key Words: Polymerase chain reaction; microreactor; DNA amplification; silicon; surface passivation.

1. Introduction

Polymerase chain reaction (PCR) provides an *in vitro* method for the rapid enzymatic amplification of fragments of DNA (*1*). In the PCR procedure, two oligonucleotide primers that are complementary to the flanking sequence of the DNA to be amplified are used to prime a DNA polymerase that performs the copying of each strand of DNA. Separation of the two strands of DNA, annealing of the complementary oligonucleotide to each strand, and the synthesis of new strands by the polymerase are performed at their optimal temperature, resulting in a three-step reaction. In the first step, the reaction mixture is heated to approx 95°C for the heat denaturation of the DNA. Then, the reaction temperature is lowered to a temperature (approx 48–55°C) that allows the

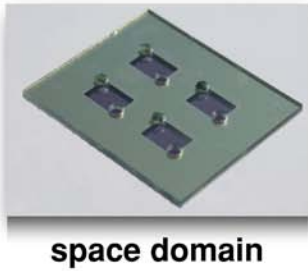
annealing of oligonucleotide primers to their complementary sequences on each strand of the target DNA, before the temperature is changed again to allow the efficient synthesis of complementary strands by the DNA polymerase (approx 70°C). After sufficient time has been allowed for the polymerase to synthesize a complete copy, the next cycle is started beginning with the denaturation of the newly synthesized double-stranded DNA. Because each strand of the target DNA serves as a template for the synthesis of its complementary strand, the target DNA is effectively doubled during the reaction. This reaction cycle is repeated many times, resulting in the exponential amplification of the target DNA, hence the name PCR.

When PCR was first introduced in 1985 (2), the procedure was time-consuming and laborious, because each reaction tube needed to be repeatedly transferred manually to a heating device preset to the respective denaturation, annealing, and polymerizing temperature. Furthermore, new DNA polymerase enzyme had to be added at each cycle, because the enzyme itself was destroyed by the high temperature necessary for denaturation of the DNA. The introduction of a heat-stable DNA polymerase from the thermophilic bacterium *Thermus aquaticus* (*Taq*) in 1988 (3) allowed the entire PCR to be conducted without having to replace the enzyme in each cycle, which, in turn, led to the introduction of so-called thermocyclers, machines that could be programmed to change the reaction temperatures at each step automatically.

Since the first description of the PCR procedure, hundreds of thousands of scientific publications mentioning the use of PCR illustrate that not only has it changed the practice of molecular biology, but it also has introduced the practice of molecular biology to many other fields. In molecular biology, PCR is commonly used for the amplification of gene fragments as a fast alternative to traditional cloning procedures, the introduction of mutations at specific sites (site-directed mutagenesis), and studies of gene expression. In clinical medi-

Fig 1. (*opposite page*) Microchip polymerase chain reaction (PCR). Chip-based PCR devices can be built using various combinations of silicon, glass, and/or plastic materials. (A) PCR reactors have are either “time-domain” devices, in which the reaction mixture is stationary and the temperature is changed, or “space-domain” devices, in which the reaction mixture is moved in a flow channel between different temperature zones. (B) Passivation of exposed surfaces in the microreactor is critical for successful PCR. Silicon and plastic surfaces can be passivated by silanization. (C) Either classic “symmetric” or asymmetric PCR can be performed efficiently and economically in chip-based microreactors. (D) Amplicons can be analyzed by electrophoresis, direct DNA sequencing, or hybridization to DNA microarrays (after asymmetrical PCR). PCR products can be subcloned into a variety of vectors.

A micro reactor design and construction
(silicon, glass, plastic)



B surface passivation



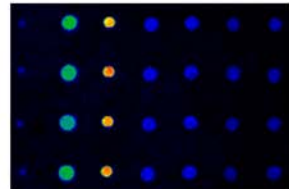
C symmetric PCR asymmetric



D electrophoresis
sequencing
cloning



hybridization



cine, it is used for the sensitive detection and genotyping of pathogenic microorganisms and the detection of mutations underlying inherited diseases, malignant transformation, or tissue typing. In forensic medicine, PCR is commonly used for paternity testing, identification of biological specimens, and identification of individuals. Applications in the basic sciences include investigations of the evolutionary relationship between species and the analysis of ancient DNA. PCR is also used for environmental, food safety, and biodefense purposes.

It has been pointed out previously (4) that one of the distinctive characteristics of PCR is its extraordinary versatility and power to create new situations for its use and those required to use it. In fact, PCR has continuously evolved and many modifications of the original procedure have been introduced.

Within a few years of the introduction of the first thermocyclers, microchip-based PCR devices were developed (5), inspired by the concept of the micrototal analysis system (6), which is now more commonly and colloquially referred to as a “lab on a chip.” Advantages of integrated devices for genetic analysis incorporating all steps from the introduction of raw sample to the determination of a given genotype include reduced sample and reagent volumes; increased speed and reliability, owing to reduction of necessary manual interventions; reduced price of mass-fabricated devices; reduced cross-contamination in disposable devices; reduced power consumption; and increased portability.

Microchip-based PCR devices (with reaction volumes from picoliters to microliters) have been realized using various combinations of silicon, glass, and/or plastic materials, such as polymethylmethacrylate, polydimethylsiloxane, or polycarbonate (5) (Fig. 1). The PCR reactors themselves have been designed either as so-called time-domain devices, in which the reaction mixture is stationary and the temperature is changed in analogy to the existing benchtop thermocyclers, or as space-domain devices, in which the reaction mixture is moved in a flow channel between different temperature zones (7). The PCR reaction is generally performed and most efficient in the liquid phase, although solid-phase PCR on glass microarrays has been reported (8). Reviews of the published literature pertaining to microchip PCR have been published recently (5,9,10).

The PCR itself has been demonstrated to function as efficiently in chip-based microreactors as in tube- or well-based benchtop thermocyclers (11). Overall, microchip-based PCR is not fundamentally different from “traditional” benchtop PCR, and established methods and protocols can easily be transferred with either no or only slight modifications. Many excellent sources are available, including review articles (1), books (12–14), and on-line guides (www.promega.com/guides/pcr_guide/default.htm), that provide detailed

information regarding protocols and applications for PCR. Specific factors that need to be taken into account regarding microchip PCR include the design of the microreactor (surface-to-volume ratio, overall size), the materials used (surface chemistry, heat mass), and the assembly procedures (e.g., bonding of glass to silicon using certain types of glue). Here, we provide detailed protocols for microchip PCR that have worked well in our experience. Although the design and manufacture of microchip PCR devices has been reviewed and covered previously (5), we include here protocols for surface passivation and bonding of glass to silicon using ultraviolet (UV) curable glue because both procedures have a major influence on the success or failure of the PCR chip.

2. Materials

2.1. Surface Passivation

1. Trimethylchlorosilane (CAS no. 75-77-4) and trimethoxymethylsilane (CAS no. 1185-55-3) (Merck, Darmstadt, Germany): the silanes should only be handled in a fume hood and stored at room temperature in a cabinet for flammable liquids.

2.2. Bonding of Glass to Silicon

1. Pyrex borosilicate glass wafers (Corning 7740) (Corning, NY).
2. UV-curing optical cement type SK-9 (Summers Optical, EMS, Hatfield, PA).

2.3. PCR Protocol

1. Stock solution of bovine serum albumin (BSA) (5 mg/mL; CAS no. 9048-46-8 from Sigma-Aldrich, St. Louis, MO) in ddH₂O: aliquot the stock solution and store at -20°C.
2. Taq (*T. aquaticus*) DNA polymerase (with license for PCR; many vendors; store following the manufacturer's recommendation): the polymerase is usually distributed with additional vials containing a 10X PCR buffer (200 mM Tris-HCl, pH 8.4, 500 mM KCl, with or without 15 mM MgCl₂). In cases in which 10X PCR buffer without magnesium is provided, a 50 mM MgCl₂ stock solution is usually also provided for convenience.
3. Ultrapure deoxyribonucleotides (dNTPs; many vendors; store at -20°C).
4. Adhesive tape (3M 5419; 3M, St. Paul, MN).

3. Methods

3.1. Surface Passivation of Silicon (see Note 1)

1. Pipet chlorotrimethylsilane onto a chip to fill the reaction chamber and incubate for 15 min at room temperature.
2. Remove the silane and dry the chamber in a nitrogen hood for 1 h.
3. Rinse the reactor three times with autoclaved deionized, ddH₂O and dry under vacuum for 1 h.

Table 1
Components of PCR Mix

Reagent	Final concentration
Autoclaved ddH ₂ O	Up to final volume
BSA (5 µg/µL)	0.5 µg/µL
10X PCR reaction buffer	1X
50 mM MgCl ₂	1.5 mM (<i>see Note 7</i>)
1.25 mM dNTP mix	200 µM each of dATP, dCTP, dGTP, dTTP
Forward primer (10 µM)	0.2–1.0 µM (<i>see Note 8</i>)
Reverse primer (10 µM)	0.2–1.0 µM (<i>see Note 8</i>)
Template DNA	0.05–1.0 ng (<i>see Note 9</i>)
<i>Taq</i> polymerase (5 U/µL)	1.25 U

3.2. Surface Passivation of Glass (*see Note 1*)

1. Silanize the glass wafers (Corning 7740) prior to bonding to the silicone wafers by treating with pure trimethoxymethylsilane in a nitrogen gas atmosphere for 30 min at 80°C.
2. Wash the glass wafers with absolute 2-propanol and dry under nitrogen gas.

3.3. Bonding of Glass to Silicon (*see Note 2*)

1. Distribute a small amount of UV glue (Sk-9; Summers Optical) onto the entire surface (except the cavities) of the silicon wafer. Align the glass wafer on top and apply slight pressure.
2. Expose the wafer for 3 h to UV light (254 nm) (Spectrolinker UV Crosslinker Spectroline, Albany, NY).
3. Treat the wafer at 80°C under vacuum (20 mbar) for 2 h, in order to remove or inactivate uncured UV-glue components such as solvents or other low molecular weight components resulting from incomplete curing, which inhibit the PCR.
4. Seal inlet and outlet holes with adhesive tape (3M 5419).

3.4. PCR Protocol (*see Notes 3 and 4*)

1. Prepare the oligonucleotides for PCR (*see Note 5*).
2. Prepare the PCR mix as in **Table 1** (*see Note 6*).
3. Add the PCR mix to the reaction chamber.
4. Program the PCR cycles (*see Note 10*).
5. Verify that the amplification has yielded the expected product by analyzing an aliquot (1 µL) of the reaction by gel electrophoresis, DNA sequencing, or microarray hybridization (*see Note 11*).

4. Notes

1. For successful PCR experiments, the inner surface of the reaction chamber has to be passivated to avoid nonspecific adsorption of the reagents, enzyme, and DNA template used in the PCR on the chamber wall resulting in poor amplification. Methods of surface passivation reported to date include silanization (silane such as trimethylchlorosilane and trimethoxysilane or silane-based compounds) and coating of the reactor surfaces with inert protein (e.g., BSA) or other biological polymers (e.g., polyadenylic acid) (15–17). The choice of surface passivation method has to be guided by the surface chemistry of the microreactor material and the fabrication method. Lee et al. (16) and Trau et al. (17) have described detailed methods for the fabrication of silicon-based PCR microreactor chips. Silicon-based PCR microreactors can effectively be passivated by the deposition of a thin silicon dioxide layer on the reactor walls during the microfabrication process (15–17). A very effective and time-proven passivation method that is applicable to silicon, glass, and plastic materials is based on the coating of the reaction chamber with a silane (15–17). In fact, so-called silanization of plastic pipet tips and reaction tubes has been a long-standing practice in molecular biology. The versatility, broad applicability, and ease of use make silanization a good general choice for surface passivation. Furthermore, in addition to surface passivation, silanes are well suited for the functionalization of surfaces. For example, silanes containing free thiols or amines can be used for the surface attachment of oligonucleotides serving as probes in DNA microarrays or solid-phase primers for solid-phase PCR (8,17).
2. We found that several other UV-curable glues did inhibit the PCR reaction despite the heat and vacuum treatment.
3. The very high sensitivity of PCR poses a formidable problem because of the constant danger of contamination, which can yield false-positive results. The importance of appropriate laboratory practice cannot be overemphasized. For example, it is good practice to use filtered pipet tips whenever possible to avoid contamination.
4. PCR in an adequately passivated microreactor is essentially similar to PCR in traditional benchtop thermocyclers albeit at greatly reduced volume and decreased reaction time. In particular, the reduced thermal mass of microchip reactors makes it possible to more quickly ramp the temperature up (e.g., 10°C/s) and down (e.g., 2.5°C/s) in microreactors compared to traditional benchtop thermocyclers (~1°C/s) (18). However, faster temperature ramping can lead to failure of amplification in the microreactor in cases in which secondary structure present at lower annealing temperature prevents annealing of the primer to its target in the microreactor but not in the benchtop reactor, because the temperature in the benchtop machine rises only slowly, leaving enough time for the target to unfold and the primer to anneal during the slow ramp up of the reactor temperature. Finally, it should be kept in mind that sufficient time has to be allotted to the synthesis step depending on the processivity (nucleotides per second)

of the DNA polymerase that is being used in the PCR and the length of the intended amplicon. For example, the most commonly used heat-stable DNA polymerase *Taq* can extend at 100 bases/s according to information from the manufacturer (Promega, Madison, WI). In general, however, it is safer to assume that polymerization proceeds at a rate of 1000 bases/min.

- Information needed to prepare primers for PCR is provided in the “Analysis Report” included by the manufacturer of the oligonucleotides. To calculate the extinction coefficient (E) use the following formula:

$$E_M = (n \times A \times 16,000) + (n \times G \times 12,000) + (n \times C \times 7000) + (n \times T \times 9600)$$

in which n is the number of the bases A, C, G, and T. Using E_M (concentration in micromolar) of each oligonucleotide, one can calculate the volume (V ; in microliters) needed to prepare the primer stock solution using the following formula:

$$V = OD_{260}/E_{mM}$$

in which E_{mM} is the concentration in millimolar. Note that primer stock solutions are usually 100–500 μM . Store at $-20^\circ C$.

- For several PCRs, a master mix is usually prepared containing all reagents except reaction-specific primers and DNA template. The volume of the master mix (V_{MM}) is calculated as follows:

$$V_{MM} = V_{PCR} \times (n_{PCR} + 1)$$

in which V_{PCR} is the final reaction volume, and n_{PCR} is the number of reactions. The number of actual reactions is increased by one in order to account for small pipetting errors.

- Amplification efficiency is influenced by the magnesium concentration in the PCR. Although most primer/template combinations work well at the “standard” magnesium concentration of 1.5 mM , the “best” concentration has to be determined empirically by varying the magnesium content of the reaction. A range of 0.5–3 mM is usually sufficient for finding the optimal concentration.
- Well-chosen and designed primers are essential for the success of the PCR (12). In our own experience, primers between 20 and 24 nucleotides with a similar G/C content between 50 and 65% have worked very well (19,20). The 5' and 3' ends of the primers should not be complementary in order to prevent the formation of hairpins or primer dimers. “Primer 3” (21), one of the best software tools for computer-assisted design of primers, is available on-line free of charge (http://frodo.wi.mit.edu/cgi-bin/primer3/primer3_www.cgi). Multiple primer pairs aimed at different targets can be added in the same PCR to perform so-called multiplex PCR (12). The optimal annealing temperature depends on the G/C content of the primers and the template and has to be determined empirically.
- In general, at least 10^2 – 10^4 copies of the DNA template should be added to the reaction mix (although single-copy amplification is possible). The accumulation of product (P) during PCR is governed by the following equation

$$P = N0 \times (1 + Y)^{n-1}$$

in which N_0 is the number of duplex template copies at the start of the PCR, n is the number of cycles, and Y is the efficiency of the reaction. In general, the efficiency is ≤ 1 . This formula does not apply for very low copy numbers ($N_0 \ll 100$) when amplification becomes stochastic (22).

10. One PCR cycle normally includes three basic steps: (1) denaturation (typically performed at 95°C for 20 s to 5 min, depending on the amount of expected secondary structure and complexity of the template); (2) annealing (the annealing temperature depends on the CG content of the primer and template; for example, for GC content <50%, try annealing temperatures between 37 and 55°C, but for GC content >50%, try annealing temperatures between 48 and 70°C); and (3) extension (see Note 3). In most cases, 25–35 cycles should be sufficient for amplification. Typically, a denaturation step of 1–5 min precedes the actual PCR cycles and an extra extension step (10 min) is sometimes added at the end of the PCR in order to extend incomplete amplicons to their final size.
11. If the PCR amplicons are to be used for hybridization to DNA microarrays, asymmetric PCR should be performed (17). In an asymmetric PCR, the primer for the target strand that is to be hybridized to the probe on the DNA microarray usually contains a label and should be present at a 100-fold excess compared to the respective (unlabeled) primer for the complementary strand.

References

1. Gibbs, R. A. (1990) DNA amplification by the polymerase chain reaction. *Anal. Chem.* **62**, 1202–1214.
2. Saiki, R. K., Scharf, S., Faloona, F., et al. (1985) Enzymatic amplification of beta-globin genomic sequences and restriction site analysis for diagnosis of sickle cell anemia. *Science* **230**, 1350–1354.
3. Saiki, R. K., Chang, C. A., Levenson, C. H., et al. (1988) Diagnosis of sickle cell anemia and beta-thalassemia with enzymatically amplified DNA and nonradioactive allele-specific oligonucleotide probes. *N. Engl. J. Med.* **319**, 537–541.
4. Bartlett, J. and Stirling, D. (2003) A short history of the polymerase chain reaction, in *Methods in Molecular Biology: PCR Protocols*, vol 226, 2nd ed. (Bartlett, J. and Stirling, D., eds.), Humana, Totowa, NJ, pp. 1–6.
5. Kricka, L. J. and Wilding, P. (2003) Microchip PCR. *Anal. Bioanal. Chem.* **377**, 820–825.
6. Reyes, D. R., Iossifidis, D., Auroux, P. A., and Manz, A. (2002) Micro total analysis systems. 1. Introduction, theory, and technology. *Anal. Chem.* **74**, 2623–2636.
7. Liu, J., Enzelberger, M., and Quake, S. (2002) A nanoliter rotary device for polymerase chain reaction. *Electrophoresis* **23**, 1531–1536.
8. Huber, M., Losert, D., Hiller, R., Harwanegg, C., Mueller, M. W., and Schmidt, W. M. (2001) Detection of single base alterations in genomic DNA by solid phase polymerase chain reaction on oligonucleotide microarrays. *Anal. Biochem.* **299**, 24–30.
9. Auroux, P. A., Iossifidis, D., Reyes, D. R., and Manz, A. (2002) Micro total analysis systems. 2. Analytical standard operations and applications. *Anal. Chem.* **74**, 2637–2652.

10. Vilknér, T., Janásek, D., and Manz, A. (2004) Micro total analysis systems: recent developments. *Anal. Chem.* **76**, 3373–3385.
11. Carles, M., Lee, T., Moganti, S., et al. (2001) Chips and Qi: microcomponent-based analysis in traditional Chinese medicine. *Fresenius J. Anal. Chem.* **371**, 190–194.
12. Dieffenbach, C. and Dveksler, G. (2003) *PCR Primer: A Laboratory Manual*, 2nd ed., Cold Spring Harbor Laboratory Press, Cold Spring Harbor, NY.
13. Innis, M., Gelfand, D., Sninsky, J., and White, T. (1990) *PCR Protocols: A Guide to Methods and Applications*, Academic, New York.
14. McPherson, M., Møller, S., Beynon, R., and Howe, C. (2000) *PCR Basics: from Background to Bench*, Springer Verlag, New York, NY.
15. Shoffner, M. A., Cheng, J., Hvichia, G. E., Kricka, L. J., and Wilding, P. (1996) Chip PCR. I. Surface passivation of microfabricated silicon-glass chips for PCR. *Nucleic Acids Res.* **24**, 375–379.
16. Lee, T. M., Hsing, I. M., Lao, A. I., and Carles, M. C. (2000) A miniaturized DNA amplifier: its application in traditional Chinese medicine. *Anal. Chem.* **72**, 4242–4247.
17. Trau, D., Lee, T. M., Lao, A. I., Lenigk, R., et al. (2002) Genotyping on a complementary metal oxide semiconductor silicon polymerase chain reaction chip with integrated DNA microarray. *Anal. Chem.* **74**, 3168–3173.
18. Woolley, A. T., Hadley, D., Landre, P., deMello, A. J., Mathies, R. A., and Northrup, M. A. (1996) Functional integration of PCR amplification and capillary electrophoresis in a microfabricated DNA analysis device. *Anal. Chem.* **68**, 4081–4086.
19. Sucher, N. J., Deitcher, D. L., Baro, D. J., Warrick, R. M., and Guenther, E. (2000) Genes and channels: patch/voltage-clamp analysis and single-cell RT-PCR. *Cell Tissue Res.* **302**, 295–307.
20. Sucher, N. J. and Deitcher, D. L. (1995) PCR and patch-clamp analysis of single neurons. *Neuron* **14**, 1095–1100.
21. Rozen, S. and Skaletsky, H. (2000) Primer3 on the www for general users and for biologist programmers, in *Bioinformatics Methods and Protocols: Methods in Molecular Biology* (Krawetz, S. and Misener, S., eds.), Humana, Totowa, NJ, pp. 365–386.
22. Lagally, E. T., Medintz, I., and Mathies, R. A. (2001) Single-molecule DNA amplification and analysis in an integrated microfluidic device. *Anal. Chem.* **73**, 565–570.

A Sensitive Sandwich DNA Array Using Fluorescent Nanoparticle Probes

Xiaojun Zhao, David T. Pierce, and Yanfu Huan

Summary

An ultrasensitive sandwich DNA array using highly fluorescent and photostable dye-doped silica nanoparticles is described. Compared to traditional sandwich arrays in which fluorophores have been used to signal target DNA molecules, the developed nanoparticle probes provide a much stronger fluorescent emission. Signal amplification of the dye-doped silica nanoparticles originates from the large number of dye molecules doped inside each individual nanoparticle. In addition, the silica matrix of the nanoparticles protects dye molecules from photobleaching. Thus, the dye-doped nanoparticles provide a constant fluorescent signal that is sufficient for detection of trace amounts of target DNA. By immobilizing a complementary DNA sequence to the target onto the nanoparticle surface, a fluorescent nanoparticle-DNA probe is formed. These nanoparticle probes are then used as superemitting reagents to perform a typical sandwich assay. By using a high-resolution fluorescent microscope, individual nanoparticle-DNA probes that have been hybridized to capture target strands can be observed clearly at low target DNA concentrations. More important, the number of the nanoparticle-DNA probes hybridized to the target DNA is proportional to the target DNA concentration in solution. By counting the number of localized fluorescent “spots” on the array, the target DNA concentration can be determined. In this chapter, detailed methods used to synthesize nanoparticle-DNA probes, fabricate the sandwich array, prepare the substrate, and quantitatively determine DNA concentration are described.

Key Words: Nanoparticles; DNA array; sandwich assay; DNA detection; fluorescence; dye molecules; DNA hybridization; photostability; signal enhancement.

1. Introduction

The DNA array has been a successful development for DNA sequencing and detection based on DNA hybridization (*1*). In general, two DNA hybridization strategies are employed with DNA arrays. The most common strategy

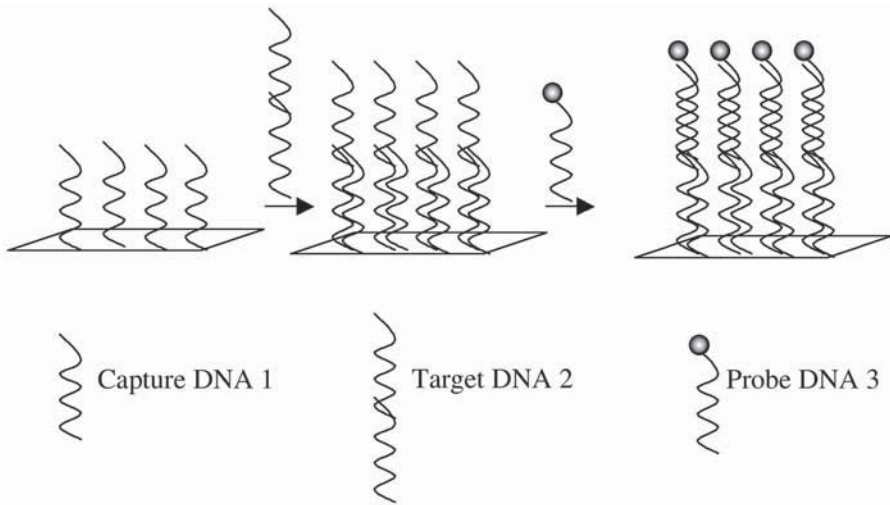


Fig. 1. Schematic diagram of sandwich DNA array.

is to hybridize directly target DNA molecules with complementary probe DNA sequences that have been immobilized on the array substrate surface. For detection, the target DNA is labeled with a fluorophore or a radioactive reagent before hybridization. After hybridization, the target DNA remains immobilized on the array surface and, thus, provides detectable signal for target sequencing (2). A significant disadvantage of this strategy is that target DNA molecules must be chemically labeled before detection. To overcome this disadvantage, an alternative hybridization strategy is used that employs three “sandwiched” DNA sequences: the capture DNA, the target DNA, and the probe DNA (3). A schematic diagram of the sandwich DNA array is shown in Fig. 1. The capture DNA is first immobilized onto the substrate surface. The sequence of the capture DNA is complementary to the target DNA but the sequence is shorter than the target. The target DNA molecules partially bind to the capture DNA during this first hybridization. The remaining sequence of the target DNA is complementary to the probe DNA molecules that have been labeled with signaling groups. As the probe DNA binds to the target sequence, the labeling group gives a detectable signal that reflects the amount of hybridized target DNA. Although one additional hybridization step is needed in the sandwich strategy, there is no need to chemically label the target DNA.

The selectivity of the sandwich DNA array benefits not only from the hybridization of two complementary sequences rather than one, but, more important,

from the sample-independent signaling ability of labeled probe molecules. Although both radioactive and fluorescent labeling are commonly used in these situations (4), the higher cost and greater safety precautions associated with radioactive materials have led to a preference toward fluorescent labeling techniques in more recent research interests (5–7). Currently, the biggest challenge in ultrasensitive detection of trace amounts of DNA sequences is the limited number of target DNA that can be labeled with fluorescent probes, which results in a fluorescent signal that is too low to be detected. Thus, without a preconcentration of the target DNA, trace detection is difficult. Moreover, most current fluorescent labeling materials are organic fluorophores owing to their advantage of high quantum yield. However, rapid photobleaching of organic fluorophores can occur during the detection process, especially when attempting to amplify emissions from a limited number of labeled sites, which results in unstable fluorescent signals.

To achieve the desired signal amplification for ultrasensitive DNA detection, several types of highly fluorescent probes have been explored. Branched DNA or DNA dendrimers (8), quantum dots (9–12), and nanoparticles (13–19) appear to be the attractive fluorescent probes. In addition, a new method based on gold nanoparticle-promoted reduction of silver can detect target DNA down to a concentration of 50 fM (20). However, newly developed dye-doped silica nanoparticles appear to show the greatest ability in emitting a highly fluorescent and photostable signal (21–24). Several advantages make dye-doped silica nanoparticles ideal fluorescent probes for ultrasensitive bioanalysis. One is a large number of dye molecules that can be doped inside a single nanoparticle, thereby providing a high fluorescent signal. Thus, when one captured target molecule is labeled with one dye-doped nanoparticle, the emission signal is greatly amplified compared to single fluorophore molecule probes. This characteristic makes ultrasensitive detection of DNA possible without extensive preconcentration of the target sequence. Another key advantage of dye-doped silica nanoparticles is the high photostability provided by the silica matrix shielding effect. Dye molecules are well protected from environmental oxygen when doped inside the silica network, which enables the fluorescent intensity of these nanoparticles to remain constant during the detection process and thus gives a more accurate signal. Finally, the silica surface serves as a biocompatible and versatile substrate for the immobilization of biomolecules. Biochemically modified nanoparticles have been developed for various applications using known immobilization mechanisms (25–31).

In this chapter, we focus on dye-doped silica nanoparticles as fluorescent labeling reagents for ultrasensitive detection of DNA in a sandwich array. We

discuss the method of synthesizing dye-doped nanoparticles based on a well-developed microemulsion system for some commonly used inorganic and organic fluorophores, such as *tris*(2,2'-bipyridyl) dichlororuthenium (II) hexahydrate (RuBpy), fluorescein, and tetramethylrhodamine (TMR). We also provide descriptions of immobilization of the probe DNA sequence onto the nanoparticle surface and immobilization of capture DNA onto the substrate using the biotin-avidin linkage as well the hybridization events followed by an imaging system to measure the fluorescent signals of the surface-bound nanoparticle-DNA probes. Finally, we discuss quantitative assay of target DNA based on fluorescent nanoparticle probe sequences, which has been found to have an excellent sensitivity and is easy to carry out.

2. Materials

All chemicals were analytical reagent grade. Distilled deionized ultrapure water (resistivity 18 $M\Omega$ -cm) was used for the preparation of all aqueous solutions in the synthesis of the nanoparticles and DNA hybridization.

2.1. Dye Molecules

1. TMR.
2. RuBpy.
3. Fluorescein.
4. Fluorescein-dextran (MW = 10,000).
5. TMR-dextran (MW = 10,000).

2.2. Chemicals for Synthesis of Dye-Doped Silica Nanoparticles

1. Acetic acid.
2. Polyoxyethylene (10) isooctylphenylether.
3. Triton X-100 ($4\text{-}[\text{C}_8\text{H}_{17}]\text{C}_6\text{H}_4[\text{OCH}_2\text{CH}_2]_n\text{OH}$; $n \sim 10$).
4. Tetraethylorthosilicate (TEOS).
5. Cyclohexane.
6. *n*-Hexanol.
7. Acetone.
8. Ethanol.
9. 10 *M* NaOH.
10. 28–30% NH_4OH .

2.3. Reagents for Surface Modification of Nanoparticles

1. Avidin.
2. Biotinylated DNA molecules (sequences can be designed based on target sequences).
3. Polyethylene glycol (PEG).
4. 25% Glutaraldehyde.

2.4. Buffers

1. Phosphate-buffered saline (PBS) buffers: 10 mM phosphate buffer (pH 7.5) and 100 mM potassium phosphate buffer (pH 7.0).
2. 1 M Tris-HCl buffer (pH 7.0) for nanoparticle surface modification.
3. Hybridization buffer: 20 mM Tris-HCl, 5 mM MgCl₂ buffer (pH 8.0).

3. Methods

3.1. Synthesis of Dye-Doped Silica Nanoparticles

Dye-doped silica nanoparticles can be synthesized by either the Stöber (32) method or the reverse microemulsion (33–36) method. Both provide a silica matrix by hydrolysis and polymerization of TEOS. The Stöber method requires a shorter synthesis time than the microemulsion method but results in relatively large, nonuniform nanoparticles. By contrast, the reverse microemulsion method provides monodisperse and smaller silica nanoparticles. Thus, the reverse microemulsion method is more commonly applied in producing silica nanoparticles.

The reverse microemulsion method is based on an isotropic and thermodynamically stable single-phase system that consists of small amounts of water, a large volume of oil, and a surfactant. The surfactant molecules lower the interfacial tension between water and oil phases (W/O), resulting in the formation of a transparent mixture. Water nanodroplets (also called water pools) are formed in the bulk oil phase and serve as nanoreactors for the synthesis of nanoparticles from various materials. The size of the water pool influences the size of the nanoparticles. By changing the molar ratio of water to surfactant (W_0 value), the size of the spherical nanoparticles is controllable. In general, the higher the value of W_0 , the larger the particle size will be. The excess base in the microemulsion initiates the polymerization reaction through hydrolysis of TEOS. The rate of the polymerization is much slower in the microemulsion in comparison with that in a bulk aqueous solution. Therefore, as the polymerization reaction continues, monodisperse silica nanoparticles are formed. The produced silica nanoparticles have very uniform size, which can be characterized by scanning electron microscopy (SEM) and transmission electron microscopy (TEM) images. Given the different applications for bioanalysis, various sizes of silica nanoparticles can be obtained by controlling the W_0 value and using different surfactants.

To obtain highly fluorescent, photostable, and biocompatible nanoparticles for bioanalysis, various dye-doped silica nanoparticles were developed (37–40). The basic idea is to entrap a large number of dye molecules inside a single nanoparticle so that each individual nanoparticle will emit a strong fluorescent signal and, thus, serve as a highly fluorescent probe.

3.1.1. Synthesis of Inorganic Dye-Doped Silica Nanoparticles

A commonly used inorganic dye molecule, RuBpy, was employed as a dopant in the W/O microemulsion (20). A W/O microemulsion solution was prepared by mixing 1.77 mL of Triton X-100 (surfactant), 1.8 mL of *n*-hexanol (cosurfactant), 7.5 mL of cyclohexane (oil), and 0.48 mL of 0.01 M RuBpy. A 100- μ L aliquot of TEOS was added to the microemulsion, followed by additional stirring for 30 min. The silica polymerization reaction was initiated by adding 60 μ L of 28% NH_4OH and then magnetically stirring for 24 h. Once the polymerization was completed, the silica nanoparticles were released by adding 20 mL of acetone, followed by sonicating and vortexing for a couple of minutes. The suspension was then centrifuged to obtain the dye-doped nanoparticles. The resultant nanoparticles were washed four times with 95% ethanol and acetone in turn. After each wash, the nanoparticles were completely dispersed in the solution. The produced nanoparticles can be stored either as water suspension for a couple of months or as a powder for a few years.

The dye-doped nanoparticles contained tens of thousands of dye molecules. However, the luminescent intensities of the dye-doped nanoparticles were not proportional to the amount of loaded dye molecules. As the amount of loaded dye was increased, the luminescent intensity of the nanoparticles was only increased up to a certain dye concentration limit. Further dye loading reduced luminescent signal owing to self-absorption of dye molecules in high concentration.

3.1.2. Synthesis of Organic Dye-Doped Silica Nanoparticles

Given the higher quantum yield of organic over inorganic fluorophores, the doping of organic dyes inside silica nanoparticles should yield more emissive probes. However, it was difficult to trap organic dye molecules inside the silica matrix using either the W/O microemulsion or the Stöber method mainly owing to the hydrophobic nature of most fluorescent organic dyes.

To address this challenge, an alternative synthetic approach was developed for organic dye-doped silica nanoparticles using organic-dextran complexes (22). Linking a highly hydrophilic dextran molecule to an organic molecule allowed the organic dye to become more easily trapped inside the water pool in the microemulsion system. However, owing to limited adsorption of the electroneutral organic dye-dextran complex to the silica matrix, the organic dye-dextran easily leached out from the nanoparticles when they were used in an aqueous solution. To more effectively trap organic dye molecules inside the silica matrix, the organic dye-dextran complex needed to be protonated and thereby positively charged. Adding HCl to the water phase in the microemulsion system firmly entrapped the organic dye-dextran complex in the silica matrix and resulted in heavily doped and highly fluorescent silica nanoparticles.

Fluorescein and TMR were commonly used organic fluorophores in bioanalysis owing to their high quantum yield, and dextran complexes of these molecules are commercially available. To synthesize TMR- or fluorescein-doped nanoparticles, a W/O microemulsion solution was prepared as described in **Subheading 3.1.1.** except that the dye solution was 0.48 mL of 1.0 mM TMR-dextran or fluorescein-dextran dissolved in pH 1.5–2.0 HCl.

Although the produced nanoparticles might aggregate, this problem could be overcome by either surface modification of nanoparticles or postcoating of the nanoparticles with functional groups (*see Note 1*). The signal enhancement and photostability of synthesized nanoparticles should be investigated before using them to fabricate DNA arrays (*see Notes 2 and 3*).

3.2. Conjugation of Nanoparticle-DNA Probes

Because of the high fluorescence intensity of dye-doped nanoparticles, they gave strong signals when employed as fluorescence probes in a sandwich DNA array. To act as DNA probes, the dye-doped nanoparticles were linked to a single-stranded DNA molecule that was complementary to part of the target DNA strand. The method of linking probe DNA strands onto a nanoparticle could be varied based on different biochemical binding approaches. The basic idea was to modify the nanoparticle surface with functional groups that were useful for subsequent surface modification and biomolecule immobilization (*41–46*). The most frequently used bioconjugation, avidin-biotin linkage, was chosen for immobilizing probe DNA strands onto the silica nanoparticles. The affinity constant between avidin and biotin was 10^{15} L/mol. Therefore, the use of avidin-biotin linkage was an effective conjugation approach to bind probe DNA onto the silica nanoparticle surface. Often, biotinylated DNA molecules that could serve as probes were commercially available. As long as avidin could be immobilized on the nanoparticle surface in a manner that retained its bioconjugate properties, biotinylated DNA could be effectively bound on the nanoparticle surface, thereby providing DNA-nanoparticle probes.

This avidin immobilization process was mainly based on electrostatic attraction. The silica surface of the nanoparticles was negatively charged, which allowed the positively charged avidin to adsorb passively on the silica surface.

A 1-mg portion of dye-doped silica nanoparticles was incubated in 2 mL of 10 mg/mL avidin solution for 12 h in 10 mM phosphate buffer (pH 7.5) at 4°C. The adsorbed avidin was immobilized on the nanoparticles by crosslinking with 1% glutaraldehyde solution for 1 h at room temperature. Any unreacted aldehyde groups were blocked by treating the nanoparticles with 1 M Tris-HCl buffer (pH 7.0) for 3 h. After each of these steps, the nanoparticles were washed three times with PBS buffer and separated from the supernatant by ultracentrifuging at 144,000g for approx 25 min. Alternatively, the nanoparticles could be sepa-

rated from the solution by using a filter membrane with a pore size of 50 nm in diameter. The resulting avidin-coated silica nanoparticles were suspended in pH 7.0 PBS buffer and conjugated to biotinylated DNA by incubating with 0.75 mL of 1 nM biotinylated DNA probe for 12 h in a humidified chamber. After washing, the DNA-nanoparticle probes were obtained. The ratio of DNA molecules to nanoparticles was adjustable (*see Note 4*).

3.3. Preparation of the Substrate of DNA Array

A glass slide was cleaned by overnight immersion in 10 M NaOH solution followed by thorough washing in distilled, deionized water. This negatively charged glass slide was then incubated in a 10 mg/mL avidin solution in 10 mM phosphate buffer (pH 7.5) for 12 h in a refrigerator (4°C). The avidin layer was stabilized by crosslinking with 1% glutaraldehyde in 100 mM potassium phosphate buffer for 1 h at room temperature and then incubated in 1 M Tris-HCl buffer (pH 7.0) for 3 h to block excess aldehyde groups. After each adsorption and immobilization step, the slide was rinsed three times with PBS buffer.

3.4. Immobilization of Capture DNA Molecules Onto Glass Substrate

Capture DNA must be immobilized onto the substrate for hybridization of target DNA molecules during a sandwich assay. The immobilization method used was based on an avidin-biotin reaction that was similar to the procedure described in **Subheading 3.2**. Specifically, a solution of 1 pM biotinylated capture DNA was incubated with the avidin-modified substrate in 10 mM PBS buffer for 12 h in a humidified chamber at 4°C. This conjugation step was followed by thorough washing with PBS buffer to remove the nonspecific bound DNA. At this stage, the substrate was ready for use in a sandwich assay.

3.5. DNA Hybridization

There were two DNA hybridization processes in the chosen sandwich assay. The first was hybridization of the target DNA molecules with the capture DNA sequences on the substrate surface. The desired concentration of target DNA was incubated with the substrate surface for 2–4 h in hybridization buffer (*see Subheading 2.4., item 3*). After a thorough, 2-min washing with the hybridization buffer, the second hybridization of 1 pM nanoparticle-DNA probe with DNA targets was performed for 2–4 h in a hybridization buffer containing 0.5% PEG. The PEG assisted in reducing physical absorption (and therefore nonspecific association) of nanoparticle probes on the substrate. The second hybridization was followed by a stringent 2-min washing to reduce any further nonspecifically adsorbed nanoparticles. The temperature of both hybridizations was determined by the number of bases in the target DNA. In general, it should be much lower than the melting temperature of the double-stranded target DNA. Incubations were conducted in a humidified chamber.

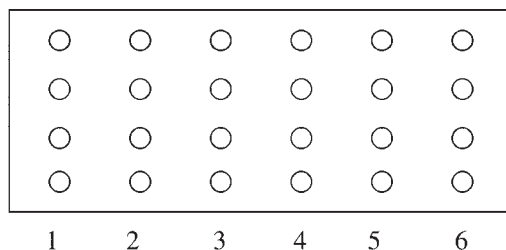


Fig. 2. DNA array substrate configured for four parallel samples of a control solution (1) and five different solutions of target DNA (2–6).

3.6. Detection of DNA on an Array

Different sequences of target DNA could be qualitatively distinguished based on the particular dye (and therefore particular fluorescence wavelength) that had been chosen for a nanoparticle probe. By assigning different dyes to different complementary probe DNAs during the stage of nanoparticle design, the same hybridized array could be used qualitatively to distinguish the presence of several different target DNAs.

The concentration for a particular target DNA could also be determined from the hybridized array by processing fluorescence images taken with a high-resolution fluorescence microscope with a laser source. For very low target DNA concentrations, the amount of target DNA could be determined by simply counting the number of nanoparticle-DNA probes observed within an image field. In this case, an objective of $\times 100$ with a high magnification of 3000 should be used and imaging over at least five different substrate areas should be performed in order to calculate an average probe number. As shown in **Fig. 2**, the array could be configured as four parallel samples for each concentration of target DNA. Thus, the final number of the fluorescent spots was an average of 20 images from four parallel samples. For investigations of signal enhancement of nanoparticles and their photostability, the fluorescent images should be taken using objectives of $\times 20$ and $\times 40$ with lower magnification.

To verify that the fluorescent spots on the fluorescence images were individual nanoparticles and not aggregates, the array could be further imaged using a scanning electron microscope. Owing to high resolution of the scanning electron microscope, any nanoparticle aggregates could be clearly distinguished.

The nonspecific binding of nanoparticle-DNA probes on the substrate could cause relatively high background signal and thereby affect any improvement of detection limits. This problem is especially serious when the sample concentration is low; thus, extra attention should be paid to this issue when performing trace determinations (*see Note 5*).

3.7. Conclusion

Using the sandwich DNA array with fluorescence nanoparticle probes, ultrasensitive DNA detection assays were achieved. The designed approach to the synthesis of dye-doped nanoparticles was very successful in obtaining highly fluorescent and photostable dye-doped silica nanoparticles. These nanoparticles exhibited an excellent signaling ability in the presence of a low number of targets. With effective surface modification procedures, nonspecific binding, physical absorption, and nanoparticle aggregation were minimized. The method is expected to be widely useful in a number of biotechnology and biomedical applications.

4. Notes

1. Aggregation is an inherent property of nanoparticles. In general, the direct characterization of dispersed nanoparticles can be done by using either imaging methods, such as SEM or TEM, or particle size analyzer based on light-scattering technique.

A modified layer on the outside of pure silica nanoparticles will assist in dispersing nanoparticles. Based on the negatively charged silica surfaces of the nanoparticles, absorption of a positively charged material on the nanoparticle surface is one simple approach, and many positively charged ions suit this requirement. Considering that a positively charged avidin molecule was chosen for the immobilization of the biotinylated probe DNA sequence onto the nanoparticles through the avidin-biotin linkage, the use of an initial avidin coating layer on the nanoparticle surface was a simple way to avoid an extra dispersion procedure in this study.

Following the aforementioned procedure for immobilizing avidin onto the nanoparticle surface, a couple of experiments can be conducted to verify whether an active avidin coating layer has been formed on the nanoparticle surface. One simple and effective method is to mix avidin-modified nanoparticles with biotinylated dye molecules. Obviously, the emission wavelength of the biotinylated dye should be different from the dopant dye used to prepare the fluorescent nanoparticles, and the presence of an active avidin layer can be confirmed by fluorescence signal from biotinylated dye molecules. With such a suitably active avidin layer, the nanoparticle probe can bind to the target DNA without agglomeration. Another method that can be used to characterize the avidin layer is to measure the typical protein absorption at 280 nm of particle suspensions by ultraviolet spectroscopy. Although this method will not indicate whether avidin has retained its ability to conjugate with biotin, it will provide a rapid assessment of avidin immobilization.

Nanoparticle aggregation can also be overcome by post-coating the nanoparticles during the synthesis process. The post-coating materials can be varied based on the particular requirements of the assay (38).

2. To assess how much signal enhancement dye-doped nanoparticles can achieve when employed as a fluorescent probe for DNA detection, a comparison of signaling ability of a dye-doped nanoparticle-DNA probe with a fluorophore-tethered DNA probe should be conducted with a sandwich DNA array. In this comparison, a particular probe DNA sequence should be selected and immobilized onto a dye-doped nanoparticle and tethered to a fluorophore, respectively. This probe DNA should complement the particular target DNA and capture DNA designed for the sandwich array. The two probes should be used to hybridize the target DNA on the substrate under the same conditions, and the fluorescent signals should be measured using a scanning fluorescent microscope. The nanoparticle probes should provide much stronger fluorescent signals than the dye molecule probes in the assay, and the exact signal enhancement can be determined by comparing of the fluorescence intensity of two probes.
3. High photostability is the other key requirement for an effective fluorescent probe. This is especially true for the detection of trace amounts of DNA on a solid phase using a microscopy image system. To obtain the greatest signal possible, a high magnification and laser power are needed. However, dye molecules are photobleached quickly under high-intensity excitation. The fluorescent signal of most organic dye molecule probes often decreases within a few seconds under these conditions, creating a problem with obtaining a stable and accurate fluorescent signal. By contrast, dye-doped nanoparticle-DNA probes emit a constant fluorescent signal over the same excitation time period. The photostability of the dye-doped nanoparticle probes and fluorophore-tethered probes on a sandwich array can be assessed using the same imaging comparisons previously described. The high photostability and a large signal amplification of the dye-doped nanoparticles provided a solid foundation for ultrasensitive detection of trace amounts of DNA targets with accurate results.
4. To achieve the highest sensitivity, the ideal nanoparticle-DNA probe is one in which each nanoparticle conjugates one probe DNA molecule so that a single target DNA can be signaled by one fluorescent nanoparticle-DNA probe. However, encounter limitations would make the binding rate of such a nanoparticle probe slow. To reach the highest sensitivity with the shortest incubation time, a ratio of approx 10 DNA probe molecules per nanoparticle should be used for optimal behavior. Although the exact number of probe DNA linked to a nanoparticle surface was difficult to determine after immobilization judging from the target DNA detection results, the DNA functionalized nanoparticle probes synthesized as described gave high sensitivity within a reasonable incubation period.
5. Using dye nanoparticles as a DNA probe, one should expect a very low detection limit. The basic idea is that one nanoparticle-DNA probe hybridizes to one target DNA sequence and, thus, brings one nanoparticle to the surface, giving approx 10^4 dye molecules to signal a single hybridization event in a small area <60 nm in diameter. With the assistance of a high-resolution scanning microscope, one should be able to observe the presence of a single nanoparticle on the substrate

surface. Theoretically, one could detect a single piece of DNA target as the hybridization occurs. However, owing to nonspecific binding and physical absorption of the nanoparticle-DNA probes on the substrate, it is difficult to achieve a detection limit down to a single piece of the target DNA. Moreover, nonspecific binding could cause very high background signals if the surface modifications of the nanoparticles and substrate are not completed, or washing steps are not efficient. To avoid false signals from nonspecific binding, proper surface modification and washing steps throughout are critical. Meanwhile, monitoring fluorescent images of control samples at each step should be carried out. For target DNA detection, it should be clearly seen that at different target DNA concentrations there are different numbers of the nanoparticle-DNA probes hybridized onto the substrate. At low target concentrations, each individual nanoparticle-DNA probe can be observed clearly. Consequently, the number of fluorescent spots on the images is proportional to the amount of the target DNA. So far, the lowest target concentration that has been effectively distinguished from the control images is 5 fM (23). There was also a linear correspondence between the target DNA concentration and the number of signaling nanoparticle DNA probes. To ensure consistency, concentrations of the capture DNA and probe DNA should be kept constant for these experiments.

Acknowledgments

We thank Dr. Weihong Tan and members of the Tan research group for invaluable assistance throughout this work.

References

1. Cotton, R. G. H. (1997) *Mutation Detection*, Oxford University Press, Oxford, UK.
2. Neary, J. T. (2000) Trophic actions of extracellular ATP: gene expression profiling by DNA array analysis. *J. Auton. Nerv. Syst.* **81**, 200–204.
3. Taton, T. A., Mirkin, C. A., and Letsinger, R. L. (2000) Scanometric DNA array detection with nanoparticle probes. *Science* **289**, 1757–1760.
4. Broketa, M., Vince, A., Drazenovic, V., Sim, R., and Mlinaric-Galinovic, G. (2001) Non-radioactive digoxigenin DNA labeling and immunologic detection of HSVPCR products. *J. Clin. Virol.* **23**, 17–23.
5. Weiss, S. (1999) Fluorescence spectroscopy of single biomolecules. *Science* **283**, 1676–1683.
6. Fang, X. and Tan, W. (1999) Imaging single fluorescent molecules at the interface of an optical fiber probe by evanescent wave excitation. *Anal. Chem.* **71**, 3101–3105.
7. Kim, J. M., Ohtani, T., Sugiyama, S., Hirose, T., and Muramatsu, H. (2001) Simultaneous topographic and fluorescence imaging of single DNA molecules for DNA analysis with a scanning near-field optical/atomic force microscope. *Anal. Chem.* **73**, 5984–5991.

8. Benters, R., Niemeyer, C. M., Drutschmann, D., Blohm, D., and Wohrle, D. (2002) DNA microarrays with PAMAM dendritic linker systems. *Nucleic Acids Res.* **30**, e10/1–e10/7.
9. Chan, W. C. W. and Nie, S. (1998) Quantum dot bioconjugates for ultrasensitive nonisotopic detection. *Science* **281**, 2016–2018.
10. Lin, Z., Su, X., Mu, Y., and Jin, Q. (2004) Methods for labeling quantum dots to biomolecules. *J. Nanosci. Nanotechnol.* **4**, 641–645.
11. Kaiser, S., Mensing, T., Worschech, L., Klopff, F., Reithmaier, J. P., and Forchel, A. (2002) Optical spectroscopy of single InAs/InGaAs quantum dots in a quantum well. *Appl. Phys. Lett.* **81**, 4898–4900.
12. Zumbuhl, D. M., Marcus, C. M., Hanson, M. P., and Gossard, A. C. (2004) Cotunneling spectroscopy in few-electron quantum dots. *Phys. Rev. Lett.* **93**, 256801/1–256801/4.
13. Cao, Y. W. C., Jin, R. C., and Mirkin, C. A. (2002) Nanoparticles with Raman spectroscopic fingerprints for DNA and RNA detection. *Science* **297**, 1536–1540.
14. Reichert, J., Csaki, A., Kohler, M., and Fritzsche, W. (2000) Chip-based optical detection of DNA hybridization by means of nanobead labeling. *Anal. Chem.* **72**, 6025–6029.
15. Taylor, J. R., Fang, M., and Nie, S. (2000) Probing specific sequences on single DNA molecules with bioconjugated fluorescent nanoparticles. *Anal. Chem.* **72**, 1979–1986.
16. Maxwell, D. J., Taylor, J. R., and Nie, S. (2002) Self-assembled nanoparticle probes for recognition and detection of biomolecules. *J. Am. Chem. Soc.* **124**, 9606–9612.
17. Pena, S. R. N., Raina, S., Goodrich, G. P., Fedoroff, N. V., and Keating, C. D. (2002) Hybridization and enzymatic extension of Au nanoparticle-bound oligonucleotides. *J. Am. Chem. Soc.* **124**, 7314–7323.
18. Li, Z., Jin, R. C., Mirkin, C. A., and Letsinger, R. L. (2002) Multiple thiol-anchor capped DNA-gold nanoparticle conjugates. *Nucleic Acids Res.* **30**, 1558–1562.
19. Park, S. J., Taton, T. A., and Mirkin, C. A. (2002) Array-based electrical detection of DNA with nanoparticle probes. *Science* **295**, 1503–1506.
20. Santra, S. M., Wang, K., Tapeç, R., and Tan, W. (2001) Development of novel dye-doped silica nanoparticles for biomarker application. *J. Biomed. Opt.* **6**, 160–166.
21. Zhao, X., Hilliard, L. R., Mechery, S. J., Wang, Y., Jin, S., and Tan, W. (2004) A rapid bioassay for single bacterial cell quantitation using bioconjugated nanoparticles. *Proc. Natl. Acad. Sci. USA* **101**, 15,027–15,032.
22. Zhao, X., Bawge, R., and Tan, W. (2004) Synthesis of organic dye doped silica nanoparticles in reverse microemulsion. *Adv. Mater.* **16**, 173–176.
23. Zhao, X., Dytocio, R. T., and Tan, W. (2003) Ultrasensitive DNA detection using highly fluorescent bioconjugated nanoparticles. *J. Am. Chem. Soc.* **125**, 11,474–11,475.
24. Zhao, X., Tapeç, R., and Tan, W. (2003) Collection of trace amounts of DNA/mRNA molecules using genomagnetic nanocaptors. *Anal. Chem.* **75**, 3476–3483.

25. Soppimath, K. S., Aminabhavi, T. M., Kulkarni, A. R., and Rudzinski, W. E. (2001) Biodegradable polymeric nanoparticles as drug delivery devices. *J. Control. Release* **70**, 1–20.
26. Harma, H., Soukka, T., and Lövgren, T. (2001) Europium nanoparticles and time-resolved fluorescence for ultrasensitive detection of prostate-specific antigen. *Clin. Chem.* **47**, 561–568.
27. Chrisey, L. A., Lee, G. U., and O’Ferral, C. E. (1996) Covalent attachment of synthetic DNA to self-assembled monolayer films. *Nucleic Acids. Res.* **24**, 3031–3039.
28. Rogers, Y., Jiang-Baucom, P., Huang, Z., Bogdanov, V., Anderson, S., and Boyce-Jacino, M. (1999) Immobilization of oligonucleotides onto a glass support via disulfide bonds: a method for preparation of DNA microarrays. *Anal. Biochem.* **266**, 23–30.
29. Osborne, M. A., Furey, W. S., Klenerman, D., and Balasubramanian, S. (2000) Single-molecule analysis of DNA immobilized on microspheres. *Anal. Chem.* **72**, 3678–3681.
30. Fang, X., Liu, X., Schuster, S., and Tan, W. (1999) Designing a novel molecular beacon for surface immobilized DNA hybridization studies. *J. Am. Chem. Soc.* **121**, 2921–2922.
31. Zhang, P. and Tan, W. (2000) Direct observation of single molecule generation at a solid-liquid interface. *Chem. Eur. J.* **6**, 1087–1092.
32. Stöber, W., Fink, A., and Bohn, E. (1968) Controlled growth of monodisperse silica spheres in the micron size range. *J. Colloid Interface Sci.* **26**, 62–69.
33. Stathatos, E., Lianos, P., DelMonte, F., Levy, D., and Tsiourvas, D. (1997) Formation of TiO₂ nanoparticles in reverse micelles and their deposition as thin films on glass substrates. *Langmuir* **13**, 4295–4300.
34. Shiojiri, S., Hirai, T., and Komasa, I. (1998) Immobilization of semiconductor nanoparticles formed in reverse micelles into polyurea via in situ polymerization of diisocyanates. *Chem. Commun.* **14**, 1439–1440.
35. Li, T., Moon, J., Morrone, A. A., Mecholsky, J. J., Talham, D. R., and Adair, J. H. (1999) Preparation of Ag/SiO₂ nanosize composites by a reverse micelle and sol-gel technique. *Langmuir* **15**, 4328–4334.
36. Shah, D. O. (1998) *Micelles, Microemulsions, and Monolayers: Quarter Century Progress at the University of Florida*, Marcel Dekker, New York, pp. 19–26.
37. Tapeç, R., Zhao, X., and Tan, W. (2002) Development of organic dye-doped silica nanoparticles for bioanalysis and biosensors. *J. Nanosci. Nanotechnol.* **2**, 1–5.
38. Wang, L., Yang, C., and Tan, W. (2005) Dual-luminophore-doped silica nanoparticles for multiplexed signaling. *Nano Lett.* **5**, 37–43.
39. Hilliard, L. R., Zhao, X., and Tan, W. (2002) The immobilization of oligonucleotides onto silica nanoparticles. *Anal. Chim. Acta* **470**, 51–56.
40. Qhobosheane, M., Santra, S., Zhang, P., and Tan, W. (2001) Biochemically functionalized silica nanoparticles. *Analyst* **126**, 1274–1278.
41. Rogers, Y. H., Jiang-Baucom, P., Huang, Z. J., Bogdanov, V., Anderson, S., and Boyce-Jacino, M. T. (1999) Immobilization of oligonucleotides onto a glass sup-

- port via disulfide bonds: a method for preparation of DNA microarrays. *Anal. Biochem.* **266**, 23–30.
42. Mascini, M., Fortunati, S., Moscone, D., Pallexchi, G., Massi-Benedetti, M., and Fabiatti, P. (1985) An L-lactate sensor with immobilized enzyme for use in vivo studies with an endocrine artificial pancreas. *Clin. Chem.* **31**, 451–453.
 43. Bangs Laboratories, 9025 Technology Drive, Fishers, IN 46038-2866, 1-800-387-0672.
 44. Bonnet, G., Tyagi, S., Libchaber, A., and Kramer, F. R. (1999) Thermodynamic basis of the enhanced specificity of structured DNA probes. *Proc. Natl. Acad. Sci. USA* **96**, 6171–6176.
 45. Zhao, X., Hilliard, L. R., Wang, K., and Tan, W. (2004) in *Encyclopedia of Nanoscience and Nanotechnology* vol. 1 (Nalwa, H. S., ed.), American Scientific Publishers, Stevenson Ranch, CA, pp. 255–268.
 46. Drake, T., Zhao, X., and Tan, W. (2004) Bioconjugated silica nanoparticles for bioanalytical applications, in *Nanobiotechnology: Methods, Concepts, and Perspectives*, (Niemeyer, Christ M Chad Mirkin, ed.), Wiley-VCH, Germany, pp. 444–458.

Microfluidic Ethanol Biobatteries on a Microchip

Shelley D. Minteer and Christine M. Moore

Summary

This chapter outlines the methods and procedures for making a microfluidic and microfabricated biofuel cell. Commercially available screen-printing carbon inks are employed as electrodes by micromolding them onto glass microchips. The carbon ink electrodes are modified with methylene green and alcohol dehydrogenase immobilized within a modified Nafion membrane to act as bioanodes in the microfluidic system. The complete biofuel cell produces power using an external platinum cathode and an integrated microfluidic bioanode. Miniaturization of power sources, such as biofuel cells, is important in applications for implementation in small technologies (i.e., sensors, bioreactors, and lab-on-a-chip technology).

Key Words: Biofuel cell; microfluidic fuel cell; microscale bioanodes; alcohol dehydrogenase.

1. Introduction

Fuel cells are gaining more attention as clean and efficient power sources because of the growing awareness for the preservation of the environment. Their use as portable power sources makes them alternatives to batteries because they are miniature, lightweight power sources (*I*). Micro proton exchange membrane fuel cells can meet the demands of advanced portable electronic devices and can be directly integrated and used as on-board power sources in the subwatt range to operate small sensors and actuators (*I*). At slightly higher outputs, they can be used to power portable electronic devices such as cell phones (~1 W) and laptop computers (~20 W) (*I*).

Silicon (Si) micromachining technologies and related thin-film processes have been the chosen procedure for fabrication (*I*). They enable the stacking of fuel cell components on a chip for compact, lightweight power generation.

Fuel cells have been built onto ceramic, Si, and polymer substrates (2). Miniature fuel cells demand a simple and compact design in order to be useful as portable power sources. The same processes can be applied to the production of a miniature biofuel cell. Miniature biofuel cells have the potential to be fast, reliable, safe, economical, and environmentally safe, owing to elimination of the potentially explosive hydrogen gas and the cost of the platinum (Pt) catalyst. They also have *in vivo* applications to power sensors and numerous applications as power supplies for lab-on-a-chip technology. Although recent research in our group has led to the largest power densities reported for biofuel cells (3,4), these power densities could be further increased by improving transport to the electrode. Currently, the macroscale biofuel cell is limited by the diffusion of the fuel to the electrode surface. Mass transport can be improved by using hydrodynamic flow and by pumping the fuel to the electrode. Microelectrodes confine the fuel to an area the size of the electrode and radial diffusion replaces the linear diffusion that exists with macroelectrodes.

The application of microfabrication and microfluidics to fuel cell or biofuel cell research has been limited. A proton-exchange membrane fuel cell on polydimethylsiloxane (PDMS) substrates using traditional photolithography was developed. However, the Pt electrodes fabricated by vapor deposition did not offer the porous surface area or catalyst area needed to generate the desired current densities (1). Other work on a membraneless vanadium redox fuel cell employed the low Reynolds numbers that occur in microchannels to eliminate the mixing of the two fuel streams (5). The only biofuel cell mentioned employed two 7- μm -diameter carbon fiber electrodes placed inside a polycarbonate support. This biofuel cell is not truly microfabricated and not a microfluidic cell. Glucose oxidase and laccase were wired to the anode and the cathode, respectively. The biofuel cell showed an increase in power densities over other cells owing to the radial mass transport at the carbon fibers, and the wiring of the enzymes added selectivity and improved electron transfer between the enzymes and the electrodes with the elimination of a compartment-separating membrane. The power densities reported were 137 $\mu\text{W}/\text{cm}^2$ (6).

By utilizing PDMS to produce microchannels, fuel can be introduced by hydrodynamic pumping. Fully integrated microelectrodes can be fabricated using a technique of micromolding carbon ink (7). The connections can be fabricated using lithography to define palladium (Pd) leads that has been sputtered on that glass surface. Once enzyme immobilization and flow dynamics are optimized, a chip that contains a fully integrated bioanode can be produced. This anode in cooperation with an external Pt wire cathode can produce power for sensors and other microchip technology.

2. Materials

2.1. Solutions and Reagents

1. Nano SU-8 developer (Microchem, Newton, MA).
2. SU-8 50 photoresist (Microchem).
3. 30% Hydrogen peroxide.
4. Methylene green solution: dissolve methylene green and sodium nitrate (both from Sigma-Aldrich) so that the final solution concentration is 0.4 mM methylene green and 0.1 M sodium nitrate in 10 mM sodium borate (Sigma-Aldrich).
5. Modified Nafion casting solution: prepare by adding 3×10^{-4} mol of tetrabutylammonium bromide to each milliliter of 5% by weight. Nafion suspension. Mix for 5 min and cast on a weigh boat. Allow the suspension to dry and soak in water overnight. Rinse and dry the membrane. Redissolve the membrane in 1 mL of ethanol.
6. Nicotinamide adenine dinucleotide and alcohol dehydrogenase (Sigma).
7. Silver colloidal paste (Ted Pella, Redding, CA).
8. JB Weld epoxy (Sulphur Springs, TX).
9. Si wafers (100 mm) (Silicon, Boise, ID).
10. Sylgard 184 (Ellsworth Adhesives, Germantown, WI).
11. Isopropanol.
12. Sulfuric acid.
13. 20-Gage copper wire.
14. High-pressure fittings (F-120).
15. Leur adapter (P-659).
16. Teflon tubing or PEEK tubing ($1/16$ -in. o.d.) (Upchurch, Oak Harbor, WA).
17. Ercon E-978 (I) carbon ink.
18. Ercon N-160 solvent thinner.
19. Soda-lime glass.
20. Pt wire.
21. Piranha solution: prepare by mixing a 70% concentration of sulfuric acid with 30% peroxide.
22. Titanium (Ti) etchant (Transene).
23. AZ 300 MIF developer.
24. SU-8 10 photoresist (Microchem).
25. AZ 1518 positive photoresist.
26. Teflon tubing (250- μ i.d.) (Upchurch).

2.2. Equipment

1. Potentiostat (CH Instruments, Austin, TX).
2. Diamond drill bit (1 mm) (Jules Borel, Kansas City, MO).
3. Spin coater (Brewer Science, Rolla, MO).
4. Near-ultraviolet (UV) flood source (Autoflood 1000; Optical Associates, Milpitas, CA).

5. Freehand software (PC Version 8.0; Macromedia, San Francisco, CA).
6. Profilometer (Alpha Step-200; Tencor, Mountain View, CA).
7. Deposition (sputtering) system (Thin Film Deposition System; Kurt J. Lesker, Clairton, PA).
8. Dremel rotary tool (Racine, WI).
9. Miniature calomel reference electrode (CH Instruments).
10. Syringe pump (Harvard Apparatus, Brookfield, OH).

3. Methods

3.1. General Fabrication of Microchip Master

1. Coat a 4-in. Si wafer with SU-8 10 negative photoresist using a spin coater operating with a spin program of 1000 rpm for 30 s to make a master for the micromolding channel or a spin program of 1750 rpm for 30 s with SU-8 50 negative photoresist for the flow channels.
2. Prebake the photoresist for 5 min at 90°C.
3. Place a negative transparency film containing the micromolding channel or flow channel design structures on top of the photoresist (*see Notes 1 and 2*).
4. Expose the negative transparency film/photoresist sandwich to UV radiation with a near-UV flood source.
5. Postbake the wafer at 90°C for 5 min.
6. Develop the wafer with Nano SU-8 developer.
7. Wash the wafer with acetone and isopropanol in order to remove any excess, unexposed photoresist that may remain on the Si wafer.
8. Measure the thickness of the photoresist with a profilometer (this corresponds to the channel depth of the PDMS structure).

3.2. General Fabrication of PDMS Channels

1. Pour a 10:1 mixture of Sylgard 184 elastomer and curing agent onto a silicon wafer.
2. Cure at 75°C for approx 2 h.
3. Remove the master wafer by cutting around the edges with a razor blade and peeling the PDMS off of the wafer carefully. The master can be reused to make more PDMS channels.

3.3. Fabrication of Pd Electrodes

1. Purchase soda-lime glass plates (7 cm wide, 10 cm long, and 1.54 mm thick) from a local glass shop.
2. Soak the glass plates for 15 min in piranha solution.
3. Rinse thoroughly with Nanopure water.
4. Dry by blowing nitrogen gas over the glass plates.
5. Argon ion sputter a 200-Å layer of Ti, for adhesive purposes, onto a glass plate.
6. Argon ion sputter a 2000-Å layer of Pd onto the Ti layer (*see Note 3*).

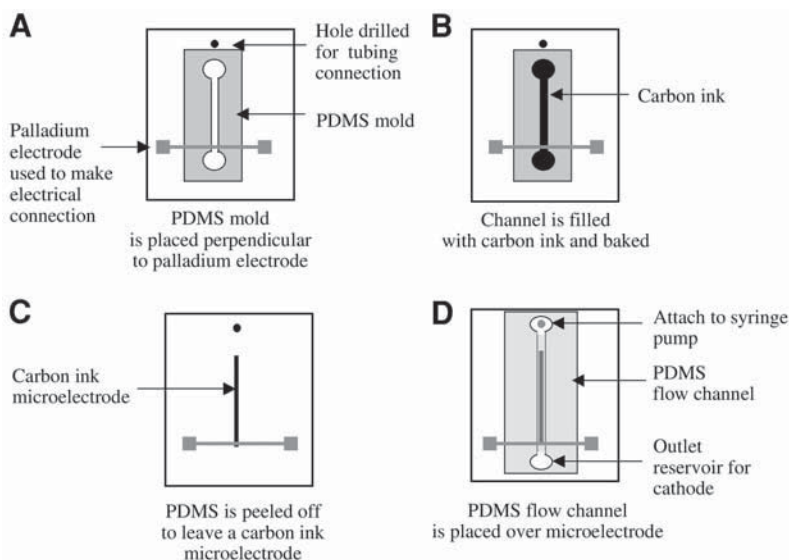


Fig. 1. Procedure for micromolding carbon ink electrodes using PDMS channels. (A) Chip before fabricating carbon ink electrodes. (B) Chip after pulling carbon ink through the mold. (C) Chip after electrode mold is removed, and (D) finished microchip.

7. Dynamically dispense AZ 1518 positive photoresist onto the Pd-coated glass plates at a rate of 100 rpm for 20 s.
8. Spin at 2000 rpm for 23 s.
9. Preexposure bake the glass plates at 95–100°C for 1 min.
10. Expose the film to 9 s of UV radiation using a near-UV flood source through a positive transparency film that contains designs for the Pd connector (*see Fig. 1A*).
11. Place the glass plates in AZ 300 MIF developer for 45 s.
12. Rinse the glass plates with water.
13. Dry by blowing nitrogen gas over the plates.
14. Postbake for 1 min at 95°C.
15. Soak in aqua regia (8:7:1 water: HCl: nitric acid) to remove the unwanted Pd.
16. Soak in Ti etchant to remove unwanted Ti from the glass plates.
17. Rinse the glass plates with acetone.
18. Rinse the glass plates with isopropanol.
19. Dry by blowing nitrogen gas over the glass plates.
20. Drill a flow access hole into each glass plate by immersing the glass plate in water and using a 1mm diamond drill bit and a Dremel rotary tool (*see Fig. 1A*).
21. Use the Dremel rotary tool (with cutting disk attachment) to remove the syringe connector portion of a Leur adapter (essentially cutting the Leur adapter in half).

22. Polish the cut side of the Leur adapter with a Dremel sanding disc.
23. Affix the polished side of the leur adapter to the glass plate with JB Weld Epoxy.
24. Cure the JB Weld Epoxy in an oven (75°C) for 2 h before use.
25. Make electrical connections to the Pd electrode by attaching a Cu wire to the Pd electrode with silver colloidal paste (*see Note 4*).

3.4. Micromolding Carbon Electrodes

1. Clean the glass plate with Nanopure water and dry with nitrogen gas.
2. Pressure seal a PDMS micromolding channel to the glass plate so that the Pd leads (with Leur fitting attached) are in contact with the channel and the channel extends to the flow access hole (*see Fig. 1A*).
3. Use high-pressure fittings to connect the Leur adapter to a syringe and syringe pump with 250- μ i.d. Teflon tubing.
4. Pump solvent thinner (N-160) through the channel for 30 min at a flow rate of 1 mL/min, to prime the channel.
5. Remove the thinner by applying a vacuum to one of the reservoirs.
6. Pump a mixture of the carbon ink and solvent thinner (mixture is 0.2% [v/w] ink in thinner) through the channel by applying vacuum (via water aspirator) to the opposite end (*see Note 5*), as shown in **Fig. 1B**.
7. After filling the channel with carbon ink, bake in an oven at 75°C for 1 h.
8. After the channel is cooled, carefully remove the PDMS from the glass plate, leaving the carbon microelectrode attached to the glass surface, as shown in **Fig. 1C**.
9. Place the chip in a separate oven at 120°C for 1 h to complete the curing.
10. Examine the electrode under a microscope to ensure that the electrode is complete and continuous (no visible holes or breaks).

3.5. Methylene Green Polymerization

1. Pressure seal a 2 \times 4 cm piece of PDMS with a 1 \times 3 cm ellipse cut out of the PDMS so that the entire length of the carbon ink electrode is exposed. This piece of PDMS will define the electrochemical cell.
2. Fill the electrochemical cell reservoir formed from the PDMS with the methylene green solution.
3. Insert a calomel reference electrode and Pt wire auxiliary electrode into the reservoir (*see Note 6*).
4. Using a potentiostat, perform seven cyclic voltammetric scans from -0.3 to 1.3 V at a scan rate of 0.05 V/s (*see Note 7*).
5. Remove the piece of PDMS.
6. Rinse the cell with Nanopure water.
7. Allow the cell to dry overnight before further modification.

3.6. Bioanode Fabrication

1. Make a fresh enzyme casting solution by mixing a 2:1 ratio of 1.0 μ M alcohol dehydrogenase with tetrabutylammonium bromide-modified Nafion solution

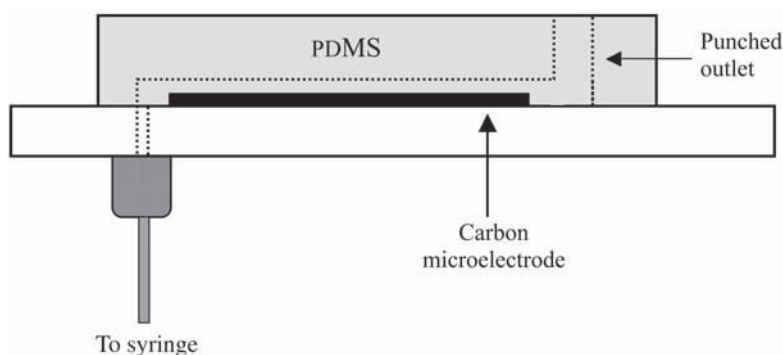


Fig. 2. Carbon ink microelectrode sealed in PDMS channel with access to flow through syringe from one end and outlet in PDMS at other end.

with 1 mg of NAD^+ for each 20 μL of tetrabutylammonium bromide-modified Nafion.

2. Place a PDMS channel that is 130 μm wide and 3.0 cm long over the carbon ink microelectrode as shown in [Fig. 1D](#) (*see Note 8*).
3. Attach a syringe (containing the enzyme casting solution) to the chip as shown in [Fig. 2](#).
4. Introduce the mixture into the channel through a syringe using a syringe pump (Harvard Apparatus) at 1.0 $\mu\text{L}/\text{min}$.
5. Once the mixture has traveled the entire length of the channel (monitored visually), allow the solvent to evaporate at room temperature.
6. After evaporation, remove the PDMS to leave a complete bioanode.

3.7. External Cathode

1. Cut a piece of 4-mm-i.d. glass tubing so that the tubing is 1 in. long.
2. Epoxy Nafion[®] 117 membrane to the end of the glass tubing using JB Weld.
3. Fill the glass tube with phosphate buffer (pH 7.15).
4. Insert a piece of 22-gage Pt wire into the glass tube.
5. Place this cathode in the reservoir at the end of the flow channel as shown in [Fig. 3](#).

3.8. Microfluidic System

1. Place a piece of PDMS with a 200- μm -wide channel over the bioanode (*see Note 8*).
2. Pump a fuel solution through the system at 0.5–10 $\mu\text{L}/\text{min}$ for 2 h to equilibrate the system.

3.9. Electrochemical Measurements

1. Pump a fuel solution containing 1.0 mM ethanol and 1.0 mM NAD^+ through the PDMS channel over the bioanode.

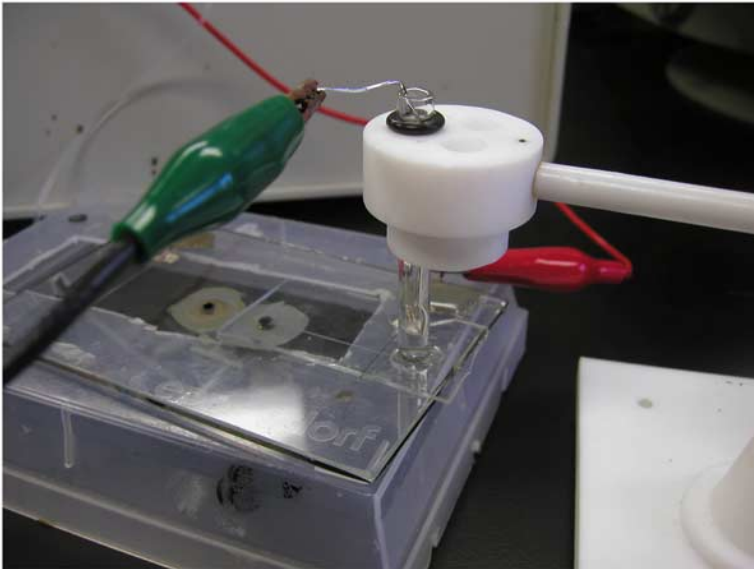


Fig. 3. Integrated microfluidic bioanode with external cathode. The cathode consists of a Pt wire in a glass tube with Nafion 117 membrane on one end and in phosphate buffer (pH 7.15).

2. Hook the bioanode and Pt wire of the cathode to the potentiostat (CH Instruments).
3. Measure the open-circuit potential.
4. Apply differing electrical loads to the circuit with the potentiostat.
5. After each electrical load is applied, measure the current produced. A plot of power density as a function of current will provide a power curve whose maximum corresponds to the maximum power that can be produced from the device. The biofuel cell can then be wired into other lab-on-a-chip devices to power sensors, pumps, and so on.

3.10. Conclusion

In the case of lab-on-a-chip technology, miniaturized, lightweight, and long-lasting energy sources are among the most urgently needed technologies. Microsystems require even smaller power sources, because weight and volume of on-board energy sources are disproportionately large compared to the systems that they power. By miniaturization, energy and materials consumed are decreased and integration with electronics is possible, leading to a simplified system in which cost is decreased without affecting performance. The market for miniaturization technology is promising owing to the use of microfluidics and microfabrication in separations, immunoassays, bioreactors, biomimetics,

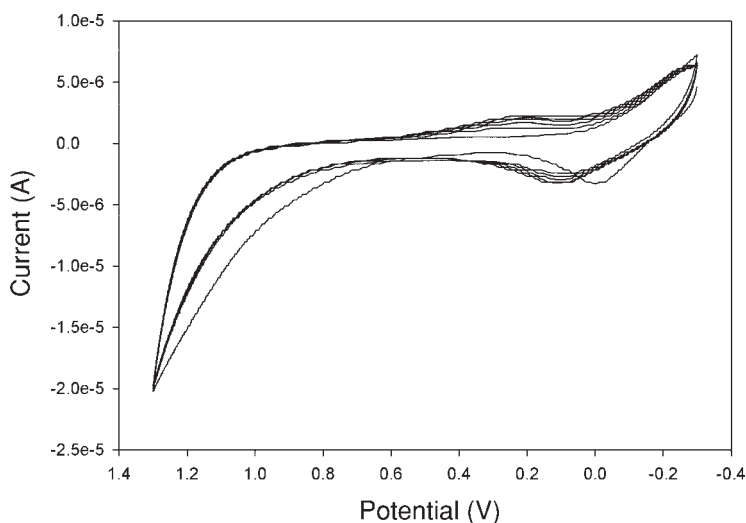


Fig. 4. Representative cyclic voltammogram of electropolymerization of methylene green on carbon ink microelectrode.

sensors, and power sources. Through the use of traditional photolithography, soft lithography, and micromolding of carbon inks, a biofuel cell can be integrated into a microchip. With the use of an external Pt cathode and an integrated bioanode on the microchip, open-circuit potentials of 0.34 V and current densities of $1.32 \times 10^{-4} \text{ A/cm}^2$ can be produced (8). This power source can be wired in series to a lab-on-a-chip device to provide power for pumps or transducers.

4. Notes

1. The transparency was made from a computer design drawn in Freehand. The design was transferred to a transparency using an image setter with a resolution of 2400 dpi by a printing service (Jostens, Topeka, KS).
2. For PDMS chips to form micromolding channels for the electrode, the design should be a line that is $45 \mu\text{m}$ wide and 2.5 cm long. For PDMS chips to form the channel for forming the enzyme layer, the design should be a line that is $130 \mu\text{m}$ wide and 3.0 cm long. For the biofuel cell flow channels, the design should be a line that is $200 \mu\text{m}$ wide and 3.0 cm long.
3. Pd was used owing to cost and availability, but Pt would also work.
4. If the colloidal silver does not produce a mechanically stable contact, one can use JB Weld to attach the wire to the glass plate and then colloidal silver paste to make the electrical contact between the wire and the Pd electrode.
5. Other commercially available screen-printing processes can be used, but we have had the best success with Ercon E-978(I) Carbon Ink.

6. Make sure that the electrodes are not touching or the system will short-circuit.
7. It is important to see the adsorption peak on the first scan of the cyclic voltammogram. If the adsorption peak near 0.0 V is not well defined (see Fig. 4), then the methylene green layer will not be active and performance will be minimal.
8. A microscope or magnifying glass may be helpful to line up the electrode and the flow channel. If they are not lined up parallel to one another, the cell will leak.

Acknowledgment

Special thanks to our collaborator R. Scott Martin, in whose laboratories many of these procedures were performed and perfected.

References

1. Shah, K., Shin, W. C., and Besser, R. S. (2003) Novel microfabrication approaches for directly patterning PEM fuel cell membranes. *J. Power Sources* **123**, 172–181.
2. Wainright, J. S., Savinell, R. F., Liu, C. C., and Litt, M. (2003) Microfabricated fuel cells. *Electrochim. Acta* **48**, 2869–2877.
3. Akers, N. L., Moore, C. M., and Minteer, S. D. (2005) Development of alcohol/O₂ biofuel cells using salt-extracted tetrabutylammonium bromide/Nafion membranes to immobilize dehydrogenase enzymes. *Electrochim. Acta* **50**, 2521–2525.
4. Akers, N. L. and Minteer, S. D. (2003) Towards the development of a membrane electrode assembly (MEA) style biofuel cell. *Proceedings of the ACS Fuel Chemistry Division* **48**, 895–896.
5. Ferrigno, R., Strook, A. D., Clark, T. D., Mayer, M., and Whitesides, G. M. (2002) Membraneless vanadium redox fuel cell using laminar flow. *J. Am. Chem. Soc.* **124**, 12,930–12,931.
6. Chen, T., Barton, S. C., Binyamin, G., et al. (2001) A miniature biofuel cell. *J. Am. Chem. Soc.* **123**, 8630–8631.
7. Kovarik, M. L., Torrence, N. J., Spence, D. M., and Martin, R. S. (2004) Fabrication of carbon microelectrodes with a micromolding technique and their use in microchip-based flow analyses. *Analyst* **129**, 400–405.
8. Moore, C. M., Minteer, S. D., and Martin, R. S. (2005) Microchip-based ethanol/oxygen biofuel cell. *Lab-on-a-chip* **5**, 218–225.

Microfluidic Chambers for Cell Migration and Neuroscience Research

Anne M. Taylor, Seog Woo Rhee, and Noo Li Jeon

Summary

This chapter describes the fabrication and use microfluidic chambers for cell migration and neuroscience research. Both microfluidic chambers are made using soft lithography and replica molding. The main advantages of using soft lithography to create microfluidic chambers are reproducibility, ease of use, and straightforward fabrication procedures. The devices can be fabricated in biology and chemistry laboratories with minimal access to clean-room facilities. First, a microfluidic chemotaxis chamber, which has been used in investigating chemotaxis of neutrophils, human breast cancer cells, and other cell types, is described. Precise and stable gradients of chemoattractants with arbitrary shapes can be generated for different applications. Second, a multicompartiment culture chamber that can fluidically isolate neuronal processes from cell bodies is described. The design of this chamber is such that only neurites grow through a series of microgrooves embedded in a physical barrier. Both devices are compatible with phase, differential interference contrast, and fluorescence microscopy.

Key Words: Soft lithography; polydimethylsiloxane; microfluidics; cell culture chamber; migration chamber; chemotaxis; compartment chamber; neuronal chamber.

1. Introduction

This chapter describes the use of soft lithography to create microfluidic chambers for cell migration studies and for culturing neurons. Microfluidics is increasingly becoming a useful tool for molecular biologists and cell biologists because of its ability to precisely control, monitor, and manipulate cellular microenvironments. Soft lithography uses polydimethylsiloxane (PDMS) as a stamp or mold to define micron-sized physical and/or chemical features. The microfluidic design is defined using a high-resolution transparency mask created using computer-aided drawing programs such as Freehand and AutoCAD.

Photolithography is used to pattern this microfluidic design onto a silicon wafer containing a layer of thick photoresist. We use the negative photoresist SU-8 because it can be used to make high structures. Once the SU-8 is patterned onto a silicon (Si) wafer, it becomes a fairly permanent structure and we use these patterned wafers as master molds to generate PDMS replicas. A solution of PDMS prepolymer is cast onto the master and cured to create a negative replica (i.e., the microfluidic chamber). PDMS is an ideal material for microfluidic chambers because it is biocompatible and optically transparent, and it can be irreversibly bonded to glass (1). In addition, PDMS is permeable to gases, making it useful for culturing cells.

Several microfluidic devices have been demonstrated for biological applications, including devices for separation of proteins and DNA, sorting and manipulation of cells, immunoassays, combinatorial screening, DNA sequencing, polymerase chain reaction, and enzymatic assays (2). A microfluidic chemotaxis chamber (MCC) has been developed to create precise gradient profiles to study neutrophil and cancer cell chemotaxis (3,4). The gradient-generating microfluidic chamber consists of a network of microchannels that produce a combinatorial mixture of starting solutions by repeatedly splitting, combining, and mixing fluid streams. At the end of the network, streams carrying different concentrations combine in a wide channel to generate a spatial gradient of soluble molecules. This device has been used to generate a gradient of laminin and other extracellular matrix (ECM) coatings on surfaces (5). A device that can generate dynamic temporal gradients has also been recently developed (6). Time-lapse microscopy is used to observe and record cell migration in response to the continuous gradient of soluble factors. The MCC has been successfully used to investigate chemotaxis of neutrophils, metastatic breast cancer cells, and several other cell types.

A multicompartiment chamber to culture neurons and isolate their processes has recently been developed to simulate microenvironments within the brain that may play a role in the pathogenesis of neurodegenerative diseases, such as Alzheimer's disease (7). Dissociated cortical and hippocampal neurons are plated into one compartment and their processes grow through a physical barrier embedded with microgrooves into a compartment containing exclusively neurites. Using a hydrostatic pressure difference, treatments to the neurites are isolated and studied exclusive of their cell bodies. In this chapter, we describe the procedures for fabricating and using the MCC for cancer cell migration and the multicompartiment culture chamber for neurons.

2. Materials

2.1. Equipment

1. Plasma cleaner (PDC-001; Harrick, Ossining, NY).
2. Laboratory oven (Fisher).
3. Photolithography-related equipment, aligner, and spinner.
4. Vacuum desiccator for degassing mixed PDMS.
5. Vacuum desiccator for silanizing wafers.
6. Syringe pumps (Harvard Apparatus, Holliston, MA).
7. Pressurized inert gas (nitrogen or argon).
8. Razor blades.
9. Round stainless steel punch (sharpened stainless steel tubes).
10. Humidified CO₂ incubator.
11. Laminar flow bench for cell culture.
12. Inverted microscope with charge-coupled device camera for time-lapse imaging.
13. Temperature-controlled and humidified box for time-lapse microscopy.

2.2. Supplies

1. Si wafers (3 in.) (Silicon Inc., Boise, ID).
2. High-resolution transparency masks (CAD/Art Services, Poway, CA).
3. Photoresists, SU-8 5 and SU-8 50 (MicroChem, Newton, MA).
4. Photoresist developer (propyleneglycolmethylether acetate [PGMEA]) (MicroChem).
5. PDMS release agent, (tridecafluoro-1,1,2,2-tetrahydrooctyl)trichlorosilane (Gelest, Morrisville, PA).
6. PDMS (Sylgard 184; Dow Corning, Midland, MI).
7. Disposable containers for mixing and degassing PDMS (plastic or paper cups).
8. Disposable stirring rods (plastic knives).
9. Scotch tape (3M Scotch 471).

2.3. Supplies for MCCs Only

1. Polyethylene tubing (PE-20; Becton Dickinson, Baltimore, MD).
2. Needles (21 gage) (Becton Dickinson).
3. Hamilton gastight syringes (250 and 500 μ L).
4. Three-way stopcock valve.
5. Disposable syringes (5 mL).

2.4. Cell Culture Supplies for MCCs

1. Metastatic human breast cancer cell line MDA-MB 231 (American Type Tissue Collection, Gaithersburg, MD).
2. Hank's balanced salt solution (HBSS) (Gibco, Carlsbad, CA).
3. 0.25% Trypsin/EDTA solution (Gibco).
4. Dulbecco's modified Eagle's medium (DMEM) (Gibco).
5. Leibovitz's L-15 medium (Gibco).

6. Bovine serum albumin (BSA) (Sigma, St. Louis, MO).
7. Fetal calf serum (FCS) (Gibco).
8. Penicillin-streptomycin (15070; Gibco).
9. Endothelial growth factor (Sigma).
10. Cell dissociation buffer (Invitrogen, Carlsbad, CA).
11. Collagen type IV (Sigma).

2.5. Cell Culture Supplies for Multicompartment Neuronal Culture Chambers

1. 0.25% Trypsin/EDTA solution (Gibco).
2. DMEM (Gibco).
3. FCS (Gibco).
4. Penicillin-streptomycin (Gibco).
5. Glass cover slip (No. 1, 24 × 40; Corning).
6. Poly-L-lysine (PLL) (mol wt = 70,000–150,000) (P1274; Sigma).
7. 99% Sodium tetraborate (100 g) (Sigma).
8. 99.5% Boric acid (100 g) (Sigma).
9. Rat (E18) primary cortical and/or hippocampal neurons (BrainBits).
10. Neurobasal media (Invitrogen).
11. B27 Nebasal Supplement (Invitrogen).
12. GlutaMAX (Invitrogen).

3. Methods

3.1. Microfluidic Chemotaxis Chamber

3.1.1. Fabrication of Master

Master molds that are used to create PDMS replicas are fabricated using photolithography (details of photolithography are included in another chapter). Masters are typically fabricated in a clean room and commercial fabrication services are available (*see Note 1*). Details of the design are described elsewhere and are beyond the scope of this chapter (**3**). The procedure for making the MCC master is shown in **Fig. 1** and is as follows (all steps are performed in a clean room):

1. Flood an Si wafer with SU-8 50 photoresist and spin at 1600 rpm for 60 s to obtain 50- μm -thick photoresist films (*see Note 2*).
2. Soft bake for 30 min at 100°C in an oven.
3. Expose the photoresist-coated wafer to ultraviolet (UV) light using a mask aligner for 1 min at 200 W. Use a high-resolution transparency mask that contains the pattern with a network of channels. The exposure time will depend on the output power of the UV lamp/mask aligner. Follow instructions from the photoresist supplier.
4. Postexposure bake at 90°C for 5 min in the oven.
5. Cool the wafer to room temperature.

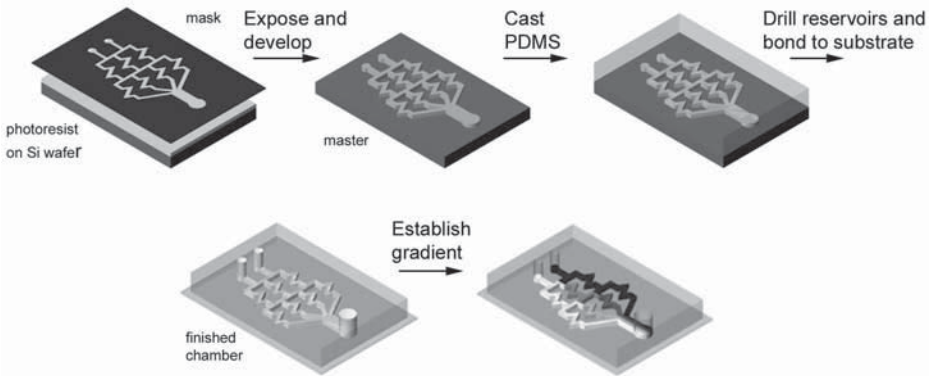


Fig. 1. Schematic of fabrication steps for the microfluidic chemotaxis chamber.

6. Develop in PGMEA for 5–10 min with gentle but thorough agitation until the unexposed area is completely developed away.
7. Rinse two to three times with fresh PGMEA solution and dry.
8. Dry and store until use.

3.1.2. Replica Molding

1. In a laminar flow hood (to minimize particulate contamination), place the patterned wafer in a clean Petri dish (100 mm), and then silanize in a vacuum desiccator using a drop of (tridecafluoro-1,1,2,2-tetrahydrooctyl)trichlorosilane placed in an open vial inside the vacuum chamber for 20 min. Silanizing the surface of the wafer allows ready release of solid PDMS from the master.
2. Make a PDMS mixture using a 10:1 ratio of prepolymer and catalyst. Thoroughly mix for 5 min and then place in a vacuum desiccator for 5 min to degas. A laboratory vacuum is satisfactory. If not properly degassed, bubbles may form and be trapped inside the PDMS, which can distort microchannels and hinder microscopy.
3. Place the master in a Petri dish and pour approx 30 g of the PDMS mixture onto the master (when using a different-size container, aim for approx 5 mm thickness). Place in a separate vacuum desiccator for another 10 min to remove bubbles trapped inside the PDMS.
4. Blow off any residual bubbles using inert pressurized gas.
5. Place the Petri dish in a laboratory oven and cure for >4 h at 70°C. The liquid PDMS mixture will become a transparent solid after curing (Fig. 1).
6. Cut the cured PDMS out of the Petri dish using a razor blade. Punch out holes in the PDMS using sharpened needles for fluidic inlets and outlets as well as cell-loading ports (see Note 3). Clean the surface by blowing off small particles with pressurized gas. Small particles will prevent irreversible bonding between glass and PDMS and cause leaks.

7. Place a glass slide and the PDMS device (microchannel side up) in a plasma cleaner and treat them for 30–60 s (medium setting in Harrick's Plasma Cleaner, approx 30 W of radio frequency [RF] power). The plasma exposure condition should be optimized for each instrument. Short plasma treatment in low RF power yields better results than longer treatments. After plasma treatment, immediately combine the two exposed surfaces to create an irreversible seal, resulting in the finished MCC (*see Note 4*).

3.1.3. Coating of Inside Surface of MCC

1. Fill channels with sterile deionized water from the outlet.
2. Coat the glass surface by pipetting 50 μL of collagen type IV (2 $\mu\text{g}/\text{mL}$) into the cell inlet. Incubate at room temperature for 30 min.
3. Rinse the channels three times with sterilized deionized water.
4. Block nonspecific protein binding with 2% BSA in Leibovitz's L-15 medium at 37°C for 2 h before use.

3.1.4. Microfluidic Connections

1. Prepare 0.2% BSA in L-15 medium with and without growth factor (*see Note 5*) and load into 250 μL Hamilton syringes with 21-gage needles. When using a flow rate of 0.1 $\mu\text{L}/\text{min}$, an 8–10-h experiment can be performed without refilling the syringe. For longer experiments, the syringe pumps can be stopped briefly to refill the syringes.
2. Connect PE20 polyethylene tubing to the syringes of the syringe pump (**Fig. 2**). Fill the tubing with media, and then insert into the top inlets in the MCC (*see Note 6*).
3. Adjust the flow rate to 0.1–10 $\mu\text{L}/\text{min}$ to create an optimum concentration gradient.

3.1.5. Chemotaxis Assay

1. Culture MDA-MB-231 cells in L-15 medium supplemented with 10% fetal bovine serum (FBS) and 1% penicillin-streptomycin at 37°C in a humidified incubator.
2. Serum starve the cells overnight in 0.2% BSA/L-15 medium before experiments. Remove the old medium from the culture flask and wash the cells with 6 mL of HBSS.
3. Incubate the detached cells for 5 min using 1 mL of cell dissociation buffer.
4. Centrifuge the detached cells at approx 150g for 5 min.
5. Wash with 0.2% BSA/L-15 medium once and resuspend in 0.2% BSA/L-15 medium.
6. Filter the cells through a 40- μm filter to obtain a single cell suspension.
7. Count the cells.
8. Using a micropipet, load 20 μL of cell suspension (100,000 cells/mL) into the MCC via the cell-loading port.

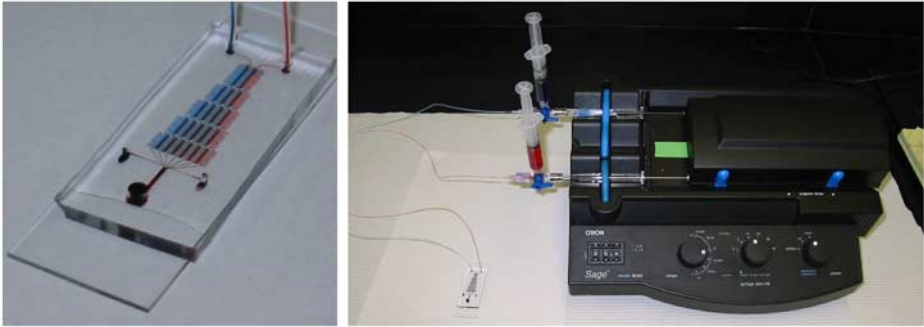


Fig. 2. Micrographs of microfluidic chemotaxis chamber and experimental setup.

9. Slow down or stop the flow inside the MCC when the cells are attached (visualized under a microscope).
10. After the cells attach, seal the loading port with tape and adjust the flow rate to 0.1–10 $\mu\text{L}/\text{min}$.
11. Place the chamber on the microscope in an enclosed environmental chamber maintained at 37°C. Acquire time-lapse images.

3.2. Multicompartment Neuronal Culture Chambers

3.2.1. Fabrication of Master

The steps to creating multicompartment chambers are largely identical to those for creating the MCC. The main difference is that the multicompartment chambers require two layers of aligned photoresist patterns to create the positive relief pattern (Fig. 3). The first thin layer (3 μm) forms the microgrooves in the barrier, and the second layer (100 μm) forms the cell culture chamber and the solid barrier. The mask designs are detailed elsewhere (7).

1. Flood an SU-8 5 photoresist on a cleaned 3-in. Si wafer and spin at 4000 rpm for 60 s (3 μm thick).
2. Soft bake the wafer for 1 min at 100°C in a leveled oven.
3. Expose the wafer through a high-resolution transparency mask (20,000 dpi; CAD/Art Services) containing 10- μm microgrooves for 30 s at 200 W.
4. Postexposure bake at 90°C for 1 min on a hot plate or 2–3 min in a drying oven.
5. Develop with PGMEA (photoresist developer) for 30 s.
6. Rinse two to three times with fresh developer solution.
7. Dry using pressurized inert gas.
8. Spin a second layer of photoresist using SU-8 50 at 1000 rpm for 60 s (100 μm thick).
9. Postexposure bake for 5 min at 100°C.

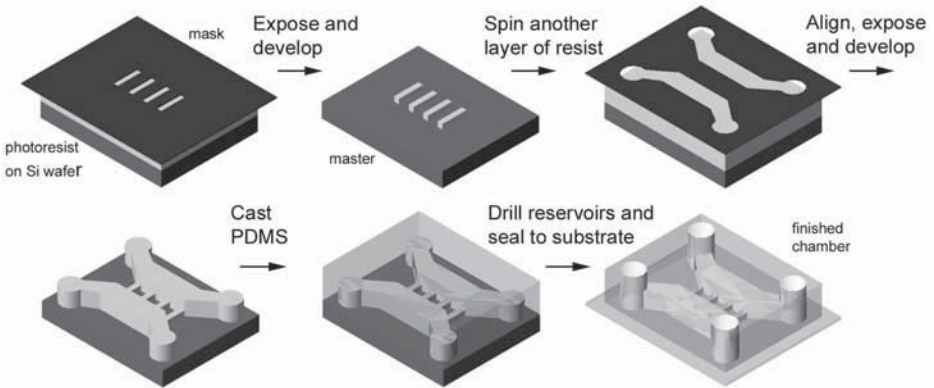


Fig. 3. Schematic of the fabrication steps for multicompartiment neuronal culture chamber. (Reproduced with permission from Langmuir, 2003, Copyright 2003 *Am. chem. Soc.* **19**(5), 1551–1556.)

10. Use a second mask to create the cell culture chamber compartments and barriers.
11. Align the chamber mask to the grooves patterned on the wafer using the alignment marks. Expose for 2 min.
12. Postexposure bake for 5 min at 90°C.
13. Develop for 5–10 min as needed. Rinse two to three times with fresh developer solution. Dry using pressurized inert gas.

3.2.2. Replica Molding of Multicompartiment Neuronal Culture Chambers

1. Repeat **step 1** in **Subheading 3.1.2**.
2. Rinse the wafer thoroughly with isopropanol, then 95% ethanol.
3. Repeat **steps 2–4** in **Subheading 3.1.2**.
4. Cure in a 70°C drying oven overnight (*see Note 7*).
5. Cut the cured PDMS out of the Petri dish using a razor blade. Use a sharpened stainless steel punch to create access holes (*see Note 3*).
6. Sterilize the device by immersing the chambers in 70% ethanol and dry in a hood for 1 h (*see Note 8*). **Steps 1–6** must be performed in a sterile laminar flow hood to minimize contamination and maintain sterility.

3.2.3. Coating of Substrate

1. Prepare 0.1 M borate buffer solution (1.24 g of boric acid, 1.9 g of sodium tetraborate, 400 mL of Nanopure water).
2. Dissolve 400 mg of PLL (1 mg/mL) in borate buffer solution by stirring for 30 min.
3. Sterilize the solution by filtering with a 2- μ m filter.
4. Clean glass cover slips using an ultrasonic cleaner in 95% ethanol for 1 h (*see Note 9*).

5. Remove the glass cover slips from the ethanol, rinse with 70% ethanol, and then dry under a laminar flow hood for 30 min.
6. Place the glass cover slips in PLL solution in a 37°C, 5% CO₂ incubator for 12 h.
7. After PLL coating, wash the glass cover slips twice in deionized water for at least 2 h.
8. Dry the glass cover slips overnight in a laminar flow hood under sterile conditions.
9. Store the coated glass cover slips in a 4°C refrigerator. Protect from light. PLL-coated glass cover slips must be used within 2 wk.

3.2.4. Assembly of Multicompartment Neuronal Culture Chambers

1. Place PDMS on the glass cover slip and lightly touch down on the PDMS until it is sealed to the glass around the chamber. This type of conformal seal is reversible, in contrast to irreversible seals formed when PDMS and glass are exposed to plasma before bonding. Usually no pressure is needed except around the barrier region in the middle of the device.
2. Use the assembled chambers within 1 to 2 h or fill the device with deionized water. Air bubbles may get trapped in the microgrooves if used after storage.

3.2.5. Loading of Cells

1. Use E18 rat cortical and/or hippocampal dissociated cell suspension with an approximate density of 3×10^6 cells/mL (see **Note 10**).
2. Load 10 μ L of cell suspension into one of the wells close enough to the channel that the cell suspension is drawn up into the channel by capillary action.
3. Load another 10 μ L into the opposite well connected to the cell channel.
4. Incubate the chamber for 5 min for the cells to attach to the glass.
5. Add 150 μ L of Neurobasal medium containing 2% B27, GlutaMAX, and penicillin-streptomycin to one of the wells.
6. After ensuring that the medium is drawn up into the channel, add an additional 150 μ L to the connecting well.
7. Add 150 μ L to each of the wells containing the cell suspension.
8. Incubate in a humidified 37°C incubator containing 5% CO₂.

3.2.6. Fluidic Isolation

Multicompartment neuronal chambers can be used to isolate chemical environments to either the somal compartment or the axonal compartment for several hours (**Fig. 4**).

1. Remove 15 μ L from one side of the chamber and add it to one of the wells in the adjoining compartment.
2. Repeat **step 1** for the other well.
3. Use 1 μ L or less of a concentrated insult (300 times the desired concentration), and gently add to each well in the compartment containing the lesser volume (see **Note 11**).

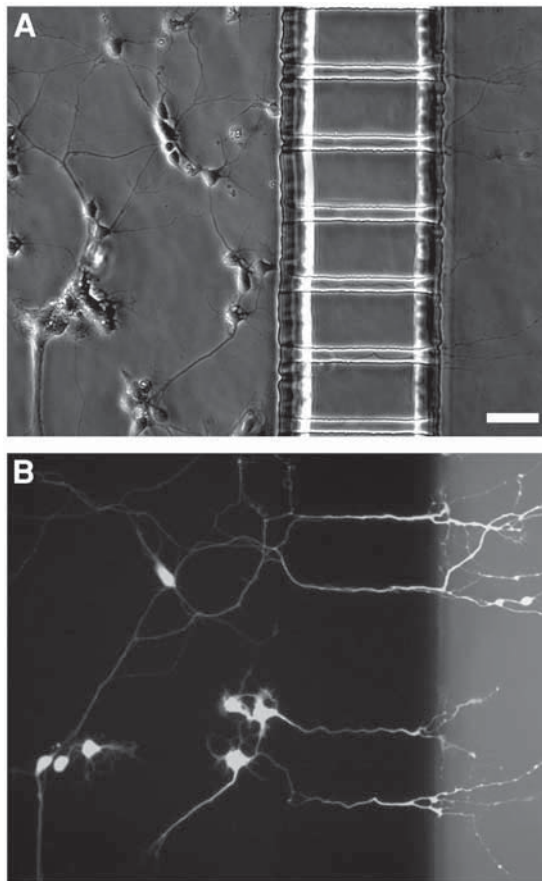


Fig. 4. Micrographs of neurons cultured in multicompartiment neuronal culture chamber. (A) A phase contrast image of CNS neurons plated in the left side. Neurites grow through microgrooves embedded in the PDMS barrier. (B) An epifluorescence image of the same field. The live cell marker (Calcein AM) and Texas Red–Dextran were loaded into the right compartment. Live neurons that have processes extending through the barrier were labeled by taking up Calcein AM. Soluble Texas Red–Dextran (light gray) was localized to the right compartment containing only processes. The scale bar is 57 μm . (Reproduced with permission from Langmuir, 2003, **19**(5), 1551–1556. Copyright 2003 *Am. Chem. Soc.*)

4. Notes

1. Electrical engineering departments in many universities may have an associated clean-room facility that may be able to fabricate masters. For example, at the University of California at Irvine, the Integrated Nanoscale Research Facility can fabricate masters for a fee (contact info@inrf.uci.edu).

2. When fabricating the master mold, the thickness of the photoresist can be controlled with spinner revolutions per minute and time. Follow the manufacturer's suggestions for photolithography.
3. Remove debris on the PDMS surface after punching the holes. Small particles are detrimental to the bonding of PDMS to glass substrate.
4. Avoid touching the PDMS surface that will be bonded to the substrate. Bonding is dependent on the cleanliness of the PDMS surface. It is a good practice to wear gloves and use tweezers when handling PDMS and glass.
5. To visualize the concentration gradient profile of growth factors, add 5 μM fluorescein isothiocyanate–dextran to the growth factor (e.g., endothelial growth factor) solutions.
6. Avoid introducing bubbles when filling the syringes and tubing with media.
7. Primary cortical and hippocampal neurons seem to be more sensitive and challenging to culture than other cell types. Be sure that the oven is dedicated for PDMS curing.
8. An alternative method is to sterilize the chambers with an autoclave.
9. We use a cover glass staining rack and a staining dish for immersing the glass in the PLL solution. Add sterile water to the PLL solution to cover the glass completely. Add 50 μL of Triton X-100 to reduce surface tension to eliminate bubbles in the PLL solution. We have additional staining dishes for subsequent washes. It is best to use the same staining dish for these steps.
10. If pregnant rats are not available, cortices and hippocampi can be ordered through BrainBits (www.brainbitsllc.com).
11. Do not add solutions close to the channel entry.

References

1. McDonald, J. C., Duffy, D. C., Anderson, J. R., et al. (2000) Fabrication of microfluidic systems in poly (dimethylsiloxane). *Electrophoresis* **21**, 27–40.
2. Sia, S. K. and Whitesides, G. M. (2003) Microfluidic devices fabricated in poly (dimethylsiloxane) for biological studies. *Electrophoresis* **24**, 3563–3576.
3. Jeon, N. L., Baskaran, H., Dertinger, S. K., Whitesides, G. M., Van de Water, L., and Toner, M. (2002) Neutrophil chemotaxis in linear and complex gradients of interleukin-8 formed in a microfabricated device. *Nat. Biotechnol.* **20**, 826–830.
4. Lin, F., Nguyen, C. M., Wang, S. J., Saadi, W., Gross, S. P., and Jeon, N. L. (2004) Effective neutrophil chemotaxis is strongly influenced by mean IL-8 concentration. *Biochem. Biophys. Res. Commun.* **319**, 576–581.
5. Dertinger, S. K., Jiang, X., Li, Z., Murthy, V. N., and Whitesides, G. M. (2002) Gradients of substrate-bound laminin orient axonal specification of neurons. *Proc. Natl. Acad. Sci. USA* **99**, 12,542–12,547.
6. Lin, F., Saadi, W., Rhee, S. W., Wang, S. J., Mittal, S., and Jeon, N. L. (2004) Generation of dynamic temporal and spatial concentration gradients using microfluidic devices. *Lab Chip* **4**, 164–167.
7. Taylor, A. M., Rhee, S., W., Tu, C. H., Cribbs, D. H., Cotman, C. W., and Jeon, N. L. (2003) Microfluidic multicompartiment device for neuroscience research. *Langmuir* **19**, 1551–1556.

Microtextured Polydimethylsiloxane Substrates for Culturing Mesenchymal Stem Cells

Erik T. K. Peterson and Ian Papautsky

Summary

Musculoskeletal tissue-engineering strategies have recently focused on the use of biomaterial scaffolds capable of guiding growth and organization of mesenchymal stem cells (MSCs), which are precursors for connective tissues. This chapter describes the methods for culturing MSCs on micropatterned polydimethylsiloxane (PDMS) substrates. MSCs are isolated from bone marrow biopsies and subcultivated before plating onto PDMS substrates. Micropatterned substrates are fabricated by casting PDMS on AZ P4620 photoresist molds. Prior to plating cells, substrates are cleaned, sterilized, and coated with fibronectin. Micropatterned growth surfaces are a useful research tool enabling the study of cell morphology and alignment in response to substrate geometry. Understanding MSC response to surface topography will assist in the design of improved scaffolds for connective-tissue repair.

Key Words: Micropatterned substrates; polydimethylsiloxane; photoresist; fibronectin; bone marrow; mesenchymal stem cells; contact guidance.

1. Introduction

In recent years, stem cells have become a subject of intense research owing to their potential applications in tissue engineering (1–6). In the case of mesenchymal stem cells (MSCs), these partially differentiated cells can produce a variety of connective tissues, including bone, cartilage, muscle, tendon, ligament, and adipose tissue (5–7). The use of MSCs in the development of tissue-engineered implants provides an attractive alternative to current techniques for connective-tissue repair. Musculoskeletal tissue-engineering strategies have recently focused on the use of biomaterial scaffolds capable of guiding growth and organization of the MSCs and extracellular matrix (ECM) (2–4,8–12).

The cellular microenvironment profoundly affects the overall behavior and development of an engineered tissue. It is now recognized that microscale surface topography can influence cell shape, alignment, motility, proliferation, gene activity, and more complex events such as tissue organization (13–23). Hence, incorporating microscale or nanoscale topographies at the cell–substrate interface may provide an attractive approach for guiding specific cell behaviors without destabilizing the delicate biochemical environment.

The first attempts to modify cellular microenvironments were carried out in the late 1950s by Weiss who investigated cell locomotion in response to surface micropatterns using a variety of substrata, including the internal collagenous layer of fish scale, plasma clots, and glass fibers (24). Although new techniques for defining micropatterned cell cultures such as microcontact printing (25,26) and laminar flow patterning (26,27) have been gaining popularity, methods involving microtextured substrates remain a versatile and enabling tool for the study of cell–substrate interactions. Today, microtextured substrates are relatively simple to fabricate via etching, polymer casting, laser ablation, or a variety of deposition techniques commonly employed in microfabrication (28). Features can be realized with high spatial resolution, from centimeter to subnanometer dimensions. Arrays of grooves, typically having equal channel and ridge widths, and cross sections resembling a square wave or V-shape are the most common micropattern geometry employed (19,22). In general, investigations found that cells align with the long axis of the grooves, and the relative degree of orientation depends on factors such as groove depth, width, and spacing between adjacent features. These cell–microtexture interactions leading to cell alignment, motility, and changes in morphology are a phenomenon known as contact guidance.

Although microtextured substrates for cell culture can be fabricated from a range of materials, casting a polymer such as polydimethylsiloxane (PDMS) offers several advantages over conventional micromachining of substrates. Once the master molds for casting are fabricated, 10–100 identical castings can be made at very low cost with minimal effort. PDMS can be purchased off the shelf as a two-component kit and can be cast and cured in any laboratory. It has excellent optical properties, which allow for a variety of microscopy techniques including phase contrast, differential interference contrast (DIC), and epifluorescence. It is permeable to CO₂ and O₂ relatively biocompatible, flexible, and durable and has good chemical resistance, although it does swell in many organic solvents (29–31). Furthermore, PDMS surfaces can be successfully modified by adsorbing proteins or via plasma processing to obtain specific surface characteristics (30–33).

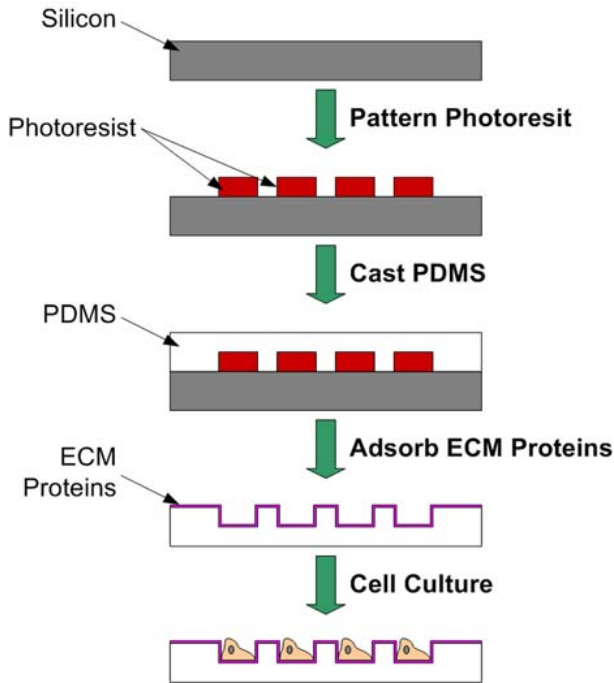


Fig. 1. Process for creating microtextured polydimethylsiloxane (PDMS) cell culture substrates.

Culturing MSCs on microtextured PDMS substrates involves several steps; this is schematically illustrated in **Fig. 1**. Although outside the scope of this chapter, mask design for creating microtextures can be performed using a layout software package, such as AutoCAD or L-Edit. For those not familiar with this process, MEMS and Nanotechnology Clearinghouse (www.memsnet.org) offers a fee-based mask design service. In the first step described, a master containing the negative microtexture pattern is fabricated. Here, positive-tone AZ P4620 photoresist (Clariant) is used to produce patterns 5–20 μm thick. This step must be performed in a clean room. If a clean room is not available, MEMS and Nanotechnology Clearinghouse also offers a variety of fee-based clean-room services. Steps similar to those described can also be used to produce patterns <1 μm thick using AZ 1500 (Clariant) or S1800 (Shipley) series photoresists, and patterns >20 μm thick can be achieved using a negative-tone SU-8 photoresist (Microchem). Once a master is fabricated, PDMS is cast to form the microtextured substrates. An example of a micropatterned PDMS sub-

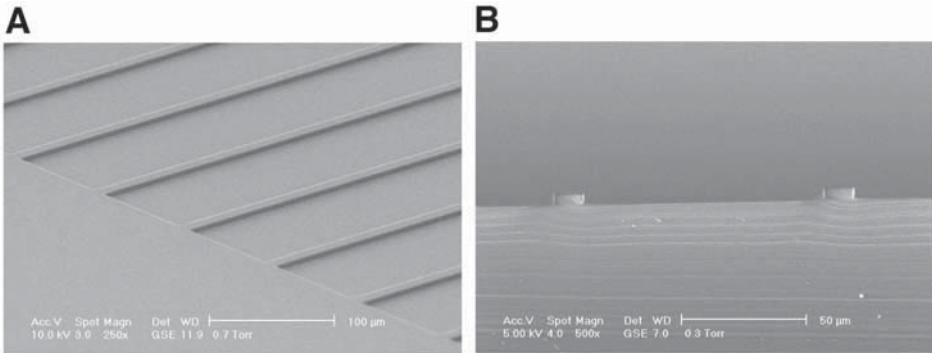


Fig. 2. Environmental SEM images of a polydimethylsiloxane (PDMS) substrate prior to plating cells: (A) top view; (B) cross section. The pattern has 10- μm ridge widths, 100- μm spacing, and 5- μm depth.

strate is shown in **Fig. 2**. This step does not require a clean-room facility and can be performed in a regular laboratory. The substrates are then prepared for cell culture by treating with oxygen plasma, cleaning, sterilizing, and coating with fibronectin. Once the substrates are prepared, they are ready for plating of cells. Freshney (34), provides an excellent review of animal cell culture techniques, and specific techniques for culturing MSCs have been presented in the literature (9,10,34–40). Although we discuss a simple method for culturing MSCs on PDMS, the basic techniques for fabricating the microtextured substrates and plating the cells may be extended to other adherent cell types. MSCs are isolated from bone marrow biopsies collected from 1-yr-old New Zealand White rabbits and expanded in culture. MSCs are then plated onto PDMS substrates and subcultured once more. Finally, MSCs on PDMS substrates are fixed in formalin and dehydrated through a series of ethanol/water dilutions. In this state, the samples can be preserved for several months. **Figure 3** shows examples of MSCs fixed on smooth and patterned PDMS substrates imaged using DIC and scanning electron microscopy (SEM). Alternatively, the samples can be analyzed by observing live cultures, although this becomes challenging if the number of substrates is large.

2. Materials

2.1. Preparation of Master

1. Silicon wafers (2 in.), one side polished, test grade; resistivity is not a factor.
2. Class 1000 or better high-efficiency particulate air flow hood, spinner, ultraviolet (UV) aligner, hot plates, ovens, deionized water supply at 18 $M\Omega\text{-cm}$ (DI H_2O).

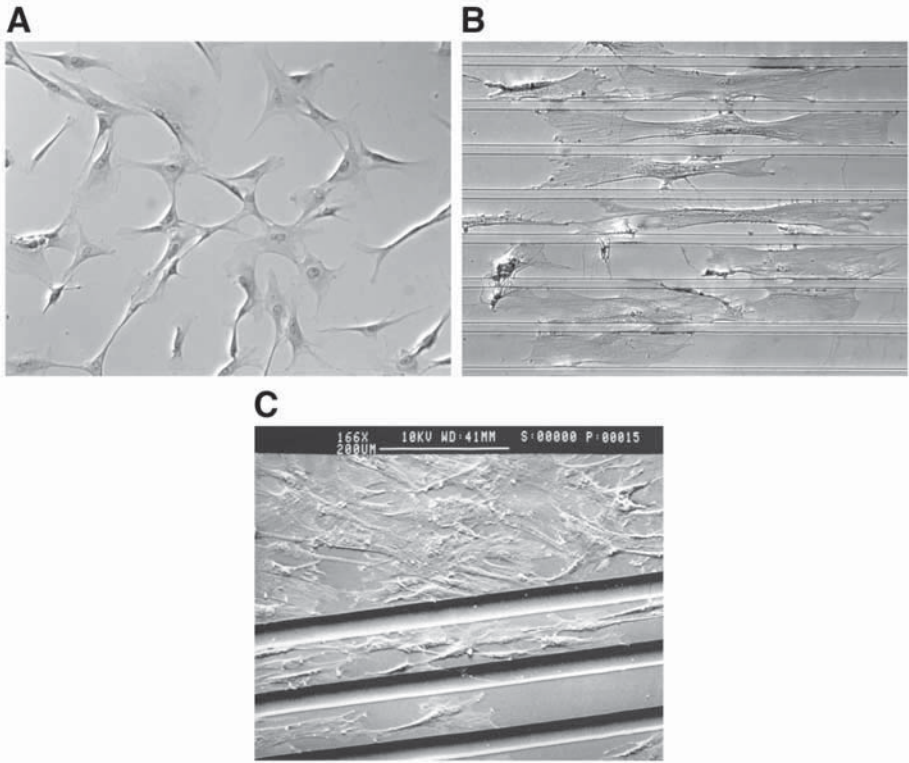


Fig. 3. Images of mesenchymal stem cells (MSCs) grown on PDMS substrates: (A) fixed cells on smooth polydimethylsiloxane (PDMS) differential interference contrast (DIC), $\times 200$; (B) fixed cells on patterned PDMS (DIC, $\times 200$) (C) scanning electron microscopy (SEM) of fixed cells on patterned PDMS ($\times 166$).

3. Acetone, methanol (MeOH), sulfuric acid (H_2SO_4), hydrogen peroxide (H_2O_2), ammonium fluoride, and hydrofluoric acid. All chemicals are electronics grade or American Chemical Society (ACS) grade (minimum).
4. Buffered oxide etchant (BOE): 1 HF:3 DI H_2O :3 NH_4F (v/v/v). Store at room temperature. This can be reused 50–80 times if kept free of dirt and debris.
5. Piranha solution: 3 H_2O_2 :7 H_2SO_4 (v/v) (*see Note 1*).
6. Pyrex Petri dishes (3 in.) and HDPE or polytetrafluoroethylene beakers.
7. AZ P4620 photoresist (store at 4–8°C) and AZ 400K developer (store at room temperature) (Clariant).
8. Level for hot plates and oven.
9. Wafer dipper and containers (Entegris).
10. Wafer-handling tweezers with Teflon coat (TechniTool).
11. Clean-room wipes.

12. Inspection microscope.
13. Surface profiler (e.g., KLA Tencor P-10).

2.2. Preparation of PDMS Substrates

1. Sylguard 184 kit (Dow Corning) containing elastomer base and curing agent.
2. Plastic cup (e.g., Dixie drink cups work well).
3. Plastic Petri dish or container to cast and cure PDMS.
4. Tape.
5. Plastic spatula.
6. Vacuum desiccator and pump.
7. Scale.
8. Leveled hot plate.
9. Pasteur pipet and bulb.
10. Syringe (5 or 10 cc).
11. Razor blade or scalpel.
12. Tweezers, sharp or needlepoint.
13. *Optional*: Positive displacement micropipet (1000 μ L) and tips, detergent.

2.3. Bone Marrow Harvest From Rabbits

1. Illinois 18-gage biopsy needles (sterile) (*see Note 2*).
2. Scalpel handle and no. 15 blades (sterile).
3. Syringes (10 cc) with leur-lock tips (sterile).
4. Heparin sodium, injectable (5000 U/mL) (Henry Schein).
5. Ethanol (200 proof) (Aaper) diluted in DI H₂O to 70% by volume.

2.4. Culture of MSCs

1. Class II laminar flow hood, CO₂ incubator, centrifuge, 37°C water bath, autoclave, inverted phase contrast microscope.
2. Sterile serological pipets (5, 10, 25 mL; Corning) and autopipettor.
3. Micropipets and sterile tips (100–1000, 10–100, 1–10 μ L; Eppendorf).
4. Hemocytometer counting chamber and lab counter.
5. T-75 tissue culture flasks (Corning).
6. Sterile centrifuge tubes (50 mL) (Falcon).
7. Sterile Pasteur pipets (9 in.) and aspiration equipment (vacuum flasks, tubing, and pump).
8. 1X Dulbecco's phosphate-buffered saline (PBS), liquid without CaCl₂ and MgCl₂ (cat. no. 14190; Gibco, Invitrogen).
9. Defined fetal bovine serum (FBS) (cat. no. SH30070; HyClone).
10. 100X Antibiotic-antimycotic (A/A), liquid (cat. no. 15240; Gibco).
11. 1X Trypsin-EDTA (0.25% trypsin, 1 mM EDTA) (cat. no. 25200; Gibco).
12. 1X Dulbecco's modified eagle's medium (DMEM) liquid, low glucose (cat. no. 11885; Gibco).
13. MSC Complete Medium (MSC-CM): DMEM, supplemented with 10% FBS and 1% A/A.

14. Trypan blue stain (0.4%) (Sigma, St. Louis, MO).
15. Glacial acetic acid, aldehyde free (Fisher).
16. Ethanol (200 proof) (Aaper) diluted in DI H₂O to 70% by volume.

2.5. Preparation of PDMS Substrates for Cell Culture

1. Class II laminar flow hood with UV light.
2. Sterile Pasteur pipets (9 in.) and aspiration equipment (vacuum flasks, tubing, and pump).
3. Petri dishes or containers for storage of PDMS substrates.
4. Tissue culture dishes (60 mm) (Falcon).
5. Ethanol, 200 proof (Aaper) diluted in DI H₂O to 70% by volume.
6. Reactive ion etcher (RIE) system with ultrahigh purity oxygen.
7. Ethanol burner.
8. Stainless steel wafer-handling tweezers (TechniTool).
9. DMEM, liquid, low glucose (cat. no. 11885; Gibco).
10. Fibronectin from rabbit plasma (1 mg) (cat. no. 341650; Calbiochem-Novabiochem).

2.6. Plating and Culturing of MSCs on PDMS Substrates

1. Class II laminar flow hood, CO₂ incubator, centrifuge, 37°C water bath, autoclave, inverted phase contrast microscope.
2. Sterile centrifuge tubes (50 mL) (Falcon).
3. Tissue culture dishes (60 mm) (Falcon).
4. Sterile Pasteur pipets (9 in.) and aspiration equipment (vacuum flasks, tubing, and pump).
5. 1X Dulbecco's PBS, liquid without CaCl₂ and MgCl₂ (cat. no. 14190; Gibco).
6. MSC-CM: DMEM supplemented with 10% of FBS and 1% A/A.
7. Ethanol (200 proof) (Aaper) diluted in DI H₂O to 70% by volume.

2.7. Fixation of MSCs on PDMS Substrates

1. 1X Dulbecco's PBS, liquid without CaCl₂ and MgCl₂ from (cat. no. 14190; Gibco).
2. Ethanol (200 proof) (Aaper) diluted in DI H₂O to 70% by volume.
3. Formalin, Fisherbrand Formalde-Fresh Solution (cat. no. SF94-4).
4. Glass cover slips (2 in., no. 1.5) (Fisher).

3. Methods

3.1. Preparation of Master (in Class 1000 or Better Clean Room)

3.1.1. Cleaning of Wafer

1. Use clean 3-in. Petri dishes. Fill one with acetone, one with MeOH, and one with piranha.
2. Rinse a wafer in running DI H₂O for 2 min.
3. Place the wafer in the Petri dish containing acetone for 2 min.

Table 1
Parameters for AZ P4620 Processing

Process parameter	Desired film thickness		
	5 μm	10 μm	20 μm
Spread speed (10 s)	500 rpm	500 rpm	500 rpm
Spin speed (30 s)	8000 rpm	2800 rpm	1000 rpm
Room temperature relaxation	5 min	5 min	5 min
65°C Oven soft bake	4 min	5 min	5 min
100°C Hot plate soft bake	4 min	5 min	5 min
65°C Oven soft bake	4 min	5 min	5 min
Room temperature relaxation	~15 min	~20 min	~20 min
Exposure ^a	50 s	90 s	120 s
Development (3.5:1)	~75 s	~2 min	~2.5–3 min

^aFor a 275-W lamp, constant intensity (CI) mode.

4. Transfer the wafer to the Petri dish containing MeOH for 2 min.
5. Rinse in running DI H₂O for 1–2 min.
6. Place the wafer in the Petri dish containing piranha for 10 min.
7. Rinse in running DI H₂O for 3–5 min.
8. Place the wafer on a dipper or in a basket and submerge in BOE solution for 20 s.
9. Rinse under running DI H₂O; the water should bead up, indicating that the oxide has been removed.
10. Blow-dry using dry N₂.
11. Dehydrate the surface of the wafer by placing it on a hot plate at 150–200°C for 20 min or in an oven at 120°C for 45–60 min.
12. Allow the wafer to cool to room temperature before proceeding with photoresist processing.

3.1.2. AZ P4620 Photoresist Processing

1. Center the clean wafer polished side up on a spinner vacuum chuck.
2. Pour about 3 mL of AZ P4620 on the center of the wafer; avoid trapping bubbles in the resist.
3. Spin coat the photoresist using spread and spin parameters from **Table 1** (see **Note 3**).
4. Place the wafer on a flat, level surface at room temperature for 5 min while covered with a Petri dish lid.
5. Soft bake on a leveled rack in a 65°C oven for 5 min, transfer to a leveled 100°C hot plate for 5 min, and then transfer to the 65°C oven for 5 min (see **Note 4**).
6. Allow the photoresist to relax at room temperature for approx 15–20 min while covered with a Petri dish (see **Table 1**).

7. Expose the photoresist to UV light using a Karl Suss Aligner (MJB3) with a 275-W lamp in vacuum contact mode. Exposure time depends on film thickness and is given in **Table 1** (see **Note 5**).
8. Fill one 500-mL beaker with 3.5 DI H₂O:1 AZ 400K developer (v/v) and one with fresh DI H₂O for rinsing.
9. Place the wafer on a dipper, submerge in developer, and agitate lightly.
10. Develop for 1–3 min (use **Table 1** to determine the exact development time based on film thickness).
11. Remove the dipper from the developer and immediately submerge in the second beaker containing DI H₂O.
12. Place the second beaker under slowly running DI H₂O for 2–3 min, but make sure that the water stream does not directly hit the wafer.
13. Gently blow-dry using dry N₂.
14. Inspect the photoresist patterns on the wafer under a microscope (see **Note 6**).
15. Check the photoresist pattern dimensions using a surface profiler.

3.2. Preparation of PDMS Substrates

1. Use a new 10-mL syringe (without needle), and withdraw the PDMS elastomer base and transfer 10 g to a cup on a scale (see **Notes 7 and 8**).
2. Use a pipet to transfer 1 g of the curing agent to the plastic cup on the scale containing the elastomer base.
3. Mix thoroughly for 2–3 min using a spatula (see **Note 9**).
4. Place the cup inside a vacuum desiccator and turn on the vacuum (25–28 in. Hg) for 20–30 min or until no bubbles are left (see **Note 10**).
5. Tape the master pattern side up to the bottom of a clean plastic Petri dish.
6. Pour degassed PDMS over the master directly from the cup (see **Note 11**).
7. Degas the filled molds a second time to remove any air bubbles introduced while pouring the PDMS.
8. Cure the PDMS on a leveled 80°C hot plate. Curing time depends on the thickness of the PDMS (thick layers will take longer than thin layers) and the curing temperature. Curing times for a thin 1- to 5-mm-thick layer of PDMS on an 80°C hot plate are given in **Table 2** (see **Note 12**).
9. Turn off the hot plate and let the PDMS cool to room temperature.
10. Use a razor blade or scalpel to cut around the patterns, and then use tweezers to carefully and slowly peel the PDMS away from the mold as shown in **Fig. 4** (see **Note 13**).
11. Clean the PDMS substrates by sonicating in 70% EtOH followed by DI H₂O for 20 min each.
12. Dry the PDMS substrates in an oven at 90°C for 1 h.

3.3. Bone Marrow Harvest From Rabbits

1. Obtain a 1-yr-old, skeletally mature, female New Zealand White rabbit within 15 min following euthanasia.
2. Place the rabbit on a dissection table on its stomach with the hind legs tucked underneath.

Table 2
Curing Times for PDMS Layers at 80°C

PDMS film thickness (mm)	Cure time
>1	1 h
1–5	1–2 h
12	4 h

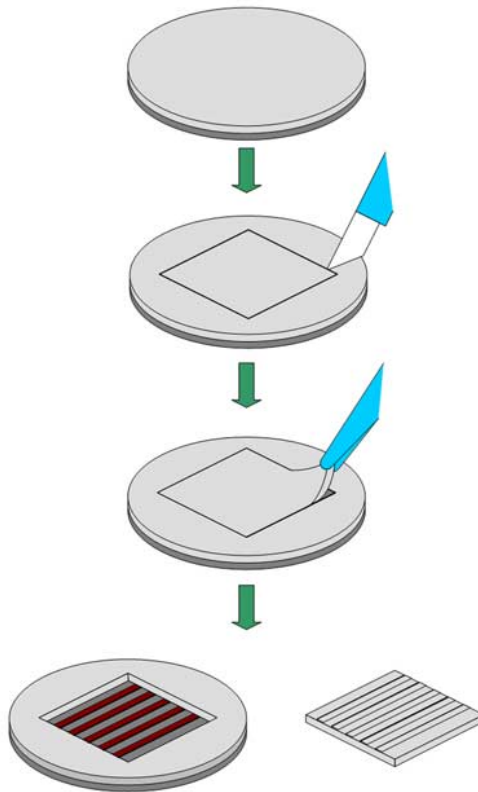


Fig. 4. Schematic diagram showing polydimethylsiloxane (PDMS) mold release.

3. Thoroughly scrub the area around the hips using 70% EtOH.
4. Use a scalpel to make a 5–6 cm incision to expose completely the iliac crest (*see Note 14*).
5. Open a sterile biopsy needle and use a syringe to flush with 3 cc of heparin (diluted to 3000 U/mL in PBS), and then replace the stylus and secure the end cap before penetrating the bone.

6. Insert the biopsy needle into the center of the incision described in **step 4** and **Note 14** while carefully rotating and pushing the tip into the bone at a compound angle approx 45° to the sagittal, transverse, and coronal planes to a depth of 2–4 mm into the bone marrow cavity.
7. Remove the stylus and connect the biopsy needle to a sterile 10-cc syringe preloaded with 2 cc of heparin (3000 U/mL).
8. Pull the bone marrow into the syringe (*see Note 15*).
9. Detach the syringe from the biopsy needle and cap it using a fresh sterile needle (with cap).
10. Invert the syringe 20–30 times to thoroughly mix the sample with heparin to avoid clotting.
11. Transport syringes containing the samples to the cell culture laboratory at room temperature.

3.4. Culture of MSCs

3.4.1. Direct Plating of Primary MSCs

1. Thoroughly clean the outside of the syringes containing bone marrow samples using 70% EtOH and wipe dry.
2. Remove the caps and carefully transfer the bone marrow samples into 25 mL of DMEM + 1% A/A at 37°C in a sterile 50-mL centrifuge tube while just keeping the tip submerged in the medium.
3. Centrifuge at 1000g for 6 min.
4. Aspirate the supernatant while carefully avoiding contact with the cell pellet.
5. Resuspend in 25 mL of DMEM + 1% A/A at 37°C.
6. Centrifuge a second time at 1000g for 6 min.
7. Resuspend in 10 mL of MSC-CM.
8. Remove a 50-μL aliquot of cell suspension.
9. Mix thoroughly with 450 μL of DMEM in a 2-mL microcentrifuge tube.
10. Withdraw 50 μL of the new suspension and mix with 50 μL of 4% acetic acid in a second 2-mL microcentrifuge tube.
11. Withdraw a 10-μL aliquot from the second tube and count the nucleated cells on the hemocytometer using phase contrast at ×100 on an inverted microscope (*see Note 16*).
12. Plate the cells (P_0 , d 0) in T-75 flasks at approx $23\text{--}25 \times 10^6$ cells per flask in a total volume of 20 mL of MSC-CM.
13. Incubate at 37°C with humidity and 5% CO₂ (*see Note 17*).
14. On d 3, gently rock each flask two times to loosen red blood cells from the growth surface, and add 5 mL of MSC-CM to each flask.
15. On d 5, gently rock each flask, wash with 10 mL of PBS, and feed with 20 mL of MSC-CM.
16. Observe colony formation using a ×100 inverted phase contrast microscope.
17. Aspirate the spent medium and feed the cells every 3 to 4 d with 20 mL of MSC-CM. At 10–14 d, once cultures become approx 40% confluent with colonies, cells are ready for the first subculture (P_1).

3.4.2. Subcultivation of MSCs (see **Note 18**)

1. Aspirate the spent medium.
2. Add 10 mL of PBS and gently rock the flasks several times.
3. Remove the wash using aspiration.
4. Add 5 mL of trypsin-EDTA to the side of each flask.
5. Rock the flasks to ensure complete coverage.
6. Aspirate approx 2–3 mL of the trypsin-EDTA.
7. Incubate at 37°C for 5 min.
8. Remove the flasks from the incubator, and use a 25-mL pipet to rinse with approx 15 mL of MSC-CM over the growth surface of the first flask.
9. Withdraw the suspension back into the pipet and rinse again (see **Note 19**).
10. Withdraw the suspension with the pipet, and use it to collect cells from the remaining flasks in the same manner.
11. Once cells have been collected from all the flasks, transfer the suspension to a 50-mL centrifuge tube.
12. Top off the centrifuge tube with MSC-CM to a total volume of 30 mL.
13. Centrifuge at 1000g for 6 min, aspirate the supernatant, and resuspend in 10 mL of MSC-CM.
14. Perform a viability count using Trypan blue. Remove a 50- μ L aliquot of cell suspension and mix with 50 μ L Trypan blue in a 2-mL microcentrifuge tube. Wait 2 to 3 min for the cells to take up the dye, and then remove a 10- μ L aliquot to load the hemocytometer for counting. Count the viable, nucleated cells.
15. Replate the cells at approx 300,000 cells per T-75 flask to expand the population further, or plate directly onto PDMS substrates at approx 5000/cm² in 60-mm Petri dishes.

3.5. Preparation of PDMS Substrates for Cell Culture

3.5.1. Plasma Treatment and Storage of PDMS Substrates

1. Clean the PDMS substrates by sonicating in 70% EtOH and then DI H₂O for 20 min each.
2. Dry the PDMS substrates in an oven at 90°C for 1 h.
3. Treat the clean, dry PDMS substrates with O₂ plasma in an RIE system at 50 W, 13.56-MHz radio frequency (RF) power, and 20-sccm O₂ flow for 20 s.
4. Store the treated PDMS substrates submerged in DI H₂O in Petri dishes until ready for plating cells (see **Note 20**).

3.5.2. Sterilization of PDMS Substrates

While performing **steps 1–3**, keep forceps in a centrifuge tube containing a small amount of EtOH and flame before use.

1. Rinse once with 70% EtOH and submerge in fresh EtOH for approx 15–20 min in clean Petri dishes.
2. Rinse and submerge several times with sterile PBS to remove any residual ethanol.
3. Transfer to sterile Petri dishes pattern side up using forceps.

4. Allow substrates to air-dry in open dishes for approx 6 h under UV light in a laminar flow hood.

3.5.3. Pretreatment of PDMS Substrates With Fibronectin

1. Dilute fibronectin in DMEM to desired concentration, approx 50 $\mu\text{g}/\text{mL}$ (*see Note 21*).
2. Place the sterile PDMS substrates in 60-mm sterile Petri dishes, and add fibronectin solution until the substrates are submerged. Swirl the dishes to ensure complete coverage.
3. Incubate at room temperature in a laminar flow hood for 30–45 min.
4. Aspirate the solution immediately prior to adding the cell suspension. Do not touch the growth surface with the pipet tip. Do not allow the PDMS surface to dry between aspiration and plating of cells.

3.6. Plating and Culturing of MSCs on PDMS Substrates

1. Resuspend the cells to approx 100,000 cells/mL in a 50-mL centrifuge tube.
2. Fill the 60-mm dishes containing the PDMS substrates with approx 6–7 mL of MSC-CM at 37°C to submerge the substrates completely.
3. Add 40,000–50,000 cells or approx 5000 cells/cm² to each 60-mm dish (i.e., 0.5 mL of suspension/dish) by pipetting the suspension onto the middle of the substrate and wait 60 s.
4. Gently swirl each dish before placing in an incubator.
5. Incubate at 37°C with humidity and 5% CO₂ for 4–6 d before fixation while making regular observations (*see Note 22*).
6. Feed with 6 to 7 mL of MSC-CM every 3 d and 24 h prior to fixation.

3.7. Fixation of MSCs on PDMS Substrates

1. Aspirate the medium and rinse once using PBS at 37°C.
2. Aspirate and replace with formalin diluted to 4% in PBS at room temperature for 30 min.
3. Aspirate the formalin and dehydrate the samples by using a series of ethanol/water dilutions according to the schedule summarized in [Table 3](#). Use Petri dishes and transfer the samples with tweezers (*see Note 23*).
4. After drying, place the samples pattern side up on clean 2-in. no. 1.5 cover slips to avoid flexing and to simplify handling (*see Note 24*).

4. Notes

1. For a typical process, in a clean 6-in. Petri dish, combine 30 mL of H₂O₂ with 70 mL of H₂SO₄. Stir with tweezers. **Caution:** this reaction is very exothermic. After use, wait for the mixture to cool before disposing. Do not store; mix a fresh solution for each use.
2. Although disposable, the needles may be used several times with careful cleaning and ethylene oxide sterilization. However, the tips will eventually become dull, and after 6–10 uses new needles are required.

Table 3
Dehydration of PDMS Substrates

Process	Time (min)
Rinse in running DI H ₂ O	4
30% EtOH	3
50% EtOH	3
70% EtOH	3
90% EtOH	3
95% EtOH	3
100% EtOH	5
100% EtOH	5
Air-dry	30

3. When spinning 10- μm and thicker layers, formation of an edge bead will become a problem during the exposure step owing to nonconformal contact with the mask photo plate. Thus, for films 10 μm and thicker, following spin coating, keep the wafer on the spinner chuck and rotate at approx 100 rpm or slower (slower is better). Use a clean-room wipe with acetone to remove the edge bead of photoresist. Alternatively, a plastic drinking straw cut at a 45–60° angle can be carefully touched to the edge of the wafer as it rotates to collect the resist buildup. In addition, when spinning at high speed, sometimes “whiskers” of photoresist will form around the perimeter, and these can also be removed using the aforementioned methods.
4. Soft bake and development times may need to be adjusted slightly depending on the ambient temperature and relative humidity in the clean room during processing.
5. When exposing for durations >60 s, better results are obtained if the exposure is performed in two or more steps with a 30-s break between doses.
6. Photoresist patterns should be inspected frequently (every 30–60 s) during the development (**step 10**) until the exact process time is determined. A final inspection should be done at the end of the development process. During the inspection, look at the corners of the smallest photoresist patterns. Convex or acute corners indicate underdeveloped photoresist and, thus, additional development time is necessary. In this case, place the wafer back in the developer for additional time and then repeat the inspection step. Concave or oblique corners indicate overdevelopment. Unfortunately, overdevelopment is a terminal problem, and the entire process must be restarted. In this case, the wafer-cleaning steps (*see Subheading 3.1.1.*) may be performed to remove the resist, and the wafers may be reused. Peeling, pitting, cracking, or “mouse bites” in photoresist patterns may also occur and are typically indicative of poor adhesion or overexposure. Poor adhesion is frequently caused by poor wafer cleaning, overdeveloping, or excessive agitation during the development. These problems are also terminal, and the entire process must be restarted.

Table 4
PDMS Curing Times for 1- to 5-mm-Thick Films

Temperature (°C)	Approximate time (h)
20	24
65	4
80	2

7. Always wear gloves and protect all work surfaces when casting PDMS. Uncured PDMS is terribly messy and sticks to everything; it is difficult to clean from surfaces and will never wash out of clothing. Incorporation of dirt can ruin results. Covering the bench top with clean aluminum foil can help reduce the amount of dust and dirt. After pouring into the cup for mixing, replace all caps immediately.
8. The PDMS is mixed at a 10:1 (m/m) ratio of elastomer base to curing agent. It is very important to maintain this ratio for consistent results. Typically, 10 g of the base and 1 g of the curing agent are sufficient. To cover a 3-in. Petri dish with a membrane a few millimeters thick, one will need 8–15 g of PDMS; to cover a 2-cm² pattern area approx 1 mm thick, one will need 1–2 g of PDMS. It can be difficult to thoroughly mix <5 g using a spatula and cup.
9. PDMS must be mixed until it becomes homogeneous and milky white owing to air bubbles stirred in.
10. To speed up the process, the vacuum can be released and pumped down a second or even third time. Each cycle bursts more air bubbles.
11. For better accuracy, a positive displacement micropipet may be used. Filling the molds on a scale provides an added degree of accuracy. Try to avoid introducing additional bubbles. If the PDMS layer is too thin (<100 μm thick), it may tear when trying to peel it later, making it very difficult to work with. Thick layers may be difficult to image using an inverted microscope owing to the short working distances of many objectives. Samples 0.5–1 mm thick seem to work best for cell culture.
12. For a 1- to 5-mm-thick sample, alternative curing conditions are summarized in [Table 4](#). Overcuring does not cause any obvious problems but has been reported to have an effect on the mechanical and optical properties of PDMS. However, temperatures higher than 80°C may degrade photoresist or melt polystyrene Petri dishes and are not recommended.
13. Avoid touching the photoresist pattern with the blade or tweezers, because this will damage the photoresist master. If cutting out square patterns, peel diagonally (from corner to corner). When cutting subsequent PDMS substrates, overcut the area to reduce the meniscus near the patterns.
14. The iliac crest can be located by an indentation on the anterior portion of the bone, marked by three raised protrusions forming a small triangle.

15. A good bone marrow biopsy will have some fatty tissue in the mixture, whereas a poor biopsy (usually owing to an incorrect needle placement) will have almost entirely blood and no visible fatty tissue. Biopsies are performed bilaterally, and no great variation in MSC cell counts seems to correlate with the volume of bone marrow withdrawn beyond 3 to 4 cc. Typically, 3–5 cc is preferred.
16. From a typical biopsy (3–5 cc), anywhere from 100 to 300×10^6 cells are collected and counted. However, not all cells will attach and survive. The dilution factor is 20 when calculating this initial cell count.
17. Caps should be loosened approximately one half turn to allow proper ventilation.
18. Cells should be subcultured after 10–14 d of P_0 , or when cells reach approx 90% confluence in subsequent passages.
19. At this point, the cells should be seen detaching and going into the suspension. If cells are still attached to the growth surface, an additional wash may be required. If this does not release the cells, the 37°C trypsin incubation period may need to be increased; however, if cells are incubated with the trypsin too long, they will become damaged.
20. Storage in water helps to maintain the hydrophilic surface following plasma treatment.
21. Fibronectin is diluted and coated based on the manufacturer's product data sheet. According to the provided protocol, a 1 mg/mL vial is thawed and diluted in 37°C serum-free medium to a final volume of 20 mL, yielding a fibronectin solution of 50 $\mu\text{g/mL}$. Adding 2 mL to a 60-mm dish should be sufficient to coat the dish at 5 $\mu\text{g/cm}^2$. However, these are only guidelines. Higher fibronectin concentrations cause the cells to grow more densely and reach confluency faster, whereas lower concentrations will have a less significant effect. In addition, MSCs have been cultured on PDMS without a fibronectin coating, resulting in lower cell densities. Without fibronectin, we have found that cells are more likely to detach or become damaged during fixation.
22. Cells should attach and spread uniformly after the first day. Cells growing on the open area of the bottoms of the dishes will reach confluence before cells growing on the PDMS substrates. Cultures should be monitored closely to obtain the desired cell density.
23. Although commonly used in fixation techniques, acetone or xylene should not be used. These chemicals cause PDMS to swell and will cause cells to crack, break off, or detach, owing to differences in compliance and expansion. Furthermore, great care should be taken to handle each substrate in the same location (far from patterns, close to edges) to avoid damaging cells with the tweezers. In addition, try not to flex the PDMS excessively during the fixation process because this may cause cells to crack or detach.
24. Although some initial shrinkage is observed (~10%), cells remain in excellent condition for several months if kept in closed containers, free of dirt and excessive moisture, and substrates are not flexed at any time.

Acknowledgments

We wish to thank David Butler (University of Cincinnati) and members of his laboratory for their help and many useful suggestions regarding the culture of MSCs. We also thank Chia-Chi Ho for the use of her microscope. This work was partially funded by a Veterans Affairs Medical Center Merit Grant to Gregory P. Boivin.

References

1. Bonassar, L. J. and Vacanit, C. A. (1998) Tissue engineering: the first decade and beyond. *J. Cell Biochem. Suppl.* **30/31**, 297–303.
2. Ringe, J., Kaps, C., Burmester, G., and Sittinger, M. (2003) Stem cells for regenerative medicine: advances in the engineering of tissues and organs. *Naturwissenschaften* **89**, 338–351.
3. Muschler, G. F., Nakamoto, C., and Griffith, L. G. (2004) Engineering principles of clinical cell-based tissue engineering. *J. Bone Joint Surg.* **86-A**, 1541–1558.
4. Oreffo, R. O. C. and Triffitt, J. T. (1999) Future potentials for using osteogenic stem cells and biomaterials in orthopedics. *Bone* **25**, 5S–9S.
5. Caplan, A. I. and Bruder, S. P. (2001) Mesenchymal stem cells: building blocks for molecular medicine in the 21st century. *Trends Mol. Med.* **7**, 259–264.
6. Pittenger, M. F., Mackay, A. M., Beck, S. C., et al. (1999) Multilineage potential of adult human mesenchymal stem cells. *Science* **284**, 143–147.
7. Caplan, A. I. (1991) Mesenchymal stem cells. *J. Orthop. Res.* **9**, 641–650.
8. Butler, D. L., Goldstein, S. A., and Guilak, F. (2000) Functional tissue engineering: the role of biomechanics. *ASME J. Biomech. Eng.* **122**, 570–575.
9. Young, R. G., Butler, D. L., Weber, W., Caplan, A. I., Gordon, S. L., and Fink, D. J. (1998) Use of mesenchymal stem cells in a collagen matrix for Achilles tendon repair. *J. Orthop. Res.* **16**, 406–4413.
10. Awad, H. A., Butler, D. L., Boivin, G. P., et al. (1999) Autologous mesenchymal stem cell-mediated repair of tendon. *Tissue Eng.* **5**, 267–277.
11. Awad, H. A. (1999) Mesenchymal stem cell seeded collagen scaffolds for tendon repair. PhD dissertation, University of Cincinnati.
12. Freed, L. E. and Vunjak-Novakovic, G. (1998) Culture of organized cell communities. *Adv. Drug Deliv. Rev.* **33**, 15–30.
13. Matsuzaka, K., Walboomers, F., de Ruijter, A., and Jansen, J. A. (2000) Effect of microgrooved poly-L-lactic (PLA) surfaces on proliferation, cytoskeletal organization, and mineralized matrix formation of rat bone marrow cells. *Clin. Oral Impl. Res.* **11**, 325–333.
14. Walboomers, X. F., Ginsel, L. A., and Jansen, J. A. (2000) Early spreading events of fibroblasts on microgrooved substrates. *J. Biomed. Mater. Res.* **51**, 529–534.
15. Soboyejo, W. O., Nemetski, B., Allameh, S., Marcantonio, N., Mercer, C., and Ricci, J. (2002) Interactions between MC3T3-E1 cells and textured Ti6Al4V surfaces. *J. Biomed. Mater. Res.* **62**, 56–72.

16. Oakley, C., Jaeger, N. A., and Brunette, D. M. (1997) Sensitivity of fibroblasts and their cytoskeletons to substratum topographies: topographic guidance and topographic compensation by micromachined grooves of different dimension. *Exp. Cell Res.* **234**, 413–424.
17. Matsuzaka, K., Walboomers, X. F., Yoshinari, M., Inoue, T., and Jansen, J. A. (2003) The attachment and growth behavior of osteoblast-like cells on microtextured surfaces. *Biomaterials* **24**, 2711–2719.
18. Mata, A., Boehm, C., Fleischman, A. J., Muschler, G., and Roy, S. (2002) Growth of connective tissue progenitor cells on microtextured polydimethylsiloxane surfaces. *J. Biomed. Mater. Res.* **62**, 499–506.
19. Flemming, R. G., Murphy, C. J., Abrams, G. A., Goodman, S. L., and Nealey, P. F. (1999) Effects of synthetic micro- and nano-structured surfaces on cell behavior. *Biomaterials* **20**, 573–588.
20. den Braber, E. T., de Ruijter, J. E., Smits, H. T. J., Ginsel, L. A., von Recum, A. F., and Jansen, J. A. (1996) Quantitative analysis of cell proliferation and orientation on substrata with uniform parallel surface micro-grooves. *Biomaterials* **17**, 1093–1099.
21. den Braber, E. T., de Ruijter, J. E., Ginsel, L. A., von Recum, A. F., and Jansen, J. A. (1998) Orientation of ECM protein deposition, fibroblast cytoskeleton, and attachment complex components on silicone microgrooved surfaces. *J. Biomed. Mater. Res.* **40**, 291–300.
22. Curtis, A. and Wilkinson, C. (1997) Topographical control of cells. *Biomaterials* **18**, 1573–1583.
23. Brunette, D. M. and Chehroudi, B. (1999) The effects of the surface topography of micromachined titanium substrata on cell behavior in vitro and in vivo. *ASME J. Biomech. Eng.* **121**, 49–57.
24. Weiss, P. (1959) Cellular dynamics. *Rev. Modern Phys.* **31**, 11–20.
25. Chen, C. S., Mrkisich, M., Huiang, S., Whitesides, G. M., and Ingber, D. E. (1997) Geometric control of cell life and death. *Science* **276**, 1425–1428.
26. Kane, R. S., Takayama, S., Ostuni, E., Ingber, D. E., and Whitesides, G. M. (1999) Patterning proteins and cells using soft lithography. *Biomaterials* **20**, 2363–2375.
27. Folch, A., Ayon, A., Hurtado, O., Schmidt, M., and Toner, M. (1999) Molding of deep polydimethylsiloxane microstructures for microfluidics and biological applications. *ASME J. Biomech. Eng.* **121**, 28–34.
28. Madou, M. J. (2002) *Fundamentals of Microfabrication: The Science of Miniaturization*, 2nd ed., CRC Press, New York, NY.
29. Kuo, A. C. M. (1999) Poly(dimethylsiloxane), in *Polmer Data Handbook*, (Mark, J. E., ed.), Oxford University Press, New York, NY, pp. 411–435.
30. Sia, S. K. and Whitesides, G. M. (2003) Microfluidic devices fabricated in poly(dimethylsiloxane) for biological studies. *Electrophoresis* **24**, 3563–3576.
31. Lee, J. N., Park, C., and Whitesides, G. M. (2003) Solvent compatibility of poly(dimethylsiloxane)-based microfluidic devices. *Anal. Chem.* **75**, 6545–6554.
32. Kim, B., Peterson, E. T. K., and Papautsky, I. (2004) Long-term stability of plasma oxidized PDMS surfaces, in *Proceedings of the 26th International Conference of the IEEE EMBS*, San Francisco, CA, September 1–5, 2004, pp. 5013–5016.

33. Toworfe, G. K., Composto, R. J., Adams, C. S., Shapiro, I. M., and Ducheyne, P. (2004) Fibronectin adhesion on surface-activated poly(dimethylsiloxane) and its effect on cellular function. *J. Biomed. Mater. Res.* **71A**, 449–461.
34. Freshney, R. I. (2000) *Culture of Animal Cells: A Manual of Basic Technique*, 4th ed. J Wiley, New York, NY.
35. Salgado, A. J., Gomes, M. E., Coutinho, O. P., and Reis, R. L. (2004) Isolation and osteogenic differentiation of bone-marrow progenitor cells for application in tissue engineering, in *Methods in Molecular Biology, vol. 238: Biopolymer Methods in Tissue Engineering* (Hollander, A. P. and Hatton, P. V., eds.), Humana, Totowa, NJ, pp. 123–129.
36. Pittenger, M. F., Mbalaviele, G., and Black, M. (2000) Mesenchymal stem cells, in *Human Cell Culture, vol. 5: Primary Mesenchymal Cells* (Koller, M. R., Palsson, B. O., and Masters, R. W., eds.), Kluwer, Boston, MA, pp. 189–208.
37. Pittenger, M. F., Flaker, A. F., and Deans, R. J. (2002) Stem cell culture: mesenchymal stem cells from bone marrow, in *Methods of Tissue Engineering* (Atala, A. and Lanza, R. P., eds.), Academic, San Diego, CA, pp. 461–469.
38. Lennon, D. P., Haynesworth, S. E., Bruder, S. P., Jaiswal, N., and Caplan, A. I. (1996) Human and animal mesenchymal progenitor cells from bone marrow: identification of serum free optimal selection and proliferation. *In Vitro Cell. Dev. Biol. Anim.* **32**, 602–611.
39. Lennon, D. P., Haynesworth, S. E., Yound, R. G., Dennis, J. E., and Caplan, A. I. (1995) A chemically defined medium supports in vitro proliferation and maintains the osteochondral potential of rat marrow-derived mesenchymal stem cells. *Exp. Cell Res.* **219**, 211–222.
40. Sekiya, I., Larson, B. J., Smith, J. R., Pochampally, R., Cui, J., and Prockop, D. J. (2002) Expansion of human adult stem cells from bone marrow stroma: conditions that maximize the yields of early progenitors and evaluate their quality. *Stem Cells* **20**, 530–541.

Contraction Study of a Single Cardiac Muscle Cell in a Microfluidic Chip

Xiujun (James) Li and Paul C. H. Li

Summary

This chapter introduces a microfluidic method to study the contraction of a single cardiac muscle cell (cardiomyocyte). This method integrates single-cell selection, cell retention, dye loading, chemical stimulation, and fluorescence measurement for intracellular calcium on one microfluidic chip. Before single-cell experiments, the bonded chip was modified in order to make the channel deep enough to accommodate a large, single cardiomyocyte. After the modification, a single heart muscle cell could be selected and retained at a cell retention structure. Fluo-4 AM was loaded in the cell for the measurement of intracellular calcium ion concentration in the cell. Subsequently, caffeine was introduced into the chamber to induce the contraction of the cardiomyocyte. During contraction, fluorescence measurement was used to monitor the intracellular calcium level, and an optical imaging system was used to monitor the shape to confirm the contraction. The resting $[Ca^{2+}]_i$ of cardiomyocyte was determined and was consistent with the value of approx 100 nM in the literature.

Key Words: Muscle cell contraction; cardiomyocyte; intracellular calcium; microfluidic chip; caffeine.

1. Introduction

Muscle contraction enables high organisms to carry out organized and sophisticated movements. At the microscale level, muscle cell (myocyte) contraction allows high organisms to carry out and control crucial internal functions, such as beating of the heart. If the heart muscle cells (cardiomyocytes) do not work well, cardiovascular disease may result (*1*). Therefore, study of the contraction of cardiomyocytes has attracted great interest. Here, a method is introduced for the contraction study of single heart muscle cells. However, this method can also be applied to the study of other muscle cells as well.

Because the components in different cells are distributed differently, single-cell analysis has generated great interest, and different approaches have been tried to conduct single-cell analysis. A capillary tube was used to sample the cells and capillary electrophoresis was subsequently employed for cell-content analysis (2–4). Since 1990, the microfluidic chip (lab-on-a-chip, micro-total analysis system [μ TAS]) has developed rapidly. This device has the advantages of short analysis time, low reagent and sample consumption, and high separation efficiency (5). In addition, the dimensions (10–100 μ m) of microfluidic channels are highly compatible with the sizes of biological cells and, thus, have made cellular assay a popular μ -TAS application (6–13). Cell retention, manipulation, and subsequent cellular analysis on-chip can be achieved by using slit- (14) or weir- (15,16) type filters, or by electrokinetic pumping (6), cell adhesion (17), and dielectrophoresis (18). Different cells, such as red blood cells (19), white blood cells (19), *Escherichia coli* cells (20,21), human KB cancer cells (22), Jurkat T-cells (16,23,24), yeast cells (6,23), HL-60 cells (7,25), and mast cells (RBL-2H3) (26), have been tested. Nevertheless, most reports are focused on the study of a group of cells, whose averaged results mask the differences among different cells or the cells at different status, rather than a single cell (16,23,27,28). Single-cell analysis will help researchers to identify this difference, which is useful for the study of the mechanisms of many diseases.

A single rabbit cardiomyocyte has a cylindrical shape with a diameter of 15–25 μ m and length of 50–100 μ m (see Fig. 1). Its long cylindrical (rather than round) shape, large cell size, and fragility make the manipulation and transport of the cell rather difficult. To date, there are only a few reports on the study of muscle cells in microfluidic chips (29).

There are several conventional approaches for the study of the muscle cell (myocyte). These include contraction force measurement (30,31), stiffness measurement, and intracellular calcium measurement (32–35). The former two methods require the attachment of the cell to a measuring apparatus (e.g., force transducer and servomotor) (36). The latter method does not require cell attachment, and fluorescent dye has been loaded into the cell cytosol to measure the change in Ca^{2+} concentration accompanying muscle cell contraction (37). This is the method we report in this chapter.

Calcium acts as a universal second messenger in a variety of cells. In the 1960s, Ebashi and Lipmann (38,39) discovered in muscle fibers an intracellular Ca^{2+} storage site, the sarcoplasmic reticulum (SR). Subsequently, they investigated the role of the Ca^{2+} -binding protein, troponin, in the contraction of striated muscle of higher vertebrates (40–42). The release of Ca^{2+} from the SR, or from the calcium channel in the cell membrane, raises the cytosolic calcium concentration. When this concentration is high enough to saturate the Ca^{2+} site on troponin C, contraction of the muscle cell occurs. If the intracellu-

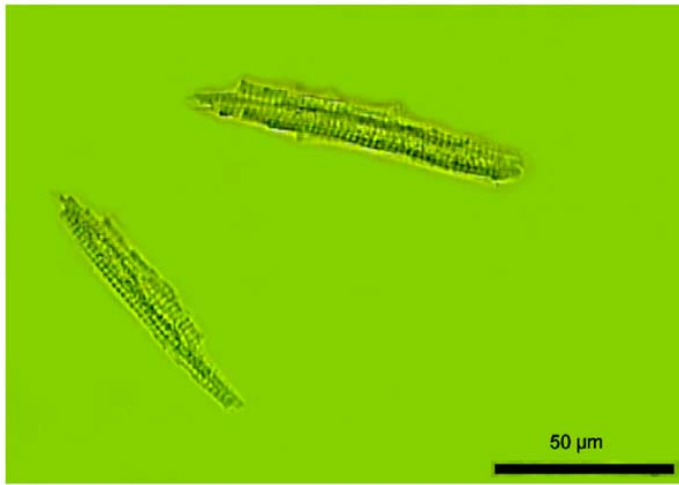


Fig. 1. Two rabbit heart muscle cells in relaxed state.

lar calcium concentration decreases, the muscle cell will relax (37). Therefore, intracellular calcium measurement is essential in the mechanistic study of cardiac activities (43–47).

Since the 1980s, fluorescence has become the most widely used method in the measurement of intracellular calcium using a variety of fluorescent probes or dyes (48,49). These probes include Indo-1, Fura-2, and Fluo-3. Although Indo-1 and Fura-2 are popular ratiometric probes that facilitate calibration, they require ultraviolet excitation, which is prone to cell damage and dye photobleaching (50). Fluo-3 can be excited by an argon-ion laser at 488 nm (visible-wavelength excitation), a popular choice for intracellular calcium measurement. Recently, Fluo-4, which is an analog of Fluo-3 with the two chlorine substituents replaced by fluorine, has become popular (51) because of its superior performance over Fluo-3. The advantages of Fluo-4 are that the hydrophobic acetoxymethyl (AM) ester of the dye can be loaded faster, that the intensity at equivalent dye concentration is higher, and that the dye is excited well by the 488-nm line of the argon-ion laser. Consequently, we choose Fluo-4 AM as the fluorescent probe for measuring the change in the intracellular calcium concentration.

We designed a microfluidic chip for the contraction study of a single cardiomyocyte. We also integrated various operations, such as cell sorting, cell retention, chemical stimulation, and intracellular calcium fluorescence measurement, on one microfluidic chip. After dye loading, a single heart muscle cell is sorted and retained in the cell retention structure in the chip. Because caffeine can induce the contraction of cardiomyocytes (33,52,53), it was intro-

duced via a reagent channel to trigger the muscle cell contraction. Meanwhile, fluorescence measurement was used to monitor the change in intracellular calcium, and an optical imaging system was used to observe the change in cellular shape. The resting value of $[Ca^{2+}]_i$ of the cardiomyocyte was determined. Furthermore, we integrated on-chip dye loading and caffeine-induced cell contraction in one experiment.

Compared with conventional methods, the microfluidic method has the following advantages:

1. It is easier to sort and retain a single cardiomyocyte in the microchannel than in the bulk solution because of the narrow size of the former.
2. Experiments on one cell can be performed for a long time without concern about cell death owing to evaporation of the cell medium.
3. There is no change in fluorescence owing to the change in the depth of liquid at the observation region.
4. There is less consumption in cells and reagents.
5. On-chip dye loading can be performed, which will minimize cell damage owing to centrifugation.

2. Materials

2.1. Chip Fabrication

The chip was fabricated through the Protolyne® Chip program of Canadian Microelectronic. The general microfabrication procedures include standard radio frequency catheter ablation (RCA) cleaning, thin-film deposition, photolithography, wet high frequency (HF) etching, access-hole formation, and chip bonding (54).

A schematic diagram of the layout of the microfluidic chip is shown in **Fig. 2**. In this chip, there are three reservoirs, three channels, one chamber, and one cell retention structure. Reservoir 1 and reservoir 2 are for cell inlet and waste outlet, respectively. Reservoir 3 is used to deliver reagents. The cell retention structure is in the form of a U-shaped barrier with a central stretch. The depth of all etched area is 19.6 μm . The width of channel 1 and 2 is 89.2 μm at the top because of undercutting of the etching and 50 μm at the bottom of the channels, whereas the width of channel 3 is 49.2 and 10 μm at the top and bottom, respectively. Other dimensions are shown in **Fig. 2**.

2.2. Enlargement of Chip Channel

A 12% HF etchant solution was used to enlarge the chip channels. When handling HF, take special safety precautions, such as the use of double plastic gloves and a face shield. In the case of spilling HF on the skin, treat by washing with a large amount of water for a long period of time and applying calcium gluconate gel (Phamascience, Montreal, Canada) to sequester any residual HF.

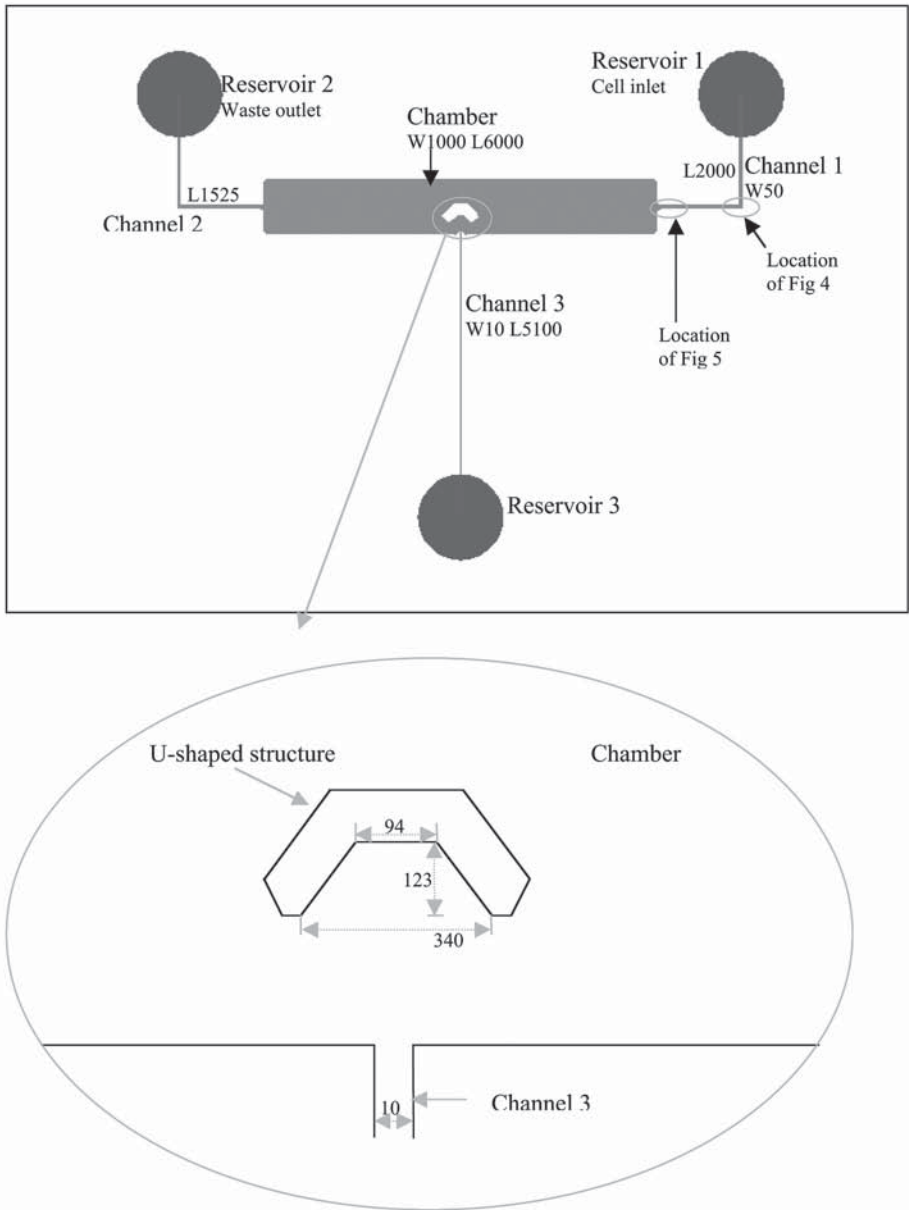


Fig. 2. Design layout of microfluidic chip. W = width and L = length in the unit (μm). The depth of all channels and the chamber is $19.6 \mu\text{m}$. The width of channel 1 and 2 is $50 \mu\text{m}$, and that of channel 3 is $10 \mu\text{m}$. The inset at the bottom shows the dimension of the cell retention structure. All specifications are those on the photomask before wet etch.

Table 1
Age-Appropriate Parameters for Isolation of Neonate Rabbit Myocyte

	Age (d)			
	3	6	10	20
Collagenase (mg/mL)	0.06	0.10	0.15	0.15–0.20
Collagenase volume (mL)	10.0	10.0	10.0	10–20
Protease (mg/mL)	0.05	0.07	0.10	0.10
Protease volume (mL)	10.0	10.0	10.0	15.0
Perfusion speed (mL/s)	1.8	1.8	1.8	2.0

2.3. Isolation of Cardiomyocytes

Ventricular myocytes were isolated from heart tissues of New Zealand white rabbits (of either sex) by a previously described method (55). The procedure is briefly described as follows:

1. After intraperitoneally injecting a rabbit with pentobarbital (65 mg/kg of body wt) and heparin (15 mg/kg body of wt), rapidly excise the heart in a 4°C Ca²⁺-free solution.
2. Perfuse the heart in the Langendorff mode; first with collagenase (Yakult, Tokyo, Japan) and then with protease (Sigma) at the age-appropriate concentrations and perfusion speeds (*see Table 1*).
3. Remove and chop the ventricles of the heart into small pieces and wash twice using storage solution (120 mM L-glutamic acid monopotassium salt [C₃H₈NO₄K], 5 mM MgCl₂, 20 mM taurine, 1 mM EGTA, 10 mM glucose, 10 mM HEPES) (*see Note 1*).

2.4. Dye Loading

1. Medium: Hank's balanced salt solution (HBSS) (Invitrogen, Grand Island, NY).
2. Fluorescent probe: first dissolve specially packaged Fluo-4 AM (50 µg, Molecular Probe, Eugene, OR) in dimethyl sulfoxide (DMSO) to make a stock solution. Then dilute in HBSS to make a 9.1 µM solution. Note that Fluo-4 AM is light sensitive and must be stored at -20°C. (*see Note 2*).
3. DMSO, >99.9% (Sigma-Aldrich, St. Louis, MO).

2.5. Measurement of Intracellular Calcium During Cardiomyocyte Contraction

1. Chemical stimulant: caffeine (Sigma-Aldrich). The reagent should be kept in a tightly sealed container when not in use.
2. Imaging system: an inverted microscope (TE300; Nikon, Mississauga, Ontario, Canada) was connected to a video camera (TK-C3180; JVC, Yokosuka, Japan). A TV set (Hitachi) and VCR system (JVC) was used for easy microscopic obser-

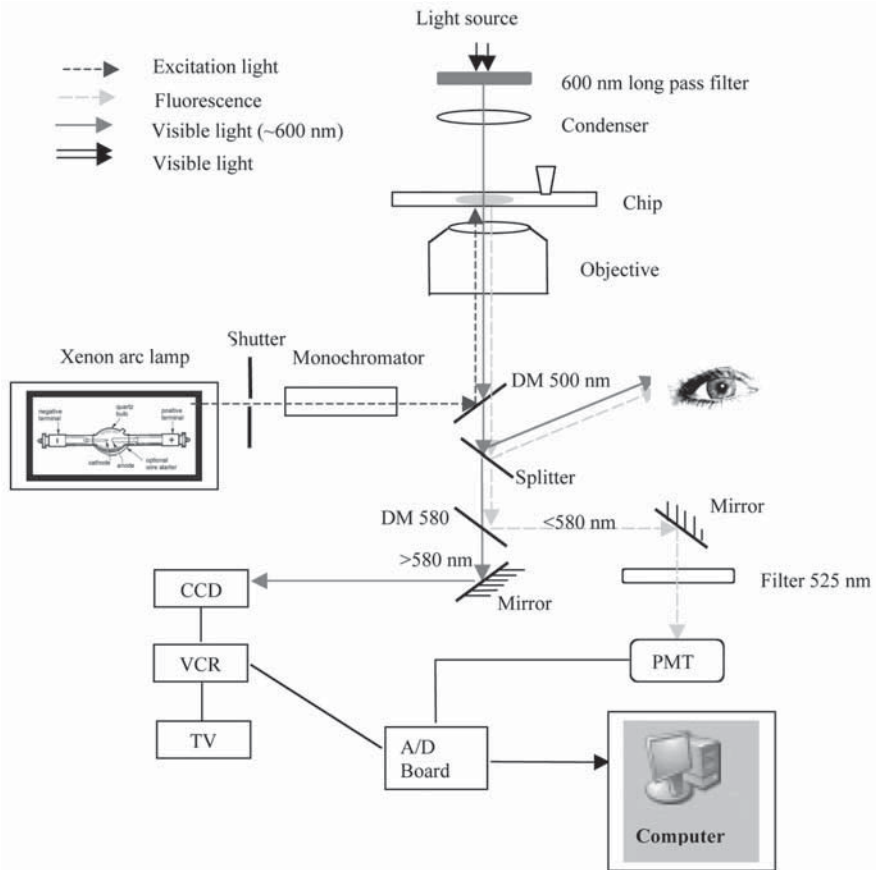


Fig. 3. Optical measurement setup including bright-field imaging system and epifluorescence measurement system. DM; dichroic mirror; CCD camera; charge-coupled device camera.

vation and video recording. A video capture card (ATI-TV wonder bt878, Markham, Ontario, Canada) was installed in an IBM PC for image capture either directly or from video recordings.

- Optical observation and fluorescence measurement: as shown in **Fig. 3**, excitation was achieved by a xenon arc lamp (Photon Technologies International [PTI], London, Ontario, Canada) coupled to a monochromator (PTI). An excitation wavelength of 480 nm was selected. The fluorescent emission at 525 nm was measured by a microphotometer consisting of an adjustable aperture and a photo-multiplier tube (PMT) (PTI) coupled to the side port of the microscope. Photometric data were collected and processed by Felix software (PTI).

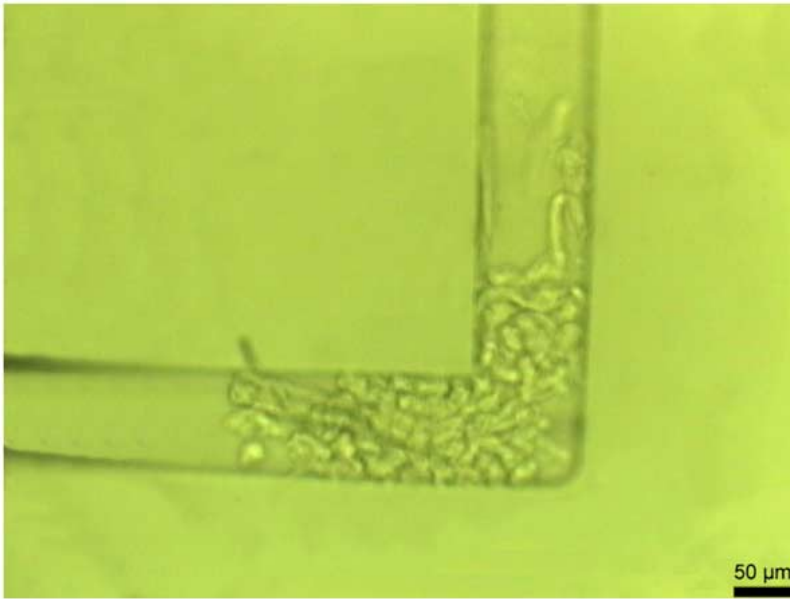


Fig. 4. The muscle cells jammed at a channel corner of the chip because of insufficient channel depth for cells to pass through. The location of this channel corner is shown in [Fig. 2](#).

3. Methods

3.1. Enlargement of Chip Channel

Because the microchips that we obtained were limited to a channel depth of about 20 μm , they were not suitable for the study of large cells. (The width of 50 μm at the bottom of the channel was too narrow for cardiomyocyte study too. Note that isotropic etching will form a rounded side wall rather than a vertical side wall.) We found that the heart muscle cells (15–25 μm in diameter, 50–100 μm long) jammed at the inlet of the reservoir. Even though some cells managed to enter the microchannel, they were jammed at a channel corner (see [Fig. 4](#)). Therefore, we applied wet HF etching in order to enlarge the cross section of the microchannels.

1. Place a chip on a microscopic stage for monitoring of the etching process.
2. Put a small amount of 12% HF in reservoirs 1 and 2 (see [Fig. 2](#) for notations). Because channel 3 is not used for cells, put only water in reservoir 3 to prevent this channel from etching. Allow the chip to etch for 45 min (see [Note 3](#)).
3. Remove all the solutions within the microchannels by suction. Examine the channel width under the microscope in order to estimate the channel depth. If the channel is not etched deep enough, repeat **step 2**.

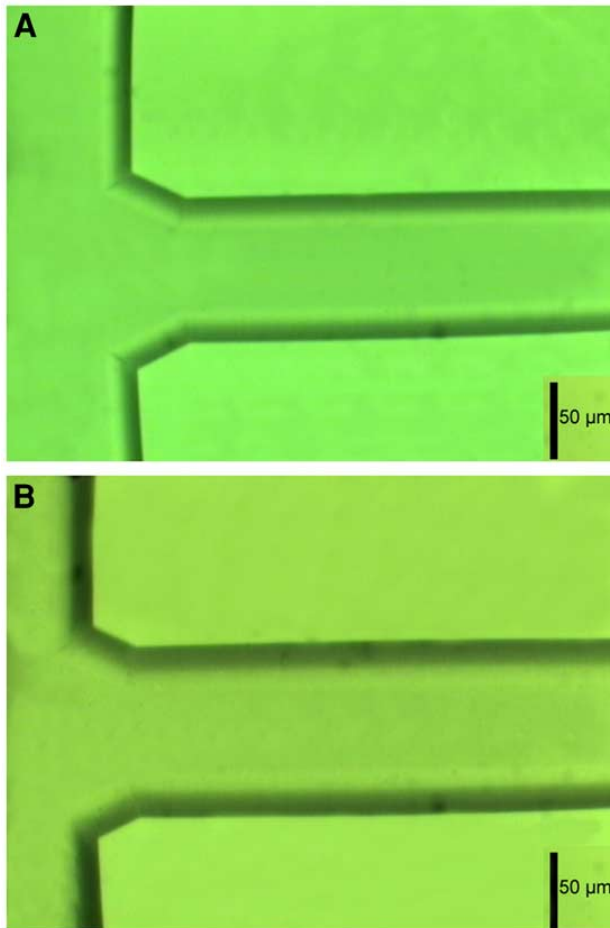


Fig. 5. Enlargement of chip channel: (A) before etching; (B) after etching. The location is shown in [Fig. 2](#).

Figure 5 shows the result of the channel etching. **Figure 5A** depicts one part of the channel before etching (*see* [Fig. 2](#) for the location), and **Fig. 5B** shows the same location of the channel after etching. It is known in isotropic etching of glass that when the channel is etched to a depth of X , the channel width will increase by $2X$. Therefore, since the channel width increased by $30.2\ \mu\text{m}$, the depth was determined to increase by $15.1\ \mu\text{m}$. This result was achieved after repeating the second step four times. For an initial channel depth of $19.6\ \mu\text{m}$, the new channel depth was determined to be approx $35\ \mu\text{m}$. This new depth proved to be sufficient in our experiments because the cells were found to go into the channel easily and no jamming of the channel occurred.

As for the quality of the etch, the channel wall surface was found to be quite smooth and no pits were noticed (*see Fig. 5B*). According to the literature, an etching rate of 9.6% HF is about 2 $\mu\text{m}/\text{min}$ (*56*). In the case of on-chip HF etching, we found that an etching rate of 12% HF was quite slow, taking about 3 h to etch 15.1 μm . The reason for this is that in the conventional method the etching is accompanied by agitation in a large space so that the etching products can be removed and no masking by the products occurs. However, during on-chip etching, the space for filling with HF is quite limited and there is no stirring. Accordingly, the etch reaction products cannot be removed, which will retard the reaction rate. Therefore, the steps of HF etching and solution removal are repeated a few times in order to achieve the desired etch depth. The etch rate could be increased by pumping HF solution through the channels, as reported previously (*57*).

3.2. Dye Loading

1. Transfer 1.5 mL of cell suspension to a 1.5-mL centrifuge vial and allow the muscle cells to settle for 3–5 min.
2. Centrifuge the cell suspension at 50g for 1.5 min (*see Note 4*).
3. After removing the supernatant, add 350 μL of 9.1 μM Fluo-4 AM solution to the cell pellet in the vial, and gently agitate the cell suspension.
4. Keep the vial in the dark for 30–40 min at room temperature to complete dye loading into the cells.
5. To remove excess external dye, centrifuge the vial again at 50g for 1.5 min. After removing the supernatant, resuspend the cell pellet in 1000 μL of HBSS solution.
6. Repeat **step 5** once.
7. Centrifuge the vial one last time. After removing the supernatant, add a proper amount (e.g., 0.4 mL) of HBSS to the cell pellet for experimentation (*see Note 5*). **Steps 5–7** should last 10–20 min, which should be sufficient to complete the hydrolysis of Fluo-4 AM ester to Fluo-4 inside the muscle cell.

Modification of the carboxylic acids group of Fluo-4 with the AM ester groups results in an uncharged molecule, Fluo-4 AM, that can permeate the cell membrane. Once inside the cell, Fluo-4 AM ester is hydrolyzed to Fluo-4, which will bind with free intracellular calcium ion to produce a change in fluorescent intensity.

To confirm the 30- to 40-min loading time and 10- to 20-min hydrolysis time, we carried out the following experiment. The dye was loaded to the muscle cells (**steps 1–3**) at time zero. After introduction of the cell in the microfluidic chip, fluorescent measurement started at 600 s. **Figure 6** shows the change in fluorescence of a heart muscle cell in the relaxed state during the Fluo-4 AM loading/hydrolysis process. For 30 min (i.e., from 0 to 1800 s), the

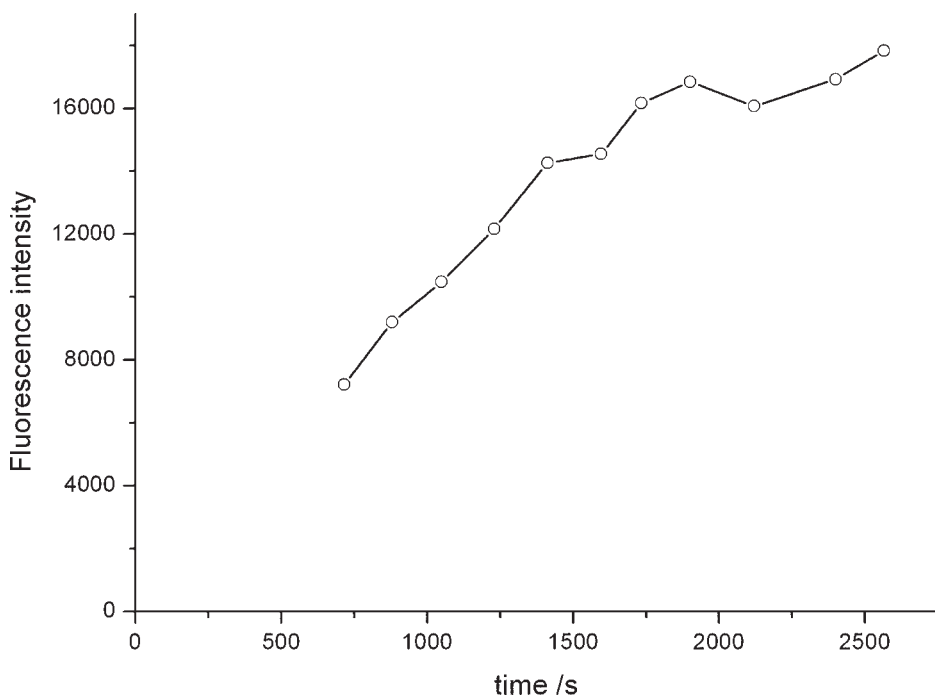


Fig. 6. Plot of fluorescence intensity vs time after off-chip dye loading and subsequent on-chip cell retention. The Fluo-4 AM used was $9.1 \mu\text{M}$ in HBSS.

rate of the change in fluorescence was rather fast. After 1800 s, the rate of change leveled off. Therefore, we are confident that 30–40 min for dye loading at room temperature and another 10–20 min for the hydrolysis of Fluo-4 AM ester should be sufficient.

3.3. Optimization of Excitation Wavelength of Fluo-4

1. Because a variable-wavelength excitation source (xenon arc lamp) is used, the optimal excitation wavelength can be found by performing an excitation scan. Essentially, measure a labeled cell in the microfluidic chip when the excitation monochromator is scanned from 400 to 550 nm.
2. After cleaning and drying the chip, also scan the empty glass microfluidic chip (without any solution) from 400 to 550 nm to check for background fluorescence of the glass using the same aperture as the muscle cell (*see Note 6*).
3. Compare the two excitation spectra, and subtract the fluorescence of the glass chip from the fluorescence of the cell in the glass chip.
4. Determine the optimal excitation wavelength from the corrected spectra in **step 3**.

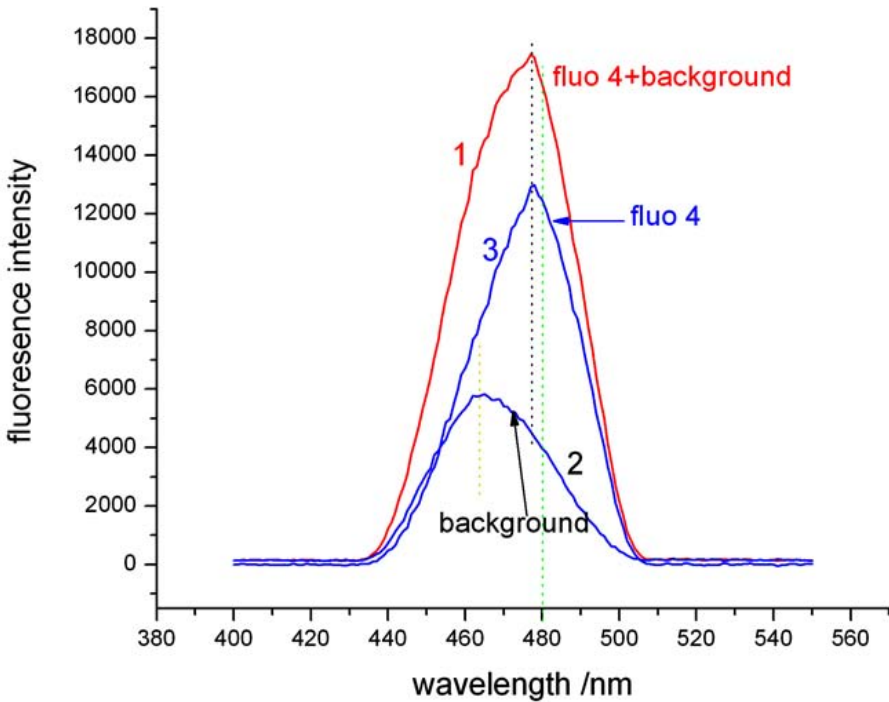


Fig. 7. Excitation spectra on contracted muscle cells for optimization of excitation wavelength for Fluo-4. Curve 1, fluorescence intensity of a Fluo 4-loaded cell plus glass chip background; curve 2, only glass chip background; curve 3, fluorescence intensity of a Fluo-4-loaded cell after background correction.

Figure 7 shows the excitation spectrum obtained for Fluo-4 in our experimental conditions. Curve 1 is the fluorescence signal of a labeled heart muscle cell in the microfluidic chip. Curve 2 is the glass microfluidic chip fluorescence background without solutions. After subtracting the fluorescence background from the fluorescence of the muscle cell placed in the glass chip, we were able to obtain the cell fluorescence (curve 3). Curve 3 shows that the maximum excitation wavelength was 478 nm. This is different from the value (494 nm) reported in the literature (51). However, these wavelengths may vary if the dye is diluted in different solutions. This discrepancy may be caused in part by the absorption/scattering by intracellular constituents (58–60), solution polarity (60,61), and/or solution viscosity (62). Actually, in order to be slightly distant from the fluorescence peak of the glass, we chose 480 nm as the excitation wavelength in our experiments.

3.4. Single-Cell Selection and Retention

To carry out single-cell analysis, one must select a single cell from the bulk of a cell suspension. In addition, to monitor the same heart muscle cell during its contraction, one must retain the cell at the same location (always within the observation aperture). This will facilitate measurement of the change in intracellular calcium during the delivery of reagents. Here, we used the cell retention structure to select and retain a single cell.

1. Add a small amount of HBSS to all three reservoirs of the chip shown in **Fig. 2** allow the HBSS to fill the chamber and channels (*see Note 7*).
2. Gently agitate the cell suspension and put a small aliquot (~5 μL) into reservoir 1.
3. While the cell is monitored from the optical imaging system (i.e., the TV monitor), adjust the cell location by modifying the liquid levels in reservoirs 1 and 2. This is achieved by adding liquid to or sucking liquid from the reservoirs with a micropipet. In this manner, a desired muscle cell can be moved to the center of the cell retention structure (*see Note 8*).
4. After the cell is adjusted to the center, add a small amount of HBSS to reservoir 3 to push the cell into the cell retention structure.

Currently there are two main approaches to transport cells in microfluidic channels. One approach is the electrokinetic method (**6,63,64**). Because of the use of a high electric field, there are some disadvantages, such as formation of gas bubbles and possible damage of the cells. Another approach to transport cells is the hydrodynamic method (**7,9,65**). This is a much gentler method to the cells, and, therefore, we adopted this method and used different solution levels to produce the hydrodynamic flow necessary to transport the cells.

A schematic diagram for the transport and retention of the muscle cell is shown in **Fig. 8**. After the cell suspension was added to the right (reservoir 1; *see Fig. 2* for notations), the cell moved from the right to the left (*see Fig. 8A*). When the cell moved close to the entrance of the cell retention structure, some HBSS was added to the left (reservoir 2). This would cause an opposing flow from the left to retard or stop the cell movement (*see Fig. 8B*). Finally, some HBSS was added to the middle channel (via reservoir 3) to push the cell into the cell retention structure (*see Fig. 8C*).

Several images were captured from the video recording depicting these selection and retention events of a cardiomyocyte and are shown in **Fig. 9**. The images were obtained by an optical microscope using a magnification of $\times 10$ in the phase contrast mode. In **Fig. 9A,B**, the cell was moving from the right to the left after the cell suspension was added from the right. In **Fig. 9C**, the cell moved farther and passed the entrance of the cell retention structure. In **Fig. 9D**, the cell moved back and stopped at the entrance by adjusting the liq-

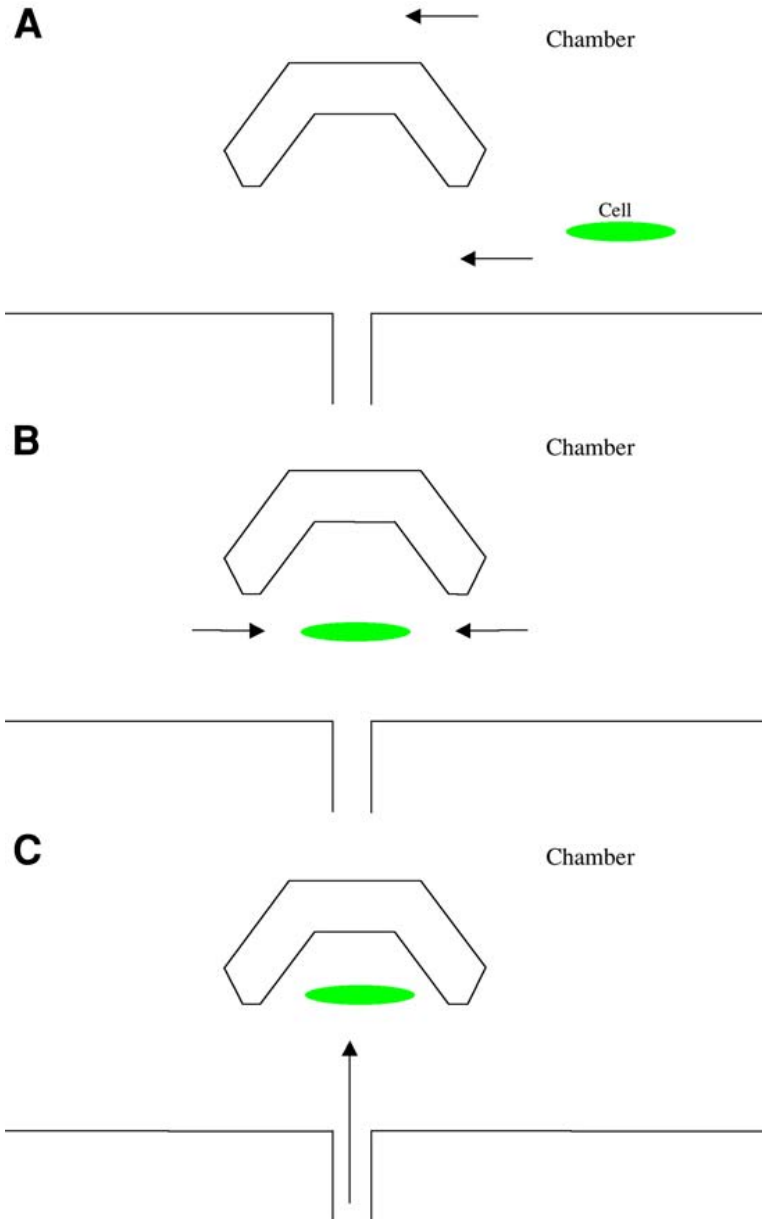


Fig. 8. Schematic diagrams showing how a single heart muscle cell was sorted and retained in the cell retention structure. (A) Cell suspension was put in reservoir 1. (B) The liquid level of reservoir 1 or 2 was adjusted to make the cell stop at the entrance of the cell retention structure. (C) HBSS solution was added to reservoir 3 to push the cell into the structure.

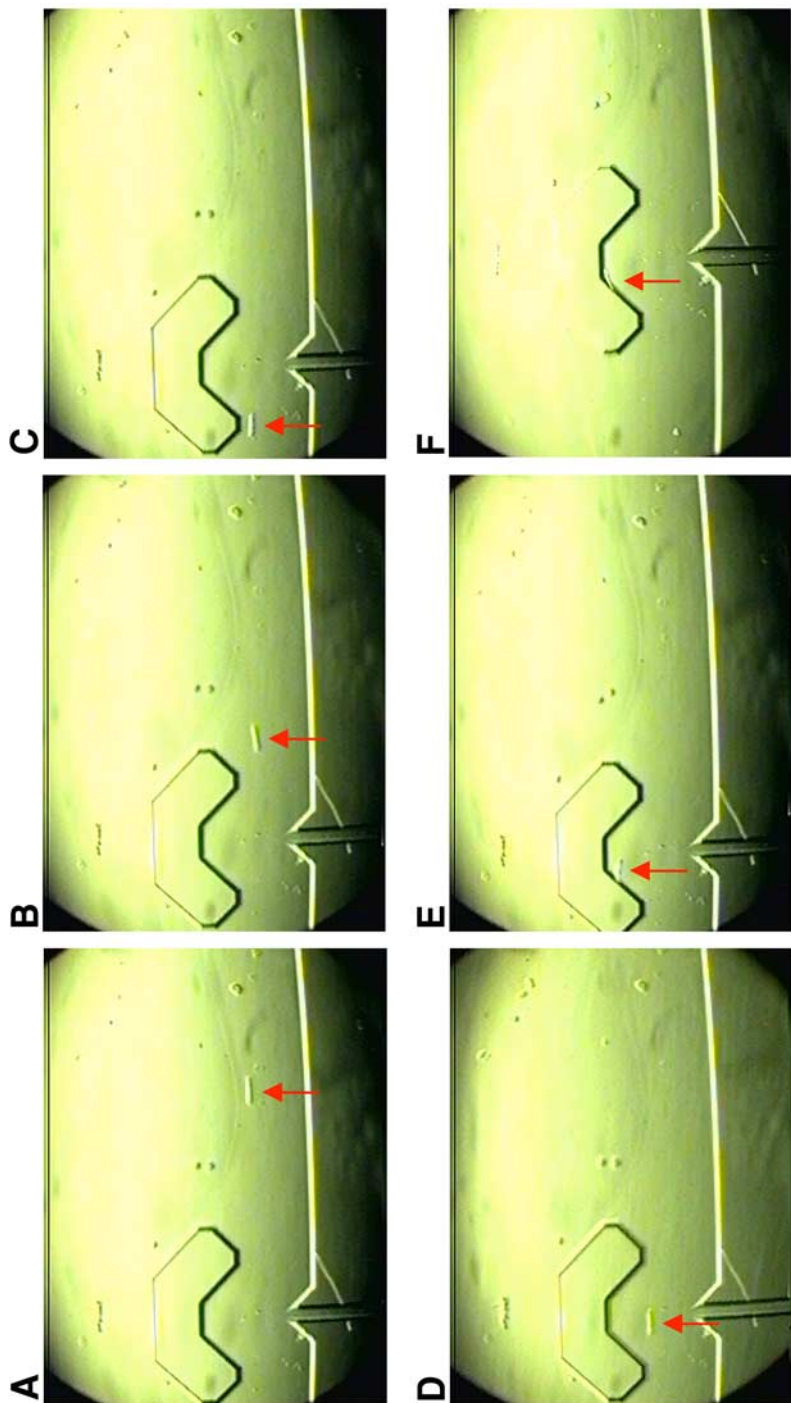


Fig. 9. Process of selecting and retaining a single heart muscle cell in cell retention structure as observed by microscope ($\times 10$) using phase contrast mode. (A,B) A cell was moving from right to left. (C,D) The liquid levels of reservoirs 1 and 2 were adjusted to make the cell stop at the entrance of the cell retention structure. (E,F) The cell was pushed into the structure by adding HBSS into reservoir 3.

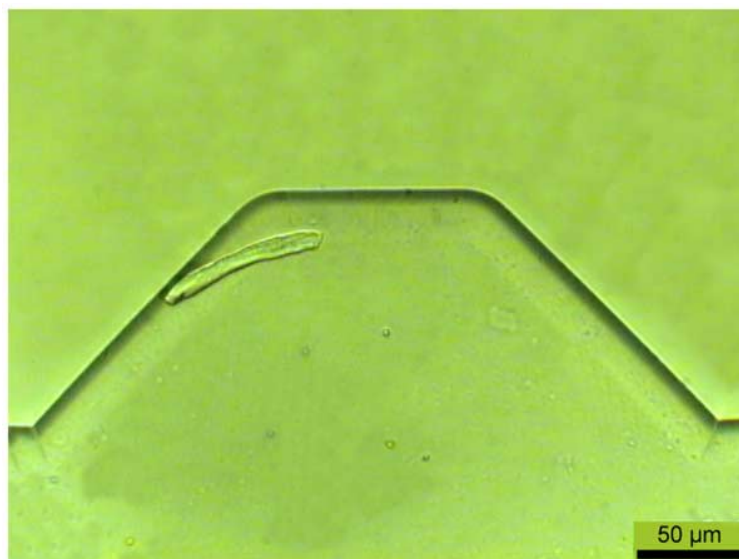


Fig. 10. Heart muscle cell retained in cell retention structure as observed under high-resolution microscope ($\times 40$).

uid levels of reservoirs 1 and 2. In **Fig. 9E,F**, the cell was pushed into the cell retention structure when a flow was administered via the central reagent channel. **Figure 10** shows a close-up view (using a $\times 40$ objective) of the heart muscle cell being selected and retained within the cell retention structure according to the aforementioned procedure.

Sometimes, more than one cell was transported to the entrance of the cell retention structure. **Figure 11A** shows a cell being retained in the cell retention structure but another cell localized at the outlet of the structure, which could have interfered with our experiment. To select one single cell, the solution level was adjusted to move the undesired cell away and retain only the desired one (*see Fig. 11B*). Because the cell outside the structure received more liquid-induced force than the one inside the structure, the cell outside the structure was easily flushed away.

3.5. Measurement of Intracellular Calcium of a Single Cardiomyocyte

1. After cell retention, adjust the aperture for fluorescence measurement by PMT to the cell size. Mark this aperture on the TV monitor. Start fluorescence measurement with the muscle cell either inside or outside the aperture (*see Note 9*).
2. Translate the chip so that the cell is outside the aperture for the fluorescence background measurement, or the cell is inside the aperture for the cell fluorescence measurement.

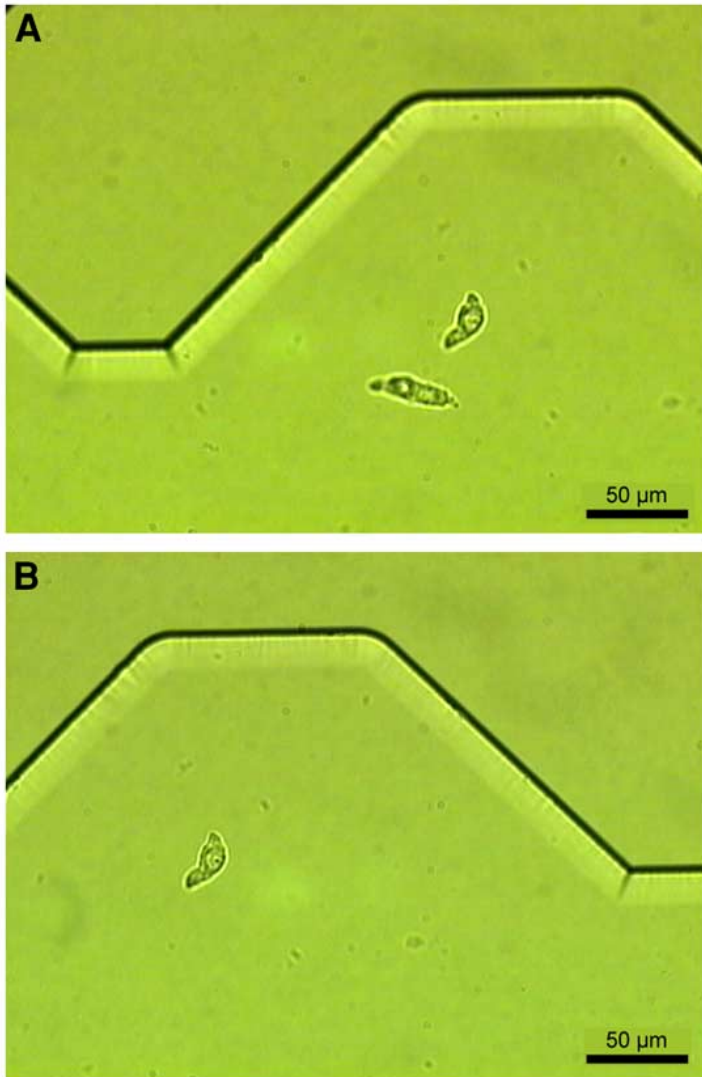


Fig. 11. Single-cell selection. (A) Two muscle cells are shown (one was within the structure and the other outside). (B) The cell inside was retained, while another cell was flushed away.

3. Add an aliquot (~5 μL) of 40 mM caffeine (in HBSS) solution to reservoir 3 to interact with the cardiomyocyte to induce its contraction. Use the PMT system to monitor the change in intracellular calcium and the optical imaging system to record the cell contraction process. If necessary, connect a syringe pump to reservoir 3 via fine Teflon tubing to introduce the caffeine (see Fig. 12) (see Note 10).

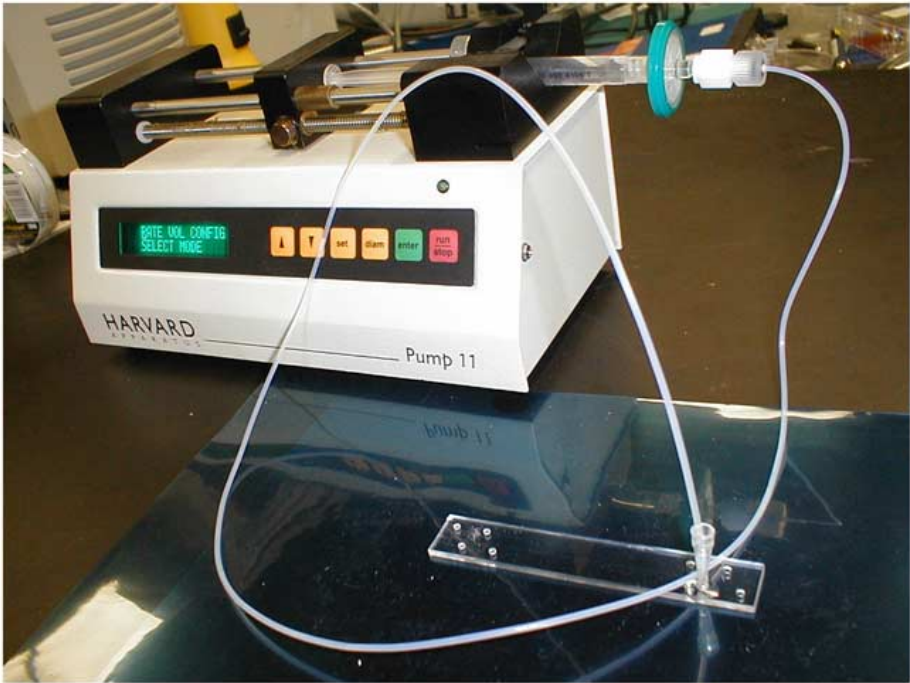


Fig. 12. Image of chip with reservoir 3 interfaced with a syringe pump for liquid delivery.

Figure 13 shows the change in the fluorescence intensity of a dye-loaded 3-d before heart muscle cell during its contraction as induced by 40 mM caffeine. At 545, 681, 855, 932, 1002, and 1088 s, the microchip was translated so that the cardiomyocyte was out of the aperture, and in each case, the fluorescence background was measured. At 929 s, 40 mM caffeine was introduced to induce contraction of the cardiomyocyte. Thereafter, the fluorescence intensity increased, and at 958 s it reached the maximum and then decreased. This is mainly because the caffeine induced the release of calcium from the SR, so the intracellular calcium concentration increased. When the calcium concentration increased to a certain high level, it triggered the contraction of a cardiomyocyte. However, the Ca^{2+} pump and Ca^{2+} channel released the high concentration of calcium to outside the cell to cause the decrease in fluorescence intensity (52,53). Meanwhile, from the imaging system, the changes in the cell shape were recorded during the contraction process. **Figure 14A** shows the long relaxed cell before the addition of caffeine, and **Fig. 14B** shows the contracted cell after the addition of caffeine, when the cell became a round body mainly because of the high concentration of caffeine.

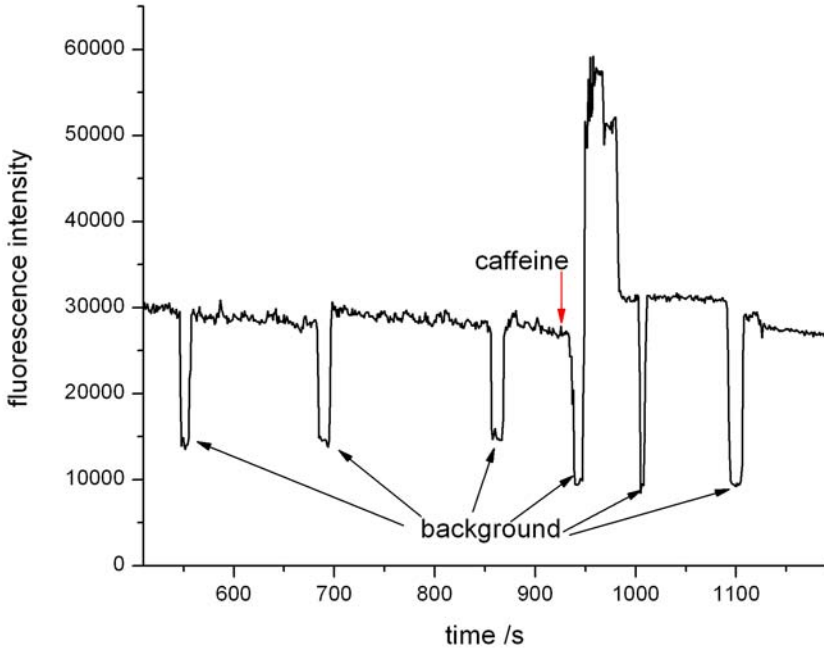


Fig. 13. Change in intracellular fluorescence as monitored during contraction of single cardiomyocyte induced by caffeine. At 928 s, 40 mM caffeine in HBSS was introduced. At 545, 681, 855, 932, 1002, and 1088 s, the microchip was moved back and forth so that the cell was momentarily out of the aperture to measure the background. Fluo-4 AM was loaded into the cell by an off-chip method.

Because 40 mM caffeine caused the unrecoverable contraction of the muscle cell, the calcium concentration is assumed to reach its cellular fluorescence maximum. In addition, the background fluorescence can be considered as the fluorescence minimum. Accordingly, the resting intracellular calcium concentration can be determined by the following **Eq. 1**:

$$\left[Ca^{2+}\right]_{i,r} = K_d \frac{F - F_{\min}}{F_{\max} - F} \quad (1)$$

in which F is the fluorescence intensity of the relaxed cardiomyocyte, F_{\min} is the background fluorescence determined from a cell-free area in a calcium-free solution, F_{\max} is the maximum fluorescence acquired after the cell contracted into a round body owing to the caffeine, and K_d is the dissociation constant of the Fluo-4 (0.35 μM) (51).

The resting intracellular calcium concentration of the relaxed cardiomyocyte is determined to be 0.14 μM , which is consistent with the value in the literature

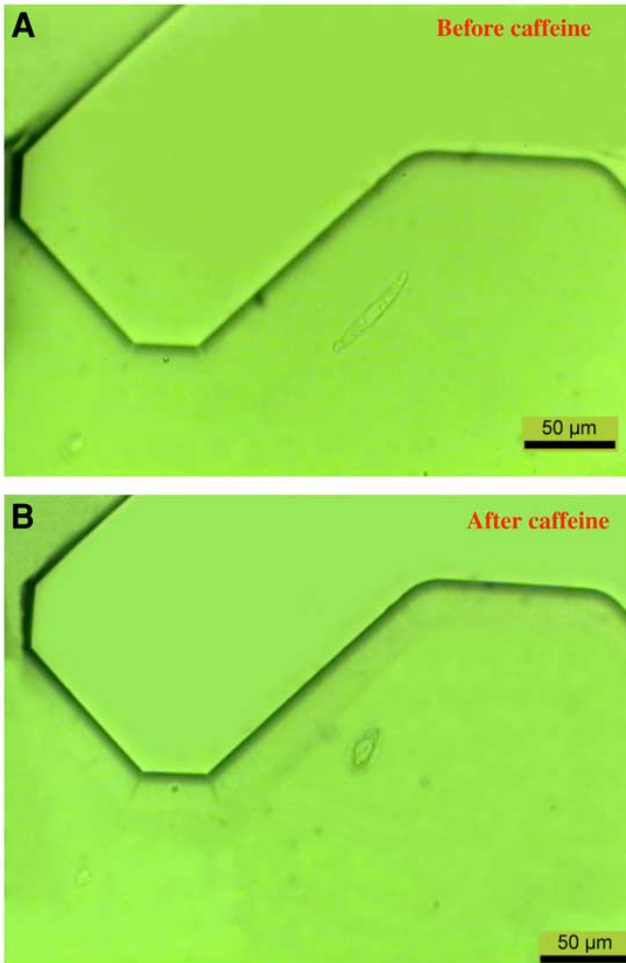


Fig. 14. Caffeine-induced contraction of single cardiomyocyte as monitored by bright-field imaging system: (A) before addition of caffeine; (B) after addition of caffeine. For other experimental conditions, see Fig. 13.

of $0.1 \mu\text{M}$ (37). It is known that this value may vary depending on the type of animal or the different ages of the muscle cells (e.g., it is $0.08\text{--}0.09 \mu\text{M}$ in smooth muscle cells [44]) (see Note 11).

3.6. On-Chip Dye Loading and Intracellular Calcium Measurement

Because the off-chip dye-loading method required centrifugation three times in order to remove excess dye, and this may cause physical damage to the delicate muscle cells, on-chip dye loading was carried out in order to eliminate

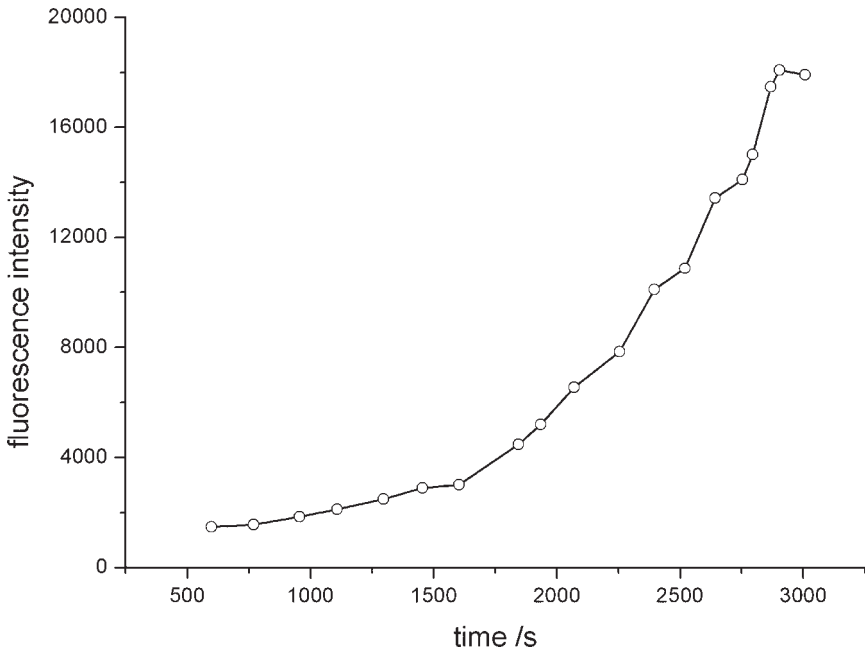


Fig. 15. Change in fluorescence intensity of a cardiomyocyte during on-chip dye loading. The concentration of Fluo-4 AM was $9.1 \mu\text{M}$ in HBSS.

the use of centrifugation and to minimize damage to the heart muscle cells. When on-chip dye loading was used, the cells were found to have better cell integrity than those using off-chip dye loading.

1. After cell retention, remove the solutions in the three reservoirs. Then, introduce a $9.1 \mu\text{M}$ Fluo-4 AM solution to the three reservoirs to carry out the on-chip dye-loading procedure.
2. Adjust the aperture for PMT measurement to barely include the muscle cell. Then, mark the position of the aperture on the TV monitor, and start fluorescence measurement to monitor the fluorescence intensity. The dye-loading procedure will take about 1 h to complete.
3. Conduct the caffeine-induced contraction experiment as described in **Subheading 3.5**.

Figure 15 shows the fluorescence intensity (after background correction) of the muscle cell during on-chip dye loading. It was found that before 1500 s, the cellular fluorescence slowly increased. After 1500 s, it started to increase at a faster rate, but after 2860 s, the fluorescence intensity leveled off. With these results, it was determined that 2860 s (47.7 min) was sufficient to complete the on-chip dye-loading procedure to obtain a constant level of Fluo-4 within the

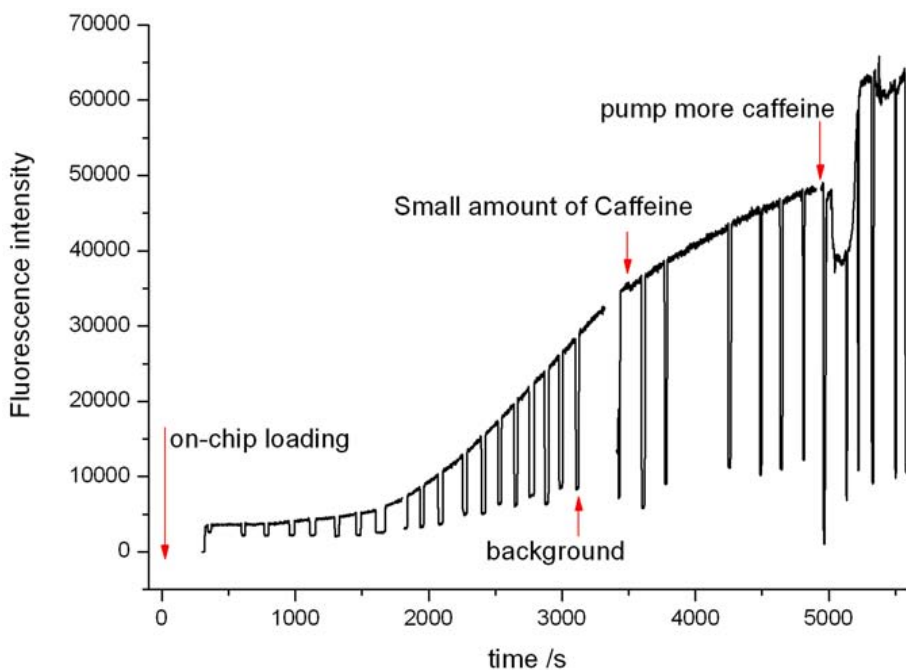


Fig. 16. Change in the fluorescence during whole process of on-chip dye loading and on-chip caffeine-induced contraction. At 3498 s, 2 μL of 40 mM caffeine was added to reservoir 3. At 4957 s, a syringe pump was used to introduce more caffeine solution to fill the whole chamber and induce muscle cell contraction.

muscle cell. After allowing another 5–10 min for hydrolysis, we were able to carry out the subsequent experiment (caffeine-induced contraction).

Figure 16 shows the change in fluorescence for the whole process of on-chip dye loading and subsequent caffeine stimulation. On-chip dye loading was carried out before 3110 s, and these raw data were used to generate **Fig. 15**. At 34,981 s, 5 μL of 40 mM caffeine was put in the reservoir 3. No contraction and no obvious change in fluorescence were observed. This may be because no obvious flow was formed (as confirmed in the imaging system) since the reservoirs were almost full of liquid. At 4951 s, a syringe pump was used to introduce more caffeine. The fluorescence intensity increased rapidly, which indicated a rapid release of calcium from the SR induced by the caffeine. The caffeine-induced contraction was also confirmed by the imaging system.

4. Notes

1. After cell isolation, dye loading and subsequent procedures should be carried out as soon as possible, because isolated heart muscle cells easily die.

2. First, 50 μL of DMSO was put into the 50- μg Fluo-4 AM vial to dissolve it. Then, five 10- μL aliquots of this solution were transferred into five different vials and stored at -20°C for future use. Aqueous buffer was not added until immediately before use because of the chemical hydrolysis of AM ester. If Fluo-4 AM ester were hydrolyzed, the Fluo-4 formed could not permeate the cell membrane. All the Fluo-4 AM solution should be prepared fresh daily.
3. Each time, on-chip etching does not need to last more than 30 min because of the buildup of the etch reaction products.
4. The heart muscle cells were easily damaged. Therefore, high-speed centrifugation of the cells could not be performed for a long time or the cells would be damaged. To reduce physical damage to the cells, the cell suspension was allowed to settle for 3–5 min before applying a short-duration centrifugation.
5. Since the cell concentrations varied after cell isolation, only a small amount of HBSS ($\sim 400\ \mu\text{L}$) was added first to avoid overdilution. If the cell density were still too high, more HBSS could be added.
6. Note that the glass chips have a background fluorescence. The excitation wavelength for maximum emission is about 468 nm. In addition, different cell media and reagents could also cause fluorescent background. Therefore, background correction should always be performed.
7. The microchannel should first be wetted with a smaller amount of HBSS; otherwise, the capillary action will cause a fast liquid flow of the heart muscle cell suspension. Cell selection and retention can be easily controlled only with a moderate liquid flow.
8. Cell selection and retention should be carried out quickly; otherwise, the heart muscle cells might settle and adhere to the channel bottom, thus making cell transport extremely difficult.
9. The aperture should be a little larger than the size of the cardiomyocyte because the cell position might change slightly during its contraction.
10. To achieve sufficient flow of caffeine for muscle cell stimulation, a syringe pump might be needed to pump the reagent through at a gentle flow rate.
11. In the experiments of caffeine-induced contraction, a lower caffeine concentration (e.g., 20 μM) could be used to contract the muscle cell slightly. Subsequently, 10 μM ionomycin could be introduced to generate the maximum cellular fluorescence (or only 10 μM ionomycin can be used to achieve the maximum fluorescence for determining $[\text{Ca}^{2+}]_i$ of the cell at relaxing status). In this manner, the intracellular calcium concentration of the contracted muscle cell can be determined.

Acknowledgments

We are grateful to Dr. Glen F. Tibbits, Jingbo Huang, Bo Liang, and Xiaoye (Helen) Sheng for providing the muscle cells and useful advice. We also gratefully acknowledge Canadian Foundation for Innovation and British Columbia Knowledge Development Fund for financial support and Canadian Institutes of Health Research for a development grant.

References

1. Bers, D. M., ed. (2001) *Excitation-Contraction Coupling and Cardiac Contractile Force*, Kluwer Academic, Dordrecht, The Netherlands, pp. 316–323.
2. Kennedy, R. T., Oates, M. D., Cooper, B. R., Nicherson, B., and Jorgenson, J. W. (1989) Microcolumn separations and the analysis of single cells. *Science* **246**, 57–63.
3. Wallingford, R. A. and Ewing, A. G. (1988) Capillary zone electrophoresis with electrochemical detection in 12.7 microns diameter columns. *Anal. Chem.* **60**, 1972–1975.
4. Jin, W., Li, X., and Gao, N. (2003) Simultaneous determination of tryptophan and glutathione in individual rat hepatocytes by capillary zone electrophoresis with electrochemical detection at a carbon fiber bundle—Au/Hg dual electrode. *Anal. Chem.* **75**, 3859–3864.
5. Harrison, D. J., Fluri, K., Seiler, K., Fan, Z., Effenhauser, C. S., and Manz A. (1993) Micromachining a miniaturized capillary electrophoresis-based chemical analysis system on a chip. *Science* **261**, 895–897.
6. Li, P. C. H. and Harrison, D. J. (1997) Transport, manipulation, and reaction of biological cells on-chip using electrokinetic effects. *Anal. Chem.* **69**, 1564–1568.
7. Yang, M., Li, C., and Yang, J. (2002) Cell docking and on-chip monitoring of cellular reactions with a controlled concentration gradient on a microfluidic device. *Anal. Chem.* **74**, 3991–4001.
8. Krüger, J., Singh, K., O'Neill, A., Jackson, C., Morrison, A., and O'Brien, P. (2002) Development of a microfluidic device for fluorescence activated cell sorting. *J. Micromech. Microeng.* **12**, 486–494.
9. Schilling, E. A., Kamholz, A. E., and Yager, P. (2002) Cell lysis and protein extraction in a microfluidic device with detection by a fluorogenic enzyme assay. *Anal. Chem.* **74**, 1798–1804.
10. Müller, T., Gradl, G., Howitz, S., Shirley, S., Schnelle, T., and Fuhr, G. (1999) A 3-D microelectrode system for handling and caging single cells and particles. *Biosens. Bioelectron.* **14**, 247–256.
11. Arai, F., Ichikawa, A., Ogawa, M., Fukuda, T., Horio, K., and Itoigawa, K. (2001) High-speed separation system of randomly suspended single living cells by laser trap and dielectrophoresis. *Electrophoresis* **22**, 283–288.
12. Dittrich, P. S. and Schwillle, P. (2003) An integrated microfluidic system for reaction, high-sensitivity detection, and sorting of fluorescent cells and particles. *Anal. Chem.* **75**, 5767–5774.
13. McClain, M. A., Culbertson, C. T., Jacobson, S. C., Allbritton, N. L., Sims, C. E., and Ramsey, J. M. (2003) Microfluidic devices for the high-throughput chemical analysis of cells. *Anal. Chem.* **75**, 5646–5655.
14. Wilding, P., Pfahler, J., Bau, H. H., Zemel, J. N., and Kricka, L. (1994) Manipulation and flow of biological fluids in straight channels micromachined in silicon. *J. Clin. Chem.* **40**, 43–47.
15. Wilding, P., Kricka, L. J., Cheng, J., and Hvichia, G. (1998) Integrated cell isolation and polymerase chain reaction analysis using silicon microfilter chambers. *Anal. Biochem.* **257**, 95–100.

16. Wheeler, A. R., Thronset, W. R., Whelan, R. J., et al. (2003) Microfluidic device for single-cell analysis. *Anal. Chem.* **75**, 3581–3586.
17. Parce, J. W., Owicki, J. C., Kercso, K. M., et al. (1989) Detection of cell-affecting agents with a silicon biosensor. *Science* **246**, 243–247.
18. Voldman, J., Gray, M. L., Toner, M., and Schmidt, M. A. (2002) A microfabrication-based dynamic array cytometer. *Anal. Chem.* **74**, 3984–3990.
19. Wilding, P., Pfahler, J., Bau, H. H., Zemel, J. N., and Kricka, L. J. (1994) Manipulation and flow of biological fluids in straight channels micromachined in silicon. *Clin. Chem.* **40**, 43–47.
20. McClain, M. A., Culbertson, C. T., Jacobson, S. C., and Ramsey, J. M. (2001) Flow cytometry of escherichia coli on microfluidic devices. *Anal. Chem.* **73**, 5334–5338.
21. Culbertson, C. T., Alarie, J. P., McClain, M. A., Jacobson, S. C., and Ramsery, J. M. (2001) Rapid cellular assays on microfabricated fluidic device, in *Micro Total Analysis Systems 2001, Proceedings μ TAS 2001 Symposium, 5th*, Monterey, CA, Oct. 21–25, pp. 285–286.
22. He, B., Tan, L., and Regnier, F. (1999) Microfabricated filters for microfluidic analytical systems. *Anal. Chem.* **71**, 1464–1468.
23. Li, P. C. H., de Camprieux, L., Cai, J., and Sangar, M. (2004) Transport, retention and fluorescent measurement of single biological cells studied in microfluidic chips. *Lab Chip*, **4**, 174–180.
24. Grad, G., Müller, T., Pfennig, A., Shirley, S., Schnelle, T., and Fuhr, G. (2000) New micro devices for single cell analysis, cell sorting and cloning-on-a-chip: the cytocon instrument, in *Micro Total Analysis Systems 2000, Proceedings of the μ TAS Symposium, 4th*, Enschede, Netherlands, May 14–18, pp. 443–446.
25. Voldman, J., Gray, M. L., Toner, M., and Schmidt, M. A. (2002) A microfabrication-based dynamic array cytometer. *Anal. Chem.* **74**, 3984–3990.
26. Matsubara, Y., Murakami, Y., Kinpara, T., Morita, Y., Yokoyama, K., and Tamiya, E. (2001) Allergy sensor using animal cells with microfluidics, in *Micro Total Analysis Systems 2001, Proceedings mTAS 2001 Symposium, 5th*, Monterey, CA, Oct. 21–25, 299–300.
27. Peng, L. X. Y. and Li, P. C. H. (2004) A three-dimensional flow control concept for single-cell experiments on a microchip (I): cell selection, cell retention, cell culture, cell balancing and cell scanning. *Anal. Chem.* **76**, 5273–5281.
28. Peng, L. X. Y. and Li, P. C. H. (2004) A three-dimensional flow control concept for single-cell experiments on a microchip (II): fluorescein diacetate metabolism and calcium mobilization in a single yeast cell as stimulated by glucose and pH changes. *Anal. Chem.* **76**, 5282–5292.
29. Li, P. C. H., Wang, W., and Parameswaran, M. (Ash) (2003) An acoustic wave sensor incorporated with a microfluidic chip for analyzing muscle cell contraction. *Analyst* **128**, 225–231.
30. Sugi, H. (1998) *Current Methods in Muscle Physiology: Advantages, Problems and Limitations*, Oxford University Press, New York.
31. Colomo, F., Poggese, C., and Tesi, T. (1994) Force responses to rapid length changes in single intact cells from frog heart. *J. Physiol.* **475**, 347.

32. Hall, J. S., Korkidis, K. A., and Maskevich, D. L. (1988) Fluorometric calcium measurement. *Nature* **331**, 729–729.
33. Yu, Z., Tibbits, G. F., and McNeill, J. H. (1994) Cellular functions of diabetic cardiomyocytes: contractility, rapid-cooling contracture, and ryanodine binding. *Am. J. Physiol.* **266**, H2082–H2089.
34. Takeishi, Y., Chu, G., Kirkpatrick, D. M., et al. (1998) In vivo phosphorylation of cardiac troponin I by protein kinase C β 2 decreases cardiomyocyte calcium responsiveness and contractility in transgenic mouse hearts. *J. Clin. Invest.* **102**, 72–78.
35. Lindner, M., Brandt, M. C., Sauer, H., Hescheler, J., Böhle, T., and Beuckelmann, D. J. (2002) Calcium sparks in human ventricular cardiomyocytes from patients with terminal heart failure. *Cell Calcium* **31**, 175–182.
36. Brandt, P. W., Colomo, F., Piroddi, N., Poggesi, C., and Tesi, C. (1998) Force regulation by Ca²⁺ in skinned single cardiac myocytes of frog. *Biophys. J.* **74**, 1994–2004.
37. Garrett, R. H. and Grisham, C. M., eds. (1999) in *Biochemistry*, 2nd ed., Saunders College Publishing, New York, pp. 540–561.
38. Ebashi, S. (1961) Calcium binding activity of vesicular relaxing factor. *J. Biochem.* **50**, 236–244.
39. Ebashi, S. and Lipmann, F. (1962) Adenosine triphosphate-linked concentration of calcium ions in a particulate fraction of rabbit muscle. *J. Cell Biol.* **14**, 389–400.
40. Ebashi, S. (1974) Regulatory mechanism of muscle contraction with special reference to Ca-troponin-tripomyosin system. *Essays Biochem.* **10**, 1–36.
41. Ebashi, S., Ebashi, F., and Kodama, A. (1967) Troponin is the Ca²⁺ receptive protein in the contractile system. *J. Biochem.* **62**, 137–138.
42. Ebashi, S. and Kodama, A. (1965) A new protein factor promoting aggregation of tropomyosin. *J. Biochem.* **58**, 107–108.
43. Morgan, K. G., Brozovich, F. V., and Jiang, M. (1988) Measurements of intracellular calcium concentration in mammalian vascular smooth muscle cells during agonist-induced contractions. *Biochem. Soc. Trans.* **16**, 493.
44. Cross, K. M. L., Dahm, L. M., and Bowers, C. W. (2000) Simultaneous measures of contraction and intracellular calcium in single, cultured smooth muscle cells. *In Vitro Cell. Dev. Biol. Anim.* **36**, 50–57.
45. Stagg, M. A., Malik, A. H., MacLeod, K. T., and Terracciano, C. M. N. (2004) The effects of overexpression of the Na⁺/Ca²⁺ exchanger on calcium regulation in hypertrophied mouse cardiac myocytes. *Cell Calcium* **36**, 111–118.
46. Shlykov, S. G. and Sanborn, B. M. (2004) Stimulation of intracellular Ca²⁺ oscillations by diacylglycerol in human myometrial cells. *Cell Calcium* **36**, 157–164.
47. Bradley, K. N., Craig, J. W., Muir, T. C., and McCarron, J. G. (2004) The sarcoplasmic reticulum and sarcolemma together form a passive Ca²⁺ trap in colonic smooth muscle. *Cell Calcium* **36**, 29–41.
48. Ridgeway, E. B. and Ashley, C. C. (1967) Calcium transients in single muscle fibers. *Biochem. Biophys. Res. Commun.* **29**, 229–234.

49. Takahashi, A., Camacho, P., Lechleiter, J. D., and Herman, B. (1999) Measurement of intracellular calcium. *Physiol. Rev.* **79**, 1089–1125.
50. Wahl, M., Lucherini, M. J., and Gruenstein, E. (1990) Intracellular Ca^{2+} measurement with Indo-1 in substrate-attached cells: advantages and special considerations. *Cell Calcium* **11**, 487–500.
51. Gee, K. R., Brown, K. A., Chen, W.-N. U., Bishop-Stewart, J., Gray, D., and Johnson, I. (2000) Chemical and physiological characterization of fluo-4 Ca^{2+} indicator dyes. *Cell Calcium* **27**, 97–106.
52. Bers, D. M. (1987) Ryanodine and the calcium content of cardiac SR assessed by caffeine and rapid cooling contractures. *Am. J. Physiol. Cell Physiol.* **253**, C408–415.
53. Weber, A. and Herz, R. (1968) The relationship between caffeine contracture of intact muscle and the effect of caffeine on reticulum. *J. Gen. Physiol.* **52**, 750–759.
54. Manz, A., Harrison D. J., Verpoorte, E. M. J., et al. (1992) Planar chips technology for miniaturization and integration of separation techniques into monitoring system. *J. Chromatogr.* **593**, 253–258.
55. Huang, J., Hove-Madsen, L., and Tibbits, G. F. (2005) $\text{Na}^+/\text{Ca}^{2+}$ exchange activity in neonatal rabbit ventricular myocytes. *Am. J. Physiol. Cell Physiol.* **288**, C195–C203.
56. Keir, R., Igata, E., Arundell, M., et al. (2002) In situ substrate formation and improved detection using microfluidics. *Anal. Chem.* **74**, 1503–1508.
57. Liang, Z., Chiem, N., Ocvirk, G., Tang, T., Fluri, K., and Harrison, D. J. (1996) Microfabrication of a planar absorbance and fluorescence cell for integrated capillary electrophoresis devices. *Anal. Chem.* **68**, 1040–1046.
58. Baker, A. J., Brandes, R., Schreur, J. H. M., Camacho, S. A., and Weiner, M. W. (1994) Protein and acidosis alter calcium-binding and fluorescence spectra of the calcium indicator indo-1. *Biophys. J.* **67**, 1646–1654.
59. Hove-Madsen, L. and Bers, D. M. (1992) Indo-1 binding to protein in permeabilized ventricular myocytes alters its spectral and Ca binding properties. *Biophys. J.* **63**, 89–97.
60. Owen, C. S. (1991) Spectra of intracellular Fura-2. *Cell Calcium* **12**, 385–393.
61. Owen, C. S., Sykes, N. L., Shuler, R. L., and Ost, D. (1991) Non-calcium environmental sensitivity of intracellular indo-1. *Anal. Biochem.* **192**, 142–148.
62. Ganitkevich, V. Y. (1998) Use of indo-1FF for measurements of rapid micromolar cytoplasmic free Ca^{2+} increments in a single smooth muscle cell. *Cell Calcium* **23**, 313–322.
63. Cabrera, C. R. and Yager, P. (2001) Continuous concentration of bacteria in a microfluidic flow cell using electrokinetic techniques. *Electrophoresis* **22**, 355–362.
64. Fu, L.-M., Yang, R.-J., Lin, C.-H., Pan, Y.-J., and Lee, G.-B. (2004) Electrokinetically driven micro flow cytometers with integrated fiber optics for on-line cell/particle detection. *Anal. Chim. Acta* **507**, 163–169.
65. Yoshida, M., Tohda, K., and Gratzl, M. (2003) Hydrodynamic micromanipulation of individual cells onto patterned attachment sites on biomicroelectromechanical system chips. *Anal. Chem.* **75**, 4686–4690.

Microscale Integrated Sperm Sorter

Yaokuang Chung, Xiaoyue Zhu, Wei Gu, Gary D. Smith,
and Shuichi Takayama

Summary

This chapter describes the design and fabrication of a passively driven microfluidic sperm sorter using soft lithographic microfabrication techniques. This self-contained device can separate motile sperm from nonmotile sperm and other cellular debris. The sorting system is small (coin sized) and structurally simple. It comprises two inlets; two outlets; a sorting channel; and arrays of horizontally oriented reservoirs that function as passively driven, constant-flow-rate pumps. Sperm with higher motility are sorted out from the rest of the semen samples based on their ability to swim through interfaces between adjacent laminar streams into separate streamlines, whereas the nonmotile sperm and debris remain in their initial streamlines. The device, which we call a microscale integrated sperm sorter, does not rely on any external power sources or controllers and incorporates all sample loading and sorting functions necessary to prepare high-quality sperm for in vitro fertilization. This self-contained, inexpensive, and portable device may also be useful for developing convenient sperm motility assays that can be used at the point of care or at home.

Key Words: Sperm sorter; passively driven pump; motility; microfluidics; soft lithography; bioassay.

1. Introduction

This chapter introduces the mechanism, materials, and fabrication of a microscale integrated sperm sorter (MISS), which is small, simple, and disposable and can sort out small amounts of healthy sperm needed in clinical settings. It not only provides an efficient, quick, and nondamaging way to sort motile sperm, but also an interesting example of designing structurally simple, yet fully functional, integrated, and self-contained microfluidic devices.

1.1. Biological Significance

1.1.1. Importance of Sperm Sorting

Approximately 5% of infertility problems are the result of abnormal or lack of sperm (1). Currently, one of the most advanced techniques to treat such sperm-related infertility is an in vitro fertilization (IVF) method called intracytoplasmic sperm injection (ICSI), in which a single sperm is directly injected into an oocyte with a tiny pipet (2). Although this method drastically reduces the number of viable sperm required for fertilization, it bypasses all natural sperm selection processes. It is, therefore, important to have an efficient, artificial, but biomimetic selection process to maximize the probability of fertilizing oocytes with high-quality sperm that will lead to successful pregnancies and healthy offspring (3).

1.1.2. Current Sperm-Sorting Techniques and Limitations

The human ejaculate contains a mixture of seminal plasma, sperm, nonreproductive cells, microorganisms, and nonspecific debris. For ICSI and other IVF procedures, the motile sperm population needs to be separated from the rest of the semen samples because the motile sperm are the most fertilizable and the nonmotile ones are not only inferior in their capability to fertilize, but can also damage the motile sperm. Primary methods commonly used for isolating motile sperm from semen samples are centrifugation, sperm migration into culture medium (swim-up), density gradient separation, or a combination of these techniques. Recovery rates, motility, morphology, and degrees of DNA integrity may vary among these methods (4).

1.1.2.1. CENTRIFUGATION

The centrifugation method uses centrifugal force generated by high-speed spinning to obtain a compact pellet of all sperm and debris and, thus, separation from the seminal plasma. Although this method is quite effective, it is reported that sperm can be damaged during centrifugation, either by physical damage of the sperm or owing to significant release of reactive oxygen species (ROS) from sperm and semen leukocytes (5). Furthermore, the extraction rates of motile sperm from initial samples can be very low (6).

1.1.2.2. SWIM-UP

To avoid damage caused by ROS in the centrifugation method, a direct swim-up separation technique has been developed. In this method, a semen sample is covered with media so that motile sperm can swim toward this top layer (4). This technique can be performed using either washed (quickly centrifuged and resuspended) or unwashed (direct) semen samples. Although this

simple technique results in good recovery with minimal sperm dysfunction, it can be time-consuming and not efficient enough to recover sperm from low-motility semen samples or patient samples that include large amounts of cellular debris.

1.1.2.3. DENSITY GRADIENT SEPARATION

Density gradient separation separates cells or particles based on their differing intrinsic densities. There is a well-referenced medium for density gradient separation, which is composed of colloidal silica coated with polyvinylpyrrolidone. Because of the heterogeneity of particle sizes, centrifugation of the medium will spontaneously form a density gradient. For sperm separations, liquefied seminal plasma is layered on an isotonic discontinuous gradient and centrifuged. Subsequent separation relies on the percentage of active sperm in the ejaculate and added force of centrifugation to isolate motile sperm from other cells. Even though this technique can selectively isolate motile sperm from debris and neutrophils, the occurrence of lower DNA integrity after density gradient separation (7) makes this method less desirable.

1.1.3. Microfluidic Sperm Sorting

The described sperm sorting is based on microfluidics, the flow of fluids through small channels. An interesting feature of microfluidics is the ability to flow different streams adjacent to each other with no turbulent mixing between the streams. Such laminar flows occur when viscous force dominates over inertial force or when the Reynolds number (Re) is small (8). Because microchannels have small dimensions, the Re in microfluidic systems is typically low (<1 for the MISS), and the flows are laminar.

1.2. Design and Fabrication of Device

The main challenge of designing a practical microfluidic sperm sorter is to integrate all components necessary for sorting while keeping the device inexpensive, easy to fabricate, simple to use, and overall compact in size. The sperm sorter described in this chapter satisfies these needs with a K-shaped channel that connects four horizontally oriented reservoirs: two for loading sperm sample and media, and another two for collecting separated motile and nonmotile sperm (see Fig. 1).

The combined reservoir arrays also serve as a passively driven pumping system that maintains a steady flow rate regardless of fluid volume in the reservoirs (9,10). Although a variety of materials may be potentially used, this chapter describes fabrication of the sperm sorter in polydimethylsiloxane (PDMS) through soft lithography (11).

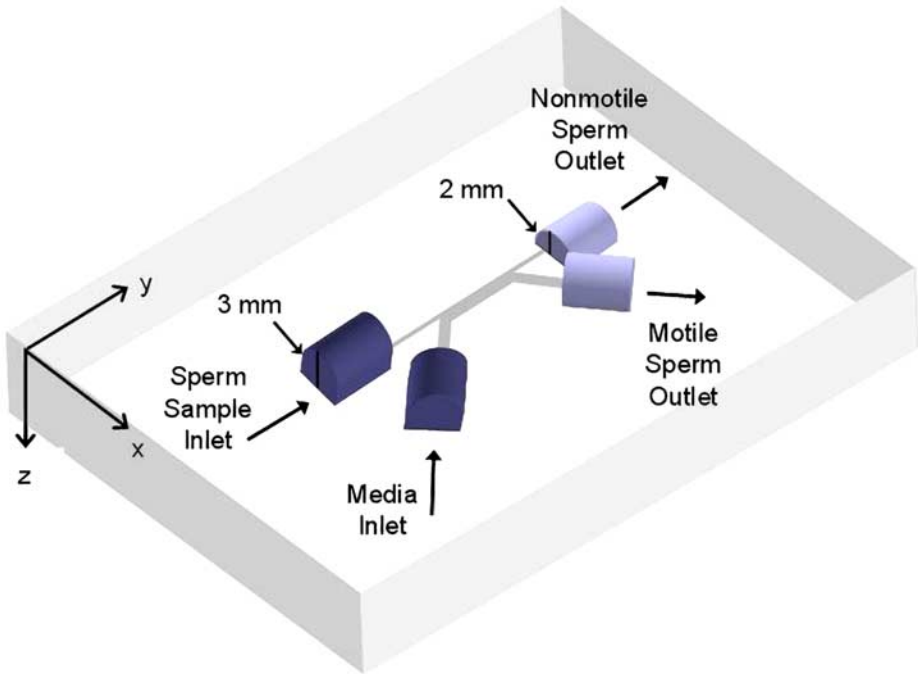


Fig. 1. Structure of MISS. (Reproduced with permission from ref. 9.)

1.2.1. Sorting Mechanism

MISS takes advantage of laminar flows in microfluidic channels together with differences in the swim velocity of motile vs nonmotile sperm. As mentioned earlier, flow in small channels is often laminar. The Re_D for flow in a tube is defined as follows:

$$Re_D = \frac{\rho \times u_m \times D_h}{\mu}$$

in which ρ is the fluid density; μ is the fluid dynamic viscosity; u_m is the mean fluid velocity over the tube cross-section; and D_h is the hydraulic diameter defined as

$$D_h = \frac{4 \times A_c}{P}$$

in which A_c and P are the flow cross-section area and the wetted perimeter, respectively. Turbulent flow occurs when the Re_D is above approx 2000 (12). For the MISS design described here,

$$Re_D \approx \frac{10^3 \text{ (kg / m}^3\text{)} \times 1.6 \times 10^{-3} \text{ (m / s)} \times 6.67 \times 10^{-5} \text{ (m)}}{855 \times 10^{-6} \text{ (N} \cdot \text{s / m}^2\text{)}}$$

Owing to this small Re , flow is laminar and allows two streams to flow adjacent to each other without turbulent mixing.

From the Stokes-Einstein equation, diffusivity is defined as

$$D = \frac{k_B \times T}{\bar{f}}$$

in which k_B is the Boltzmann's constant, which is approx 1.38×10^{-23} J/K; T is the absolute temperature; and \bar{f} is the frictional drag coefficient, which is related to the dimension of the particle and the fluid properties such as viscosity. For a spherical particle, the friction drag coefficient is defined as $\bar{f} = 6 \times \pi \times \mu \times R$, in which R is the sphere radius. Nonmotile human sperm, approximated to be a spherical particle with a diameter of $6 \mu\text{m}$, have a diffusivity of 1.5×10^{-13} m^2/s in water at room temperature. Such a particle or nonmotile sperm would need 690 s to diffuse just $10 \mu\text{m}$. By contrast, motile human sperm swim faster than $20 \mu\text{m}/\text{s}$ at room temperature (13).

In the multiple laminar flow system of the MISS, a media stream intersects with a sample stream and creates an interface. Nonmotile sperm and miscellaneous cellular debris remain in the initial streamline, owing to their low diffusivity, and, finally, exit into a waste outlet. Unlike nonmotile particles, high-motility sperm can actively swim across the interface and be sorted into a separate, motile sperm outlet. This mechanism allows the MISS to sort motile sperm away from nonmotile sperm and debris efficiently and without harm in a gentle biomimetic manner.

1.2.2. Flow Control

A key factor for successful sorting with the MISS is to control flow rates. The absolute flow rate of the fluid is crucial for determining the total time that sperm spend to sort themselves out by motility. A longer residence time may allow an increasing number of sperm with low forward motility to enter the collecting stream; a shorter residence time may allow selection of sperm with higher motility. The relative flow rates between the sample stream and the collecting stream are important for determining the position of the fluid interfaces, as well as the purity and recovery rate of the motile sperm. If the sperm sample stream is too thin, the throughput decreases. If the sperm sample stream is too wide, then even nonmotile sperm and debris may collect in the motile sperm outlet. The MISS is designed to give sperm a residence time of approx 20 s in the main separation channel, and the width of the sample stream is approximately equal to or a little smaller than the sample inlet and nonmotile sperm outlet (9,10).

The key to achieving the desired flow control in the MISS is to use horizontally oriented fluid reservoirs. In this reservoir design, a constant pressure drop is maintained regardless of the volumes of fluid in the reservoirs, enabling

constant fluid flow rates and a stable laminar flow interface for sorting (**Fig. 1**). In a typical design, the inlet and outlet reservoirs are 3 and 2 mm in height, respectively. The combination of hydrostatic force produced from the 1-mm height difference between inlets and outlets and a net capillary force imbalance resulting from the differences in reservoir size provides the pressure drop across the reservoirs needed to drive the flow through this microchannel system. Because of the relatively small size of the reservoirs, surface tension keeps fluids and sperm suspensions within the horizontally oriented reservoirs and prevents the liquid from spilling out. The horizontal reservoir configuration causes the fluid meniscus to move horizontally rather than vertically, thus keeping the height difference and, hence, the hydraulic pressure between the inlet and outlet reservoirs constant. This contrasts with conventional gravity-driven pumping mechanisms, in which flow rate decreases over time owing to changes in fluid levels associated with the use of vertically oriented reservoirs open to the atmospheric pressure. In a typical MISS design, the sperm inlet and non-motile sperm outlet have a width of 100 μm and a length of 5000 μm . The width and length of the media inlet and motile sperm outlet is 300 and 5000 μm , respectively. The main separation channel's width is 500 μm , and its length is 5000 μm . All channel heights are 50 μm .

1.2.3. Sorting Procedure and Results

In a typical sorting test, semen samples from human subjects are obtained with institutional review board (IRB) approval. To begin, the channels and reservoirs of the MISS are filled with media. When the channel walls are made hydrophilic, the fluid will spontaneously wick into the channels. Once the channels are filled with liquid, the fluids in the outlet reservoirs are emptied, except for a small amount of liquid sufficient to form a concave meniscus. Finally, a sperm sample is loaded into the sperm sorter inlet, while taking precautions not to overfill the reservoirs.

Typical experiments have shown an increase in motile sperm purity from 10 to >98% after a single passage through the device using washed human semen. The gentle and reliable microfluidic sorting mechanism and the steady fluid flows generated by the passively driven pumping system provide a simple yet generally consistent sorting capability. The main problem that one encounters is channel clogging, which can occur when the sample is too highly concentrated or includes an excess of large debris. This device also works well with unwashed human semen (**10**). In a typical experiment, sperm motility increased from 44 ± 4.5 to $98 \pm 0.4\%$ following processing. However, it is important to note that if unwashed semen is of high viscosity, the isolation is less efficient for the design described owing to slower flow rates.

1.2.4. Soft Lithography

The fabrication procedures used for constructing the MISS takes advantage of a set of microfabrication methods called “soft lithography,” which uses molding to replicate microfeatures into elastomers. These patterned elastomers are then used as masks, stamps, molds, or microchannels. Soft lithography is advantageous for many microfluidic applications because it allows fabrication of microchannel structures more rapidly and with low equipment costs compared to surface/bulk micromachining (14). Soft lithography has been used extensively in microfluidic applications to fabricate components such as sensors, mixers, sorters, and cell culture chambers (11). This chapter specifically describes the use of soft lithographic methods to fabricate the MISS.

2. Materials

1. SU-8 (MicroChem, Newton, MA): this is a negative, near-ultraviolet (UV), epoxy photoresist. Compared with other photoresists, SU-8 is distinguished for its ability to produce thicker and/or higher-aspect-ratio structures while using standard contact lithography equipment. This feature is owing to SU-8’s low optical absorption in the UV range as opposed to the higher absorptions of other sensitive photoresists. SU-8 fills the need for fabricating the relatively thick microchannels required for the MISS (15–17).
2. PDMS: this is a transparent, thermosetting polymer that consists of a base and a curing agent component. This class of materials (silicon rubber) has been thoroughly used for specific clinical applications such as contact lenses and various implanted devices. PDMS (Sylgard 184) is obtained from Dow Corning. The curing agent is normally added to the base in a 1:10 weight ratio. The weighted components are mixed with an electric mixer or by hand and degassed under vacuum until no bubbles remain in the mixture. After degassing, the PDMS can be cast against photoresist patterned silicon (Si) wafers. Detachment of the cured PDMS from the Si wafer gives a PDMS slab with open-channel features that can then be sealed against PDMS, glass, plastic, or other flat surfaces.

For microfluidic applications, PDMS is useful because of several important properties, including mechanical flexibility, gas permeability, and optical transparency. Its elasticity and hermetic self-sealing properties make multilayer construction of PDMS-based devices relatively straightforward. Although the surface of PDMS is inherently hydrophobic, it can be made hydrophilic through a plasma oxidation treatment, surface coating, or surface grafting. Plasma treatment will also allow permanent bonding of PDMS to other treated PDMS, Si, or glass.

3. Epotek epoxy: Epotek UVO-114 (Epoxy Technology, Billerica, MA) is a viscous epoxy that cures into a stiff solid once exposed to sufficient UV light. This material can be used to create a rigid replica of microfeatures present in elastomeric PDMS. In a typical procedure, a piece of PDMS is placed with microfeatures facing down on prepoured Epotek in a Petri dish. After degassing

and eliminating bubbles underneath the PDMS, the Epotek and PDMS structure are exposed for 90 min to strong UV from a UV chamber (3D Systems) to form a solid mold.

4. Semen samples: the semen samples that we tested were obtained with IRB approval from men undergoing evaluation for infertility after a minimum of 3 d of abstinence. Before sorting experiments, a semen sample analysis was performed to assess semen volume, pH, viscosity, liquefaction, sperm count, sperm motility, sperm agglutination, strict sperm morphology, and cell contamination. Semen samples with forward progression spermatozoa were selected for experimental use.
5. Bovine serum albumin (BSA) fraction V (Sigma, St. Louis, MO).
6. Phosphate-buffered saline (PBS) (Invitrogen, Carlsbad, CA).
7. HEPES-buffered human tubal fluid with 0.2% BSA (processing medium) (Irvine Scientific).
8. Propidium iodide (PI) (Molecular Probes).
9. (Tridecafluoro-1,1,2,2-tetrahydrooctyl)-1-trichlorosilane (United Chemical Technologies).

3. Methods

This section describes the details of the MISS microfabrication along with the procedure for using the MISS for sperm sorting. The simple structure of the device makes it suitable for fabrication through a variety of techniques using various materials. Here, we describe a typical procedure used in our laboratory.

3.1. Fabrication of Microfluidic Sperm Sorter

Although the structure of the MISS is simple, the coexistence of defined structures with both micrometer- and millimeter-length scales makes fabrication a challenge. Procedures such as photolithography are excellent for making micrometer features but are limited in making features with millimeter height. On the other hand, methods for milling and machining millimeter-sized objects are often not well suited for precise fabrication of microchannels. It is because of this challenge of making multiscale structures that the fabrication procedures described next are rather lengthy. Once a good master mold with all the structures is obtained, subsequent MISS devices can be more readily fabricated simply through casting.

3.1.1. Fabrication of a Mask

The first step is to prepare a photomask with channel features for further microfabrication. Although chrome masks are generally used in conventional photolithography, they are expensive and often require long lag times to obtain. In rapid prototyping with contact photolithography, it is convenient to use transparency film masks, which are lower yet sufficient in resolution and much

cheaper and quicker to obtain than chrome ones. A typical mask would be 5×7 in. and is drawn with readily available software such as AutoCAD. The AutoCAD dxf files are converted to gbr files by conversion software such as LinkCAD. Finally, the gbr files are printed at 20,000 dpi by CAD/Art Services (www.outputcity.com). A resolution of 20,000 dpi is sufficient to fabricate microchannels with widths as low as $1.25 \mu\text{m}$. This resolution is more than sufficient since the minimum width of the sperm sorter is $100 \mu\text{m}$.

3.1.2. Fabrication of an Si Master With Channel Features

Once the transparency mask is obtained (a K-shaped channel in the case of the MISS), contact photolithography is used to fabricate a master mold of the K-shaped microchannel features. PDMS prepolymer can then be cast against this master to generate a PDMS replica.

1. Spin hexamethyldisilazane (HMDS) primer over a Si wafer to help promote adhesion of SU-8. SU-8 is a typical epoxy-based negative photoresist that cures or hardens with UV exposure. Then spin coat SU-8 (MicroChem) photoresist onto the Si wafer. A high-resolution transparency mask defines the eventual channel architecture. The mask selectively permits UV light through to induce or prevent curing of spin-coated photoresist on a wafer. The detailed procedure is as follows:

Precoat HMDS primer	Step 1: 500 rpm	10 s
	Step 2: 1000 rpm	10 s
	Step 3: 3000 rpm	30 s
Coat SU-8	Step 1: 750 rpm	60 s
	Step 2: 1500 rpm	30 s
	Step 3: 2000 rpm	30 s
Soft bake	Step 1: 65°C	10 min
	Step 2: 95°C	15 min
Exposure		4 min, 30 s
Postexposure bake	Step 1: 65°C	3 min
	Step 2: 95°C	9 min
Develop	Immerse the wafer under and spray with MicroChem SU-8 Developer until the unpolymerized substrate is gone; then dry with a gentle stream of nitrogen.	

2. To prevent PDMS from bonding to the wafer, silanize the wafer using $\text{C}_8\text{H}_4\text{Cl}_3\text{F}_3\text{Si}$, TFS. Perform silanization by chemical vapor deposition of silane in an evacuated desiccator for 10 min, with the substrates hung upside down above a cover glass coated with a 1:1 ratio mixture of mineral oil and silane.

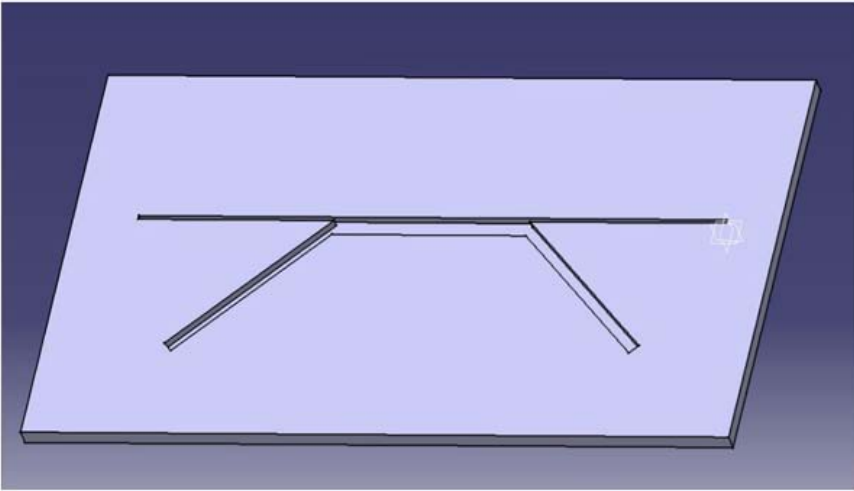


Fig. 2. First PDMS mold cast against pattern fabricated by photolithography.

3.1.3. Fabrication of an Epoxy Mold

Because of to the fragility of Si wafers, we often prepare an epoxy replica, which is stronger and easier to manipulate.

1. Make a PDMS mold of the Si wafer with photoresist channel features (Fig. 2). Pour degassed PDMS on the wafer to form a flat PDMS sheet approx 4 to 5 mm thick. If the PDMS is too thin, it will easily bend and deform in the epoxy molding step.
2. Cure and remove the PDMS mold from the silanized wafer, and put it on the epoxy prepolymer. To avoid bubbles trapped underneath the PDMS, precoat the PDMS surface with channel features with copious epoxy prepolymer, and then swiftly flip the channel feature side down onto a Petri dish prefilled with epoxy prepolymer from one end to the other, pushing potentially trapped air to one side.
3. Remove any residual bubbles from the epoxy with a needle, and then further degas it under vacuum until all bubbles are gone. It regularly takes 2 h for the degassing process.
4. Expose the epoxy in a UV chamber for 90 min to harden. The wavelength ranges from 280 to 400 nm.
5. Peel off the PDMS slab after the epoxy mold is cured.

3.1.4. Fabrication of a Master Mold With Both Microchannel Features and Millimeter-Sized Reservoirs

1. Glue small metal (typically steel or copper) cuboids or cylinders (2- to 3-mm radius) onto the solid epoxy surface using Superglue to form horizontally oriented fluid reservoirs that serve as steady-flow, passively driven pumps (Fig. 3).

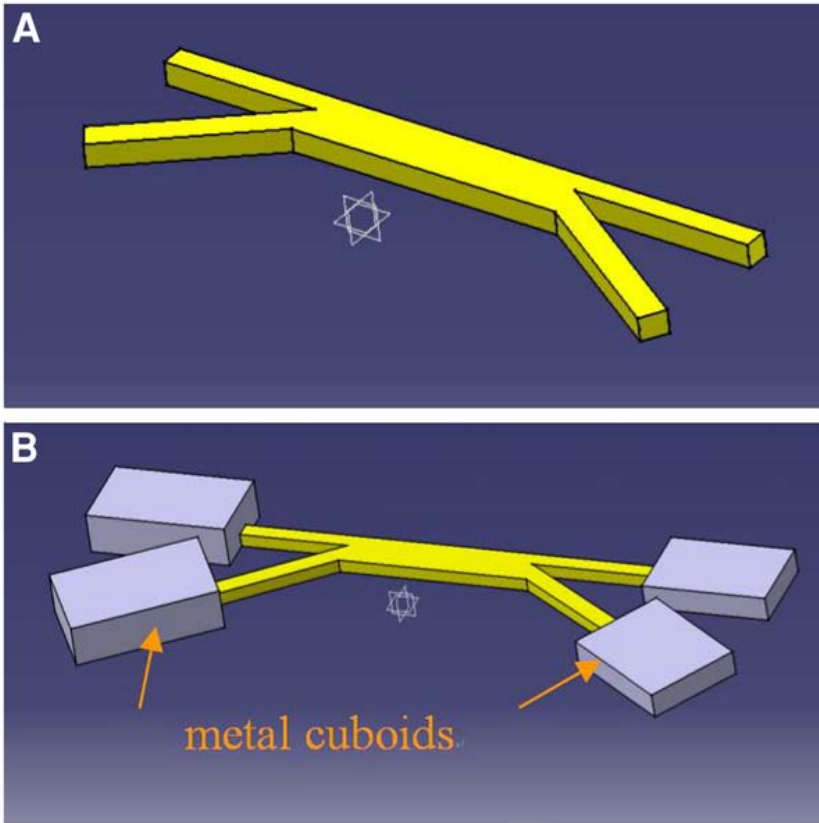


Fig. 3. (A) Epoxy mold without metal cuboids; (B) epoxy mold with cuboids glued to the wafer.

The cuboid or cylinder can be of any material as long as it is not chemically reactive or does not inhibit PDMS crosslinking. Low-viscosity glue is desirable, so that it can be dispensed accurately with a narrowed tip using a micropipettor (*see Note 1*). Overdispensing glue will change the desired shape of the reservoirs, which serve as passively driven pumps.

2. Pour degassed PDMS on this epoxy mold.
3. Cure the PDMS at 60°C for at least 60 min.
4. Remove the cured PDMS slab from the epoxy mold with the metal reservoirs still glued to it. This slab provides a second PDMS structure (Fig. 4).
5. Make a second epoxy mold by casting against the second PDMS structure. This second epoxy mold, which has the combined microchannel and millimeter-sized reservoir features (*see Fig. 5*), is made by repeating steps 2–4 in Subheading 3.1.3. This will be the master mold used for subsequent fabrication of the PDMS-based MISS (Fig. 5).

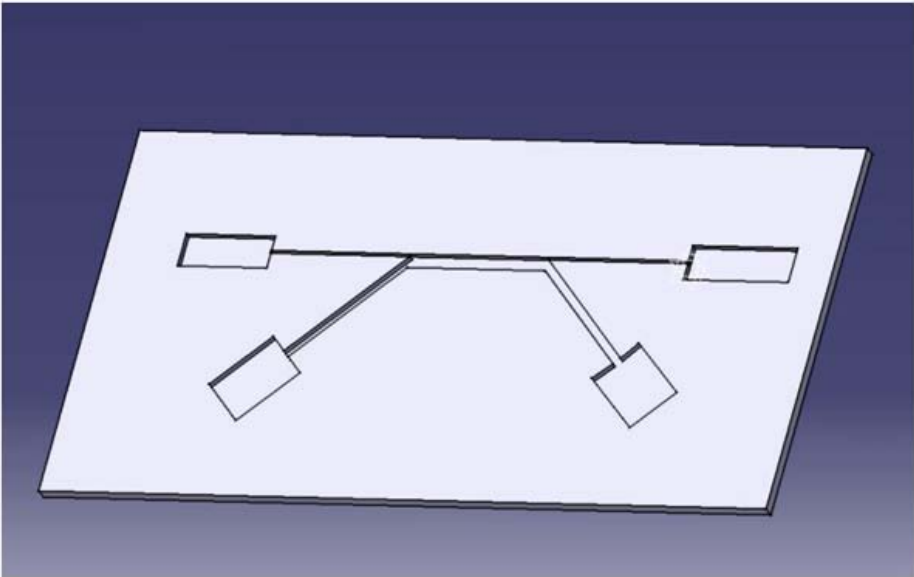


Fig. 4. The second PDMS structure.



Fig. 5. The final epoxy mold.

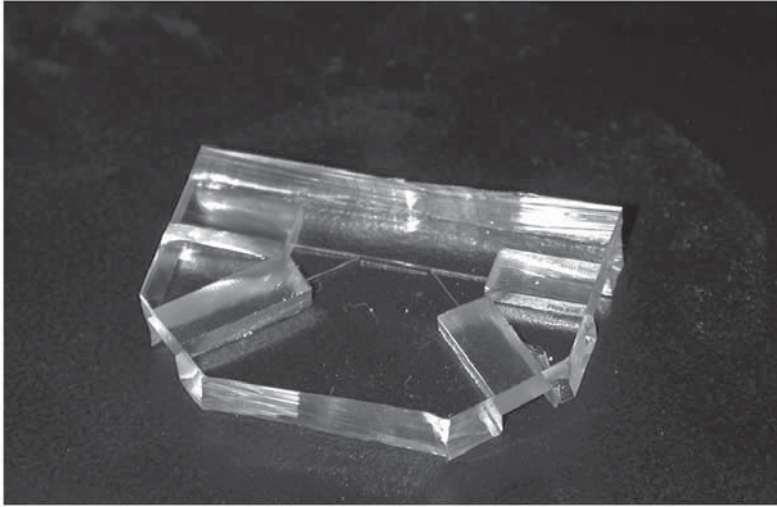


Fig. 6. Top layer of MISS.

3.1.5. Final Assembly

The final step of the fabrication involves bonding of the PDMS mold with a flat substrate (typically PDMS or glass) to obtain an enclosed channel system.

1. Pour degassed PDMS on the epoxy mold to a thickness of 4 mm to form microfluidic channels with horizontally oriented reservoirs. This piece will be the top layer of the final device (**Fig. 6**).
2. Pour degassed PDMS on flat Petri dishes to form the bottom part of the MISS to a thickness of 2 mm (**Fig. 7**).
3. Partially cure both PDMS layers by leaving them at room temperature overnight or at 60°C for 20 min.
4. Put the two partially cured PDMS layers together and cure the combined structure at 60°C for an additional 60 minutes to obtain the closed channel structure (**Fig. 8**) (see **Notes 2** and **3**).

3.2. Plasma Oxidation of Sperm Sorters

The purpose of plasma oxidation of sperm sorters is to make the channel hydrophilic to facilitate introduction of fluids into the channels. PDMS is inherently hydrophobic and aqueous solutions are difficult to introduce into channels. Furthermore, nonspecific adsorption causes sperm to stick to the surfaces of the channels and reservoirs, thus reducing the yield. To change the surface property of PDMS devices from hydrophobic to hydrophilic, we use plasma oxidation to activate the surface and make the surface transiently hydrophilic for a few hours. We typically plasma oxidize the whole device in a plasma

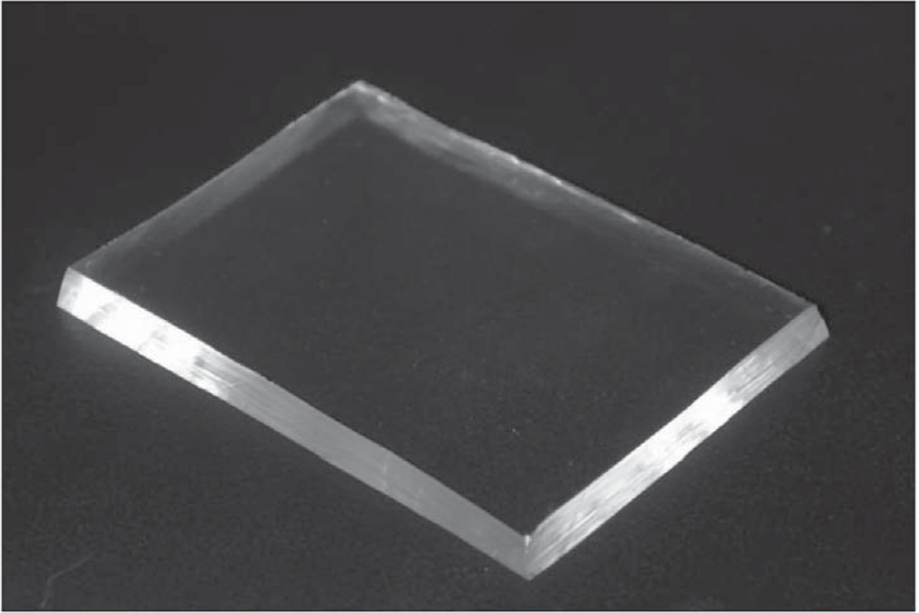


Fig. 7. Bottom layer of MISS.

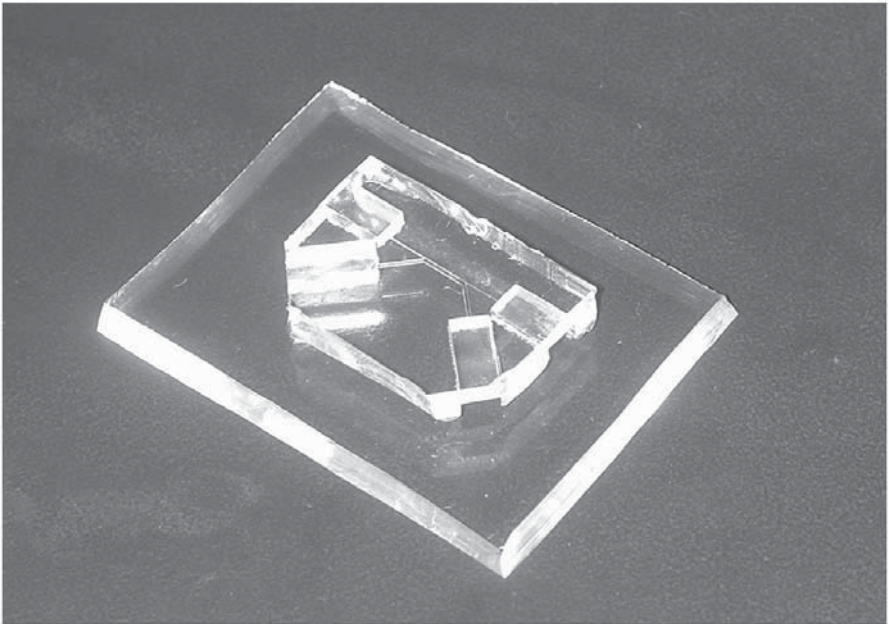


Fig. 8. The bonded structure.

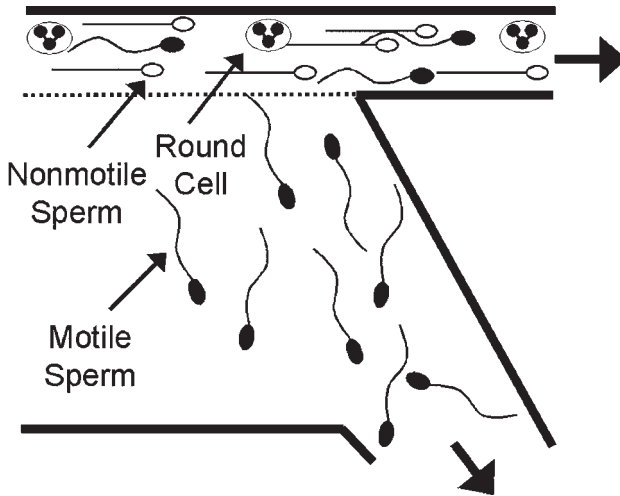


Fig. 9. Schematic illustration of sperm-sorting process. (Reproduced with permission from ref. 9.)

chamber for 10 min to make the surface transiently hydrophilic. If the device is hydrated and stored in a humid environment immediately after plasma treatment, channel surfaces can remain hydrophilic indefinitely (*see Notes 4 and 5*). Following plasma oxidation, channels and reservoirs are further coated with a 1% BSA solution (dissolved in PBS) to minimize nonspecific adsorption of cells to channel walls (*see Notes 6 and 7*).

3.3. Sorting Sperm With a MISS

A typical sorting experiment would be as follows:

1. Add 60 μL of processing medium to the media inlet.
2. After media wicks through the channel to the outlets, add 2 μL of medium to each of the outlet reservoirs.
3. Add a 50- μL semen sample to the sample inlet. All positions can be seen in [Fig. 1](#). The semen and media flow at a constant flow rate from the inlet to the outlet (*see Notes 8 and 9*). Owing to the laminar flows and motility differences between sperm, most nonmotile sperm exit the upper outlet, whereas a significant portion of the motile sperm will exit out the lower outlet ([Fig. 9](#)).
4. Analyze the number of motile sperm using a Makler counting chamber (Sefi-Medical, Haifi, Israel) while taking dilution factors into account.
5. Visualize nonmotile sperm (more precisely, membrane-compromised sperm) by adding 3 μL of PI (60 mM dissolved in processing medium; Molecular Probes) to sperm samples prior to sorting and using a Texas Red filter set (577-nm excitation, 620-nm emission) to view red fluorescence.

6. Record images and movies on an inverted microscope (Nikon TE 330) with a charge-coupled device camera (Hamamatsu ORCA-100).

The MISS system enables straightforward, gentle, and reliable sorting of motile, morphologically normal spermatozoa from a mixture using microfluidics. The MISS is structurally simple, straightforward to fabricate, cost-effective, and a stand-alone device that is fully functional without any external power sources or controls (9). It is ideal for sorting small volumes of samples and can provide high-quality (motile and of good morphology) sperm even from debris-laden samples (10).

4. Notes

1. It is possible to glue metal reservoirs directly on the Si wafer with channel features without making the first epoxy mold. However, the wafers are fragile and can break easily owing to cutting and peeling of PDMS on the wafer. It is also not necessary to make the second epoxy mold; the PDMS can be cast directly against the first epoxy mold with metal cuboids glued on it.
2. Occasional leaks occur at the reservoir's edges (i.e., at the interface between the main PDMS device, the substrate, and air) owing to capillary action and result in cross-contamination between reservoirs. To solve this problem, we dabbed and cured small amounts of PDMS at the PDMS-substrate interface between reservoirs. The amount of PDMS dabbed should be limited to prevent the risk of it being wicked into the channels.
3. Alternatively, glass cover slides can be used as the bottom layer whenever the bonding performed is through plasma oxidation treatment (17). A glass bottom is originally hydrophilic; however, the bonding technique using plasma oxidation is sensitive to experimental conditions and can sometimes be difficult to reproduce reliably.
4. Plasma oxidation can be used to bond permanently a flat PDMS surface to unsilanized glass, silicon, or PDMS. A typical procedure would involve facing two surfaces (to be bonded) up in the oxidation chamber, and oxidizing for 30 s with 40 mA at 200–800 mtorr under oxygen plasma. The two sides would then be immediately brought into contact after oxidization (within minutes) and hermetically sealed, followed by incubating in a 60°C oven or baking on a heating plate for 1.5 h to ensure full, irreversible bonding. Plasma oxidation only temporarily changes the PDMS surface to hydrophilic. For bonding purposes, it is important that the PDMS surface be oxidized only briefly, and that oxidized surfaces be brought into contact with each other immediately thereafter. Short oxidizations activate functional groups (hydroxyl) on the PDMS surface. The functional groups from each surface will form chemical bonds and, hence, make bonding irreversible. If the oxidization is long (>10 min), the surface will be degraded and will not be able to form chemical bonds between surfaces. Plasma oxidization keeps the PDMS surface hydrophilic only transiently if the surface is kept dry. To elongate the device's hydrophilicity, an aqueous solution

should be introduced into the channel within 10 min after oxidation. Incubation with 1–5% BSA solution also helps to maintain the hydrophilicity. It is also possible to dry and save the device after bonding; oxidize again for 10 min immediately before the introduction of liquid.

5. Devices can be entirely UV sterilized after their production, because all components are transparent. Autoclaves can also be used.
6. The channel surface can be coated with BSA and then dried for storage. The channel may be receptive for the introduction of liquid later without using plasma oxidization. This will allow users without a plasma oxidizer to use the device. BSA is a common blocking protein with negative charges that can make surfaces hydrophilic. However, it will not create a channel surface as hydrophilic as plasma oxidization would, and often liquid needs to be aspirated for the channel to be air/bubble free.
7. After plasma oxidation, devices can also be immersed in a water-filled ziplock bag (or other tight-sealing container) for long-term storage to keep the channels hydrophilic.
8. Clogging is an issue that often occurs in the sperm sample inlet. Although it is relatively desirable that clogging occur at the sperm inlet (rather than outlets or media inlet) since purity is not compromised, clogging is still a challenge. Most clogs are eliminated by pushing on the channel from the top with a pipet tip or finger.
9. Along with channels, reservoirs also need to be as hydrophilic as possible. Lower contact angles result in less contact angle hysteresis and more stable flows. Reservoirs should not be overfilled so that the liquid meniscus is bulging outward and, thus, changes the surface tension. In addition, it is preferable to add sperm sample after filling other inlet and outlet reservoirs.

References

1. Mosher, W. D. and Pratt, W. F. (1991) Fecundity and infertility in the United States: incidence and trends. *Fertil. Steril.* **56**, 192–193.
2. Palermo, G., Joris, H., Devroey, P., and Van Steirteghem, A. C. (1992) Pregnancies after intracytoplasmic injection of single spermatozoon into an oocyte. *Lancet* **340**, 17–18.
3. Schultz, R. M. and Williams, C. J. (2002) *Science* **296**, 2188–2190.
4. Tukur, K. E. and Jansen C. M. A. (2003) Sperm separation techniques: comparison and evolution of gradient products, in: *The Art and Science of Assisted Reproductive Technique + Art*. (Allahbadia, G. N. and Basuray-Das, R., eds.) Jaypee Medical Publishers, New Delhi, India, pp. 218–221.
5. Aitken, R. J. and Clarkson, J. S. (1988) Significance of reactive oxygen species and antioxidants in defining the efficacy of sperm preparation techniques. *J. Androl.* **6**, 367–376.
6. Englert, Y., Van de Bergh, M., Rodesch, C., Bertrand, E., Biramane, J., and Legreve, A. (1992) Comparative auto-controlled study between swim-up and Percoll preparation of fresh semen samples for in-tro fertilization. *Hum. Reprod.* **3**, 399–402.

7. Zini, A., Finelli, A., Phang, D., et al. (2000) Influence of semen processing technique on human sperm DNA integrity. *Urology* **6**, 1081–1084.
8. Weigl, B. H., Bardell, R. L., and Cabrera, C. R. (2003) Lab-on-a-chip for drug development. *Adv. Drug Deliv. Rev.* **55**, 349–377.
9. Cho, B. S., Schuster, T. G., Zhu, X., Chang, D., Smith, G. D., and Takayama, S. (2003) Passively driven integrated microfluidic system for separation of motile sperm. *Anal. Chem.* **75**, 4671–1675.
10. Schuster, T. G., Cho, B. S., Keller, L. M., Takayama, S., and Smith, G. D. (2003) Isolation of motile spermatozoa from semen samples using microfluidics. *Reprod. BioMed. Online* **7(1)**, 75–81.
11. Whitesides, G. M., Ostuni, E., Takayama, S., Jiang, X., and Ingber, D. E. (2003) Soft lithography in biology and biochemistry. *Annu. Rev. Biomed. Eng.* **3**, 335–373.
12. White, F. M. (1999) *Fluid Mechanics*, 4th ed., McGraw Hill, Columbus, OH.
13. World Health Organization. (1999) *WHO Laboratory Manual for the Examination of Human Semen and Sperm–Cervical Mucus Interaction*, 4th ed., Cambridge University Press, Cambridge, UK.
14. Xia, Y. and Whitesides, G. M. (1998) Soft lithography reviews. *Angew. Chem. Int. Ed.* **37**, 550–575.
15. Gadre, A., Kastantin, M., Li, S., and Ghodssi, R. (2001) An integrated BioMEMS fabrication technology. *Intl. Semiconductor Device Res. Symp.* 1–4.
16. Carlier, J., Arscott, S., Thomy, V., et al. (2004) Integrated microfluidics based on multi-layered SU-8 for mass spectrometry analysis. *Micromech. Microeng.* **14**, 619–624.
17. Duffy, D. C., McDonald, J. C., Schueller, O. T. A., and Whiteside, G. M. (1998) Rapid prototyping of microfluidic systems in poly(dimethylsiloxane). *Anal. Chem.* **70**, 4974–4984.

Index

A

Advanced nucleic acid analyzer
(ANAA), 103
Agarose gel, 110
Alcohol dehydrogenase, 157, 162
Annealing, 98
Antibody, 89
Antibody immobilization, 77–78, 83–95
Avidin, 144

B

Beads, 47–49
Bioanode, 157–166
Biochip, *see* BioMEMS
Biofuel cell, 157–166
BioMEMS, 5, 9, 12–13, 115
Bioseparation, 65–81
Biotinylated DNA, 144, 147
Bone marrow biopsies, 179
Bovine serum albumin (BSA), 89–90,
108, 137, 172, 241

C

Caffeine, 199, 215, 217, 220
Cancer cell chemotaxis, *see* Chemotaxis
Capillary electrophoresis (CE), 1, 27,
99, 110–115
Cardiac muscle cell, *see* Cardiomyocyte
Cardiomyocyte, 199–225
Cell culture chamber, 167–177, 184–185,
189–191
Cell retention, 191, 199, 211–214
Cellular debris, 227
Ceramics, 102
Chemical stimulation, 199
Chemotaxis, 167–177

Chlorotrimethylsilane, 108
Chrome-gold layer, 55–56
Collagenase, 204
Compartment chamber, 167
Computer aided design (CAD), 19, 25,
50, 53, 167, 235
Contact guidance, 179
Continuous-flow, 97, 116–119
Convective-flow, 97, 119–122
Cuboids, 236–237
Cyclic olefins, 102, 114

D

Denaturation, 98
Density gradient separation, 229
Descumming, 10
Dichloromethylsilane, 108
DNA amplification, 97–140
DNA analysis, 97, 141–155
DNA array, 141–155
DNA detection, *see* DNA analysis
DNA hybridization, 84, 110, 141, 148
dNTP, 98, 135–136
Double-tee injection system, 33
Dye-doped silica nanoparticles, 141–155
Dyes, 141–155, 201, 204–205, 208, 241

E

Electromagnet, 68, 70–75
Electroosmotic flow, 52, 58, 84
Electrophoresis, 87
Electroplating, 72–74
Enzymes, 109, 137, 157, 162
Extension, 98
External heat, 103–105, 112–114

F–G

Fibronectin, 179, 191
 Fluid dynamic viscosity, 230
 Fluorescein, 87, 89, 144, 147
 Fluorescent probes, 102, 141–155,
 209–210, 241
 Fluorescent labeling, 89, 143
 Friction drag coefficient, 231
 Gas chromatograph, 1
 Gold, 11, 23, 26, 55

H

Hexamethyldisilazane (HMDS), 108, 235
 Hybridization, *see* DNA hybridization
 Hydraulic diameter, 230
 Hydrogel, 83–95
 Hydrolysis, 145, 220

I

Immobilization, 147, 157, 162–163
 Immunoassay, 66, 80, 83–95
 Integrated heat, 103, 106–107, 112–114
 Intracellular calcium, 199–200, 214–220
 Intracytoplasmic sperm injection
 (ICSI), 228
 In vitro fertilization (IVF), 228

L–M

Laminar flow, 180, 229–231, 241
 Laser ablation, 27–38, 86
 Laser fluence, 27
 Lift-off technique, 23–26
 Lithography, 5, 28
 Lysis, 115
 Magnetic force, 75–76
 Magnetic moment, 75
 Magnetic particle, 65–81
 Magnetic separation, 65–81
 Magnetic susceptibility, 75
 Magnetization density, 75
 Mean fluid velocity, 230
 Methylene green, 157, 162, 165
 Mesenchymal stem cells, *see* Stem cells

Microelectromechanical systems
 (MEMS), 5, 12–15

Microfabrication, 5–38
 Microfluidic fuel cell, 157–166
 Microfluidics, 1, 5, 11–12, 17–20, 47
 Microgrooves, 173
 Microlithography, 5
 Micromolding, 157–158, 162
 Micropatterned substrates, 167–197
 Microreactor, 1, 131
 Micro total analysis system (μ TAS), 1, 47
 Microvalves, 79
 Migration chamber, 167
 Miniature analytical thermal cycling
 instrument (MATCI), 103
 Molding, 17
 Motile sperm, 227, 241
 Motility, 227
 Muscle cell contraction, 199–225

N

Nafion, 159–162
 Nanoparticles, 141–155
 Neuronal chamber, 167–177
 Neutrophils, 167–177
 Nonmotile sperm, 227
 Nonspecific binding, 149

P

Packed column, 47
 Passivation, 97, 108, 123, 131, 135–136
 Passively driven pump, 227, 229, 236
 Pattern transfer, 11
 PCR amplicons, 139
 Permalloy, 71–75
 Photobleaching, 143
 Photoinitiation, 87
 Photolithography, 2, 5–15
 Photoresist, 5–11, 19, 25, 55, 71, 73,
 179, 186–187
 Photostability, 141, 151
 Plasma oxidation, 239–241
 Polyacrylamide gel, 83–95, 103

- Polycarbonate (PC), 85–87, 102, 134
Polydimethylsiloxane (PDMS), 12, 17–21, 34, 102, 134, 158–162, 167–168, 170–172, 179, 180–187, 190–191, 229, 233, 235–239
Polyethylene glycol (PEG), 108, 144, 148
Polyimide, 102
Poly-L-lysine (PLL), 170, 174–175
Polymerase chain reaction (PCR), 97–140
Polymethylmethacrylate, 33, 85–87, 134
Polypropylene insert, 106–108, 111–112
Polytetrafluoroethylene (PTFE), 116–117
Polyvinyl pyrrolidone (PVP), 108
Preconcentration, 47
Primers, 98, 138
Profilometer, 160
Propyleneglycolmethyl ether acetate (PGMEA), 168, 173
Protease, 204
- Q–S**
- Quartz, 102
Replica molding, 12, 165
Reverse microemulsion, 145
Reversible glass bonding, 39–43
Reynolds number, 158, 229
Room temperature bonding, 39–43
Sandwich assay, 141–155
Screen-printing carbon inks, 157
Silanes, 19, 108, 119
Silicon oxide, 108
Silicon wafer (Si wafer), 1, 19, 23–26, 70, 73–75, 134, 157–158, 173, 182
Soft lithography, 2, 5, 12, 17–21, 28, 167, 229, 233
Solid phase extraction, 47–64
Sperm motility assay, 227–244
Sperm sorter, 227–244
Sputter coating, 26, 158, 160
Stem cells, 179–199
Sterilization, 190
Stober method, 145–146
SU-8, 12, 17–21, 102, 159–160, 170, 173, 233
Superparamagnetic particle, 65, 69
Surface modification, 147
- T**
- Tetramethylrhodamine (TMR), 144, 147
Thermus aquaticus (Taq), 98, 109, 132
Teflon, 116–118, 120, 159, 162, 183, 215
Temperature ramping, 131
Tetraethylorthosilicate (TEOS), 144–146
Thermocycler, 99–100, 103, 110
Tris(2,2-bipyridyl)dichlororuthenium (II) (RuBpy), 144, 146
Triton X-100, 108, 144, 146
Turbulent flow, 230
Tween-20, 108
- U–W**
- Ultraviolet curable glue, 131, 135
Water nanodroplets, 145